University of Essex

Biochemical and Molecular Characterisation of the FADDosome

Sylwia Jencz

A thesis submitted for the degree of
DOCTOR OF PHILOSOPHY

School of Life Sciences
University of Essex

October 2019

ABSTRACT

An anti-metabolite drug, 5-FU (5-fluorouracil), is widely used in the treatment of colorectal cancer. However, acquisition of resistance by cancer cells is the main cause of the limited clinical use of 5-FU, which needs to be overcome to widen and lengthen its utility. Therefore, it is necessary to investigate the factors and pathways involved in 5-FU-induced apoptosis. Chemotherapeutic agents, such as 5-FU, are believed to exert their anti-cancer effect by initiation of apoptosis via the intrinsic cell death pathway, which requires activation of caspase-9. However, our group has recently discovered that 5-FU-induced cell death is initiated by activation of caspase-8, whereas caspase-9 was found to be dispensable for this process. Moreover, our group has found that upon treatment with 5-FU, caspase-10 is upregulated, which leads to the formation of a newly discovered apoptosis-inducing protein complex, FADDosome. This study is composed of two parts. In part I, the functional and interactional analysis of the main FADDosome constituents revealed that caspase-10 has the ability to activate caspase-8 *in vitro*. Moreover, it was found that FADD and caspase-8 possibly interact via a novel, DED-independent mechanism *in vitro*. In part II, our group discovered that the ATR, Chk1 and Chk2 kinases are activated in 5-FU-treated HCT116 cells and play a key role in the 5-FU-induced DNA damage signal transduction towards caspase-10 upregulation and FADDosome formation. It was found that activation of Chk1 and Chk2 as well as induction of p53 are regulated in an ATR-dependent manner in response to 5-FU. It was discovered that when Chk1 and Chk2 are inhibited, the 5-FU-treated HCT116 cells appear to shift to an alternative cell death mechanism, mediated by another newly discovered apoptosis-inducing complex, the FLIPosome. The obtained results provide new insights into the roles of the proteins and mechanism involved in the FADDosome formation and apoptosis regulation in colorectal cancer cells treated with 5-FU.

ACKNOWLEDGMENTS

I would like to sincerely thank my supervisor, Dr Ralf Zwacka, for his knowledge, advice, patience and guidance. Thank you for the time and effort that you put into introducing me to the area of molecular biology and cancer research as well as supporting me with completion of my research work and writing-up this thesis. I am also grateful to my co-supervisor, Dr Andrea Mohr, for her knowledge, experience, advice and giving me the opportunity to explore on my own.

I would also like to acknowledge my first advisor at the University of Essex, Dr Jonathan Worrall, for his wisdom, advice and valuable discussions, which were very helpful on numerous occasions.

I would like to thank my friends and colleagues that I worked with in Dr Zwacka's lab as well as other labs within the University of Essex. Special thanks and gratitude to Yasamin Mehrabadi for her friendship, advice and support. Thank you all for a nice and friendly atmosphere during our work together.

Finally, I would like to thank my family, friends and my beloved partner, Slawomir Chmielewski, for your love, support, understanding and encouragement during my studies. Thank you all for being there for me, especially when I needed you the most. I am very grateful for all the wonderful moments that we have shared together.

TABLE OF CONTENTS

LIST OF FIGURES

LIST OF TABLES

LIST OF ABBREVIATIONS

5-FU	5-fluorouracil
ANOVA	analysis of variance
Apaf-1	apoptotic protease activating factor-1
APS	ammonium persulfate
AMC	Ac-DEVD 7-amino-4-methylcoumarin
ATM	ataxia telangiectasia-mutated
ATR	ataxia telangiectasia and Rad3-related protein
ATRIP	ATR-interacting protein
Bak	Bcl-2 homologous antagonist
Bid	BH3 interacting-domain death agonist
BSA	bovine serum albumin
CAD	caspase-activated DNase
CARD	caspase-recruitment domain
CDK(s)	cyclin-dependent kinase(s)
Chk1/2	checkpoint kinase 1/2
CXCL1	chemokine (C-X-C motif) ligand 1
cFLIP	cellular FLICE-inhibitory protein
DD	death domain
DSB	double-strand breaks
DED(s)	death effector domain(s)
DISC	death-inducing signalling complex
DMF	dimethyl fumarate
DNA	deoxyribonucleic acid
DNA-PK(s)	DNA-dependent protein kinase(s)
FADD	Fas-associated via death domain

GST	glutathione S-transferase
GuHCl	guanidine hydrochloride
His	polyhistidine
HMGB1	high-mobility group B1 protein
HRP	horseradish peroxidase
IAPs	inhibitors of apoptosis
ICAD	inhibitor of caspase-activated DNase
IL-6/8	interleukin 6/8
IMAC	immobilized metal ion affinity chromatography
IPTG	isopropyl β-D-1-thiogalactopyranoside
JNK	c-Jun-terminal kinase
LRRs	leucine-rich repeats
MALS	multiangle light scattering
MCP-1	monocyte chemoattractant protein-1
MEFs	mouse embryonic fibroblasts
MIF	macrophage migration inhibitory factor
MOMP	mitochondrial outer membrane permeabilisation
MRN	MRE11–RAD50–NBS1
Nemo	NF-κB essential modulator
NMR	nuclear magnetic resonance
NPM1	nucleophosmin
NSAIDs	nonsteroidal anti-inflammatory drugs
Nec-1	necrostatin-1
PARP	poly (ADP-ribose) polymerase
PBS	phosphate-buffered saline
PCNA	proliferating cell nuclear antigen
PIDD	p53-induced protein with death domain
PIKKs	phosphoinositide 3-kinase (PI3K)-related kinases

PP1/5	protein phosphatase 1/5
PP2A	protein phosphatase 2A
PP2C	protein phosphatase 2C
PPM1D	protein phosphatase 1D
PVDF	polyvinylidene difluoride
PYD	pyrin domain
RAIDD	CASP2- and RIPK1-domain-containing adaptor with death domain
RFC4/5	replication factor C subunit 4/5
RIP1/3	receptor-interacting protein 1/3
RNA	ribonucleic acid
RPA	replication protein A
SDS	sodium dodecyl sulphate
SEC	size exclusion chromatography
ssDNA	single-stranded DNA
tBid	truncated Bid
TBS	Tris-buffered saline
TBST	Tris-buffered saline tween 20
TLR	toll-like receptor
TNF	tumour necrosis factor
TNF-R1	tumour necrosis factor receptor 1
TRADD	TNF-R1-associated via death domain
TRAF-1/2	TNF-R1-associated factor 1/2
TRAIL-R1/2	TNF-related apoptosis-inducing ligand receptor 1/2
Trx-1	Thioredoxin-1
UPA	uncharacterised protein domain conserved in UNC5, PIDD and ankyrins
vFLIP	viral FLICE-inhibitory protein

Wip1	wild-type p53-induced phosphatase-1
XIAP	X-linked inhibitor of apoptosis protein
ZU5	ZO-1 and Unc5-like

LIST OF PUBLICATIONS

Mohr, A., Deedigan, L., Jencz, S., Mehrabadi, Y., Houlden, L., Albarenque, S.-M. and Zwacka, R.M. (2018). Caspase-10: a molecular switch from cell-autonomous apoptosis to communal cell death in response to chemotherapeutic drug treatment. *Cell Death & Differentiation*, 25(2), 340–352.

CHAPTER 1

LITERATURE REVIEW

1.1. Colorectal Cancer and Its Resistance to 5-Fluorouracil

Colorectal cancer has been reported to be the fourth leading cause of cancer-related deaths throughout the world (Brody, 2015). Currently, 5-FU (5-fluorouracil), a pyrimidine anti-metabolite drug, is the most widely used therapeutic in the treatment of colorectal cancer (Longley, 2003; De Angelis et al., 2006; Thant et al., 2008). However, despite the significant advancement of cancer-related research and improvement of anti-tumour therapies, colorectal cancer still remains a major public health problem worldwide.

The anti-cancer effect of 5-FU is associated with its ability to induce apoptosis, which is a major goal of the anti-tumour intervention (Hong et al., 2014; Lopez and Tait, 2015). Nevertheless, it has been reported that colorectal cancer can acquire resistance to 5-FU during the treatment (Thant et al., 2008). Moreover, the reduced response to 5-FU is a major cause of the limited clinical use of this cytotoxic drug (Longley et al., 2003; Zhang et al., 2008). Unfortunately, the molecular mechanisms leading to development of the resistance to 5-FU still remain unclear. Therefore, our aim is to examine the molecular pathways and factors involved in induction of cell death in response to 5-FU and thereby to investigate the potential mechanisms responsible for acquisition of the resistance to 5-FU in human colorectal cancer cells.

1.2. What Is Apoptosis?

Apoptosis (a-po-toe-sis) is a term that was first introduced by Kerr et al. (1972). The term describes a form of the programmed cell death, which is a conserved process (Zhang and Yu, 2013; Fuchs and Steller, 2015), involved in maintaining of tissue homeostasis by removal of damaged cells, organelles and molecules, such as proteins. Apoptosis plays a key role in aging and development of multi-cellular organisms and is necessary for maintaining of the cell population in tissues. This process also functions as a defence

mechanism in inflammation and immunity, and in response to anti-tumour treatments, such as chemotherapy or irradiation. Any dysregulation of the programmed cell death, leading to insufficient or excessive apoptosis, contribute to development of a wide range of human diseases, including cancer, infection, inflammation, neurodegeneration (Alzheimer's, disease and Parkinson's disease), developmental and immunological disorders (Elmore, 2007; Fuchs and Steller, 2011; Galluzzi et al., 2018). It was reported that abnormalities in the regulation of apoptosis contribute to development of therapeutic resistance in cancer cells (Bauer and Hefand, 2006; Zhang and Yu, 2013; Koff et al., 2015).

When cell death occurs, a variety of morphological features and changes can be observed. Depending on the mechanisms, which are used in order to dispose of the dead cells and their fragments, programmed cell death can be classified into three different forms. Type I cell death, known as apoptosis, is characterised by cytoplasmic shrinkage, chromatin condensation, DNA fragmentation, plasma membrane blebbing, cytoskeleton protein degradation and formation of apoptotic bodies, which are degraded within lysosomes of the neighbouring cells that use phagocytosis. During type II cell death, called autophagy, the cells undergo extensive cytoplasmic vacuolization followed by lysosomal degradation by surrounding cells. Type III cell death, named necrosis, which does not manifest any of the characteristics of the type I or II cell death, terminates by removal of dead cells without the involvement of phagocytosis and lysosomes (Fuchs and Steller, 2011; Galluzzi et al., 2018). It was believed that necrosis functions as a passive form of programmed cell death, however recently some studies reported the involvement of proteins responsible for regulation of this process. The regulated form of necrosis is referred to as "necroptosis". It can be blocked by using a small molecule inhibitor Nec-1 (Necrostatin-1) (Fuchs and Steller, 2011).

1.3. Apoptotic Pathways

Next to morphological features, apoptosis is characterised by an energy-dependent cascade of molecular and biochemical events. According to the conventional model of apoptosis, two main and distinct molecular networks are involved in initiation of the programmed cell death, namely the extrinsic/death receptor pathway and intrinsic/mitochondrial pathway.

The extrinsic apoptotic pathway is known to be induced by extracellular stimuli, such as death ligands, which can interact with their cognate death receptors (Figure 1). The death receptor family belongs to the TNF (tumour necrosis factor) receptor superfamily. Death receptors are composed of two domains: a cysteine-rich extracellular domain and an intracellular (cytoplasmic) domain, termed death domain. The latter consists of 80 amino acids (Ashkenazi and Dixit, 1998) and is necessary for transmitting the death signals from the cell surface to the cytoplasmic signalling networks. To date, the best described death receptors are: TNF-R1 (tumour necrosis factor receptor 1), CD95 (Fas/Apo1), Apo3 (DR3), TRAIL-R1 and TRAIL-R2 (TNF-related apoptosis-inducing ligand receptor 1 and 2) also known as DR4 and DR5 (death receptor 4 and 5), respectively (Elmore, 2007; Li et al., 2013; Bertsch et al., 2014; Brenner et al., 2015; Peter et al., 2015) (Figure 1).

Moreover, the extrinsic apoptotic network requires involvement of specific death ligands, that bind to their corresponding death receptors, which form trimers and are localised on the surface of the cell membrane (Elmore, 2007; Fuchs and Steller, 2015). Binding of the ligands contributes to recruitment of the cytoplasmic adapter proteins, such as FADD (Fas-associated via death domain) in the CD95- and TRAIL-R1/2-mediated extrinsic pathways or TRADD (TNF-R1-associated via death domain) in the TNF-R1-regulated network. Adapter proteins utilise their corresponding death domains to interact with the

death receptors. Next, in the TNF-R1 apoptotic pathway, FADD binds to TRADD (Wajant, 2002). The role of FADD in the extrinsic apoptotic pathways is to recruit pro-caspase-8, leading to formation of the DISC (death-inducing signalling complex), at which caspase-8 undergoes auto-processing and activation. Subsequently, activated caspase-8 can cleave the effector caspases, such as caspase-3, which in turn triggers the execution phase of the cell death mechanism (Gonzalvez and Ashkenazi, 2010; He et al., 2015; Mohr et al., 2015) (Figure 1).

On the other hand, the intrinsic apoptotic pathway is typically triggered in response to intracellular signals, such as DNA damage caused by chemotherapy, UV or irradiation (Figure 1). Moreover, it is known that DNA lesions contribute to activation of the tumour suppressor p53, which is believed to mediate the transcriptional activation of numerous factors involved in initiation of the cell death program (Kamer et al., 2005; Liu et al., 2010; Fuchs and Steller, 2015). The intrinsic apoptotic network is regulated by the Bcl-2 family of proteins, including Bcl-2, Bcl-X2, Mcl-1, Bid (BH3 interacting-domain death agonist), Bak (Bcl-2 homologous antagonist) and Bax. Initiation of this pathway occurs via induction of MOMP (mitochondrial outer membrane permeabilisation), which leads to the release of cytochrome c and Smac/DIABLO into the cytosol. Together with Apaf-1 (apoptotic protease activating factor-1), cytochrome c forms a complex termed Apoptosome, at which caspase-9 is activated, leading to execution of cell death. It has been reported that depending on the cell type, the extrinsic and intrinsic apoptotic pathways can converge at the mitochondrial level and influence one another (Ashkenazi and Dixit, 1998; Shen et al., 2008; Cullen and Martin, 2009; Li et al., 2015) (Figure 1).

Next to the extrinsic and intrinsic apoptotic networks, an additional apoptotic pathway has been described, which requires involvement of T-cells and contributes to perforin-granzyme-dependent apoptosis. In this pathway, cell death is induced via either granzyme A or granzyme B (Elmore, 2007).

A common feature of the apoptotic pathways is the involvement of the pro-apoptotic cysteine proteases called caspases, which function as the key mediators of programmed cell death and are involved in initiation of the execution pathway. Caspases are expressed as inactive proenzymes and activated in the extrinsic, intrinsic and granzyme B-dependent apoptotic pathways by proteolytic processing events, known as the cascade of caspases (Cullen ad Martin, 2009). The granzyme A-mediated network is induced in parallel in response to the single stranded DNA damage, without involvement of the caspases. The cascade of caspases contributes to amplification of the apoptotic signal and subsequent cell death (Figure 1). Activation of caspases is an irreversible process. These enzymes possess a proteolytic activity and although they can recognize different amino acid sequences within their substrates, the common feature of all caspases is to cleave other proteins at aspartic acid residues. Currently, caspases can be categorised into the following groups: (I) initiator caspases: caspase-2, -8, -9 and -10; (II) effector (executioner) caspases: caspase-3, -6 and -7; as well as (III) inflammatory caspases: caspase-1, -4 and -5 (Elmore, 2007).
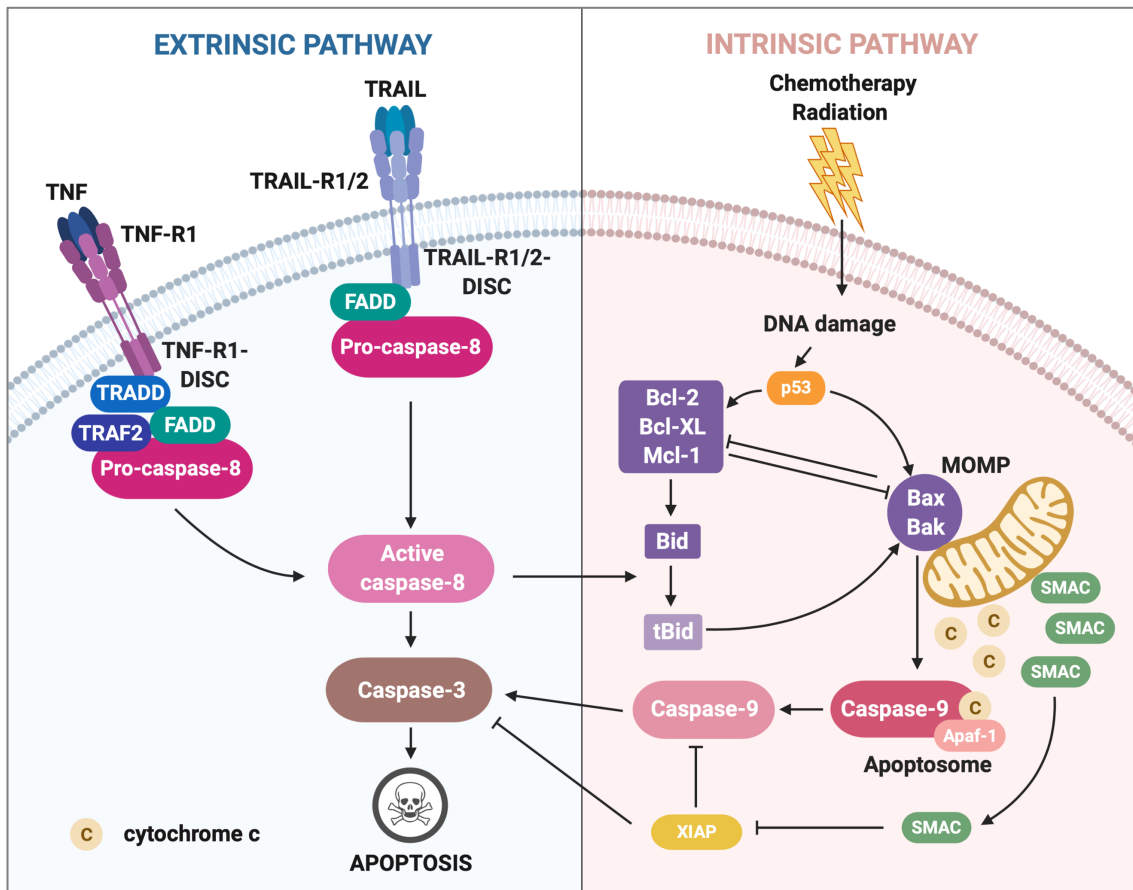
Figure 1. The conventional model of apoptosis.
The extrinsic pathway is triggered by binding of the death ligand to its cognate death receptor. Such interaction leads to induction of the death receptor, which recruits the adaptor molecules, such as FADD or TRADD and pro-caspase-8. These events contribute to formation of the DISC (death-inducing signalling complex), at which caspase-8 is activated and in turn, activates caspase-3, leading to initiation of apoptosis. On the other hand, the intrinsic apoptotic pathway is induced in response to the cytotoxic stimuli (such as DNA damage) and regulated by p53 and the Bcl-2 family of proteins. Activated p53 positively regulates expression of Bak and Bax, which together with tBid (truncated Bid) initiate MOMP (mitochondrial outer membrane permeabilisation) and subsequently contribute to the release of cytochrome c. The cytosolic cytochrome c interacts with Apaf-1 and as a result, forms a complex called Apoptosome, which contributes to caspase-9 activation and subsequent initiation of the cascade of caspases followed by the cell death induction. Another molecule, named Smac/DIABLO is also released from mitochondria into the cytosol, where it inhibits the anti-apoptotic protein XIAP (X-linked inhibitor of apoptosis protein). Such inhibition releases the molecular brake that XIAP exerts on caspase-3 and caspase-9.[1]

---

[1] Image created with BioRender.com

1.4. Extrinsic/Death Receptor Apoptotic Pathway

In the CD95- and TRAIL-R1/TRAIL-R2-mediated apoptotic pathway, the adapter protein FADD is recruited to the death receptor and associates with pro-caspase-8 or pro-caspase-10. An interaction between these molecules is believed to occur via their cognate death effector domains. This leads to formation of the DISC, at which pro-caspase-8 is cleaved and activated. An active enzyme is released to the cytosol, which contributes to initiation of apoptosis either by caspase-8-mediated cleavage of Bid or by activation of caspase-3, -6, -7 during the execution phase (Ohtsuka et al., 2003; Lavrik et al., 2005; He et al., 2015; Mohr et al., 2015). The extrinsic apoptotic pathway can be inhibited by cFLIP (cellular FLICE-inhibitory protein), which associates with FADD and pro-caspase-8 or -10 and as a result, prevents the DISC formation and blocks activation of caspase-8 or -10 (Lavrik et al., 2005; Elmore, 2007).

The TNF-R1-regulated signalling network requires formation of the DISC, which consist of TNF-R1, TRADD, FADD and TRAF-1/2 (TNFR-associated factor). Similar to the CD95- and TRAIL-R1/TRAIL-R2-mediated apoptotic pathway, pro-caspase-8 is recruited to the TNF-R1-DISC and cleaved at the complex. Activated caspase-8 proteolytically processes the executioner caspases (caspase-3, -6 and -7), leading to initiation of the cell death. TNF-R1 can also form other signalling platforms, such as a membrane-bound complex I and cytoplasmic complex II. Complex I requires association of TNF-R1 with TRADD, RIP1 (receptor-interacting protein 1) and TRAF 1/2, which triggers the non-canonical pathways, including NF-κB-signalling network and JNK (c-Jun-terminal kinase) vie the TRAF-2-dependent mechanism (Lavrik et al., 2005; Elmore, 2007). Complex II requires association of TRADD and RIP1 with their binding partners, FADD and caspase-8. This complex can be inhibited by cFLIP (Micheau and Tschopp, 2003).

1.4.1.   The Roles of Caspase-8 and Caspase-10

The role of caspase-8 in the initiation of the extrinsic apoptotic network has been thoroughly investigated and is currently relatively well understood (Fuchs and Steller, 2015). In addition, there is evidence that caspase-8 can be involved in initiation of non-conventional apoptotic pathways triggered by anti-cancer drugs, such as etoposide (Feoktistova et al., 2011; Imre et al., 2011; Biton and Ashkenazi, 2011; Tenev et al., 2011) as well as participate in TRAIL-mediated inflammation responses (Henry and Martin, 2017).

Similar to caspase-8, caspase-10 is believed to play a role in induction of the death receptor-dependent apoptotic pathway. It was demonstrated that this cysteine protease shares a significant sequence similarity with caspase-8. Additionally, it was reported that the catalytic domains of both caspases are identical in 46% of their protein sequence. Moreover, the Casp10 and Casp8 genes are located on the same chromosomal 2q33-34 region in humans. To date, no homologue of human caspase-10 has been found in mice, which is considered as one of the possible reasons for the little focus on caspase-10-related research (Wachmann et al., 2010; McIlwain et al., 2013). Therefore, our understanding of the physiological functions of caspase-10 in the apoptotic network is still fairly poor (Filomenko et al., 2006; McIlwain et al., 2013).

It has been suggested that, due to the shared structural homology, caspase-10 can functionally substitute caspase-8 in death receptor-induced signalling pathways, depending on the cell type (Kischkell et al., 2001). On the contrary, according to Sprick et al., (2002), it is very unlikely that caspase-10 can replace caspase-8 in mediating the TRAIL- and CD95-dependent apoptosis. Therefore, further and more detailed investigation is required to clarify this issue. It was reported that both uncleaved and cleaved variants of caspase-10 can proteolytically process Bid, leading to formation of

tBid, which in turn can contribute to initiation of apoptosis (Wachmann et al., 2010). Such observations led to the conclusion that caspase-8 and -10 share substrate specificity and their functions may partially overlap (Parrish et al., 2013; Riley et al., 2015).

Furthermore, there are only few studies, which investigated and described the role of caspase-10 and its activity in the initiation of the programmed cell death in response to chemotherapy. It was shown by some studies *in vitro*, that treatment with anti-tumour drugs (such as doxorubicin and etoposide) and arsenic dioxide can promote transcription of the Casp10 gene via activation of p53 and phosphoacetylation of histone H3, respectively, in cancer cells (Filomenko et al., 2006). Interestingly, some of the findings suggest that caspase-10 plays an active role in initiation of cell death in a FADD-dependent and death receptor-independent manner in response to cytotoxic chemotherapeutics (Park et al., 2004; Filomenko et al., 2006; Lee et al., 2007). Such apoptosis-inducing mechanisms were observed in human lymphoblastic leukaemia cells treated with paclitaxel (taxol) (Park et al., 2004) as well as in human U937, HeLa and 293T cell lines exposed to etoposide (Filomenko et al., 2006).

Nevertheless, there are no reports describing the role of caspase-10 and its upregulation or activity in triggering apoptosis in colorectal cancer cells treated with 5-FU. Additionally, the exact details of how the caspase-10-mediated initiation of cell death is driven in response to doxorubicin, etoposide and arsenic dioxide, mentioned above, still remain enigmatic. In summary, our poor understanding of how caspase-10 together with its chemotherapy-induced upregulation and/or activation might contribute to initiation of apoptosis in cancer cells requires further investigation.

1.5. Intrinsic/Mitochondrial Apoptotic Pathway

During intrinsic apoptotic pathway, which can be triggered without the involvement of the death receptors, activated p53 positively regulates the overexpression of the key pro-apoptotic proteins, namely Bak and Bax. Moreover, upon induction of the intrinsic apoptotic network, the pro-apoptotic protein Bid undergoes the caspase-8-mediated cleavage, which in turn leads to formation of truncated Bid (tBid). Bak, Bax and tBid contribute to induction of MOMP (Tait and Green, 2010; David, 2012). As a result, the pro-apoptotic cytochrome c (Liu et al., 1996) and the IAPs (inhibitors of apoptosis) antagonist named Smac/DIABLO (Verhagen et al., 2000) are released. The cytosolic cytochrome c can interact with Apaf-1 and consequently, forms a complex called Apoptosome (Cullen and Martin, 2009; Li et al., 2015). Formation of the Apoptosome stimulates initiation of a cascade of caspases, which consists of subsequent proteolytic processing events leading to activation of downstream caspases and consequently, induction of cell death.

1.5.1. Regulation by Bcl-2 Family Members

The mitochondrial pathway functions as an initial stage of the intrinsic apoptotic network and is mostly regulated by the Bcl-2 family of proteins, which are responsible for controlling of the release of pro-apoptotic proteins, such as cytochrome c, Smac/DIABLO, and the serine protease HtrA2/Omi (van Loo et al., 2002; Garrido et al., 2005; Wang and Youle, 2009) from the mitochondrial intermembrane space into the cytosol. Upon intracellular stimuli, such as DNA damage, toxins, chemotherapeutic agents, UV radiation, viral infection or stress signals, the inner mitochondrial membrane undergoes changes, which contribute to opening of the pores, loss of the transmembrane potential and finally, induction of MOMP, which is one of the main

characteristics of the intrinsic network (Elmore, 2007; Wang and Youle, 2009; Márquez-Jurado et al., 2018).

The regulators of these events, Bcl-2 family of proteins, consist of at least 25 members and can be divided into two classes: pro-apoptotic proteins, which include Bcl-10, Bak, Bax, Blk and Bok, as well as anti-apoptotic proteins, including Bcl-2, Bcl-G, Bcl-L10, Bcl-Rambo, Bcl-w, Bcl-X, Bcl-XS, Bcl-XL, Mcl-1, A1 and Bag. The anti-apoptotic members of the Bcl-2 family can be inhibited by the BH3-only family of proteins, which share a BH3 motif and due to their function act as pro-apoptotic factors. The BH3-only family includes: Bad, Bid, Bim, Bik, Puma, Noxa, Bmf and Hrk (Elmore, 2007; Wang and Youle, 2009). It was demonstrated that the key regulators of the mitochondrial apoptotic pathway are Bak and Bax, at which the intracellular signals converge (Zong et al., 2001). These factors play a critical role in determining, whether cells undergo apoptosis or inhibit the process. Bak and Bax can be negatively or positively regulated by the members of the anti-apoptotic Bcl-2 and BH3-only protein families, respectively (Elmore, 2007; Wang and Youle, 2009) (Figure 2).

In healthy cells, Bak is normally located inside the mitochondria, whereas Bax residues in cytosol and translocates to mitochondria upon initiation of apoptosis (Figure 2). During cell death, both proteins undergo conformational changes and subsequent oligomerisation, which is necessary for mitochondrial membrane permeabilisation and subsequent release of cytochrome c (Leber et al., 2007) (Figure 2). Until recently, it was unclear, how changed conformation and oligomerisation of Bak and Bax contributes to permeabilisation of the mitochondrial membrane. It was reported by Uren et al. (2017), that Bak and Bax form symmetric homodimers, that act as a basic unit for pore formation, which was confirmed by biophysical, biochemical and structural studies. Each dimer contains a transmembrane domain, which allows anchoring inside the mitochondria and an extended hydrophobic surface, localised on the mitochondrial outer membrane. It was

proposed that Bak and Bax have a preference for forming of the lipid pores over proteinaceous ones, however the exact mechanism still remains unclear (Uren et al. 2017).
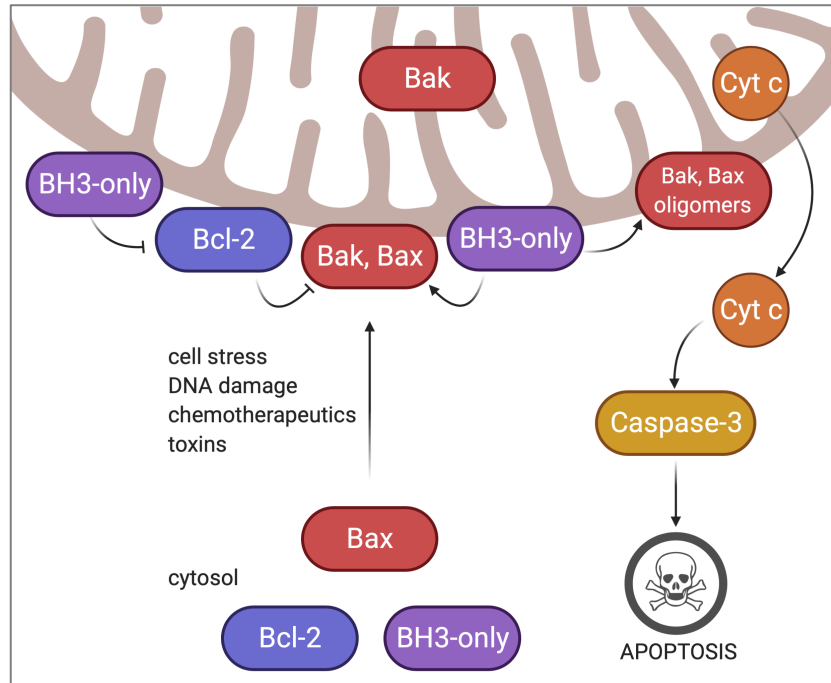
Figure 2. Activation and oligomerisation of Bak and Bax followed by release of cytochrome c and apoptosis.
Upon initiation of the mitochondrial pathway, the pro-apoptotic factors Bak and Bax translocate to the mitochondria outer membrane and oligomerise in order to trigger MOMP. The anti-apoptotic Bcl-2 family proteins inhibit Bak and Bax, whereas pro-apoptotic BH3-only family proteins positively regulate these factors. Additionally, BH3-only family proteins negatively regulate the Bcl-2 proteins. During MOMP, cytochrome c is released to the cytosol, leading to caspase-3 activation and apoptosis (Uren et al., 2017).[2]

The existence of the "cross-talk" between the extrinsic and intrinsic/mitochondrial apoptotic pathways has been widely reported. One of the examples is the caspase-8-mediated cleavage of Bid (BH3 interacting-domain death agonist), which occurs in type II cells, when the cascade of caspases cannot be induced due to existence of XIAP. Until being cleaved, Bid remains inactive and is located in the cytosol. After the caspase-8-mediated cleavage and activation, a truncated fragment of Bid (tBid) localises to mitochondria, and then, together with activated Bax initiates the release of cytochrome

---

[2] Image created with BioRender.com

c leading to induction of intrinsic apoptotic pathway (Li et al., 1998; Luo et al., 1998; Wang, 2001; Kamer et al., 2005).

1.5.2. Roles of Cytochrome c and Smac/DIABLO

Cytochrome c is a pro-apoptotic protein, which is released during MOMP into the cytosol. Other proteins, that are also released during the process include Smac/DIABLO and HtrA2/Omi (Loo et al., 2002; Garrido et al., 2006; Wang and Youle, 2009). These molecules are involved in activation of the caspase-dependent mitochondrial network. In particular, cytochrome c is known to interact with Apaf-1 and consequently, forms a complex called Apoptosome (Cullen and Martin, 2009; Li et al., 2015). At the complex, Apaf-1 binds to pro-caspase-9, which in turn forms clusters, leading to its activation and execution of the cell death. The apoptotic function of cytochrome c has been demonstrated by numerous genetic and biochemical studies *in vitro* and *in vivo* (Liu et al., 1996; Hakem et al., 1998; Kuida et al., 1998; Hao et al., 2005). Furthermore, Smac/DIABLO and HtrA2-Omi bind to the IAP (Inhibitors of apoptosis) and play a key role in neutralizing the inhibitory effects of IAP on effector caspases activity, which consequently promotes execution of apoptosis (Wang and Youle, 2009). In particular, Smac/DIABLO binds to XIAP, however association with cIAP1 and cIAP2 has also been reported (Srinivasula et al., 2000). Nevertheless, various studies suggest that Smac/DIABLO can play more complex roles in apoptosis. One of the splicing variants, Smac beta can sensitise cells to apoptosis, despite lacking its ability to associate with IAPs. Such observation suggests, that acting as an IAP antagonist is not the only function of Smac (Roberts et al., 2001). It was also reported that Smac3, another splicing variant of Smac, is involved in XIAP autoubiquitination and degradation (Fu et al., 2003). Other studies have demonstrated that knocking-out Smac in HCT116 cells lead to the delayed release of cytochrome c and resistance to NSAIDs (nonsteroidal anti-inflammatory drugs) (Kohli et al., 2004).

1.5.3. Regulation by p53

The tumour suppressor protein p53, encoded by TP53 gene, functions as a sensor of the cellular stress and mediates transient and permanent cell cycle arrest as well as plays a critical role in tumorigenesis prevention by being involved in regulation of numerous processes, including apoptosis, DNA repair and oncogenes activation (Russo et al., 2005; Collavin et al., 2010; Li et al., 2015). p53 is known to induce and regulate the intrinsic apoptotic pathway, however, it has been described that this tumour suppressor can be also involved in mediating and promoting the extrinsic apoptotic network (Ryan et al., 2001; Li et al., 2015). p53 is a transcription factor, which consists of characteristic domains, including: N-terminal transactivation domain (1 – 92 residues), a central core sequence-specific DNA-binding domain (100 – 300 residues) and C-terminal tetramerization and regulatory domain (323 – 393 residues) (Stavridi et al., 2005) (Figure 3).
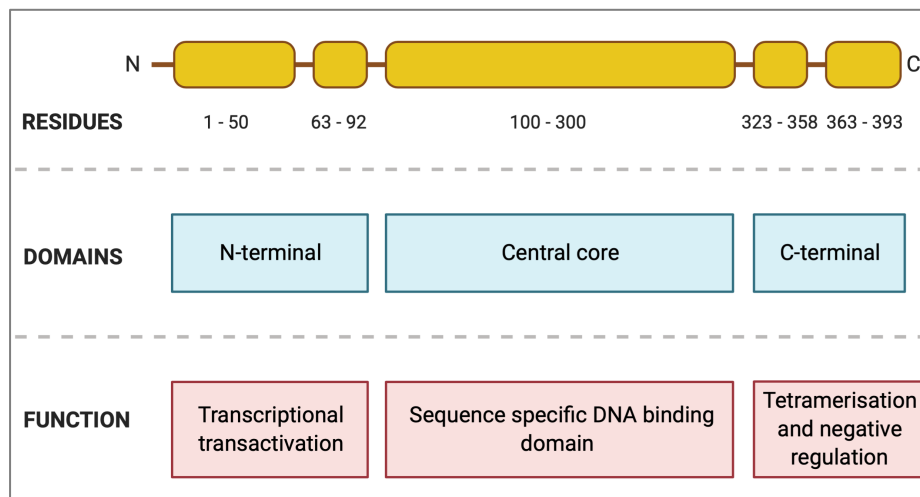
Figure 3. Domains of the tumour suppressor p53 and their functions.
The p53 protein structure consists of several domains. To date, the following domains have been identified: N-terminal domain (responsible for transcriptional transactivation), the central core domain (a sequence specific DNA binding domain), and the C-terminal domain (it encompasses the tetramerization and negative regulation domain) (Stavridi et al., 2005).[3]

---

[3] Image created with BioRender.com

Mutations in the TP53 gene and deactivation of p53 are described as one of the most frequently occurring events associated with the subsequent development of a wide range of human cancers (Kandoth et al., 2013). Inactivation of p53 happens as a result of a single monoallelic missense mutations, which mainly occur in the DNA-binding domain. Typically, p53 is expressed as a stable, full-length protein, which lacks its sequence-specific DNA-binding activity due to the mutations (Brosh and Rotter, 2009).

Depending on the mechanism, p53-mediated apoptosis can be regulated transcriptionally or non-transcriptionally. To date, numerous p53 targets have been found and include: the pro-survival Bcl-2 and Bcl-XL as well as pro-apoptotic Bcl-2 proteins (Bax, Puma, Noxa and Bid), which can be regulated negatively and positively by p53, respectively (Oda et al., 2000; Sax et al., 2002; Shen et al., 2008). It was demonstrated by *in vitro* studies that, when Puma is overexpressed, Bax expression is also elevated, which leads to the change of Bax conformation and induction of the mitochondrial apoptotic pathway (Liu et al., 2003).

Moreover, it was reported, that Noxa can be translocated to the mitochondria and associate with pro-survival members of the Bcl-2 family, which in turn contributes to activation of caspase-9 (Oda et al., 2000). Other examples of p53 targets include the death receptors (such as Fas, DR4, DR5, CD95), PIDD (p53-induced protein with death domain) and Wip1 (wild-type p53-induced phosphatase-1), which have been shown to be positively regulated by p53 (Wu et al., 1997; Sheikh et al., 1998; Lu et al., 2008; Amaral et al., 2010; Li et al., 2015).

Wip1, also known as serine/threonine protein phosphatase 1D (PPM1D), is involved in regulation of cell cycle checkpoints in response to stress associated with DNA damage (Yamaguchi et al., 2007; Lu et al., 2008; Song et al., 2010; Lowe et al., 2013; Song et al., 2013). Wip1 belongs to the PP2C (protein phosphatase 2C) family of proteins

(Yamaguchi et al., 2007). Moreover, this Mg2+/Mn2+-dependent monomeric enzyme consists of two domains, including the N-terminal and C-terminal domain. It has been reported that he N-terminal domain performs a catalytic function and is more conserved than the non-catalytic C-terminal domain (Kleiblova et al., 2013).

1.6. Execution Cell Death Network

Execution pathway, at which the extrinsic, intrinsic and granzyme B-mediated networks converge, begins with processing and activation of the effector (executioner) caspase-3, -6 and -7. The execution phase of apoptosis is considered as the final pathway of the programmed cell death. The effector caspases promote activation of cytoplasmic endonuclease and proteases. The endonuclease degrades the genetic material within the nucleus, whereas the proteases digest the cytoskeletal and nuclear proteins. Moreover, caspase-3, -6 and -7 proteolytically process a variety of substrates, such as PARP (poly (ADP-ribose) polymerase), cytokeratins, NuMA (nuclear protein) and the alpha fodrin (plasma membrane cytoskeletal protein). Cleavage of these substrates gives rise to the biochemical and morphological changes observed in the cells undergoing apoptosis (Elmore, 2007).

The most important of the executioner caspases is caspase-3, which is cleaved and activated by the initiator caspases, including caspase-8, -9 and -10. Upon initiation of the execution pathway, caspase-3 activates the endonuclease CAD (caspase-activated DNase) by cleavage of ICAD (inhibitor of caspase-activated DNase), which typically functions as an inhibitor of CAD. In dividing and growing cells, ICAD forms a complex with CAD, which supresses the activity of CAD. After CAD is released and activated, it metabolises chromosomal DNA localised in nuclei, which leads to condensation of the chromatin. Moreover, caspase-3 is involved in formation of the apoptotic bodies by mediating the cytoskeletal reorganization and fragmentation of the cell (Elmore, 2007).

1.7. Targeting Apoptosis in Cancer

It is known that tumours and their therapy-resistance can frequently develop as a result of dysregulation of the apoptotic pathways (Owens et al., 2013; Koff et al., 2015). Such dysregulation is typically associated with the enhanced or impaired expression of the critical proteins involved in both positive and negative regulation of the cell death. In particular, overexpression of IAPs as well as an unbalanced expression of the proteins that belong to the Bcl-2 family (mainly Bax, Bcl-2 and Bcl-XL) are known to contribute to tumorigenesis. Moreover, IAPs and Bcl-2 family of proteins have been implicated in the development of resistance to chemotherapy and radiation, what was demonstrated by many studies *in vitro* (Violette et al., 2002; LaCasse et al., 2008; Owens et al., 2013; Ehrenschwender et al., 2014).

Occurrence of mutation or damage in the TP53 gene leads to disruption of the p53-mediated DNA damage recognition and repair or apoptosis. Another protein, which is involved in DNA damage repair and mediates regulation of the cell cycle progression is ATM (ataxia telangiectasia-mutated). This kinase is activated in response to DNA double strand breaks, which in turn leads to ATM-mediated phosphorylation of p53. Thus, disruption of activation and functions of ATM and p53 promotes tumorigenesis (Kurz and Lees-Miller, 2004; Kitagawa and Kastan, 2005; Elmore, 2007).

Members of the IAP family have been widely studied as therapeutic targets for the treatment of cancer, spinal cord injuries, stroke and multiple sclerosis (Elmore, 2007). Targeting and inhibition of these proteins in cancer cells holds a significant promise in the treatment of various malignancies. Among eight currently known members of IAPs family, survivin, cIAP1, cIAP2 and XIAP are described as the most commonly overexpressed apoptotic regulatory proteins, which in turn can lead to enhanced

inhibition of cell death and development of a wide range of human cancers (LaCasse et al., 2008; Owens et al., 2013; Koff et al., 2015).

To date, many promising IAP-targeted therapies have been developed and include application of single-stranded antisense oligodeoxynucleotides, adenoviruses expressing dominant-negative mutants of a target gene and most importantly small molecules inhibitors (Smac mimetics), which function as IAP antagonists (Owens et al., 2013; Bai and Wang, 2014; Koff et al., 2015) (Figure 4). Upon binding to the Smac mimetics, IAPs undergo ubiquitination and degradation by proteasomes. Loss of IAPs triggers two events: (I) formation of a protein complex, consisting of RIP1, FADD and caspase-8, which induces apoptosis and (II) activation of non-canonical NF-κB pathway, production of TNF-α and autocrine/paracrine cell death (Varfolomeev et al., 2007) (Figure 4). The effect of the Smac mimetics in cancer cells has been investigated in combination with other treatments, including chemotherapy, radiotherapy, small molecular inhibitors of kinases, death receptor agonists, proteasome and Bcl-2. Responses to such treatments were examined on xenograft mouse models and by using *in vitro* studies (Fulda and Vucic, 2012). Interestingly, it has been demonstrated by the pre-clinical studies that targeting IAPs with Smac mimetics can contribute to the enhancement of sensitivity to the clinically used anti-cancer drugs, including 5-FU, in various tumours (Owens et al., 2013; Koff et al., 2015).

Small molecule inhibitors were also developed for anti-apoptotic Bcl-2 family of proteins (Figure 4). These inhibitors are non-peptide molecules, which can mimic the pro-apoptotic BH3-only proteins (BH3 mimetics). The BH3 mimetics compete with the pro-apoptotic Bcl-2 family members and bind to anti-apoptotic Bcl-2 family proteins, which leads to the release of the pro-apoptotic proteins (Figure 4). The advantage of some BH3 mimetics is to exhibit their antitumor activity by specific binding to their targets. Some of the compounds have been already advanced into clinical trials and were conducted in

patients with lymphoma, leukaemia and small-cell lung cancer (Wilson et al., 2010; Gandhi et al., 2011; Roberts et al., 2012). Leukaemia showed a substantial susceptibility to the treatment with BH3 mimetics (Robert et al., 2012), whereas the response of solid tumours was limited. This was mostly caused by overexpression of Mcl-1, the anti-apoptotic protein, which belongs to the Bcl-2 family (Konopleva et al., 2006). Further approaches and strategies are focused on developing pan Bcl-2 inhibitors or Mcl-1 selective inhibitors to treat solid tumours (Bai and Wang, 2014).

Another group of small inhibitors includes Mdm2/p53 interaction antagonists, which mimic the p53 binding residues and target Mdm2 (Bai and Wang, 2014) (Figure 4). Several of these inhibitors have advanced to the clinical trials, including RO-5503781, MI-77301 and CGM097 (http://clinicaltrials.gov). The mode of action of Mdm2 antagonists is associated with their ability to bind with Mdm2, which in turn contributes to stabilisation and activation of p53, followed by cell cycle arrest and apoptosis in cancer cells with wild type p53 (Tovar et al., 2006). The response to treatment with Mdm2 inhibitors is currently examined in various cancers, including solid tumours, leukaemia and acute myeloid leukaemia (Bai and Wang, 2014).
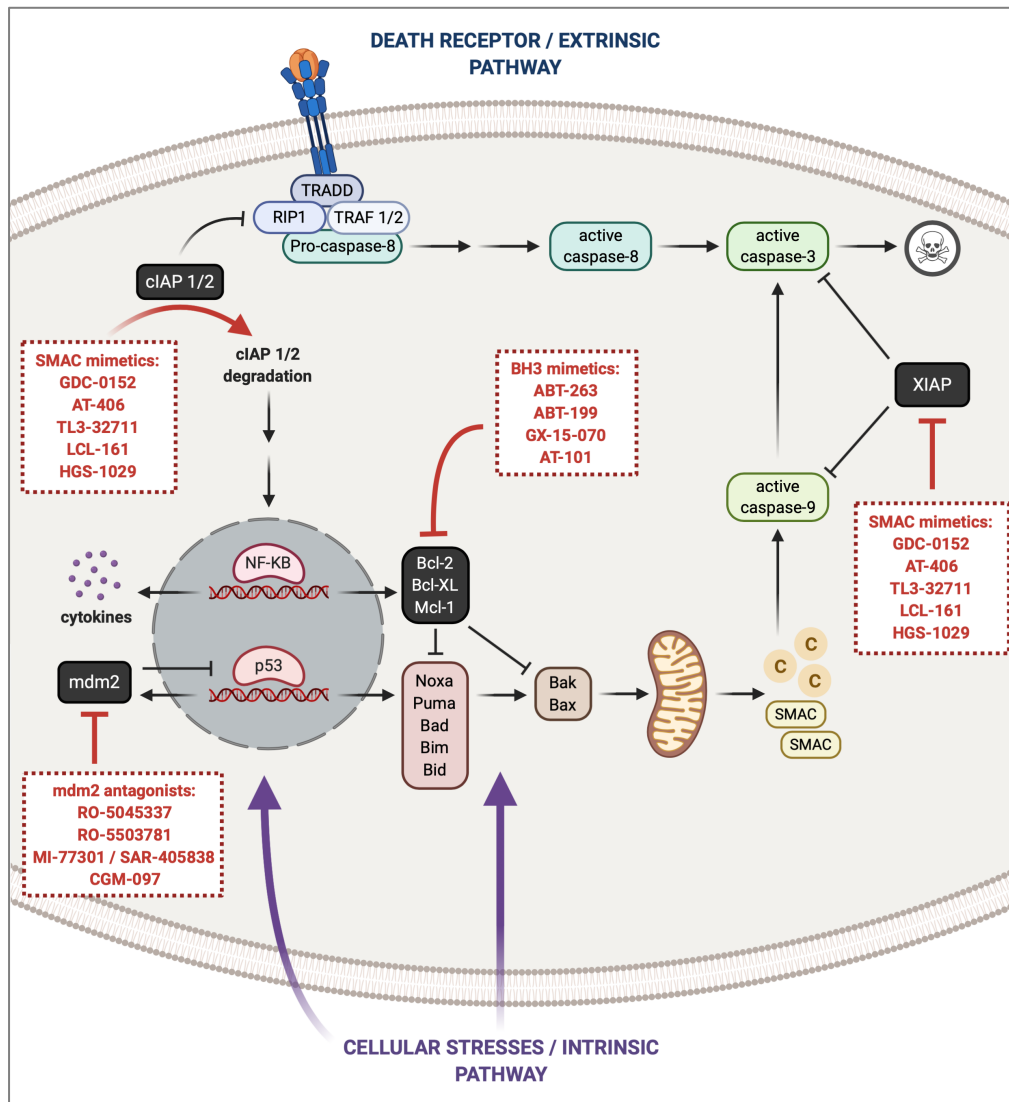
Figure 4. Proteins involved in regulation of apoptotic pathways and small-molecule inhibitors targeting these proteins.

Inhibitors of apoptosis (IAPs), such as cIAP1/2 prevent cell death by ubiquitination of RIP1. This event blocks DISC formation in the extrinsic apoptotic pathway and subsequent activation of caspase-8 at the complex. cIAP1/2 are also involved in regulation of the canonical and non-canonical NF-κB-mediated pathway. Another inhibitor of apoptosis, XIAP, blocks cell death by inhibition of caspase-3 and -9, which are involved in the intrinsic apoptotic network. However, Smac can prevent the XIAP-mediated inhibition of caspases. The small molecule inhibitors, named Smac mimetics, can bind to IAPs, including cIAP1/2 and XIAP, and thereby antagonise their inhibitory effects. Upon initiation of the intrinsic apoptotic pathway, pro-apoptotic Bak and Bax function as the effectors of MOMP, which leads to the release of cytochrome c. The BH3 mimetics compete with the pro-apoptotic Bcl-2 family members for binding to anti-apoptotic Bcl-2 family proteins, which leads to their inhibition and subsequent release of Bak and Bax. The tumour suppressor, p53 promotes apoptosis by transcriptional regulation of genes that express proteins involved in apoptosis. This transcription factor can also activate Bak and Bax. The Mdm2 protein functions as a regulator of the stability and transcriptional activity of p53 by negative-feedback loop. The small molecule inhibitors, Mdm2 antagonists, outcompete p53 for binding to Mdm2 (Bai and Wang, 2014).[4]

---

[4] Image created with BioRender.com

1.8. Non-Conventional Pathways and Signalling Protein Platforms Involved in Cell Death Induction

The programmed cell death is a tightly controlled process, that is regulated by various molecular factors and mechanisms. Conventionally, it is believed that cell death is triggered by the extrinsic/death receptor pathway and the intrinsic/mitochondrial pathway. Moreover, to date, numerous signalling protein complexes involved in the regulation of apoptotic networks have been described. These include the well-known protein platforms, such as DISC (Lavrik et al., 2005; Elmore, 2007; Fuchs and Steller, 2015) TNF complex II, (Micheau and Tschopp, 2003), Apoptosome (Cullen and Martin, 2009; Li et al., 2015), PIDDosome (Tinel and Tschopp, 2004), TLR (toll-like receptor) complexes (Vercammen et al., 2008) and RIP1-platform accompanied by TNF-α secretion (Biton and Ashkenazi, 2011).

Recently, it has become more evident that cancer cells subjected to the chemotherapy-based treatments can undergo apoptosis that is induced by molecular mechanisms, which are not covered by the classical models of programmed cell death. The strict division into the intrinsic and extrinsic apoptotic networks has been recently challenged by findings from our laboratory (Mohr et al., 2018) as well as other studies, which remodelled the molecular mechanisms responsible for initiation of programmed cell death in response to various cytotoxic agents. Moreover, there is more evidence that cytotoxic stress-induced cell death can be regulated and initiated by newly discovered protein complexes, such as RIPoptosome (Feoktistova et al., 2011; Tenev et al., 2011), FADDosome and FLIPosome (Mohr et al., 2018).

1.8.1. Apoptosis Can Be Caspase-9-Independent

It has been shown in our research that caspase-9 (classified as an initiator caspase), which is believed to play a key role in initiation of the conventional intrinsic/mitochondrial apoptotic pathway, is not essential for induction of apoptosis in cancer cells treated with 5-FU (Mohr et al., 2018). Importantly, some of the first findings regarding initiation of casapse-9-independent apoptosis go back to late 1990s, when Hakem et al., (1998) demonstrated, that Casp9-/- mouse splenocytes are sensitive to UV and can undergo apoptosis. Additionally, this study suggests that induction of the programmed cell death in the absence of caspase-9 depends on both stimulus and cell type, what implies the existence of multiple cellular death networks.

Furthermore, Marsden et al., (2002) showed that activation of the cascade of caspases could be regulated by the Bcl-2 protein and did not require involvement of the Apoptosome (a protein complex consisting of cytochrome c, Apaf-1 and caspase-9) in mouse lymphocytes and fibroblastoid cells subjected to cytokine withdrawal or treatment with dexamethasone, etoposide and γ-irradiation. The study suggests that caspase-9 is not required for induction of apoptosis in haematopoiesis and that the main function of the Apoptosome is rather to accelerate, but not to initiate the cascade of caspases (Marsden et al., 2002). Later studies confirmed that the loss of caspase-9 did not lead to evasion of apoptosis in response to diverse insults, however, it contributed to the partial and transient resistance to etoposide and dexamethasone in MEFs (Marsden et al., 2004; Delft et al., 2009) and thymocytes (Delft et al., 2009).

Numerous *in vitro* studies reported that the acquired resistance to chemotherapy is associated with the p53 status, in addition to the level of major regulatory proteins involved in initiation of intrinsic apoptotic network. In fact, mutations in TP53 gene and loss of p53 function occur commonly in the majority of human cancers (Violette et al.,

2002; Longley et al., 2003; Boyer et al., 2004; Muller and Vousden, 2013). Similar to others, we showed that the deficiency of p53 provides protection against 5-FU in isogenic knockout HCT.p53-/- cells treated with 5-FU for 48 h, when compared with wild-type HCT116 cells subjected to the same treatment (Longley et al., 2003; Boyer et al., 2004).

Conventionally, it is believed that p53 is activated in response to DNA damage, which in turn contributes to positive regulation of pro-apoptotic Bax and Bak proteins followed by cytochrome c release and caspase-9 activation. Nevertheless, the finding that caspase-9 is not essential for 5-FU-induced apoptosis refutes the classical model of programmed cell death. Taken together, our results showing that HCT.p53-/- cells are protected against the treatment with 5-FU and the caspase-9 findings, summarised above, lead to a conundrum that requires different models and answers with respect to apoptosis induction in response to chemotherapeutic drugs.

1.8.2. PIDDosome

The PIDDosome complex was initially studied and first reported by Tinel and Tschopp (2004). Their research provided answers for the role of caspase-2, which is known as the initiator caspase involved in the DNA-damage response and stress-induced apoptosis. Tinel and Tschopp (2004) demonstrated that caspase-2 is activated at the PIDDosome, a protein platform that encompasses PIDD and an adapter protein RAIDD (CASP2- and RIPK1-domain-containing adaptor with death domain; also known as CRADD) (Tinel and Tschopp, 2004). However, there is also evidence that caspase-2 can be activated without involvement of PIDD, e.g. in dying neurons or in cell extracts *in vitro* (Manzl et al., 2009; Ribe et al., 2012).

PIDD is a ~100 kDa protein, which was first characterised by Lin et al., (2000) and contains a C-terminal death domain (DD). The protein sequence also comprises N-

terminal LRRs (leucine-rich repeats), ZU5 (ZO-1 and Unc5-like) domains and UPA (uncharacterised protein domain conserved in UNC5, PIDD and ankyrins). It has been reported that PIDD possess autoproteolytic activity and can cleave itself into three fragments: PIDD-N, PIDD-C and PIDD-CC, which sizes are 48 kDa, 51 kDa and 37 kDa, respectively. Different transcription and splice variants of PIDD were also identified. The adapter protein RAIDD contains the C-terminal DD and N-terminal caspase-recruitment domain (CARD), which associate with PIDD DD and caspase-2 CARD, respectively. Apart from the CARD domain, caspase-2 also contains two subunits, p19 and p12 (Sladky et al., 2017) (Figure 5).
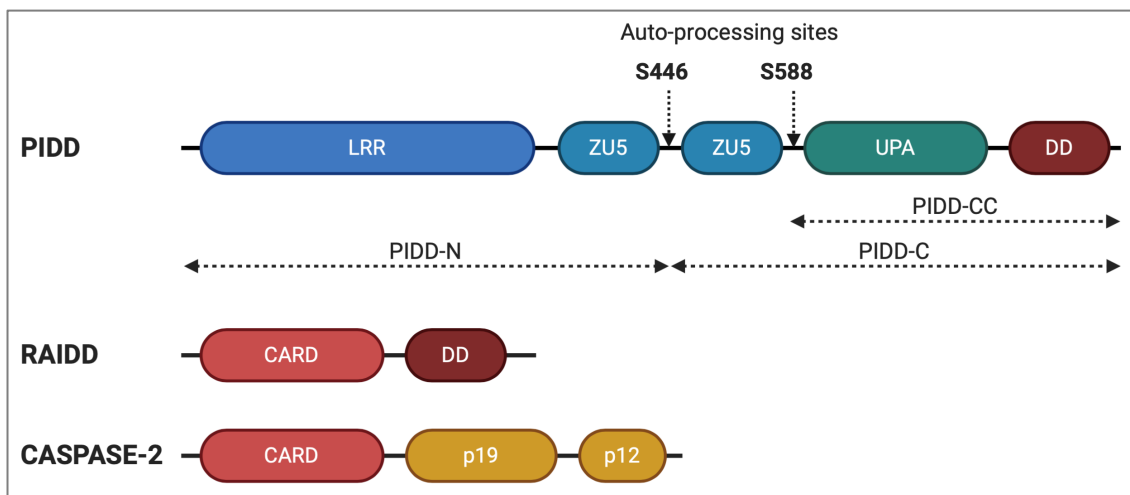
Figure 5. Domain organisation of the PIDDosome complex constituents.
The domains of PIDD include: N-terminal LRRs (leucine-rich repeats), ZU5 (ZO-1 and Unc5-like) domains, UPA (uncharacterised protein domain conserved in UNC5, PIDD and ankyrins) and C-terminal death domain (DD). The structure of RAIDD comprises N-terminal CARD and C-terminal DD domains. Caspase-2 contains three domains, including N-terminal CARD, p19 and p12. The DD and CARD of the adapter protein RAIDD interact with PIDD DD and caspase-2 CARD, respectively, to form the PIDDosome complex. the cleavage fragments, PIDD-N, PIDD-C and PIDD-CC, resulting from PIDD auto-processing are also indicated (Sladky et al., 2017).[5]

In order to elucidate the molecular mechanisms responsible for caspase-2 activation at the PIDDosome, Tinel and Tschopp (2004) overexpressed various DD- and CARD-containing proteins in 293T cells. By using immunoprecipitation, the authors examined,

---

[5] Image created with BioRender.com

which molecules could bind to caspase-2. Tinel and Tschopp (2004) found, that the only interaction partners of caspase-2 were RAIDD and PIDD, and subsequently, reconstituted the caspase-2-activating complex, which they termed PIDDosome. Examination of the cell lysates extracted from non-stimulated HeLa, 293T and Jurkat T cells as well as Ramos B lymphocytes showed that the PIDDosome complex could be also formed spontaneously under more physiological conditions. The gel filtration analysis of the 293T and Jurkat T cell revealed that caspase-2, RAIDD and PIDD eluted in fractions corresponding to the size of ~670 kDa, confirming that these molecules can form a stable, high molecular weight protein platform (Tinel and Tschopp 2004).

The authors also wondered about the physiological function of the capsase-2 activation at the PIDDosome complex. In order to examine that, Tinel and Tschopp (2004) investigated the effect of PIDD overexpression in HeLa and Ramos B lymphocytes exposed to genotoxic drugs and compared the results with the control wild-type and PIDDΔDD-expressing cells. They observed that upon treatment with doxorubicin or etoposide, the PIDD-overexpressing cells can undergo apoptosis, whereas most of the control cells remained viable. Moreover, it was reported, that in the presence of overexpressed PIDD, almost all caspase-2 molecules were processed and the activity of the effector caspase-3 was strongly increased. These findings showed that PIDD-mediated caspase-2 activation can sensitise cells to apoptosis in response to genotoxic drugs (Tinel and Tschopp, 2004).

Studying of erythroleukaemia cell line by Lin et al. (2000) allowed to find that PIDD functions as a direct transcriptional target of p53. Moreover, p53-dependent transcription of the Pidd gene was observed in mouse embryonic fibroblast exposed to γ-irradiation as well as in AML-4 (leukaemia) and MCF7 (breast cancer) cells. Additionally, the authors found that apoptosis could be induced in cells lacking p53 and supressed in cells with knocked down PIDD (Lin et al., 2000). Moreover, it was reported that application of

antisense nucleotides targeting PIDD mRNA delayed apoptosis induction in p53-overexpressing K562 (myelogenous leukaemia) cells (Lin et al., 2000). The same phenomenon was observed in H1299 cells with increased p53 expression accompanied by application of RNA interference against PIDD mRNA (Baptiste-Okoh et al., 2008). In parallel, other proteins involved in the cell death regulation and controlled in the p53-dependent manner were described, namely Puma and Noxa. It has been confirmed by various studies *in vivo* that Puma and Noxa, but not PIDD, were required for the p53-mediated DNA damage response and cell death induction (Villunger et al., 2003; Kim et al., 2009; Manzl et al., 2009). Additionally, it was suggested that PIDD can play a role outside of the p53-mediated pathways, as it was still expressed at low levels in p53-lacking HCT116 and HEK-239 cells (Tinel e al., 2007). Induction of the basal PIDD expression, independent of p53, was also reported by Cuenin et al. (2008), which suggests different mechanisms involved in regulation of PIDD levels in cells.

It was described that the PIDD-originating segments, in particular PIDD-C and PIDD-CC, can perform different functions within cells and form complexes with various proteins (Sladky et al., 2017). For example, PIDD-CC is a key component of the RAIDD- and caspase-2-containing PIDDosome complex, involved in mediation of cell death. On the contrary, PIDD-C forms a protein platform with RIP1 and Nemo (Sladky et al., 2017)/ It was proposed that Nemo is ubiquitinated and degraded at the complex, which contributes to a subsequent activation of NF-κB signalling pathway and cell survival. It was shown by numerous *in vitro* and *in vivo* studies that PIDD is indeed involved in NF-κB activation (Bock et al., 2012; Bock et al., 2013), but it does not play a role in the cell survival or DNA repair. Further experiments have demonstrated that the PIDD-C/RIP1/Nemo complex is most likely involved in inflammation (Bock et al., 2013). Furthermore, the MS-analysis of the overexpressed PIDD revealed that its full-length form or PIDD-C can form a complex, which comprises PCNA (proliferating cell nuclear antigen), RFC5 (replication factor C subunit 5) and RFC4 (replication factor C subunit 4).

The complex is localised in the nucleus and involved in translesion DNA synthesis (Logette et al. 2011). The exact role of the PIDD-N fragment still remains to be defined (Sladky et al., 2017).

Various reports, inspired by the findings obtained by Tinel and Tschopp (2004), investigated the role of PIDD in triggering of the caspase-2-mediated cell death (Bock et al., 2012; Janssens and Tinel, 2012). Studying p53-deficient zebrafish embryos, which were resistant to radiotherapy, revealed that upon inhibition of the Chk1 (checkpoint kinase 1), the cell death could be restored. Interestingly, it was found that the cell death in zebrafish embryos was independent of caspase-3, -8 and -9, Bcl-2, Noxa, Puma, cytochrome c, p63 or p73, could not be blocked by Bcl-2 overexpression, but required involvement of caspase-2 and was regulated by the ATM/ATR (ataxia telangiectasia and Rad3-related protein)/caspase-2 signalling network (Sidi et al., 2008). Importantly, it was reported that this mode of cell death was conserved in various human tumours, however it was only partially confirmed by *in vivo* studies (Manzl et al., 2013). Other reports examined the ATM/ATR/caspase-2 signalling axis induced upon Chk1 inhibition and found that activated ATM, but not ATR, was associated with PIDD (Ando et al., 2012), which contributed to formation of the PIDDosome formation and subsequent initiation of caspase-2-mediated apoptosis in HeLa cells. On the other hand, ATM-mediated assembly of the PIDDosome suppressed an interaction between PIDD and RIP1, which indicated that ATM can regulate the mode of PIDD action (pro-survival vs. pro-apoptotic) in the cells (Ando et al., 2012). Interestingly, binding of ATM to PIDD was also observed in response to irradiation or etoposide alone, without inhibition of Chk1, however the combined treatment was more efficacious in promoting of the PIDDosome formation (Ando et al., 2012). Nevertheless, it still remains enigmatic, how caspase-2 drives this type of cells death.

Interestingly, at the same time, it was demonstrated that using siRNA to target PIDD or RAIDD expression did not affect the processing of caspase-2 in HCT116 cells treated with 5-FU (Vakifahmetoglu et al., 2006). Moreover, it was reported that PIDD-overexpressing mouse fibroblasts could trigger apoptosis dependent on RAIDD, but not caspase-2. These findings indicated that PIDD could be involved in initiation of the cell death, which did not require engagement of caspase-2 (Berube et al., 2005). Manzl et al., (2009) examined the role of PIDD in ell death induction by using PIDD-deficient mice. The authors observed that caspase-2 was activated in the etoposide-treated primary lymphocytes, which were unable to form the PIDDosome complex. Similar, the loss of RAIDD did not affect the levels of caspase-2 activation in the cells. Moreover, mouse lymphocytes and SV40-transformed MEFs (mouse embryonic fibroblasts) were susceptible to apoptosis independent of PIDD and caspase-2 in response to DNA damage, endoplasmic reticulum stress and growth factor deprivation as well as TNF and FAS-mediated cell death initiation.

Taken together, these findings suggest the existence of alternative functions of capsase-2 and its activation mechanisms, other than PIDDosome, in response to DNA damage (Manzl et al., 2009). Importantly, the authors suggested that, upon DNA damage, processing of caspase-2 occurs downstream of MOMP and Apoptosome, and requires involvement of Apaf-1 and caspase-9, which is in contrast to other reports describing that caspase-2 activation takes place upstream of mitochondria in HeLa and Jurkat cells (Guo et al., 2002; Robertson et al., 2002; Robertson et al., 2004). Interestingly, similar to Manzl et al. (2009), the most recent study by Fava et al. (2017) demonstrated that PIDD-mediated caspase-2 activation is not involved in cell death initiation and DNA damage-induced p53 activation. Instead, it was found that the PIDDosome-regulated caspase-2 activation contributes to activation of p53 in the process of centrosome amplification and can function as a sensor of aberrant centrosome numbers (Fava et al., 2017). These findings indicate that PIDD plays an important role in cell differentiation

and organogenesis (Sladky et al., 2017). Interestingly, it was recently discovered that NPM1 (nucleophosmin), an oncogenesis regulator, which is often found to be mutated or dysregulated in acute myeloid leukaemia and other tumours, is directly involved in the PIDDosome formation in response to DNA damage (Sidi and Bouchier-Hayes, 2017).

To conclude, many contradictions arise from the initial findings indicating that the PIDDosome promotes apoptosis in response to DNA damage and other stimuli, and subsequent results showing that the PIDDosome constituents demonstrate inconsistent phenotypes and that the complex formation is regulated in a differential fashion under various experimental conditions. These contradictions require different models and answers with respect to identification of the upstream and downstream regulators of the PIDDosome, functions of PIDD and caspase-2, and other molecular pathways that these proteins are potentially involved in.

1.8.3.   RIPoptosome

The study by Geserick et al. (2009) was first to describe the RIPoptosome, a novel cytosolic protein platform encompassing caspase-8, RIP1, FADD and cFLIP isoforms (Figure 6). The complex was identified upon induction of the cell death by CD95 and in response to IAP antagonist-mediated depletion of cIAPs (Geserick et al., 2009). The RIPoptosome contributes to induction of the cell death machinery in various cancer cell lines exposed to cytotoxic and genotoxic stresses. To date, there have been many reports describing that the RIPoptosome formation occurs in response to a wide range of stimuli, including DNA damage, IAPs depletion, accumulation of RIP1, exposure to chemotherapeutics and application of Smac mimetics. It was demonstrated that the RIPoptosome can be assembled in response to application of IAP antagonists (Smac mimetics) alone or in combination with TLR3 stimulation (Feoktistova et al., 2011) and DNA-damaging anti-tumour drugs, such as etoposide (Tenev et al., 2011; Riley et al.,

2015). The most recent studies reported that RIPoptosome-mediated cell death can be also induced in response to: (I) treatment with BV6 plus glucocorticoids in acute lymphoblastic leukaemia (Belz et al., 2014), (II) overexpression of ZFP36 in glioblastoma (Selmi et al., 2015), (III) application of dimethyl fumarate (DMF; FDA approved as Tecfidera®) and targeting Thioredoxin-1 (Trx-1) in T-cell lymphomas and leukaemias (Schroeder et al., 2017).

Caspase-8, RIP1, FADD and cFLIP are also components of the TNF-induced complex II. However, the RIPoptosome is formed without involvement of the TNF-R1 and TNF signalling, which indicates that this protein platform functions as an independent signalling complex (Schilling et al., 2014) (Figure 6). In the RIPoptosome, caspase-8 is cleaved and activated, which leads to initiation of the cell death. Importantly, Feoktistova et al., (2011) and Tenev et al., (2011) have identified RIP1 to be the core driver of the complex assembly, hence the term RIPoptosome. Apart from caspase-8, RIP1, FADD and cFLIP isoforms, the complex may also contain caspase-10, however this depends on the cell type and stimulation. Moreover, depending on the expression levels and activity of these molecular components, the cells can either undergo caspase-dependent apoptosis or RIP1-RIP3-dependent necroptosis (Feoktistova et al., 2011).

Conventionally, the above mentioned RIPoptosome constituents are believed to be involved in triggering the extrinsic/death receptor apoptotic pathway (Micheau and Tschopp, 2003; Lavrik et al., 2005; Elmore, 2007). In the classical model of apoptosis, capase-8 (and also caspase-10) can be recruited to CD95 or TRAIL receptors in a FADD-dependent manner in response to interaction of the death receptors with their complementary death ligands. Such events lead to formation of the DISC, at which caspase-8 and -10 undergo multimerization followed by proteolytic cleavage and activation. Finally, active caspase-8 and -10 can proteolytically process and activate their

downstream targets, such as caspase-3, -6 and -7 (classified as effector caspases) (Ohtsuka et al., 2003; Yu et al., 2009; He et al., 2015; Koff et al., 2015).

The molecular mechanisms responsible for the RIPoptosome formation, its regulation and RIPoptosome-mediated cell death induction in cancer cells exposed to various stimuli have been widely studied and are currently well understood. Feoktistova et al., (2011) reported, that the loss of IAPs caused by Smac mimetics contributed to enhancement of the cell death induced by poly(I:C) in HaCaT and MET-1 but not A5RT3 cells. Importantly, it was described that knocking down of cIAP1 in HaCaT cells contributed to sensitisation of the cells to TLR3-mediated cell death. The cells were further sensitised in response to IAP inhibitors. Such results indicate, that cIAP1 plays the decisive role in TLR3-induced apoptosis and necroptosis, whereas cIAP2 is involved in the cell death resistance (Feoktistova et al., 2011). These findings also argue that TLR3-mediated cell death is controlled in a cell type-specific manner.

At the same time, Tenev et al. (2011) found that the treatment with etoposide contributes to a strong reduction of cIAPs and XIAP in different tumour cell lines, which leads to formation of the RIPoptosome. Moreover, it was demonstrated by Tenev et al. (2001) camptothecin and tenoposide also caused degradation of cIAP1, cIAP2 and XIAP, but only the latter triggered formation of the caspase-8/RIP1/FADD complex. Similar results were obtained by Belz et al., (2014), which demonstrated that a combination of the IAP inhibitor BV6 and glucocorticoids (dexamethasone) lead to a strong reduction of the cIAP1, cIAP2 and XIAP. Additionally, Belz et al., (2014) observed that upon the treatment, the activity of caspase-8 and production of ROS were significantly increased. As a result, these events led to the RIPoptosome formation and cell death induction in tumour cells (Belz et al., 2014). Furthermore, Tenev et al. (2011) found that cIAPs regulate the RIPoptosome formation by targeting RIP1, caspase-8, caspase-8/cFLIP heterodimers, but not FADD, for ubiquitination and degradation. These results were

supported by the observation that application of the proteasome inhibitor, lactacysting, promoted the RIPoptosome formation.

Taken together, the results obtained by Feoktistova et al. (2011), Tenev et al. (2011) and Belz et al. (2014) showed that degradation of IAPs drives the RIPoptosome assembly and the RIPoptosome-mediated cell death induction, which was observed in various cancer cells lines exposed to a wide range of stimuli. These findings indicate that the RIPoptosome is not cell type- nor stimulus specific, but rather a fairly common cell death induction mechanism. In addition to that, another function of cIAPs was discovered, as it was found that these proteins regulate the complex assembly by targeting of the RIPoptosome components for ubiquitination and subsequent degradation. This suggest that cIAPs play different roles in the context of RIPoptosome.

A very recent study by Schroeder et al. (2017) discovered another mechanism responsible for the RIPoptosome formation and subsequent cell death induction. The authors examined the effect of DMF-mediated suppression of Trx-1, which functions as a main regulator of NF-κB transcriptional activity. It was reported that active NF-κB can promote survival of various tumours, including T-cell lymphomas and leukaemias via positive regulation of the IAPs and cFLIP expression in the cells. Thus, Schroeder et al. (2017) wondered, whether targeting of Trx-1 could antagonise NF-κB, downregulate IAPs and cFLIP, and in turn contribute to formation of the RIPoptosome and subsequent cell death. First, the authors confirmed that DMF-mediated inhibition of NF-κB leads to depletion of cIAP2 and cFLIP, but not XIAP and Bcl-2 family members and caused cell death in HH (human lymphoma), SeAx (cutaneous T-cell lymphoma cell line) and CEM (T-cell leukaemia cell line) cells. Moreover, the study has demonstrated that application of DMF caused an increase of caspase-8 activity in the cells. The RIPoptosome was also formed in response to the treatment, which was confirmed by investigation of the caspase-8/RIP1/FADD interactions by using the proximity ligation assay and co-

immunoprecipitation of caspase-8. Thus, in addition to the previous findings, it appears that the RIPoptosome can be formed indirectly by inhibition of NF-κB, leading to the loss of cIAP2 and cFLIP, which provides more insights into the mechanisms responsible for the complex assembly.

It was discovered that RIPoptosome mediates different modes of cell death, namely apoptosis and necroptosis (Figure 6). Feoktistova et al., (2011) demonstrated that, regardless of the IAPs status, application of zVAD or Nec-1 alone barely affected the poly(I:C)-induced apoptosis and TLR-3-mediated HMGB-1 release. Interestingly, when zVAD and Nec-1 were used in combination, the HMGB-1 release was supressed, and the cells were rescued from apoptosis. Additionally, the analysis of the cell morphology revealed that the depletion of IAPs and blocking of caspases with zVAD lead to TLR3 stimulation followed by induction of RIP1-mediated necroptosis. Thus, these findings indicate that the RIPoptosome can trigger both apoptosis and necroptosis (Figure 6).
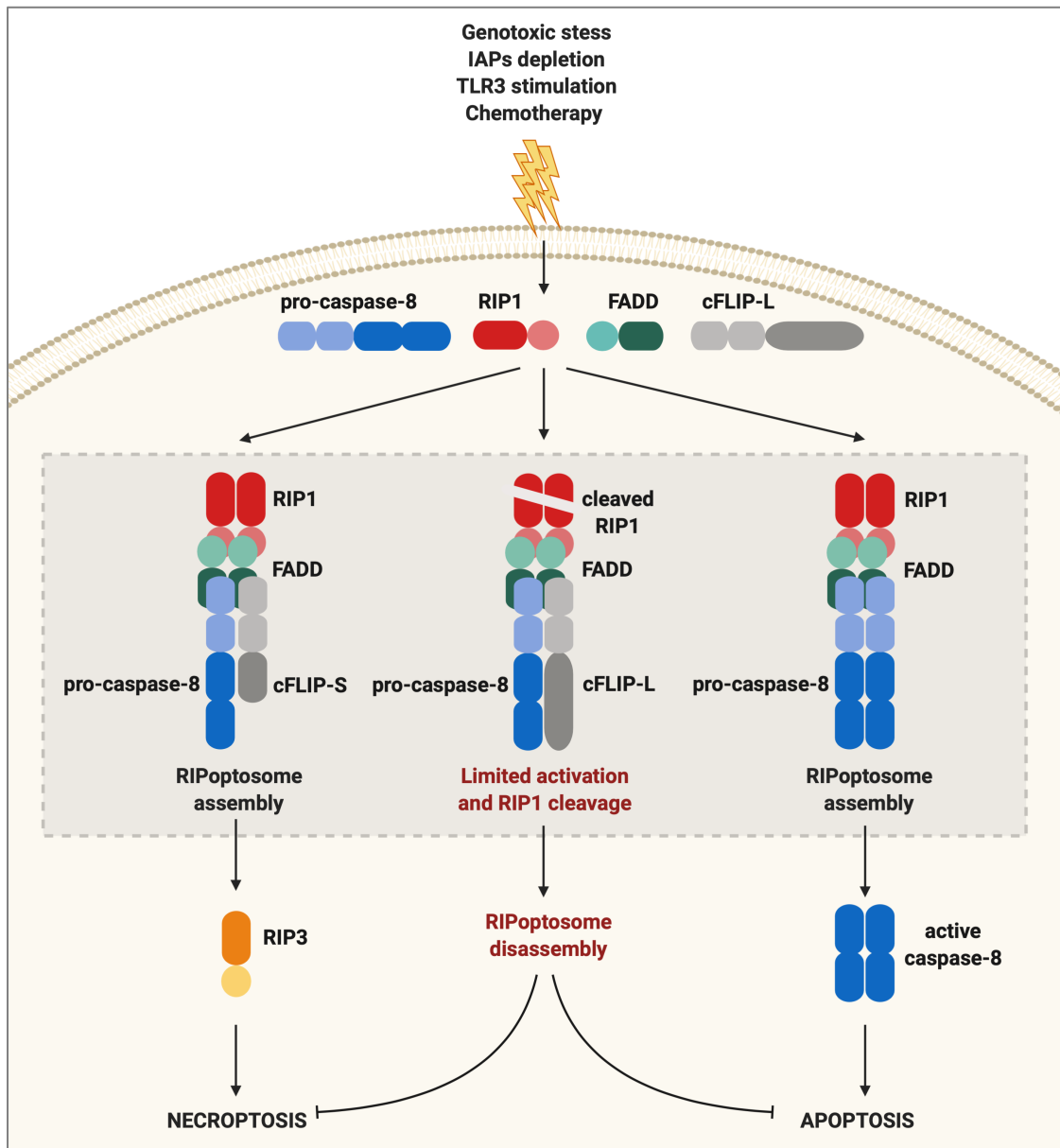
Figure 6. Activation and signalling of the novel cell death-inducing protein platform, RIPoptosome and its regulation by cFLIP isoforms.

Upon intracellular stimuli, the RIPoptosome complex, which consists of RIP1, FADD and caspase-8, is formed in tumour cells. At the complex, caspase-8 is activated and initiates apoptosis (right panel). The RIPoptosome also regulates the RIP3-dependent necroptosis (left panel). Different cFLIP isoforms control the RIPoptosome assembly and the mode of the cell death (apoptosis vs. necroptosis). In the presence of cFLIP-L, the caspase-8/cFLIP-L heterodimers are formed, which cause that the process of caspase-8 activation is limited. This in turn leads to the RIP1 cleavage and RIPoptosome disassembly (middle panel). Moreover, cFLIP-S positively regulates the RIPoptosome formation and promotes a shift towards the RIP1-RIP3-dependent necroptosis in tumour cells (left panel) (Imre et al., 2011).[6]

---

[6] Image created with BioRender.com

Similar to the results obtained by Feoktistova et al. (2011), observations by Tenev et al. (2011) also demonstrated that the RIPoptosome mediates different cell death modes (caspase-dependent apoptosis vs. caspase-independent necroptosis). The authors reported that the application of Nec-1 completely and partially blocked caspase activation in etoposide-treated HT1080 cells and MDA-MB-231 cells, respectively, in response to etoposide. However, in both cases formation of the RIPoptosome was strongly reduced. Exposure to a combination of Nec-1 and zVAD inhibited the etoposide-induced cell death machinery, however it promoted the RIP3-mediated activation of caspases in MDA-MB-231 cells (Tenev et al., 2011). Such findings indicated, that etoposide induces apoptotic cell death in HT1080 cells, whereas in MDA-MB-231 cells both apoptosis and necroptosis are triggered in response to the treatment. Moreover, these results further confirmed the involvement of the RIPoptosome in mediation of different cell death modes. However, it is noteworthy, that the mode of the cell death triggered in response to etoposide depends on the cell type.

Similar to Feoktistova et al. (2011) and Tenev et al. (2011), Schroeder et al. (2017) also demonstrated that RIPoptosome can be involved in induction of both apoptosis and necroptosis. As mentioned, administration of DMF induced the RIPoptosome formation and caspase-8 dependent apoptosis in HH, SeAx and CEM cells. In order to assess, whether RIPoptosome can mediate necroptosis, the authors used CD4+ T-cells, isolated from patients with the Sézary Syndrome. Such T-cells are characterised by strongly increased activity of NF-κB and elevated levels of cIAP2 and cFLIP. DMF-mediated inhibition of NF-κB led to the RIPoptosome formation and induction of the cell death in CD4+ T-cells, which could be inhibited by treatment with combination of zVAD and Nec-1, but not by zVAD alone. Similar effects were observed in CEM cells. These results indicate, that inhibition of capase-8 activity leads to a switch to the necroptotic mode of the cell death in tumour cells and confirms the involvement of the RIPoptosome in both apoptosis and necroptosis.

Identification and analysis of the RIPoptosome components was performed by using co-immunoprecipitation of caspase-8 in response to: (I) treatment with Smac mimetics plus poly(I:C) (Feoktistova et al., 2011) or etoposide (Tenev et al., 2011), (II) stimulation with BV6 plus dexamethasone, (III) exposure to etoposide alone (Selmi et al., 2015), (IV) overexpression of ZFP36 (Selmi et al., 2015) and administration of DMF (Schroeder et al., 2017). The caspase-8 complex, induced upon TLR3-stimulation, contained RIP1, FADD, cFLIP (p43 cleavage fragment) and caspase-10 (p47/p43 segment) (Feoktistova et al., 2011). Similarly, stimulation of HT1080 and MDA-MB-231 cells with Smac mimetics and etoposide allowed co-purification of caspase-8 bound to RIP1, FADD and cFLIP-L (Tenev et al., 2011). The caspase-8/RIP1/FADD complex was also found in response to the BV6 plus dexamethasone treatment in Jurkat and Reh cells (Belz et al., 2014), upon overexpression of ZFP36 (Selmi et al., 2015) and after application of DMF in CEM and SeAX cells (Schroeder et al., 2017).

However, Tenev et al. (2011), Belz et al. (2014), Selmi et al. (2015) and Schroeder et al. (2017) did not detect caspase-10 within the RIPoptosome, which was in contrast the results obtained by Feoktistova et al. (2011). It is noteworthy, that each group used different cell lines and treatments to induce the RIPoptosome assembly and cell death. Therefore, the levels of caspase-10 could be different, depending on the cell type and/or stimulus or it might be inducible in some cell types but not others. Nevertheless, the biological significance and the activity of caspase-10 in terms of the RIPoptosome formation and its role in the complex activation still remain enigmatic and requires further examination and clarification (Feoktistova et al., 2011).

In order to examine the composition of the RIPoptosome in more detail, Feoktistova et al. (2011) and Tenev et al. (2011) performed chromatographic gel filtration analysis followed by caspase-8 immunoprecipitation of the selected elution fractions. The complex was extracted from: (I) cFLIP-S-overexpressing HaCaT cells treated with z-VAD

alone (control) or with the IAP antagonist plus z-VAD combination (Feoktistova et al., 2011), and (II) HT1080 cells exposed to z-VAD alone (control) or to the etoposide/Smac mimetics/z-VAD combination. The RIPoptosome components were detected in elution fractions corresponding to the size of ~2MDa by both groups. Interestingly, it was observed that caspase-8 and RIP1 were mostly detectable in their monomeric forms (Feoktistova et al., 2011) and overall, only small proportions of the total caspase-8, RIP1 and FADD were associated with the RIPoptosome (Feoktistova et al., 2011; Tenev et al., 2011). These findings suggest that other molecules might be present within the complex, however further studies are required to identify the yet unknown RIPoptosome components. Feoktistova et al. (2011) detected caspase-8, RIP1 and cFLIP-S in the fractions corresponding to ~2MDa in response to zVAD alone and combined with IAP antagonist. Similarly, Tenev et al. (2011) also detected caspase-8 and RIP1 in the fractions corresponding to ~2MDa after exposure to z-VAD alone and the etoposide, Smac mimetics and z-VAD combination. Interestingly, the subsequent immunoprecipitation of the selected gel filtration fractions at ~2MDa led to the co-purification of RIP1 by both groups, and additionally cFLIP-S and FADD by Tenev et al. (2011). None of these proteins were co-purified in the controls. Therefore, the role of the uncomplexed RIPoptosome components detected in the ~2MDa range in response to z-VAD alone and the exact mechanisms whereby IAPs influence the complex assembly requires further investigation and clarification.

Interestingly, a recent study by Jang et al. (2014) proposed a mechanism and a molecular model for the formation and an overall structure of the RIPoptosome core by investigation of the interactions between RIP1 and FADD death domains. The authors expressed and purified the proteins of interest (RIP1 DD, residues 583−664 and FADD DD, residues 93−184), reconstituted the RIP1 DD/FADD DD complex *in vitro*, which was in turn examined by using electron microscopy and gel filtration. Electron microscopy showed a population of the monodispersed and homogeneous particles, which were

structurally similar to the Fas DD/FADD DD complex (Wang et al., 2010). Gel filtration analysis resulted in elution of the RIP1 DD/FADD DD complex in the range corresponding to ~120 kDa. Using MALS (multiangle light scattering) allowed to determine the molecular weight of the protein platform at 118.7 kDa and therefore confirmed the gel filtration result. MALS was also used to assess the stoichiometry of the RIP1 DD/FADD DD complex. It was revealed that the protein platform consists of five RIP1 DDs and five FADD DDs. Furthermore, Jang et al. (2014) performed a mutational analysis of the complex formation *in vitro* by using pull-down assays and gel filtration. The mutations were generated in both RIP1 DD and FADD DD, and were based on the previously resolved Fas DD and FADD DD structure (Wang et al., 2010). Additionally, FADD DD was fused with the $(His)_6$ tag. The pull-down and gel filtration results confirmed that RIP1 DD and FADD DD can form a stable protein platform, which resembles the Fas DD/FADD DD complex. These findings suggest that the molecular mechanisms responsible for the RIPoptosome and Fas-DISC assembly are similar. Therefore, the authors proposed a schematic model of the RIPoptosome (Jang et al., 2014).

The study by Jang et al. (2014) provides interesting and important insights into the general formation mechanism used by death domains in terms of the RIPoptosome assembly. The authors assume that the other members of the DD superfamily, which apart from the DD, encompasses CARD, DED (death effector domain) and PYD (pyrin domain), form protein platforms and interact by using molecular mechanisms similar to those used by DDs. Nevertheless, to date there have been no reports, that tested and confirmed such hypothesis. Moreover, the study by Jang et al. (2014) contains a few limitations. Provided that the authors investigated the RIPoptosome formation mechanisms by using truncated fragments of RIP1 and FADD, without including the other components, namely caspase-8 and cFLIP-S, the proposed model provides only a part of the answer on how the complex is assembled. Moreover, the presence of caspase-8 and/or cFLIP-S might affect the stoichiometry and the structural conformation

of the complex as well as its components, which might differ from the described model. Therefore, further biochemical studies, which would aim to reconstitute the RIPoptosome complex *in vitro* by using caspase-8, RIP1, FADD and cFLIP-S, preferably at their full-length forms, are necessary to provide more details regarding the RIPoptosome structure and assembly mechanism.

cFLIP was identified by Feoktistova et al. (2011) and Tenev et al. (2011) as a critical regulator of the cell death induction and RIPoptosome formation (Figure 6). It was observed that knocking down of cFLIP led to a strong sensitisation to TLR3- or Smac mimetic- and etoposide-induced cell death (Feoktistova et al., 2011; Tenev et al., 2011). Additionally, Smac mimetics and etoposide combination caused an increased RIPoptosome formation (Tenev et al., 2011). Interestingly, in the absence of IAPs, various cFLIP isoforms were shown to regulate the RIPoptosome assembly and play a role in the switch between cell death modes (apoptosis vs. necroptosis) in a differential manner (Feoktistova et al., 2011). Upon treatment with IAP antagonist, overexpression of cFLIP-L completely blocked the cell death and RIPoptosome formation in HaCaT cells. In contrast, overexpressed cFLIP-S promoted the cell death and the complex assembly as well as contributed to the increase of the RIP1 levels in the absence of IAPs in HaCaT cells. Interestingly, the study reported that in the cFLIP-S-expressing cells caspase-8 activity within the RIPoptosome was blocked. It was also found that increased levels of cFLIP-S favoured initiation of the RIP1-RIP3-meadiated necroptosis. In contrast to HaCaT findings, analysis of HeLa cells showed an inhibition of the TLR3-mediated cell death in the presence of both overexpressed cFLIP isoforms. However, similar to HaCaT results, overexpressed cFLIP-S, but not cFLIP-L, promoted formation of the RIPoptosome complex. On the contrary, the protein complex assembly was not observed in human keratinocytes (PKs) with supressed IAPs functions. These results indicate that formation of the RIPoptosome highly depends on the cell type. The findings also argue, that the cFLIP isoforms perform opposite functions in terms of the regulation

of the complex assembly, and that this process depends on the stoichiometry of the proteins (Feoktistova et al., 2011).

Further study by Feoktistova et al., (2012), in which the authors investigated the role of stoichiometry of the molecular components in terms of the RIPoptosome formation and cell death induction, described that the decision point for the complex assembly lies in the balance between RIP1 and cIAPs. This was shown by an increased cell death initiation and promotion of the RIPoptosome formation in HaCaT cells in response to the induced expression of RIP1. In this case, cIAP1 was also recruited to the complex. In other words, elevation of RIP1 levels or, as shown by previous study, depletion of IAPs leads to RIPoptosome assembly, followed by initiation of apoptosis or necroptosis. Another decision point regards the switch between the apoptotic and necroptotic modes of cell death. Feoktistova et al., (2012) proposed that the switch to necroptosis depends on the regulation of the RIP1/RIP3 interaction by caspase-8/cFLIP heterodimers. In particular, the authors assume that increased interaction between caspase-8 and cFLIP-L contributes to the RIP1 cleavage and, as a result, leads to the RIPoptosome disassembly and blocks cell death induction (Figure 6). On the other hand, it was demonstrated that preferable binding of caspase-8 and cFLIP-S prevents the RIP1 cleavage, which promotes the RIP1/RIP3 interaction and RIP1/RIP3-dependent initiation of necroptosis (Feoktistova et al., 2012) (Figure 6). The role of RIP3 in triggering of the necroptotic cell death was supported by reconstitution of RIP3 expression in HeLa cells, which were in turn susceptible to necroptosis in the absence of IAPs. Moreover, overexpression of cFLIP-S in these cells contributed to the increase of the cell death, which was dependant on RIP3, but not caspase-8 (Feoktistova et al., 2012). Taken together, previous and these findings indicate that the balance between cFLIP-S and RIP3 is critical for execution of necroptosis in the cells.

Nevertheless, the question still remains, whether RIP3 functions as one of the components of the RIPoptosome in the necroptotic cell death, or whether this protein is regulated, directly or indirectly, downstream of the complex. Due to some limitations, Feoktistova et al. (2011) and Tenev et al., (2011) were unable to detect RIP3 after performing caspas-8 co-immunoprecipitation, thus the exact function and activity of RIP3 in induction of RIPoptosome-mediated necroptosis still remains unclear.

Taken together, the recent findings indicate that caspase-8 is not only activated via the classical pathway of the death receptor triggering, but also by a novel, intracellular complex, the RIPoptosome. Alternatively, when apoptosis is blocked, the complex can switch to the necroptotic mode of the cell death. Thus, targeting the RIPoptosome for novel therapeutic approaches holds a significant promise in sensitisation of the treatment-resistant tumours to cell death.

1.8.4. FADDosome and FLIPosome

Similar to the previous reports, our group has described another example of a protein platform, which contains caspase-8 and contributes to initiation of cell death in response to chemotherapeutic compounds (Mohr et al., 2018). This recently discovered complex, which we refer to as FADDosome (Figure 7), has been shown to initiate the cell death in cancer cells subjected to treatment with 5-FU, irinotecan or raltitrexed without requirement for induction of the death receptor signalling pathways (Mohr et al., 2018).

As already mentioned, upon treatment with 5-FU apoptosis is induced in caspase-9-independent manner and, contrary to the Feoktistova et al. (2011) and Tenev et al. (2011) findings, it does not require formation of the RIPoptosome complex. However, we observed that p53 was necessary for execution of apoptosis in 5-FU-treated cancer cells. Moreover, we found that p53 plays an important role in execution of apoptosis via

mitochondrial network in HCT116 cells, but is dispensable for the caspase-8-mediated cell death. Thus, we have demonstrated that upon exposure to 5-FU, caspase-8 is activated in the p53-independent manner (Mohr et al., 2018).

Further experiments have shown that caspase-10 was upregulated in response to 5-FU and this process was independent of p53. The immunoprecipitation of caspase-8 led to co-purification of caspase-10 and FADD, but not cIAP2 or the death receptors. The observation was supported by studying of the 5-FU-treated HCT116 and 293 cells, which were overexpressing caspase-10- and FADD, respectively. The results have shown that caspase-10 and FADD could be co-immunoprecipitated with caspase-8 in HCT116 cells, whereas caspase-8 and -10 could be co-precipitated with pulled-down FADD in 293 cells. The sucrose gradient analysis unveiled that the size of the caspase-10/caspase-8/FADD complex was ~2 MDa (Mohr et al., 2018) and the result was similar to the observed size of the RIPoptosome (Feoktistova et al., 2011, Tenev et al., 2011). The immunoprecipitation of caspase-8 led to co-purification and identification of other constituents of the FADDosome, namely RIP1 and TRAF2. We found that caspase-10 and RIP1 were necessary for the recruitment of TRAF2 to the complex, which could in turn promote ubiquitination and degradation of cFLIP-L (Mohr et al., 2018) (Figure 7).
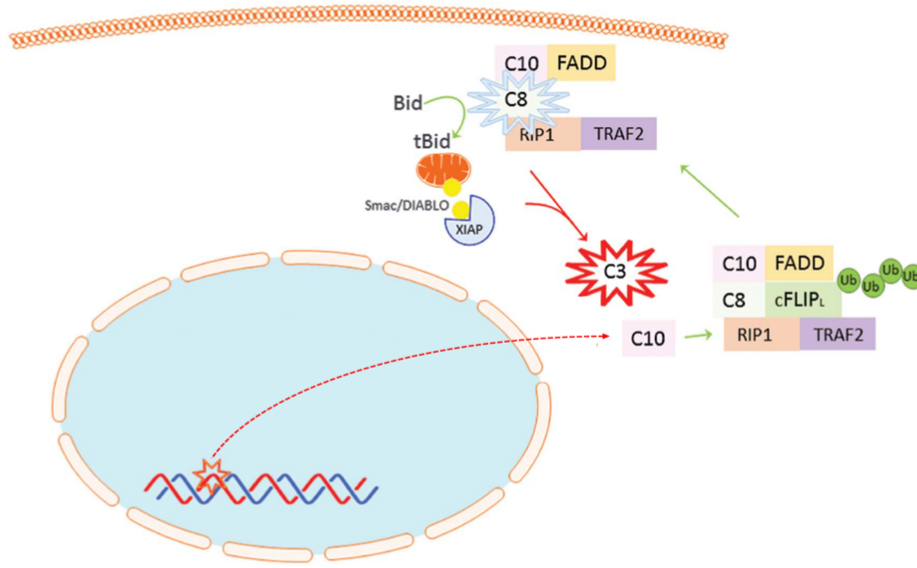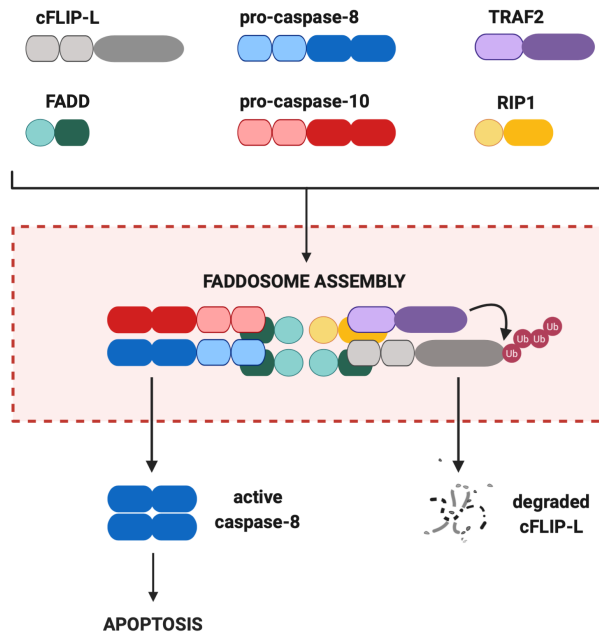
Figure 7. The FADDosome-mediated cell death induction and a model of the protein-protein interactions within the complex.
A. Upon DNA damage (indicated by the red star) caused by anti-cancer drugs, such as 5-FU, caspase-10 is upregulated in the p53-independent manner, which leads to formation of the novel apoptosis-inducing protein platform, FADDosome, encompassing caspase-10, caspase-8, FADD, RIP1 and TRAF2. At the complex, caspase-8 is cleaved and activated, which leads to activation of caspase-3 and subsequent induction of apoptosis (adapted from Mohr et al., 2018).
B. Within the FADDosome, FADD possibly acts as a scaffold and binds to caspase-10, caspase-8 and cFLIP-L. Moreover, RIP1, which is also recruited to the complex, interacts with FADD. Next, TRAF2 binds to RIP1 and ubiquitinates cFLIP-L, leading to its degradation. Moreover, cleavage and activation of caspase-8 at the complex is possibly facilitated and/or mediated by caspase-10. [7]

---

[7] Image created with BioRender.com

Moreover, we observed that the loss or inhibition of any of these factors in cancer cells exposed to 5-FU promotes a switch to an alternative cell death mechanism, which required assembly of the FLIPosome platform consisting of cFLIP-L and caspase-8 (Figure 8). Moreover, our results showed that in the absence of caspase-10 and RIP1, cIAP1 undergoes degradation in response to 5-FU. At the FLIPosome, cFLIP-L is cleaved by caspase-8, leading to generation of the cFLIP-p43 fragment and subsequent NF-κB activation, TNF-α expression and autocrine/paracrine cell death (Figure 8). Importantly, our group has demonstrated that FLIPosome-mediated apoptosis is p53-independet and overall, more efficacious than the FADDosome, which might provide a great advantage in the treatment of tumours with impaired p53 functions (Mohr et al., 2018).

Although we have identified caspase-10 to act as the core driver of the FADDosome assembly in 5-FU-induced apoptosis, the exact molecular mechanisms whereby upregulated caspase-10 forms the FADDosome and recruits other constituents requires clarification. Moreover, it still remains to be defined, what molecular factors and signalling pathways regulate the FADDosome and FLIPosome formation in response to chemotherapeutic drugs.
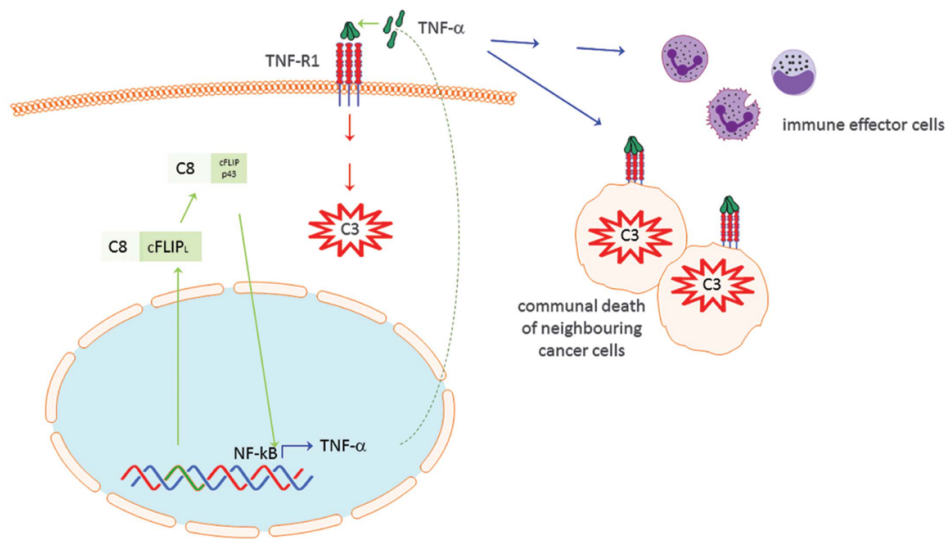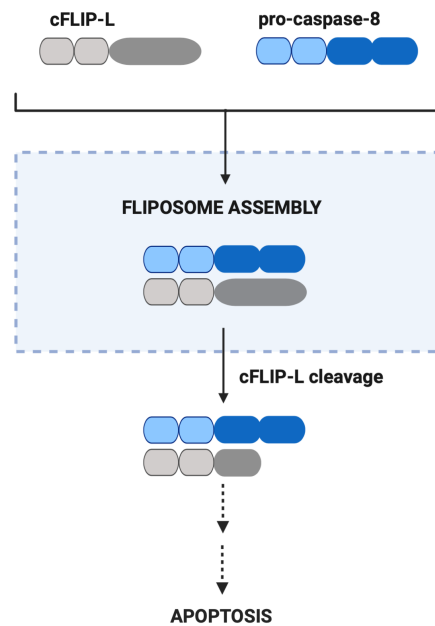
Figure 8. The FLIPosome-mediated cell death induction and a model of the protein-protein interactions within the complex.
A. The 5-FU-treated cells lacking caspase-10, RIP1, TRAF2 or ATR switch to an alternative mode of apoptosis, mediated by another novel cell-death-initiating protein platform, FLIPosome, which leads to cleavage of cFLIP-L, followed by NF-κB activation and TNF-α production. Finally, these events lead to initiation of the autocrine/paracrine cell death (adapted from Mohr et al., 2018). **B.** In the process of the FLIPosome assembly, caspase-8 binds to cFLIP-L, which contributes to the caspase-8-mediated processing of cFLIP-L to cFLIP-p43.[8]

---

[8] Image created with BioRender.com

In parallel, Henry and Martin (2017) discovered another protein platform, which similarly to the complex described by our group, was also termed FADDosome. The authors examined the role of TRAIL receptor signalling pathway in mediating NF-kB and MAPK activation, cytokine production and inflammation signalling. Henry and Martin (2017) discovered that upon TRAIL stimulation, cancer cells can form a pro-inflammatory complex, consisting of caspase-8, FADD and RIP1.

Henry and Martin (2017) studied the TRAIL-induced cytokine production in various cancer cell lines. They found that the secretion of IL-6 (interleukin 6), IL-8 (interleukin 8), CXCL1 (chemokine (C-X-C motif) ligand 1), MIF (macrophage migration inhibitory factor) and MCP-1 (monocyte chemoattractant protein-1) was significantly increased in HeLa cells. The cytokine production was also observed in PancTu-1, HCT116, HaCaT, 3LL and primary human prostate epithelial cells after application of TRAIL. These findings indicate that TRAIL-mediated cytokine synthesis is a general property of the TRAIL-R signalling pathway. In addition, Henry and Martin (2017) described that stimulation of the TRAIL receptor contributed to production of pro-inflammatory molecules, which are involved in induction of chemotaxis of neutrophils and monocytes towards in the cells.

Furthermore, zVAD-mediated inhibition of caspase activity led to suppression of apoptosis induction, but not the cytokine/chemokine production in HeLa and HT29 exposed to TRAIL, indicating that inflammatory responses occur independent of caspase activity and can be uncoupled from apoptotic pathways (Henry and Martin, 2017). Next, the authors wondered, what molecular factors are involved in the TRAIL-mediated inflammatory response. The results revealed that knocking down of RIP1, FADD and TAK1, but not TRADD, abolished the cytokine/chemokine production in HeLa cells upon TRAIL stimulation. Surprisingly and unexpectedly, the authors found that caspase-8 knockdown inhibited the inflammatory responses in TRAIL-treated HeLa cells, which was in contrast to the results obtained after application of zVAD. In addition, knocking down

of caspase-8 and FADD in HT-29 and HCT116 cells blocked TRAIL-mediated cytokine/chemokine secretion. In order to further confirm the role of caspase-8 in the TRAIL-induced inflammatory signalling, Henry and Martin (2017) used CRIPR/Cas9 and deleted Casp8 gene in HeLa and HCT116 cells, which similar to the previous results, abolished the inflammatory responses in the tested cell lines. These findings were supported by the observation that the re-introduction of wild-type caspase-8, caspase-8 active site (C360A) mutant and caspase-8 linker (D374A/D384A) restored the cytokine/chemokine production in HeLa.Casp8-/- and HCT.Casp8-/- cells in response to TRAIL. On the contrary, application of the caspase-8 oligomerization (F122G/L123G) mutant did not restore the TRAIL-induced cytokine/chemokine production in the cells. Taken together, these results indicate that TRAIL-mediated inflammatory response in tumour cells require caspase-8 to act as a scaffold, whereas activity or proteolytic processing of caspase-8 are dispensable for this process.

Co-immunoprecipitation of caspae-8 allowed to identify other molecules involved in TRAIL-mediated inflammatory signalling, namely caspase-10, FADD, RIP1, cFLIP, TRAF2, TAK1, Nemo and A20, indicating formation of a protein complex. Henry and Martin (2017) suggested that TRAIL receptor can form a transmembrane complex I, followed by detachment and subsequent generation of the cytosolic complex II, which would resemble the formation of the TNF-signalling complex I and II. The TRAIL-R complex II was termed the FADDosome. Importantly, the authors found that caspase-8 is critical for the recruitment of RIP1 and other components to the complex, which was confirmed by failed co-purification of caspase-10, RIP1, cFLIP and A20 after using biotinylated-TRAIL, co-immunoprecipitation of FADD and ligand-mediated precipitation of the TRAIL receptor protein complex in HeLa.Casp8-/- cells (Henry and Martin, 2017).

It is noteworthy, that in comparison to the FADDosome discovered by our group (Mohr et al., 2018), the FADDosome described by Henry and Martin (2017) encompassed

additional components (such as TAK1, Nemo and A20) and performed a distinct function (TRAIL-mediated inflammatory signalling). Thus, despite the fact, that these two complexes share the same name, they are most likely different.

Such contradictions and refinements in our knowledge provide new insights into how apoptosis is triggered in tumour cells subjected to treatment with cytotoxic and genotoxic drugs. Therefore, it is currently possible to develop novel approaches for examination of the molecular mechanisms and targeting of factors involved in development of the drug-resistance in cancer cells.

1.9. Interactions Between Caspase-10, Caspase-8, FADD and cFLIP

It is believed that the protein-protein interactions between caspase-10, -8, cFLIP and FADD are possible due to the presence of DEDs in the structures of these molecules (Riley et al., 2015). It was described that FADD also contains the death domain, which is structurally similar to DED and allows this adaptor protein to interact with the death receptors. A few models for the DISC assembly at the levels of DEDs interactions have been proposed, which demonstrated an association between the death receptors, caspase-8 and FADD. Interestingly, it was proposed that the stoichiometry of the caspase-8 and FADD molecules at the DISC equals 9:1, and that one FADD molecule has the ability to associate with multiple DED-containing proteins, namely pro-caspase-10, pro-caspase-8 and cFLIP. In this model, binding of multiple molecules to FADD would result in forming so called "chains". Such chains were observed by studying of fluorescently tagged caspase-8 in single cells (Dickens et al., 2012; Schleich et al., 2012). In contrast, a report by Riley et al. (2015) described that upon a sub-apoptotic DISC stimulation, even at high levels, the ratio between FADD and caspase-8 (or cFLIP)

was 1:2. Therefore, the exact stoichiometry of the molecules involved in the DISC formation remains to be defined.

Furthermore, it had been described that FADD promotes an interaction between caspase-8 (and similarly, caspase-10) molecules, which stimulates forming dimers by these caspases (Wachmann et al., 2010; Parrish et al., 2013). To date, several studies have determined the interaction of FADD with death receptors and its role in the DISC formation (Scott et al., 2008; Wang et al., 2010). The biochemical structures of FADD DD or DED domains have also been resolved (Eberstadt et al., 1998; Berglund et al., 2000). There is only one report available, which describes the structure of full-length FADD and proposes a model illustrating the mechanisms responsible for the interaction between FADD and zymogen caspase-8 (Carrington et al., 2006). The nuclear magnetic resonance (NMR) spectroscopy data revealed that the FADD structure is comprised of 12 α helices (6 per domain) and that both C- and N- protein termini are oriented in a way allowing them to face one another. The main aim of the study was to identify the specific binding surface for pro-caspases, located on the DED of FADD. In order to do that Carrington et al., (2006) used a set of FADD proteins containing different mutations that could affect the binding of pro-caspase-8, however, all the FADD mutants could still interact with the CD95 death receptor. The results obtained by CD95 co-immunoprecipitation allowed identifying the potential residues in FADD, which can be responsible for binding of procasapse-8 and these include: S12, R38, D44 and E51. Importantly, these sites can be found within helices α1 and α4 of FADD.

In order to further elucidate the binding mechanisms between FADD and pro-caspase-8, Carrington et al., (2006) used the MC159 protein, also known as viral FLICE-inhibitory protein (vFLIP) containing two DED domains, DED1 and DED2, which, due to their structural similarity, have been suggested to function as the equivalents of the pro-caspase DED2 and FADD DED, respectively. The analysis of the MC159 biochemical

structure unveiled that DED2 helices $\alpha 1$ and $\alpha 4$ can interact with DED1 helices $\alpha 2$ and $\alpha 5$. Further investigation showed that the FADD/pro-caspase-8 interaction engages F122 and L123 residues within pro-caspase DED2. Such observations were confirmed by using pro-caspase-8 proteins containing mutations of both residues, which impaired the interaction between inactive pro-caspase-8 mutant and FADD in 293T cells (Carrington et al., 2006). To conclude, these results suggest that pro-caspases can bind to FADD through their DED2, but not DED1.

A successful dimerization of caspases leads to their cleavage and subsequent activation, which is necessary for initiation of apoptosis in the cells. Only one study by Keller et al., (2009) has investigated the molecular mechanisms driving the dimerization of caspases so far, but it provides great insights into how this process works on structural level. Keller et al., (2009) investigated the structure of the zymogen caspase-8 as well as the mechanisms responsible for its activation together with associated conformational changes. In this study, a set of various recombinant caspase-8 constructs was used, including active-, cleavage- and dimerization-site mutants, which were established by introducing C360A, D374A/D384A and F468A single amino acid substitutions, respectively. Their biochemical structures were determined by using NMR methods. The obtained data revealed that an inactive caspase-8 represents the typical caspase fold and can only form monomers. It has been reported that the uncleaved form of the enzyme constitutes a highly flexible fragment termed linker. The linker consists of 40 residues and serves as a connection between p18 and p11 subunits of zymogen caspase-8.

It was shown that the structures of the inactive and active forms of caspae-8 do not differ significantly between each other. The most important differences are associated with the topology of the linker and the loop regions. Interestingly, the study revealed that conformation of the zymogen caspase-8 does not allow interacting with any substrates,

because the necessary binding pocket cannot be formed by the uncleaved enzyme. However, due to its flexibility, the linker has the ability to change its conformation, so that it becomes convenient for substrates to interact with the enzyme. Such observation explains the occurrence of occasional events, when zymogen caspase-8 reveals its basal activity.

Most importantly, Keller et al., (2009) demonstrated that the mechanisms of the induced proximity model are mainly responsible for triggering the dimerization of caspase-8 but are not directly involved in its proteolytic processing. Caspase-8 can only be cleaved after successful dimerization, which plays a crucial role in initiation of conformational changes of the zymogens followed by the cleavage of the linker (Figure 9). These observations were supported by using the dimerization-site mutant (F468A), which, despite the presence of the active Cys360 site, was not able to process itself nor interact with the used substrate, Ac-DEVD 7-amino-4-methylcoumarin (AMC). In addition, Keller et al., (2009) reported that dimerization is also necessary for triggering the catalytic activity of caspase-8, as it allows formation of the binding pocket.

It has been described, that caspase-8 can be fully activated, when both Asp374 and Asp384 cleavage sites, present in the linker, are proteolytically processed (Figure 9). Such conclusion was supported by using the single cleavage-site mutants and the AMC substrate. It was demonstrated that the D374A and D384A mutants showed a slight reduction in their activity, in comparison with the wild-type caspase-8. Most importantly, the dimerization process was decreased in both cases (Keller et al., 2009). Therefore, it is crucial for zymogen caspase-8 molecules to form dimers and to be cleaved in order to achieve its full activity potential (Figure 9).
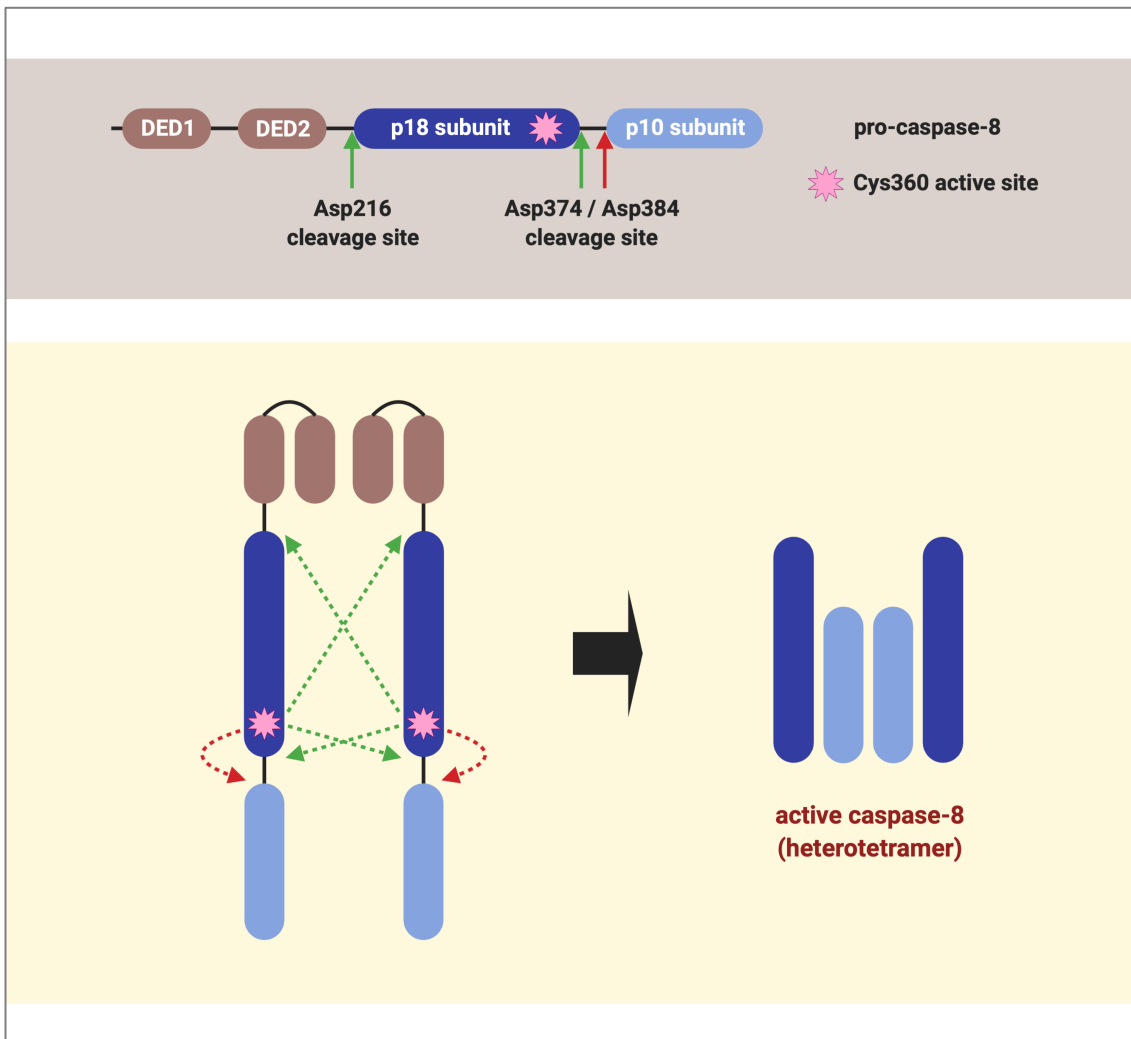
Figure 9. Model for cleavage and activation of caspase-8.
Inactive pro-caspase-8 molecules come into close proximity and form dimers. Dimerization promotes conformational changes of the pro-caspase-8 molecules, which facilitate their cleavage. First, pro-caspase-8 undergoes self-cleavage at the Asp384 site (indicated by red arrows), which leads to the release of the p10 subunit. Secondly, pro-caspase-8 undergoes trans-proteolytic cleavage at the Asp374 and Asp216 sites (indicated by green arrows). As a result, these events lead to formation of the active caspase-8 heterotetramer composed of the p18 and p10 subunits (Keller et al., 2009).9

---

9 Image created with BioRender.com

1.10. DNA Damage Response

Investigation and analysis of the interactions and functional relationships between the FADDosome components still leaves the question, what factors drive the formation of the complex. In this context, we wondered, what signalling pathways and molecular constituents are involved in the regulation of the FADDosome formation in response to 5-FU. While upregulation of caspase-10 in response to 5-FU might be a part of the answer, the exact details of how the signal from the damaged DNA is transduced towards the FADDosome still remain unknown.

Therefore, two serine/threonine kinases, ATR and ATM (Kamer et al., 2005; Shiloh and Ziv, 2013) as well as their substrates, the serine/threonine kinases Chk1 and Chk2, respectively, are the potential candidates, which we believe might play a role in promoting the caspase-10 upregulation and subsequent FADDosome formation in response to 5-FU. To be more specific, we hypothesise that upon genotoxic stress, the ATR/Chk1- and/or ATM/Chk2-mediated pathways are triggered in cancer cells and in turn, trigger a signalling cascade, which is responsible for induction of the caspase-10 upregulation and the FADDosome assembly. Therefore, it is essential to investigate the molecular mechanisms and factors involved in the signal transduction from the 5-FU-induced DNA damage site as well as in the formation of the FADDosome or other apoptosis-inducing complexes.

Conventionally, ATM and ATR are known to play a crucial role in recognition of DNA lesion (caused by anti-cancer drugs, UV or irradiation) and subsequent initiation of the DNA damage response (Kamer et al., 2005; Shiloh and Ziv, 2013; Blackford and Jackson, 2017) (Figure 10). These kinases are known to activate a wide range of targets by preferential phosphorylation at the pS/pTQ motif (Matsuoka et al., 2007; Shiloh and Ziv, 2013; Blackford and Jackson, 2017). It has been described that upon the genotoxic

stress, ATR and ATM can phosphorylate and activate the downstream Chk1 and Chk2, respectively (Table 1). After being activated, Chk1 and Chk2 phosphorylate a wide range of targets involved in the DNA damage response, which as a result can initiate DNA repair and cell survival or apoptosis (Zinkel et al., 2005; Matsuoka et al., 2007; Liu et al., 2010; Liu et al., 2011; Shiloh and Ziv, 2013).

Conventionally, the roles of Chk1 and Chk2 is to delay the cell cycle progression upon occurrence of DNA damage, and subsequently to promote DNA repair or cell death initiation (Figure 10). Moreover, these kinases are involved in signalling pathways mediating the damage-induced transcription and chromatin remodelling (Bartek and Lukas, 2003). Induction of these mechanisms is critical to protect cells against DNA damage progression and cancer. Furthermore, it has been reported that the core DNA damage response signalling pathway is formed by ATM/Chk2, ATR/Chk1, p53 and p21 (Jaarsveld et al., 2019) (Figure 10).

1.10.1. The Roles of ATM- and ATR-Mediated Signalling Pathways in the DNA Damage Response

ATM and ATR are known as the members of phosphoinositide 3-kinase (PI3K)-related kinases (PIKKs) family of proteins (Abraham, 1998). These kinases were discovered over 20 years ago and since then have been widely investigated (Blackford and Jackson, 2017). The gene encoding for ATM was identified by Savitsky et al. (1995), which followed the initial studies on patients suffering from A-T (Gotoff et al., 1967; Taylor et al., 1975; Houldsworth and Lavin, 1980; Painter and Young, 1980), a rare inherited autosomal-recessive genetic condition (Taylor et a., 2015). The main features of this genetic condition are: (I) the progressive neurological decline, which leads to the loss of

voluntary movement coordination, including abnormal gait (ataxia) and (II) dilated blood vessel (telangiectasia) (Blackford and Jackson, 2017).

Sequencing of the Rad3 gene (Seaton et al. 1992; Bentley et al. 1996), which was first found in yeast and involved in regulation of the cell-cycle checkpoints and DNA repair (Savitsky et al. 1995), was an initial step towards identification of ATR. It was later discovered that Rad3 shared a structural similarity with ATM (Bentley et al., 1996). Moreover, the subsequent studies by Bentley et al. (1996) and Cimprich et al. (1996) identified and cloned the human counterpart of the yeast Rad3 gene, which was then named ATM- and Rad3-related (ATR) (Bentley et al., 1996). With the discovery of ATM and ATR, numerous studies have been conducted, which allowed to greatly improve our knowledge and understanding of ATM and ATR in the DNA damage response.

It has been described that ATM can sense double strand breaks (DSBs) (Kamer et al., 2005; Zinkel et al., 2005; Matsuoka et al., 2007; Liu et al., 2011; Shiloh and Ziv, 2013), whereas ATR is involved in cellular response to the occurrence of single-stranded DNA (ssDNA) (Zinkel et al., 2005; Liu et al., 2010; Liu et al., 2011). Interestingly, it is believed that induction of DSBs contributes to relocation of ATM to the DNA lesion site and its activation, however the molecular mechanism involved in this process is still not well understood. Additionally, the occurrence of DSBs leads to recruitment of MRN (MRE11–RAD50–NBS1) complex, which similarly to ATM, acts as a sensor of the DNA damage. The interaction between activated ATM and MRN complex at the lesion site leads to initiation of a DNA damage-mediated signalling cascade (Shiloh and Ziv, 2013). Moreover, it has been described that the MRN complex is not required for the activation of ATM at the DNA damage site, however it is crucial for the ATM-mediated DNA damage response (Hartlerode et al., 2015) (Figure 10).

On the other hand, the single-stranded DNA (ssDNA) gaps are first recognised by replication protein A (RPA), which is regulated by Bid and believed to function as an initial sensor of ssDNA. Following the association of Bid-regulated RPA to the DNA damage site, ATR and its regulator, namely ATR-interacting protein (ATRIP), are recruited to the RPA-coated ssDNA and as a result, form the DNA damage sensor complex. As a consequence, ATR can be activated within the complex and, similarly to ATM, can then in turn phosphorylate its downstream substrates (Liu et al., 2010; Liu et al., 2011) (Figure 10).

In the non-stressed human cells, ATM remains inactive and typically forms homodimers. Following the DNA damage, this kinase can phosphorylate itself at Ser1981, which in turn leads to dissociation of the ATM homodimers and formation of phosphorylated monomers. The autophosphorylation-driven monomerization of ATM is believed to be crucial to activate its function in triggering of the DNA damage response (Bakkenist and Kastan, 2003). Moreover, it has been reported, that autophosphorylation at Ser367 and Ser1893 are also required for ATM activation, which allows this kinase to reach its full activity potential (Kozlov et al., 2006; Kozlov et al., 2011). However, some reports have demonstrated that in mice the phosphorylation of ATM at Ser367, Ser1899 and Ser1987, which function as the equivalents of the human phosphorylation sites, are not required to induce the activity of this kinase (Daniel et al., 2008). Another study has reported that in frogs (*Xenopus*), autophosphorylation of ATM is dispensable to initiate the monomerization of this kinase (Lee and Paull, 2005). This indicates that ATM monomerization is critical for its activation and allows this molecule to perform its functions in the DNA damage response. However, it is very likely that the role of autophosphorylation in the ATM activation is not a conserved process among different species (Awasthi et al., 2016).

It has been shown by various reports that ATR can by phosphorylated at Ser435, Ser428 and Thr1989 (Daub et al., 2008; Dephoure et al., 2008). A study by Liu et al., (2011) demonstrated that phosphorylation of ATR at Thr1989 occurred in response to DNA damage caused by UV irradiation, ionizing radiation and hydroxyurea *in vivo*. A subsequent co-immunoprecipitation of ATRIP (ATR-interacting protein) with the phosphorylated ATR revealed that this kinase undergoes phosphorylation at the ATR-ATRIP complex. Moreover, the authors found that phosphorylation at Thr1989 occurred only in the chromatin fractions, indicative of ATR phosphorylation on chromatin. Further experiments performed by Liu et al., (2011) demonstrated that phosphorylation at Thr1989 was crucial for ATR function, as it was found that mutation of this site abrogated the ATR-driven phosphorylation of its main substrate, namely Chk1 after exposure to UV irradiation. Moreover, the authors showed that phosphorylation of Thr1989 was not mediated by any other kinase, but occurs as a result of autophosphorylation, as it was observed that caffeine (a pan inhibitor of ATR and ATM), but not inhibitors of CDKs (cyclin-dependent kinases), ATM or DNA-PKs (DNA-dependent protein kinases), was able to block the ATR phosphorylation at Thr1989 in response to UV irradiation. Furthermore, Liu et al., (2011) reported that phosphorylation at this site also depends on ATRIP and RPA activity. Taken together, phosphorylation at Thr1989 is regarded as a hallmark of DNA-damage mediated ATR activity.

The molecular mechanisms and factors involved in initiation of the ATM- and ATR-mediated DNA damage response are summarised in Table 1.

Table 1. Main characteristics of the ATM- and ATR-controlled mechanisms and factors involved in initiation of the DNA damage response.

Kinase	DNA damage recognised	Other proteins and complexes involved[a]	Formation of the DNA damage sensor complexes[b]	Main targets[c]
ATM	double strand breaks (DSBs)[1, 3, 4]	MRN (MRE11–RAD50–NBS1) complex[4]	ATM is relocated to and activated at the DSB site in response to DNA damage, followed by recruitment of MNR complex to the lesion site[4]	Checkpoint kinase 2 (Chk2)[4]
ATR	single-stranded DNA (ssDNA)[2, 3]	Bid-regulated Replication Protein A (RPA) and ATR-interacting protein (ATRIP)[2, 3]	Bid-controlled RPA (initial sensor) is recruited to and coats ssDNA, followed by association of ATR-ATRIP complex and subsequent activation of ATR[2, 3]	Checkpoint kinase 1 (Chk1)[2, 3]

[1] Matsuoka et al., 2007; [2] Liu et al., 2010; [3] Liu et al., 2011; [4] Shiloh and Ziv, 2013
[a] Proteins and complexes that, similarly to ATM and ATR, function as sensors and associate with the DNA lesion as well as interact with the respective kinase.
[b] Molecular mechanisms responsible for interactions between ATM and ATR, and the respective protein complexes at the DNA damage sites
[c] Targets of ATM and ATR, which are phosphorylated and activated after formation of the DNA damage sensor complexes. These targets can in turn activate their downstream substrates and as a result, induce a DNA damage response signalling cascade.

1.10.2. The Roles of Chk1 and Chk2 in the DNA Damage Response

Similar to ATM and ATR, the Chk1 and Chk2 kinases also belong to the phosphoinositide 3-kinase (PI3K)-related kinases (PIKKs) family of proteins (Bartek and Lukas, 2003). The first studies on Chk1 and Chk2 knockout and knockdown mouse models, which were conducted about two decades ago, provided new insights into the biological requirement of these kinases. It was demonstrated that, despite the overlapping functions of Chk1 and Chk2 in checkpoint signalling, the loss of Chk1, but not Chk2, disrupted the mammalian development and viability (Liu et al., 2000; Takai et al., 2000, Hirao et al., 2002; Takai et al., 2002). It was found that the Chk1-deficient mice were lethal at an early embryonic stage (Liu et al., 2000; Takai et al., 2000), which was the main cause of the

limited studies on the role of Chk1 in cell-cycle checkpoint regulation *in vivo* (Bartek and Lukas, 2003). On the contrary, it was observed that the loss of Chk1 in DT-40 lymphoma cells did not affect the cell division, but instead promoted sensitisation of the cells to cell death caused by severe DNA damage, which could not be repaired. Moreover, further studies on Chk1 knockdowns revealed, that Chk1 was responsible for regulation of Cdc25A and required for the S-phase, intra-S-phase and G2/M checkpoints after exposure to irradiation and drugs-induced DNA-damage (Zhao et al., 2002; Gatei et al., 2003; Sørensen et al., 2003; Xiao et al., 2003).

In contrast to Chk1 knockdowns, the Chk2-deficient mice were viable and fertile. Moreover, it was observed that these mice were only prone to tumour development when subjected to treatment with carcinogens (Takai et al., 2002; Hirao et al., 2002). It was reported that Chk2 plays a role in the intra-S phase checkpoint induced by DSB in HCT-15 human colon carcinoma cells lacking Chk2 (Falck et al., 2001; Falck et al., 2002). Moreover, several studies demonstrated that mice lacking Chk2 exhibited radioresistance as well as defective p53-regulated transcription and apoptosis (Jack et al., 2002; Takai et al., 2002). Taken together, these results confirmed that the functions of Chk1 and Chk2 in regulation of various cell-cycle checkpoints were partly overlapping, whereas their biological requirements for development and viability of embryos were found to be fairly distinct.

It is believed that Chk1 and Chk2 are dependent on and regulated by ATR and ATM, respectively, however there is some evidence that a close "crosstalk" exists between these proteins (Gatei et al., 2003; Sørensen et al., 2003; Zabludoff et al., 2008; Matthews et al., 2013). Interestingly, Chk1 and Chk2 phosphorylate and regulate numerous downstream effectors, of which some are overlapping, and some are unique for each kinase. The most common substrates of Chk1 and Chk2 is p53 and its negative regulator, Mdm2 (Bartek and Lukas, 2003) (Figure 10). The roles of these kinases and

their targets in the DNA damage response are well understood. However, only a few molecular links to the cell death induction have been established for Chk1 and Chk2 so far (Gonzalez et al., 2003; Urist et al., 2004). In contrast, the most recent studies demonstrated that the increase of Chk1 and Chk2 activation in response to chemotherapeutic drugs, such as cisplatin or doxorubicin, leads to resistance development in tumour cells rather than apoptosis induction (Jaarsveld et al., 2019). Taken together, it remains to be unravelled, whether and to what extent Chk1 and Chk2 are involved in regulation and initiation of cell death in response to a variety of treatments including 5-FU.
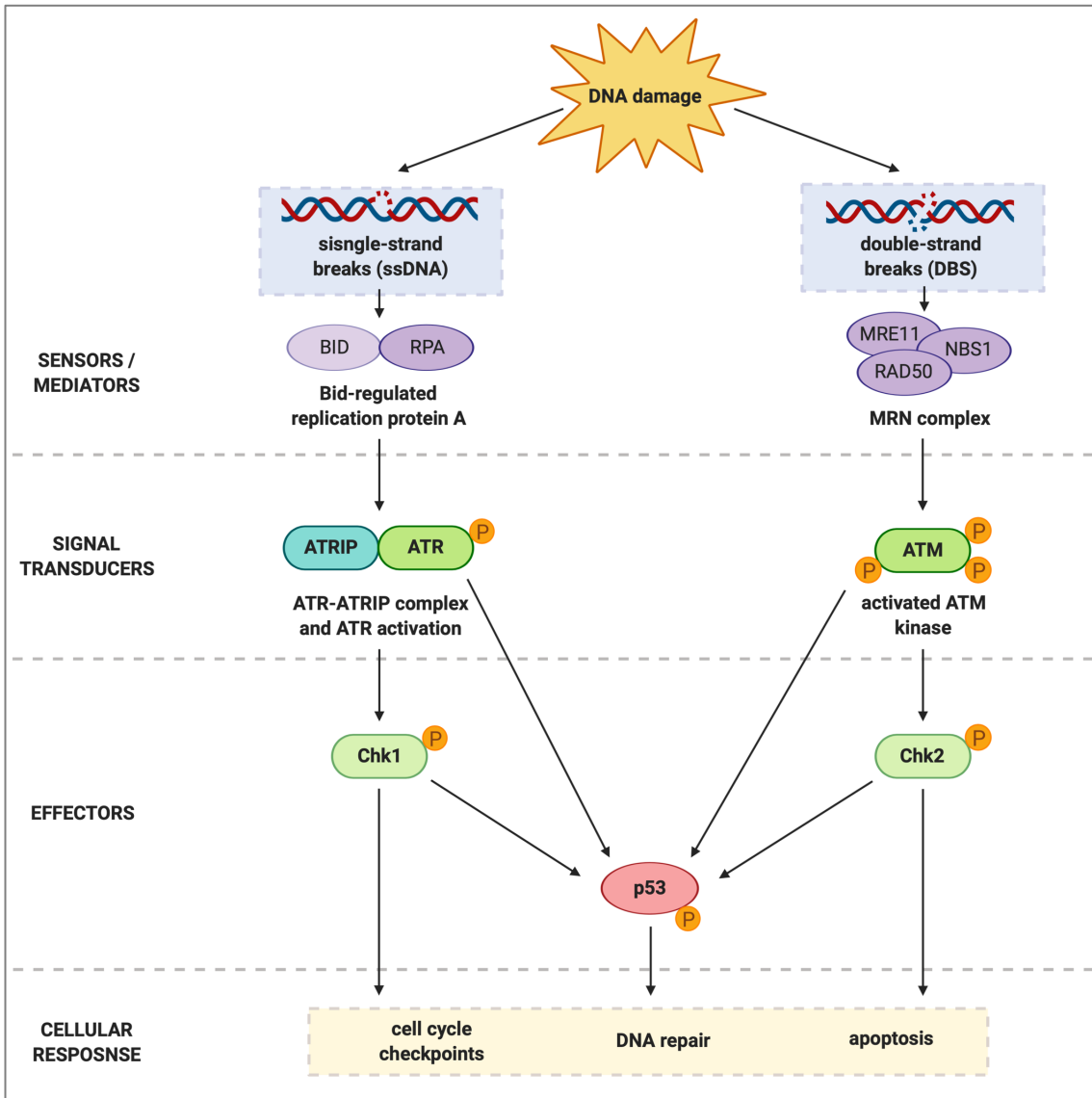
Figure 10. The ATR/Chk1- and ATM/Chk2-signalling pathways in the DNA damage response.
Upon induction of the ssDNA (left panel), Bid-regulated RPA is recruited to the site of the lesion, followed by recruitment if the ATR-ATRIP complex. At the complex, ATR is phosphorylated and activated. On the other hand, upon occurrence of the DSB (right panel), the MRN complex is formed at the site of the lesion. The complex consists of MRE11, RAD50 and NBS1 proteins. Next, ATM is relocated to the DNA damage site, at which it undergoes phosphorylation and activation. Activated ATR and ATM phosphorylate their downstream substrates, Chk1 and Chk2, respectively, as well as p53. Depending on the levels of the DNA damage, the DNA damage response either leads to the DNA repair or apoptosis induction (Ryan et al., 2016).[10]

---

[10] Image created with BioRender.com

1.10.3. ATM and ATR Signalling in Caspase-Mediated Apoptotic Pathways

To date, a few molecular links to the apoptosis induction, which requires involvement of various caspases, such as caspase-2, -3 and -8, have been established for ATM and ATR (Cicca and Elledge, 2010). It has been reported that ATM is involved in caspase and cytokine signalling in HeLa cells in response to extensive DNA damage (Biton and Ashkenazi, 2011) (Figure 11A). It was demonstrated that upon genotoxic stress, ATM promotes formation of a RIP1-reguated protein complex accompanied by secretion of TNF-α, which does not require involvement of p53. The adaptor protein FADD and initiator caspase-8 are then recruited by RIP1, which leads to cleavage and activation of caspase-8. This event contributes to caspase-8-mediated processing of caspase-3 and induction of apoptosis (Figure 11A). In parallel, extensive DNA damage also induces ATM-mediated signalling towards the RIP1-dependent production of proinflammatory cytokines, including interleukin 6 and 8 (IL-6 and IL-8, respectively), which alert neighbouring cells of the damage (Biton and Ashkenazi, 2011) (Figure 11A).

Moreover, both ATM and ATR were found to be involved in DNA-damage signalling towards another initiator caspase, namely caspase-2, in MEFs, HeLa and HCT.p53-/- cells (Sidi et al., 2008; Ho et al., 2009; Ando et al., 2012). It was reported that ATM/ATR/caspase-2-mediated pathway is triggered independently of p53, Bcl-2 and caspase-3 (Sidi et al., 2008) However, upon some treatments, such as with lidamycin, the further downstream pathway of ATR, ATM and caspase-2 requires involvement of the executioner caspase-3, which is then cleaved and activated, leading to initiation of apoptosis (Pan et al., 2009). Interestingly, a study by Ando et al. (2012) has linked ATM and ATR to regulation of the PIDDosome complex formation (Figure 11B). The authors found that these kinases are required for PIDD phosphorylation, which is in turn

necessary for binding of RAIDD. These events lead to recruitment of caspase-2 and

assembly of the PIDDosome, at which caspase-2 undergoes activation (Ando et al.,

2012) (Figure 11B).
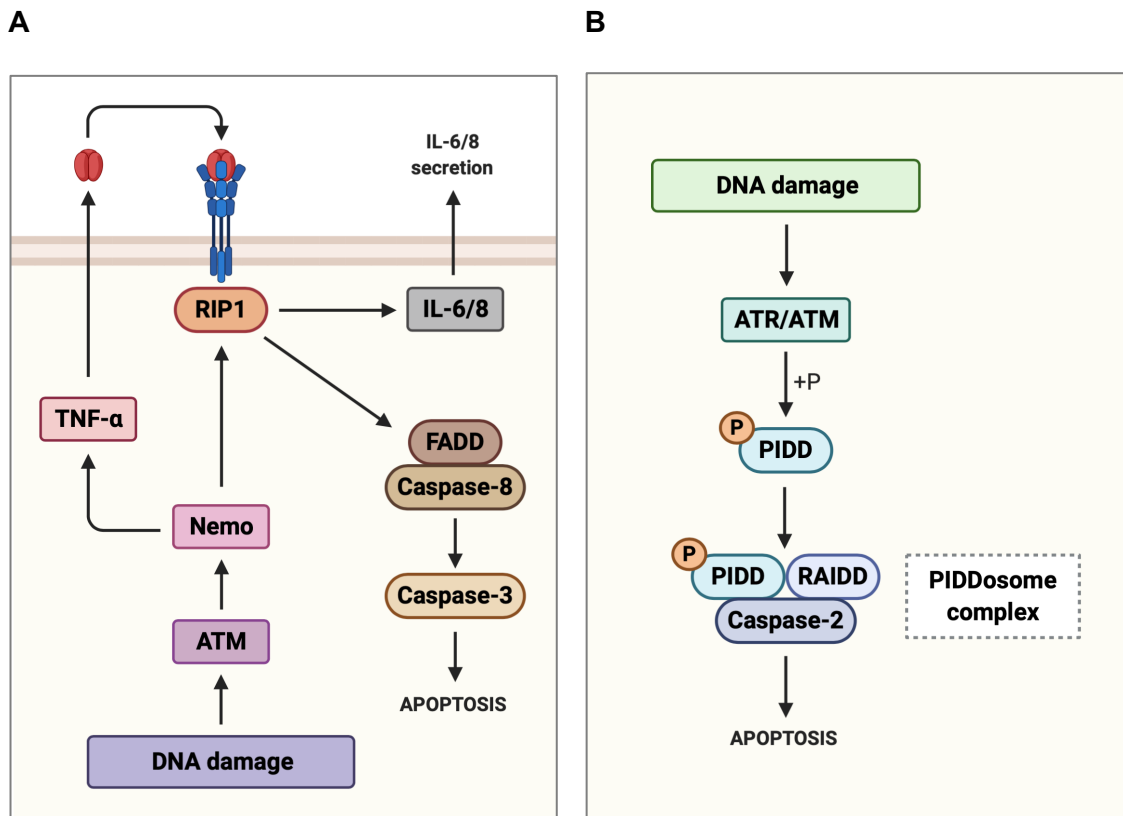
Figure 11. Roles of ATM and ATR in apoptotic pathways mediated by caspases.
A. Upon extensive DNA damage, ATM signals towards Nemo, which in turn promotes formation
of the RIP1-regulated TNFR-1 complex. The DNA damage-induced signalling from ATM to Nemo
also leads to production of TNF-α, which is involved in induction of the feedforward signalling loop
towards the TNFR-1 receptor. The adaptor protein FADD and initiator caspase-8 are then
recruited by RIP1. As a result, caspase-8 undergoes cleavage and activation, and in turn
processes caspase-3, which eventually leads to initiation of apoptosis. Moreover, the ATM-
mediated signalling from the DNA damage site also promotes the RIP1-regulated production of
proinflammatory cytokines, such as interleukin 6 (IL-6) and 8 (IL-8). Secretion of the cytokines
alerts neighbouring cells of the DNA damage (Biton and Ashkenazi, 2011). **B.** Occurrence of the
DNA lesions induces the ATR/ATM-mediated signalling towards PIDD, which in turn undergoes
phosphorylation and activation. As a result, activated PIDD interacts with RAIDD and recruits
caspase-2. These events lead to formation of the PIDDosome complex, at which caspase-2 is
activated, leading to initiation of apoptosis (Ando et al., 2012).[11]

---

[11] Image created with BioRender.com

It has been reported that upon induction of the DNA damage, ATM and ATR are activated in prostate cancer (DU145 and PC3 cells) (Garcia et al., 2015), whereas ATR alone undergoes activation in keratinocytes (HaCaT cells) (Kemp and Sancar, 2016). It was described that these kinases promote apoptotic signalling towards caspase-3, which plays a key role in initiation of cell death in response to DNA lesions in DU145, PC3 and HaCaT cells (Garcia et al., 2015; Kemp and Sancar, 2016). Moreover, in prostate cancer, activation of ATM and ATR contributes to induction of Chk1, phosphorylation of H2AX and downregulation of Cdc25C (Garcia et al., 2015). In keratinocytes and similar to findings described by others (Sidi et al., 2008, Pan et al., 2009; Biton and Ashkenazi 2011), the ATR-regulated caspase-3 activation and apoptosis are induced without involvement of p53 (Kemp and Sancar, 2016).

Taken together, in many human cancers, ATM and ATR play a critical role in signalling from the DNA damage site towards various caspases, such as the initiator caspase-2 and -8 as well as the executioner caspase-3, leading to induction of apoptosis. Therefore, in this study, inspired by the ATM/ATR-mediated signalling towards the caspase-dependent apoptotic pathways, it was hypothesised that these kinases are also involved in the 5-FU-induced caspase-10 upregulation and FADDosome formation in colorectal cancer cells.

1.11. Research Motivation

Previously, our group demonstrated, that upon treatment with 5-FU, irinotecan or raltitrexed, apoptosis can be induced in a caspase-8-dependent manner, without involvement of the death receptor signalling network (Mohr et al., 2018). We have shown that apoptosis is triggered through involvement of a protein complex termed FADDosome, which is formed upon exposure to the chemotherapeutic drugs. We have identified the main constituents of the FADDosome, namely caspase-10, caspase-8,

FADD, RIP1 and TRAF2. At the FADDosome, caspase-8 is activated in the p53-independent manner, leading to initiation of apoptosis. We found that when ATR, caspase-10, RIP1 or TRAF2 are inhibited or lost, 5-FU-treated cancer cells are able to switch to an alternative cell death mechanism, which requires assembly of the FLIPosome platform consisting of cFLIP-L and caspase-8 (Mohr et al., 2018).

Nevertheless, the biological importance and the exact roles of the main FADDosome components in promoting the 5-FU-induced complex formation and caspase-8 activation, still remain unclear. Thus, understanding the roles of factors and mechanisms involved in the FADDosome is crucial, in order to design better therapeutic approaches and help overcome resistance in cancer cells.

Since treatment with cytotoxic drugs leads to DNA damage in many cases, the question raised, how the signal from the DNA-damage site is translated into cell death signals in cancer cells. The serine/threonine kinases ATR and ATM are known to play a crucial role in sensing DNA lesions and triggering of the conventional DNA damage response machinery. Upon genotoxic stress, ATR and ATM phosphorylate and activate the downstream Chk1 and Chk2, respectively. Another target, which is phosphorylated by ATR and ATM is the tumour suppressor p53. After being activated, Chk1, Chk2 and p53 regulate a wide range of targets involved in the DNA damage response, which as a result can initiate DNA repair and cell survival or apoptosis. To date, a few studies reported that ATR and ATM play a role in the DNA damage-initiated cell death signalling. In particular, these kinases have been linked to signalling towards the caspase-2-, caspase-3- and caspase-8-mediated apoptotic pathways. Thus, it is assumed that ATR and/or ATM could also be involved in signalling from the DNA damage site towards caspase-10 and FADDosome in response to 5-FU. Moreover, our knowledge of the roles of Chk1 and Chk2 in genotoxic stress-induced cell death remains incomplete and requires investigation.

In our previous report we demonstrated that HCT.p53-/- cells were protected from apoptosis triggered by the 5-FU treatment (Mohr et al., 2018). Additionally, our group found that caspase-9, which has been reported to be crucial for the initiation of the classical intrinsic apoptosis cascade, was dispensable for the 5-FU-induced apoptosis (Mohr et al., 2018). These findings suggested that the resistance of HCT.p53-/- cells to 5-FU was not associated with inhibition of the conventional apoptotic pathway. With respect to that, our group found that p53 was involved in the transcriptional regulation of TRAIL-R2 (DR5) in HCT116 cells exposed to 5-FU (Mehrabadi, 2018). It was also discovered, that DR5 was not involved in caspase-8 activation, as described in the classical model of apoptosis, but in activation of JNK in responses to 5-FU (Mehrabadi, 2018). Thus, it is hypothesised that ATR and/or ATM can potentially regulate the TRAIL-R2/JNK axis via p53 after treatment with 5-FU. Moreover, it was shown that JNK can phosphorylate and regulate Bid (Dhanasekaran and Reddy, 2008), which suggests that the potential meeting point of the FADDosome and the p53-mediated TRAIL-R2/JNK signalling network possibly occurs downstream of Bid.

Taken together, a better understanding of the functions of the ATR/Chk1- and ATM/Chk2-signalling pathways in the DNA damage-induced apoptosis is important, as it might help with finding ways of pushing cancer cells into the cell death response, which is the main goal of the anti-tumour approaches. In this context, it is essential to investigate the molecular mechanisms and factors involved in the signal transduction from the 5-FU-induced DNA-damage site leading to initiation of apoptosis in cancer cells. Better understanding of the roles of these pathways is a key point to be addressed, as it might help to bypass resistance in cancer cells and to reduce the toxic side effects of anti-tumour treatments.

1.12. Aims and Objectives

The aims of this study are:

- to investigate the functional relationships and interactions between the main FADDosome constituents, namely caspase-10, caspase-8, FADD and cFLIP-L in terms of the complex formation and caspase-8 activation (Figure 12A, B, C and D);

- to analyse the ATR/Chk1- and ATM/Chk2-signalling pathways and to identify factors involved in regulation of the FADDosome formation and apoptosis in cancer cells treated with chemotherapeutic drugs (Figure 13).

With respect to the first aim, it is hypothesised that upregulated caspase-10 competes with cFLIP-L for binding to caspase-8, which in turn leads to formation of the FADDosome and not the FLIPosome (Figure 12B). It is assumed that within the complex, FADD functions as the binding partner of caspase-10, caspase-8 and cFLIP-L and that these proteins interacts via their cognate DED domains (Figure 12B). It is also postulated that the decrease of the caspase-10 levels or its loss promotes an interaction between caspase-8 and cFLIP-L, causing a switch to the FLIPosome (Figure 12B). Moreover, it is hypothesised that at the FADDosome, activation of caspase-8 is mediated by caspase-10, which in addition might be facilitated by FADD (Figure 12C). These hypotheses are based on how caspase-10, caspase-8, c-FLIP-L and FADD are conventionally believed to interact and function as well as on what is known about the assembly mechanisms of the other novel apoptosis-inducing protein platforms, such as RIPoptosome.

In order to test these hypotheses, the wild type and mutated variants of human recombinant ΔDEDs caspase-10, ΔDEDs caspase-8, ΔDEDs cFLIP-L and FADD-FL, which are expressed in *E. coli* and purified using column chromatography, are used. This is followed by characterisation of the functional relationships and interactions between the proteins of interest using activity and pull-down assays performed in a cell free setting.
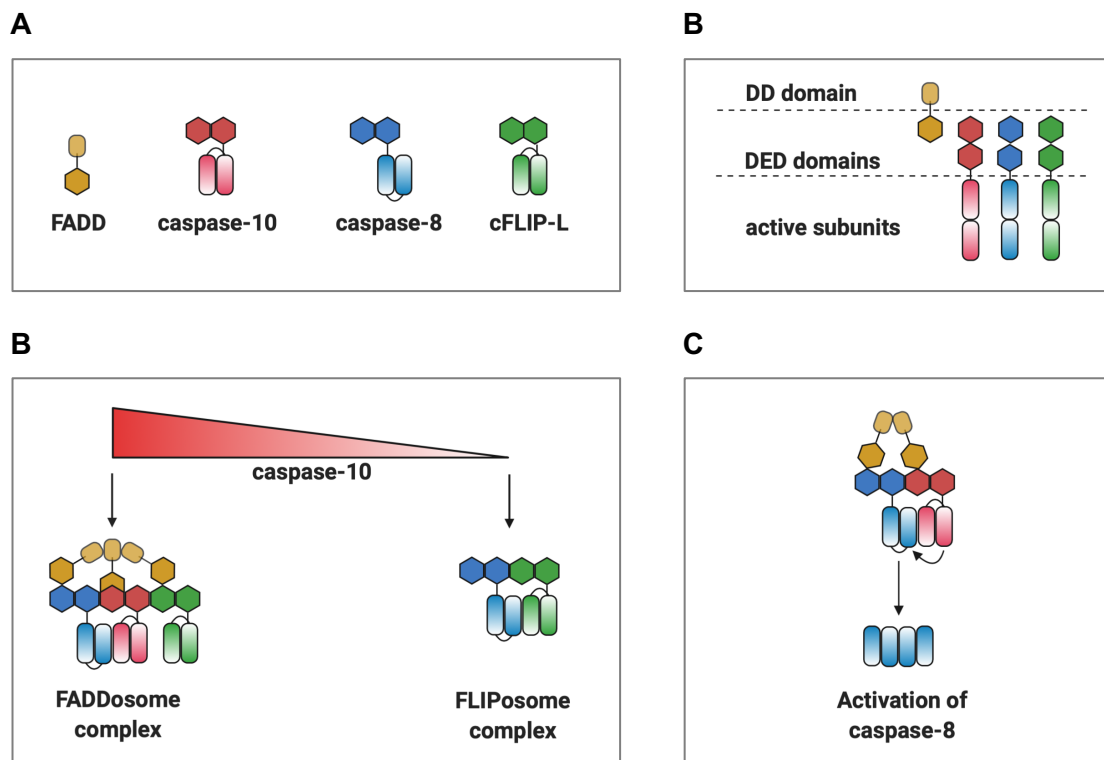
Figure 12. Hypotheses related to the interactions and functional relationships between the FADDosome components.
A. The main FADDosome components include FADD, caspase-10, caspase-8 and cFLIP-L. **B.** Domain organisation of FADD, caspase-10, caspase-8 and cFLIP-L. **C.** In the present study, it is hypothesised that the FADDosome is formed, when upregulated caspase-10 outcompetes cFLIP-L for binding to caspase-8. On the other hand, it I assumed that when the caspase-10 levels are reduced or the protein is lost, caspase-8 binds to cFLIP-L, which promotes formation of the FLIPosome. Moreover, the interaction between caspase-10, caspase-8, cFLIP-L and FADD within the FADDosome possibly occurs by involvement of their cognate DED domains. **C.** It is assumed that caspase-8 is cleaved and activated at the complex in the caspase-10-dependent manner. Additionally, FADD might be also involved in this process and facilitate it by interacting with caspase-10 and caspase-8.[12]

---

[12] Image created with BioRender.com

To address the second aim of this research, a model of 5-FU-induced apoptosis in colorectal cancer cells was proposed (Figure 13). In this model, it is hypothesised that ATM and/or ATR functions as the key sensors of the 5-FU-induced DNA damage. It is assumed that in response to such damage, ATM and ATR are activated and in turn, are involved in phosphorylation and activation of Chk1 and Chk2 as well as induction of p53. It is postulated that the sensed 5-FU-induced DNA damage is translated into apoptotic signals, which in turn contributes to the p53-independent caspase-10 upregulation and subsequent FADDosome formation. Moreover, in the current study, it is hypothesised that activated ATM and/or ATR are also involved in regulation of a distinct, p53-mediated TRAIL-R2/JNK signalling pathway. Since it was found previously that Bid can be phosphorylated by JNK, It is assumed that the FADDosome and the p53-driven TRAIL-R2/JNK axis converge downstream of Bid (Figure 13). Thus, the proposed model and hypotheses are based on our previous findings as well as on the knowledge of the pathways and factors involved in the DNA damage response and the intrinsic/mitochondrial apoptotic network.

To address these hypotheses, human colon cancer HCT.shctrl cell line, which is a derivative of HCT116 cells, is used. HCT.shctrl cells were selected in this study, as they function as control for other HCT116 knockdown cell lines. HCT.shctrl and HCT116 cells respond to 5-FU in the same manner. In order to assess the effect of 5-FU on proteins phosphorylation/activation and regulation of molecular pathways in cancer cells, the analytic methods, such as Western blot, Nicoletti assay and flow cytometry, are used.
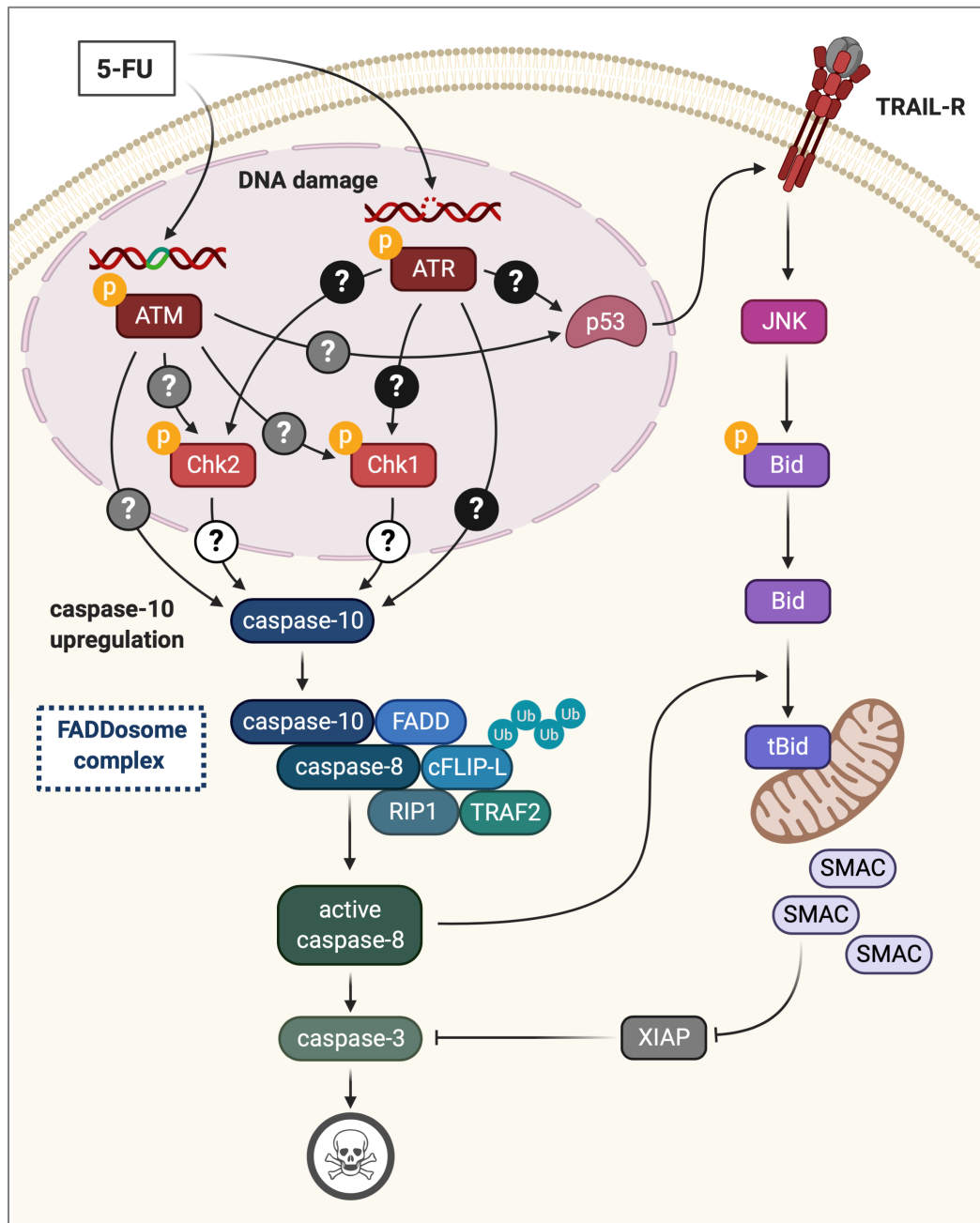
Figure 13. The hypothetical molecular model of the 5-FU-induced apoptosis.
In the proposed model of apoptosis, it is hypothesised that upon 5-FU-induced DNA damage, ATR and/or ATM can act as the critical sensors of such damage and in turn, can be phosphorylated and activated. It is also hypothesised, that this event would lead to the subsequent phosphorylation and activation of Chk1 and/or Chk2 and accumulation of p53. It is assumed that after sensing the 5-FU-induced DNA damage, ATR and/or ATM together with Chk1 and/or Chk2, could translate the sensed lesion into the apoptotic signals in cancer cells. It is believed that this leads to caspase-10 upregulation, followed by FADDosome complex formation and initiation of apoptosis. In addition, in this model, it is hypothesised that ATR and/or ATM regulate the p53-driven TRAIL-R2/JNK axis and Bid phosphorylation. It is assumed that in the further downstream pathway, dephosphorylated Bid is cleaved to tBid by caspase-8, which functions as a meeting point of the FADDosome and TRAIL-R2/JNK pathways.[13]

---

[13] Image created with BioRender.com

Following research objectives would facilitate the achievement of the first aim:

- design of protein expression constructs and cloning into pET-28a vector

- expression of ΔDEDs caspase-10 (wild type), ΔDEDs caspase-8 (wild type), ΔDEDs cFLIP-L (wild type) and FADD-FL

- purification of wild type proteins

- expression of ΔDEDs caspase-10 (C401A), ΔDEDs caspase-10 (D415A), ΔDEDs caspase-8 (C360A) and ΔDEDs caspase-8 (D374A/D384A)

- purification of selected mutated proteins

- design of protein expression constructs and cloning into pGEX-4T-3 vector

- expression of ΔDEDs caspase-10 (C401A), ΔDEDs caspase-10 (D415A), ΔDEDs caspase-8 (C360A) and ΔDEDs cFLIP-L (wild type and D376A mutant)

- purification of selected mutated proteins

- analysis of the role of caspase-10 and/or FADD in the caspase-8 cleavage *in vitro* in terms of the FADDosome

- assessing, whether FADD can interact with caspase-8, cFLIP-L and/or caspase-10 *in vitro* in terms of the FADDosome

- investigating the competition between caspase-10 and cFLIP-L for binding to caspase-8 *in vitro* in terms of the switch from FADDosome to FLIPosome and *vice versa*.

Following research objectives would facilitate the achievement of the second aim:

- analysis of ATR, ATM, Chk1 and Chk2 phosphorylation and p53 induction levels in 5-FU-induced apoptosis

- exploring the roles of ATR and ATM in Chk1 and Chk2 phosphorylation and p53 induction in response to 5-FU

- investigating the roles of ATR and ATM in caspase-10 upregulation and formation of the FADDosome after treatment with 5-FU

- assessing the roles of Chk1 and Chk2 in caspase-10 upregulation in response to 5-FU and etoposide

- establishing, whether inhibition of Chk1 and/or Chk2 activation contributes to a switch to the FLIPosome mode of apoptosis after exposure to 5-FU

- exploring the roles of ATR and ATM in regulation of the p53-mediated TRAIL-R2/JNK axis, JNK activation and Bid phosphorylation.

CHAPTER 2

MATERIALS AND METHODS

2.1 <u>Materials</u>

Cell Lines

Table 2. List of cell lines.

Cell lines	Source/Manufacturer	Description
HCT116	ATCC, Manassas, VA, USA	Human colorectal carcinoma cells
HCT.shctrl	Cell line stock of the lab	Human colorectal carcinoma cells – control knockdown
HCT.shATR	Cell line stock of the lab	Human colorectal carcinoma cells – ATR knockdown
HCT.shCaspase-10	Cell line stock of the lab	Human colorectal carcinoma cells – caspase-10 knockdown
HCT.p53-/-	Cell line stock of the lab (gift from Bert Vogelstein)	Human colorectal carcinoma cells – p53 knockout

Antibodies

Table 3. List of primary antibodies.

Primary antibodies	MW of target protein (kDa)	Catalogue number	Manufacturer
ATM	250	A6093	Sigma, St. Louis, MO, USA
ATR	230	A300-138A	Bethyl Laboratories, Montgomery, Texas, USA
Caspase-10	59	M059-3	Medical & Biological Laboratories, Woburn, MA, USA
Caspase-8/p18	55	SC-5263	Biotechnology, Santa Cruz, CA, USA
CuZnSOD	17	MAB3418	R&D Systems, Minneapolis, MN, USA
Chk1	52	2360S	Cell Signalling Technology, Beverly, MA, USA

Primary antibodies	MW of target protein (kDa)	Catalogue number	Manufacturer
Chk2	61	2662S	Cell Signalling Technology, Beverly, MA, USA
cIAP1	72	AF8181	R&D Systems, Minneapolis, MN, USA
FADD (Clone 1F7)	25	05-486	Clone 1F7, Upstate (Millipore), Billericay, MA, USA
GST-tag	26	2625S	Cell Signalling Technology, Beverly, MA, USA
(His)$_6$-tag	2	AB18184	Abcam, Cambridge, England, GB
p21	21	SC-6246	Biotechnology, Santa Cruz, CA, USA
p53	53	SC-126	Biotechnology, Santa Cruz, CA, USA
phospho-Chk1	54	8191S	Cell Signalling Technology, Beverly, MA, USA
phospho-Chk2	62	2197S	Cell Signalling Technology, Beverly, MA, USA
phospho-ATM	250	5883S	Cell Signalling Technology, Beverly, MA, USA
phospho-ATR	230	30632S	Cell Signalling Technology, Beverly, MA, USA

Table 4. List of secondary antibodies.

Secondary antibodies	Species	Catalogue number	Manufacturer
Anti-goat IgG-HRP (horseradish peroxidase)	mouse	SC-2354	Biotechnology, Santa Cruz, CA, USA
Anti-mouse IgG-HRP (horseradish peroxidase)	goat	SC-2005	Biotechnology, Santa Cruz, CA, USA
Anti-rabbit IgG-HRP (horseradish peroxidase)	mouse	SC-2357	Biotechnology, Santa Cruz, CA, USA
Anti-sheep IgG-HRP (horseradish peroxidase)	rabbit	SC-2770	Biotechnology, Santa Cruz, CA, USA

Bacteria Strains

Table 5. List of bacteria strains.

Strain	Manufacturer	Genotype
E. coli TOP10 competent cells	ThermoScientific, Waltham, MA, USA	F- mcrA Δ(mrr-hsdRMS-mcrBC) φ80lacZΔM15 ΔlacX74 nupG recA1 araD139 Δ(ara-leu) 7697 galE15 galK16 rpsL (Str^r) endA1 λ-
E. coli BL21(DE3) competent cells	ThermoScientific, Waltham, MA, USA	F$^-$ dcm ompT hsdS (r$_B$$^-$ m$_B$$^-$) gal λ(DE3)
E. coli BL21-RIL competent cells	Agilent Technologies, Santa Clara, CA, USA	F$^-$ ompT hsdS (r$_B$$^-$ m$_B$$^-$) dcm+ Tet^r gal endA Hte [argU ileY leuW Cam^r]

Cloning

Table 6. List of plasmids used for cloning and protein expression.

Plasmids	Manufacturer
pET-28a vector	Merck, Kenilworth, NJ, USA
pGEM®-T Easy Vector	Promega, Madison, WI, USA
pGEX-4T-3 vector	GE Healthcare, Chicago, IL, USA

Table 7. List of enzymes used for cloning.

Enzymes	Manufacturer
Restriction enzymes	ThermoScientific, Waltham, MA, USA
T4 ligase enzyme	ThermoScientific, Waltham, MA, USA

Table 8. List of commercial kits.

Commercial Kits	Manufacturer
GenElute™ Gel Extraction Kit	Sigma, St. Louis, MO, USA
GenElute™ Plasmid Miniprep Kit	Sigma, St. Louis, MO, USA
QuickChange® II Site-Directed Mutagenesis kit	Stratagene, San Diego, CA, USA
Pierce® BCA Protein Assay Kit	ThermoScientific, Waltham, MA, USA
SuperSignal™ West Pico Trial Kit	ThermoScientific, Waltham, MA, USA

Protein purification

Table 9. List of columns used for protein purification.

Protein Purification Columns	Manufacturer
IMAC 5 ml His-trap FF nickel-nitrilotriacetic (Ni-NTA) acid-sepharose column	GE Healthcare, Chicago, IL, USA
SEC 120 ml HiLoad Superdex 75 16/60 column	GE Healthcare, Chicago, IL, USA

Solutions

Table 10. List of buffers and solutions.

Solution	Recipe
Anode I buffer	300 mM Trizma base, 20% (v/v) methanol
Anode II buffer	25 mM Trizma base, 20% (v/v) methanol
Antibody dilution buffer	3% (w/v) bovine serum albumin (BSA) in TBS-Tween 20
Blocking buffer	5% (w/v) non-fat dry milk in TBS-Tween 20
Buffer A	50 mM Trizma base [pH 7.5], 500 mM NaCl, 20 mM imidazole
Buffer A*	50 mM Trizma base [pH 7.5], 1 M NaCl, 20 mM imidazole
Buffer A**	50 mM Trizma base [pH 7.5], 500 mM NaCl, 80 mM imidazole

Solution	Recipe
Buffer B	50 mM Trizma base [pH 7.5], 500 mM NaCl, 500 mM imidazole
Buffer C	50 mM Trizma base [pH 7.5], 100 mM NaCl
Buffer D	8 M urea, 50 mM Trizma base [pH 7.5], 500 mM NaCl, 20 mM imidazole
Calcium chloride	100 mM, sterilised
Cathode buffer	25 mM Trizma base, 40 mM hexanoic acid, 20% (v/v) methanol
Cellular lysis buffer (bacteria cells)	50 mM Trizma base, 100 mM NaCl, 1 mM EDTA, 50 mM MgCl$_2$
Coomassie stain buffer	40% (v/v) methanol, 10% (v/v) acetic acid, 0.1% Coomassie Brilliant Blue R-250
Coomassie destain buffer	40% (v/v) methanol, 10% (v/v) acetic acid
Nicoletti buffer	50 µg/ml propidium iodide, 0.1% (w/v) sodium citrate, 0.1% (w/v) Triton X-100
NP-40 lysis buffer (cancer cells)	50 mM Trizma base [pH 7.4], 10% (v/v) glycerol, 0.5% (v/v) NP-40, 150 mM NaCl, 1 mM MgCl$_2$,1 mM CaCl$_2$, 1 mM KCl, protease inhibitor cocktail tablet
Protein loading buffer	65 mM Trizma base [pH 6.8], 10% (v/v) glycerol, 4% (w/v) SDS, 4% (v/v) β-mercaptoethanol, 0.2% (w/v) bromophenol blue
SDS-PAGE running buffer (10x)	192 mM glycine, 25 mM Trizma base, 1% (w/v) SDS
Solubilisation buffer for inclusion bodies	6 M guanidine hydrochloride or 8 M urea, 500 mM NaCl, 20 mM Trizma base [pH 8.0]
TAE buffer (50x)	50 mM EDTA [pH 8.0], 2 M Trizma base, 1 M acetic acid
TBS-Tween 20 buffer	10 mM Trizma base [pH 8.0], 150 mM NaCl, 0.1% Tween 20
Triton X-100 lysis buffer (cancer cells)	2.5 mM EDTA, 1% (v/v) Triton X-100, 30 mM Trizma base [pH 7.5], 150 mM NaCl, 10% (v/v) glycerol, protease inhibitors cocktail tablet

Reagents

Table 11. List of reagents

Chemical reagents	Manufacturer
1,2-bis-(dimethylamino)-ethane (TEMED)	Sigma, St. Louis, MO, USA
5-Fluorouracil (5-FU)	Sigma, St. Louis, MO, USA
Acrylamide-bis-acrylamide	Sigma, St. Louis, MO, USA
Agarose	Sigma, St. Louis, MO, USA
Aminohexanoic acid	Sigma, St. Louis, MO, USA
Ammoniumpersulfate (APS)	Sigma, St. Louis, MO, USA
Ataxia telangiectasia mutated protein (ATM) inhibitor (KU55933)	Stratech, Newmarket, England, GB
Ataxia telangiectasia and Rad3-related protein (ATR) inhibitor (AZD6738)	Stratech, Newmarket, England, GB
BCA protein assay reagent (bicinchoninic acid)	Pierce/ThermoScientific, Waltham, MA, USA
Bovine serum albumin (BSA)	Sigma, St. Louis, MO, USA
Calcium chloride	Sigma, St. Louis, MO, USA
Checkpoint kinase (Chk) inhibitor (CHIR-124)	Stratech, Newmarket, England, GB
DNA ladders	ThermoScientific, Waltham, MA, USA
Enhanced chemiluminescent (ECL) Western blotting substrate	Pierce/Thermoscientific, Waltham, MA, USA
Ethylene-dinitrilo-tetraacetic acid (EDTA)	Sigma, St. Louis, MO, USA
Ethanol	Sigma, St. Louis, MO, USA
Etoposide	Sigma, St. Louis, MO, USA
Glycerol	Sigma, St. Louis, MO, USA
Glycine	Sigma, St. Louis, MO, USA
Guanidine hydrochloride (GuHCl)	Melford, Ipswich, England, GB
Imidazole	ThermoScientific, Waltham, MA, USA
Isopropyl β-D-1-thiogalactopyranoside (IPTG)	Sigma, St. Louis, MO, USA

Chemical reagents	Manufacturer
Laemmli buffer	Sigma, St. Louis, MO, USA
Luria-Bertani (LB) medium	Sigma, St. Louis, MO, USA
Luria-Bertani (LB) agar	Sigma, St. Louis, MO, USA
Magnesium chloride	Sigma, St. Louis, MO, USA
Methanol	Sigma, St. Louis, MO, USA
Nickel sulphate	ThermoScientific, Waltham, MA, USA
Phosphate-buffered saline (PBS)	Sigma, St. Louis, MO, USA
PhosStop phosphatase inhibitor cocktail tablets	Roche, Basel, Switzerland
Ponceau S stain solution	Sigma, St. Louis, MO, USA
Pre-stained protein marker, broad range (7-175KDa)	New England Biolabs, Ipswich, MA, USA
Propidium iodide solution	Sigma, St. Louis, MO, USA
PVDF (polyvinylidene difluoride) membrane	GE Healthcare, Chicago, IL, USA
Non-fat dry milk powder	Tesco PLC, Welwyn Garden City, England, GB
Sodium chloride	Sigma, St. Louis, MO, USA
Sodium citrate	Sigma, St. Louis, MO, USA
Sodium-dodecyl-sulphate (SDS)	Sigma, St. Louis, MO, USA
SYBR Safe	Roche, Basel, Switzerland
Thrombin	Melford, Ipswich, England, GB
Triton X-100	Sigma, St. Louis, MO, USA
Trizma base	Sigma, St. Louis, MO, USA
Trypsin/EDTA solution	Lonza, Basel, Switzerland
Tween 20	Sigma, St. Louis, MO, USA
Urea	Melford, Ipswich, England, GB
Western blot chemiluminescence reagent	SuperSignal West Pico, Thermo Scientific

Table 12. List of SDS-PAGE gels and reagents.

Reagent	6% separating gel (9 ml)	10% separating gel (9 ml)	12% separating gel (9 ml)	15% separating gel (9ml)	4% stacking gel (1.5 ml)
H_2O	5.22 ml	4.32 ml	3.87 ml	3.2 ml	1.1 ml
30% acrylamide	1.35 ml	2.25 ml	2.7 ml	3.375 ml	187.5 µl
1.5 M Tris [pH 8.8]	2.25 ml	2.25 ml	2.25 ml	2.25 ml	-
0.5 M Tris [pH 6.8]	-	-	-	-	200 µl
10% APS	90 µl	90 µl	90 µl	90 µl	15 µl
10% SDS	90 µl	90 µl	90 µl	90 µl	15 µl
TEMED	3.6 µl	3.6 µl	3.6 µl	3.6 µl	1.5 µl

2.2 **Methods**

Cell Culture

The cells used in this study include: HCT.shctrl (stable HCT116 human colorectal carcinoma cells knockdown control), HCT.shATR and HCT.shCaspase-10 (stable HCT116 human colorectal carcinoma cells knockdowns), and HCT.p53-/- (HCT116 knockout). All cell lines are derivatives of the HCT116 cells (human colorectal carcinoma cells) (ATCC®). The details of the HCT116 cell line characteristics are summarised in Table 13.

Table 13. Characteristics of the HCT116 cell line (ATCC®).[1]

Characteristic	Description
Organism	*Homo sapiens*
Tissue	Colon
Morphology	Epithelial
Culture properties	Adherent
Disease	Colorectal carcinoma
Age	Adult
Gender	Male
p53 tumor suppressor status	Wild type
Ras proto-oncogene status	Mutated in codon 13

[1] Retrieved from the American Type Culture Collection (ATCC) webpage (https://www.lgcstandards-atcc.org/en.aspx).

The HCT.shctrl, HCT.shATR and HCT.shCaspase-10 and HCT.p53-/- were grown in McCoy's 5A medium. Upon reaching 70-80% confluence, the cells were washed with 5 ml 1 x PBS (phosphate buffer saline). The cells were then trypsinised by addition of 2 ml

of trypsin/EDTA solution followed by incubation for 2-5 minutes at room temperature until the cells detached from the culture flask. Next, 12 ml of fresh medium was added to neutralise the trypsin/EDTA solution. 2 ml of suspended cells were transferred into a new flask containing 12 ml of fresh medium (sub-culturing ratio = 1:6). The cells were incubated at 37ºC and 5% CO_2. The sub-culturing of the cells was performed every 3 days.

Generation of Stable Knockdown Cell Lines

The HCT116 derived stable knockdown cell lines were generated in the Mohr/Zwacka laboratory using RNA interference (RNAi). In order to knock down the target genes, the small hairpin (sh) motifs, which are listed in Table 14, were used.

Table 14. Small hairpin motifs used for generation of stable HCT116 knockdowns.

Target gene	Small hairpin motif	Reference
ATR (shATR)	5′–GATCCCCGGCGTCGTCTCAGCTCGTCT TCAAGAGAGACGAGCTGAGACGACGCC TTTTTGGAAA–3′	Ariumi et al. (2005)
Caspase-10 (shCaspase-10)	5′–GCATTGACTCAGAGAACTTAA–3′	Mohr et al. (2018)

Sense and antisense oligos containing the short-hairpin sequences and 5' and 3' overhangs with the *BbsI* and *EcoRI* sites, respectively, were hybridised to generate double stranded DNA (dsDNA) fragments. The generated dsDNA fragments were then cloned into a modified pU6.ENTR plasmid (Life Technologies). The resulting pU6.ENTR plasmids were utilised to generate the pAd.sh vectors using the LR Clonase II system (Life Technologies) and the pBlockiT.sh plasmids (Life Technologies), which were then used to generate stable knockdown cell lines. For stable knockdowns generation, transection of the respective pBlockiT.sh plasmids into cells was performed using the

FuGene HD system (Promega). The transfected cells were then grown for three days and split into selection medium supplemented with blasticidin. Arising clones were picked, transferred to 24-well tissue culture plates and assessed for gene silencing using Western blot. A cell line generated with empty vectors, namely HCT.shctrl, was utilised as RNAi control.

Drug Treatments

In order to induce apoptosis, cells at 50-60% confluence were subjected to treatment with (I) 5-Fluorouracil (PBS) at 200 µM concentration and (II) etoposide (DMSO) at 100 µM concentration. The cells were then incubated at 37ºC and 5% CO_2 for 24 h. In order to induce inhibition of selected proteins, cells were exposed to (I) ATM inhibitor KU55933 (DMSO) at 2 µM concentration, (II) ATR inhibitor AZD6738 (DMSO) at 2 µM concentration or (III) Chk1/Chk2 inhibitor CHIR124 (DMSO) at 250 nM concentration. The cells were pre-treated with respective inhibitors 30 minutes prior to the addition of 5-FU or etoposide at the concentrations described above. The cells were then incubated at 37ºC and 5% CO_2 for 24 h.

Western Blot

In order to prepare cell extracts, cells were treated with 5-FU alone (24 h), 5-FU plus ATR inhibitor AZD6738 (24 h) or/and ATM inhibitor KU55933 (24 h), etoposide alone (24 h), 5-FU or etoposide plus Chk1/Chk2 inhibitor CHIR124 (24 h). Cells were harvested after 24 h, washed with PBS and lysed in Triton X-100 cellular lysis buffer for 20 min on ice. The lysates were centrifuged at RCF=17000 for 10 min at 4°C. Protein concentration was determined by using Pierce® BCA Protein Assay Kit (ThermoScientific) and following the manufacturer's protocol. Equal amounts of protein samples (50 µg of protein) were separated in 6%, 10% or 12% SDS-PAGE. Transfer of proteins onto PVDF

membrane (GE Healthcare) was performed at 60 mA constant current for 40 min. The transfer was visualised by using Ponceau S stain. The PVDF membrane was incubated in blocking buffer (3% non-fat dry milk solution TBST buffer) for 1 h at room temperature followed by incubation in primary antibody (1:1000 dilution) at 4ºC overnight. Next day, the blots were washed in TBST buffer (three times for 5 min) and incubated in secondary antibody (1:5000 dilution) for 1 h at room temperature. Following another wash in TBST buffer (three times for 5 min), the membrane was incubated in enhanced chemiluminescence substrate (SuperSignal™ West Pico Trial Kit (ThermoScientific) for 30 sec and visualised by using Fusion-FX Chemiluminescence System (Vilber Lourmat).

DNA Hypodiploidy/Nicoletti Assay (Apoptosis Measurement)

Apoptosis measurement was performed according to Nicoletti et al. (1991) (DNA hypodiploidy assay). After 48 h of treatment with 5-FU alone, Chk1 inhibitor CHIR124 alone or in combination with 5-FU, cell culture supernatant, PBS wash-solution and trypsinised cells were collected and centrifuged at RCF=2300 for 1 min. The cells were resuspended and lysed in 200 µl Nicoletti buffer (50 µg/ml propidium iodide, 0.1% (w/v) sodium citrate, 0.1% (w/v) Triton X-100). The fluorescence intensity was measured by using BD Accuri C6 flow cytometer (BD Biosciences) and analysed by Venturi One software. For each sample, 1000 events were measured, and each measurement was repeated three times.

Cloning into Expression Vector pET-28a

The ΔDEDs segments of caspase-10, caspase-8 and cFLIP-L genes (hereafter referred to as ΔDEDs caspase-10 (wild type), ΔDEDs caspase-8 (wild type) and ΔDEDs cFLIP-L (wild type)) and the gene of full-length FADD (hereafter referred to as FADD-FL) were amplified by PCR. The primers for PCR reactions were designed to generate DNA

inserts with desired restriction enzyme sites at their ends. The resulting PCR products were subcloned into pGEM-T-Easy vector and transformed into *E. coli* TOP10 competent cells. Selected bacteria clones were analysed for the presence of the desired inserts, which were then cut from the pGEM-T-Easy constructs by using restriction digest.

The ΔDEDs caspase-10 (wild type), ΔDEDs caspase-8 (wild type) and ΔDEDs cFLIP-L (wild type) fragments were inserted into the *Nde1* and *BamH1* sites of pET-28a vector. The ΔDEDs caspase-10 (C401A), ΔDEDs caspase-10 (D415A), ΔDEDs caspase-8 (C360A) and ΔDEDs caspase-8 (D374A/D384A) variants were then generated by using the QuickChange II site-directed mutagenesis kit (Stratagene). The FADD-FL insert was cloned into the *Nco1* and *EcoR1* sites of the pET-28a vector. The constructs were validated by sequencing.

Conditions for insert amplifications and site-directed mutagenesis are summarised in the Tables 15 and 16, respectively.

Table 15. Components list and conditions for insert amplification by using PCR.

Component	20 µl reaction	Conditions
Nuclease-free water	15 µl	Initial denaturation: 95ºC, 2 min
PCR master mix buffer (10x)	2 µl	Denaturation: 95ºC, 30 s
Forward primer (20 µM)	1 µl	Annealing: 58ºC, 30 s
Reverse primer (20 µM)	1 µl	Elongation: 72ºC, 50 s
DNA template (~20 ng/µl)	1 µl	Number of cycles: 25

Table 16. Components list and conditions for site-directed mutagenesis.

Component	30 µl reaction	Conditions
Nuclease-free water	21.6 µl	Initial denaturation: 95ºC, 2 min
Reaction buffer (10x)	3 µl	Denaturation: 95ºC, 50 s
DMSO	1.8 µl	Annealing: 60ºC, 1 min
dNTPs	0.6 µl	Elongation: 72ºC, 13 min
Forward primer (75 ng/µl)	1 µl	Final extension: 72ºC, 10 min
Reverse primer (75 ng/µl)	1 µl	Number of cycles: 25
DNA template (~15 ng/µl)	1 µl	

Forward (FP) and reverse (RP) primers used for PCR amplification and site-directed mutagenesis are listed in the Tables 17 and 18, respectively.

Table 17. Primers list for PCR amplification of ΔDEDs caspase-10 (wild type), ΔDEDs caspase-8 (wild type), ΔDEDs cFLIP-L (wild type) and FADD-FL inserts (pET-28a system).

Construct	Restriction sites	PCR primers
pET-28a / ΔDEDs caspase-10 (wild type)	Nde1, BamH1	FP: **CATATG**AGTGAATCACAGACTTTGGAC RP: **GGATCC**TCAATCAGAAGGGAAGAC
pET-28a / ΔDEDs caspase-8 (wild type)	Nde1, BamH1	FP: **CATATG**GTTAAGACATTCTTGGAAGCC RP: **GGATCC**CTAGGAAACGCTGCTCCACC
pET-28a / ΔDEDs cFLIP-L (wild type)	Nde1, BamH1	FP: **CATATG**AAAGAACAAAGACTTAAGGAAC RP: **GGATCC**TTATGTGTAGGAGAGGATAAG
pET-28a / FADD-FL	Nco1, EcoR1	FP: **CCATGG**ACCCGTTCCTGGTGCTGC RP: **GAATTC**GACGCTTCGGAGGTAGATG

Table 18. Primers list for site-directed mutagenesis of the ΔDEDs caspase-10 and ΔDEDs caspase-8 constructs (pET-28a system).

Construct	Site-directed mutagenesis primers
pET-28a / ΔDEDs caspase-10 (C401A)	FP: ATCCAGGCC**GCC**CAAGGTGAAGAG RP: CTCTTCACCTTG**GGC**GGCCTGGAT
pET-28a / ΔDEDs caspase-10 (D415A)	FP: ATCGAAGCA**GCC**GCTCTGAACCCT RP: AGGGTTCAGAGC**GGC**TGCTTCGAT
pET-28a / ΔDEDs caspase-8 (C360A)	FP: ATTCAGGCT**GCC**CAGGGGGATAA RP: TTATCCCCCTG**GGC**AGCCTGAAT
pET-28a / ΔDEDs caspase-8 (D374A/D384A)	FP (374A): GTTGAGACT**GCC**TCAGAGGAGCAA RP (374A): TTGCTCCTCTGA**GGC**AGTCTCAAC FP (384A): TTAGAAATG**GCC**TTATCATCACCT RP (384A): AGGTGATGATAA**GGC**CATTTCTAA

Cloning into Expression Vector pGEX-4T-3

Empty pGEX-4T-3 vector was modified by insertion of DNA sequences containing C-terminal (His)$_6$ tag with thrombin or TEV site into *Sal1* and *Not1* sites of the plasmid. These DNA fragments were generated by hybridization of sense and antisense oligonucleotides encoding for the thrombin-(His)$_6$ or TEV-(His)$_6$ peptides. The oligonucleotides were designed to generate the respective restriction enzyme overhangs after hybridization. The ΔDEDs caspase-8 (C360A), ΔDEDs caspase-10 (C401A), ΔDEDs caspase-10 (D415A) and ΔDEDs cFLIP-L (wild type) inserts were generated by PCR amplification and subcloned into pGEM-T-Easy in the same manner as described for the pET-28a system. The inserts were then cut from the pGEM-T-Easy constructs by using restriction digests.

The resulting ΔDEDs caspase-8 (C360A), ΔDEDs caspase-10 (C401A), ΔDEDs caspase-10 (D415A) and ΔDEDs cFLIP-L (wild type) fragments were then cloned into

BamH1 and *Sal1* sites of the pGEX-4T-3/thrombin-(His)$_6$ and pGEX-4T-3/TEV-(His)$_6$ backbones. Additionally, ΔDEDs cFLIP-L (D376A) variants were generated by site-directed mutagenesis. The constructs were validated by sequencing.

PCR and site-directed mutagenesis were performed as described previously for pET-28a constructs. Components and conditions for each reaction are summarised in the Tables 15 and 16.

Oligonucleotides used for hybridization and primers used for PCR amplification and site-directed mutagenesis are listed in the Tables 19, 20 and 21, respectively.

Table 19. Oligonucleotides list for generation on thrombin-(His)$_6$ or TEV-(His)$_6$ peptides used for modification of the pGEX-4T-3 vector.

Peptides	Restriction sites	Oligonucleotides
Thrombin-(His)$_6$	Sal1, Not1	Forward: **TCGACCTGGTGCCGCGCGGCAGC**GGCAGCAGCCATCATCATC ATCATCACAGCA**GC** Reverse: **GGCCGC**TGCTGTGATGATGATGATGATGGCTGCTGCC**GCTGC CGCGCGGCACCAGG**
TEV-(His)$_6$	Sal1, Not1	Forward: **TCGACGGAGAAAATCTTTATTTTCAAGGT**GGCAGCAGCCATC ATCATCATCATCACAGCA**GC** Reverse: **GGCCGC**TGCTGTGATGATGATGATGATGGCTGCTGCC**ACCTT GAAAATAAAGATTTTCTCCG**

Table 20. Primers list for PCR amplification of the ∆DEDs caspase-8 (C360A), ∆DEDs caspase-10 (C401A and D415A) and ∆DEDs cFLIP-L (wild type) inserts (pGEX-4T-3 system).

Construct	Restriction sites	PCR primers
pGEX-4T-3 / ∆DEDs caspase-8 (C360A)	BamH1, Sal1	FP: **GGATCC**AGTGAATCACAGACTTTGGAC RP: **GTCGAC**ATCAGAAGGGAAGACAAG
pGEX-4T-3 / ∆DEDs caspase-10 (C401A and D415A)	BamH1, Sal1	FP: **GGATCC**GTTAAGACATTCTTGGAAGCC RP: **GTCGAC**GGAAACGCTGCTCCACCTGC
pGEX-4T-3 / ∆DEDs cFLIP-L (wild type)	BamH1, Sal1	FP: **GGATCC**AAAGAACAAAGACTTAAGGAAC RP: **GTCGAC**TGTGTAGGAGAGGATAAGTTTC

Table 21. Primers list for site-directed mutagenesis of the ∆DEDs cFLIP-L construct (pGEX-4T-3 system).

Construct	Site-directed mutagenesis primers
pGEX-4T-3 / ∆DEDs cFLIP-L (D376A)	FP: GCCTCTTGGAGGTG**GCT**GGGCCAGCGATGAAG RP: CTTCATCGCTGGCCC**AGC**CACCTCCAAGAGGC

Preparation of *E. coli* Competent Cells

The *E. coli* competent cells were prepared by transferring 200 µl of *E. coli* TOP10 strain preculture grown overnight at 37ºC into 10 ml LB Broth. Following incubation at 37ºC for 2 h, the culture was centrifuged at RCF=2103 for 10 min. Bacteria cells were resuspended in 5 ml of chilled 100 mM CaCl₂. After being incubated for 30 min on ice, cells were centrifuged at RCF=2103 for 10 min. Then, the resuspension, incubation and centrifugation steps were repeated. Finally, bacteria cells were resuspended in 500 µl of 100 mM CaCl₂ and incubated on ice for 1 h.

Transformation of *E. coli*

For transformation of *E. coli*, protein expression vectors or DNA ligations were used. The amount of DNA inserts required for ligation reactions was calculated by using the following formula:

$$ng\ of\ insert = \frac{ng\ of\ vector\ x\ insert\ size\ (bp)\ x\ F}{vector\ size\ (bp)}/insert\ concetration\ (\frac{\mu g}{\mu l})$$

$F = vector\ to\ insert\ molar\ ratio$

DNA ligations were performed using a standard protocol. 100 µl of *E. coli* competent cells and 1 µl of expression vectors (25-50 ng/µl) or 4 µl of DNA ligations were mixed and then incubated on ice for 30 min. In order to heat-shock bacteria cells, the bacteria and DNA mixture was incubated at 42ºC for 30 s in a water bath. Then, the mixture was put back on ice for 2 min. Following addition of 300 µl of SOC medium, the mixture was incubated on a shaker at 37ºC for 1 h. Finally, the mixture was plated onto agar plates containing ampicillin (pGEM-T-Easy constructs), ampicillin and chloramphenicol (pGEX-4-T3 constructs) or kanamycin (pET-28a constructs). The plates were incubated at 37ºC overnight.

Protein Expression with pET-28a Constructs

Cultures of *E. coli* BL21(DE3) (*E. coli* strain B F$^-$ dcm ompT hsdS(r$_B^-$ m$_B^-$) gal λ(DE3)) competent cells were used for expression of the ΔDEDs caspase-10 (wild type), ΔDEDs caspase-10 (C401A), ΔDEDs caspase-10 (D415A), ΔDEDs caspase-8 (wild type), ΔDEDs caspase-8 (C360A), ΔDEDs caspase-8 (D374A/D384A), ΔDEDs cFLIP-L (wild type) and FADD-FL constructs. Cell cultures were grown at 37ºC for 2-3 h in LB Broth containing kanamycin. When cultures density (OD) reached A$_{600}$ = 0.6-0.8, protein

expression was induced by addition of isopropyl β-D-1-thiogalactopyranoside (IPTG) to the final concentration of 0.02 mM for ΔDEDs caspase-10 (C401A) and ΔDEDs caspase-10 (D415A), and 0.1 mM for ΔDEDs caspase-10 (wild type), ΔDEDs caspase-8 (wild type), ΔDEDs caspase-8 (C360A), ΔDEDs caspase-8 (D374A/D384A), ΔDEDs cFLIP-L (wild type) and FADD-FL. Cell cultures were shaken at 18°C for 15 h (overnight). The details of protein expression conditions for each construct are summarised in Table 22.

Table 22. List of expression conditions for pET-28a constructs.

Construct	Medium	IPTG	Temp.	Time
ΔDEDs caspase-10 (wild type)	LB medium	0.1 mM	18°C	15 h (overnight)
ΔDEDs caspase-10 (C401A)	LB medium + 1% glucose	0.02 mM	18°C	15 h (overnight)
ΔDEDs caspase-10 (D415A)	LB medium + 1% glucose	0.02 mM	18°C	15 h (overnight)
ΔDEDs caspase-8 (wild type)	LB medium or LB medium + 1% glucose	0.1 mM	18°C	15 h (overnight)
ΔDEDs caspase-8 (C360A)	LB medium	0.1 mM	18°C	15 h (overnight)
ΔDEDs caspase-8 (D374A/D384A)	LB medium	0.1 mM	18°C	15 h (overnight)
ΔDEDs cFLIP-L (wild type)	LB medium	0.1 mM	18°C	15 h (overnight)
FADD-FL	LB medium	0.1 mM	18°C	15 h (overnight)

Protein Expression with pGEX-4T-3 Constructs

Cultures of *E. coli* BL21-RIL (*E. coli* strain B F⁻ ompT hsdS(r_B^- m_B^-) dcm+ Tet^r gal endA Hte [argU ileY leuW Cam^r]) competent cells were used for expression of the control GST/thrombin-C-(His)$_6$ ΔDEDs caspase-8 (C360A), ΔDEDs caspase-10 (C401A), ΔDEDs caspase-10 (D415A), ΔDEDs cFLIP-L (wild type) and ΔDEDs cFLIP-L (D376A) constructs. Cell cultures were grown at 37°C for 2-3 h in LB Broth containing

chloramphenicol and ampicillin. When cultures density (OD) reached A_{600} = 0.6-0.8, protein expression was induced by addition of IPTG to the final concentration of 0.1 mM. Cell cultures were shaken at 30°C for 3 h. The details of protein expression conditions for each construct are summarised in Table 23.

Table 22. List of expression conditions for pGEX-4T-3 constructs.

Construct	Medium	IPTG	Temp.	Time of expression
GST/thrombin-C-(His)$_6$	LB medium	0.1 mM	30°C	3 h
ΔDEDs caspase-8 (C360A)	LB medium	0.1 mM	30°C	3 h
ΔDEDs caspase-10 (C401A)	LB medium	0.1 mM	30°C	3 h
ΔDEDs caspase-10 (D415A)	LB medium	0.1 mM	30°C	3 h
ΔDEDs cFLIP-L (wild type)	LB medium	0.1 mM	30°C	3 h
ΔDEDs cFLIP-L (D376A)	LB medium	0.1 mM	30°C	3 h

Lysis Conditions

Following protein expression, bacteria cultures were harvested by centrifugation at RCF=3578 for 10 min, resuspended in cold lysis buffer (50 mM Tris, 100 mM NaCl, 1 mM EDTA, 50 mM MgCl$_2$), stirred for 30 min and disrupted by sonication (pulsing: 30 s, rest: 30 s, number of cycles: 20) at 4°C. The cell debris and inclusion bodies were separated from soluble fraction by high-speed centrifugation at RCF=15.821 for 30 min at 4°C. In order to determine the level of protein solubility, lysate, supernatant and cell pellet samples were analysed on 12% or 15% SDS-PAGE. The gels were stained in Coomassie Brilliant Blue buffer for minimum 1 h (up to 15 h overnight) at room temperature with gentle agitation. Then, the gels were destained in Coomassie destain buffer for a minimum of 1 h (up to 15 h overnight) at room temperature with gentle

agitation. Due to accumulation of expressed proteins in insoluble inclusion bodies, cell pellets were collected for solubilisation under denaturing conditions.

Inclusion Bodies Solubilisation

Bacteria inclusion bodies harbouring desired proteins were resuspended in 25 ml solubilisation buffer (6 m GuHCl or 8 M urea, 500 mM NaCl, 20 mM Trizma base, [pH 8.0]; Table 22) and stirred for 1 h followed by sonication for 10 cycles with 30 s pulsing and 30 s rest at 4°C, and centrifugation at RCF=15821 for 20 min at 4°C to separate cell debris. After centrifugation, supernatants were collected, and cell pellets were resuspended in 25 ml solubilisation buffer followed by sonication and centrifugation steps as previously. Supernatants were collected for purification on IMAC (5 ml Ni-NTA column, GE Healthcare).

Table 23. List of inclusion bodies solubilisation methods.

Proteins – pET-28a system	Solubilisation method
ΔDEDs caspase-10 (wild type)	**GuHCl**
ΔDEDs caspase-10 (D415A)	**GuHCl**
ΔDEDs caspase-8 (wild type)	**GuHCl**
ΔDEDs caspase-8 (C360A)	**GuHCl or Urea**
ΔDEDs cFLIP-L (wild type)	**GuHCl**
FADD-FL	**GuHCl**
Proteins – pGEX-4T-3 system	**Solubilisation method**
ΔDEDs caspase-10 (D415A)/thrombin-C-(His)$_6$	**Urea**
ΔDEDs cFLIP-L (D376A)/thrombin-C-(His)$_6$	**Urea**

Protein Purification

Supernatants containing desired proteins were loaded at 1-2 ml/min flow-rate onto IMAC (5 ml Ni-NTA) column (GE Healthcare) pre-equilibrated with Buffer D and washed with Buffer D at 2-3 ml/min flow-rate using manual pump. Flow-through was collected. The column was disconnected and attached to AKTA PrimePlus. Linear urea gradient (100 ml, 100 % gradient) using Buffers D and A was then carried out to refold the proteins immobilised in Ni-NTA matrix. The refolding was performed at 1 ml/min flow-rate. Elution was performed with linear imidazole gradient (50 - 100 ml, 100 % gradient) using Buffers A and B, which were applied at 2 ml/min until UV plateaus. Protein eluates were collected as 5 ml fractions, pooled and dialysed overnight at 4°C in Buffer C. The dialysed supernatant was concentrated at RCF=3739 at 4°C in Centricon tubes (Vivaspin 20, 10 kDa MWCO) to ~10 ml. The N-$(His)_6$ tag (pET-28a system) or N-GST and C-$(His)_6$ tags (pGEX-4T-3 system) of successfully purified proteins were removed by adding 125 units of thrombin (Sigma) followed by slow rotation overnight at 4°C. The supernatants were then re-applied onto IMAC column in the same manner as previously described. The flow-through fractions containing the proteins of interest were collected, concentrated to 2 ml in Centricon tubes (Vivaspin 20, 10 kDa MWCO) and further fractionated at 0.8 ml/min flow-rate on SEC (120 ml Superdex 75 16/60 column) column (GE Healthcare), pre-equilibrated with Buffer C. Selected protein eluates in the major elution peak at 280 nm were collected as 2 ml fractions, pooled and examined for purity on 12% or 15% SDS-PAGE. The gels were stained in Coomassie Brilliant Blue buffer and destained in Coomassie destain buffer in the same manner as previously described. In order to further confirm the presence of the desired proteins, selected protein fractions were subjected to Western blot analysis or mass spectrometry. Fractions containing the proteins of interest were concentrated, subjected to circular dichroism spectroscopy and stored as 200 μl aliquots at -20°C.

Mass Spectrometry

In order to confirm identity of purified proteins, matrix-assisted laser desorption/ionisation (MALDI) mass spectrometry analysis was carried out. The protein of interest, which was purified using column chromatography and suspended in Buffer C, was loaded and run on 12% SDS-PAGE. The gel was stained in Coomassie Brilliant Blue buffer and destained in Coomassie destain buffer in the same manner as previously described, followed by thorough wash in water. The gel was cut around the band of interest and the resulting gel slice was subsequently reduced, followed by digestion into peptides using trypsin. The peptides were separated using liquid chromatography (nano-flow LC system with reverse phase column). Determination of masses and confirmation of sequences of the peptides were carried oud using an Orbitrap Elite MS/MS spectrometer, which was coupled to the liquid chromatography device. In order to confirm the identity and origin of analysed protein, the detected peptide sequences were then matched against a protein database. All MALDI analyses and sample preparations were performed at the Functional Genomics and Proteomics Facility, School of Biosciences, University of Birmingham.

Circular Dichroism Spectroscopy

Chirascan Circular Dichroism Spectrometer (Applied Photophysics) was set up according to the manufacturer's protocol. Required parameters for circular dichroism data measurement were set up by using Chirascan software and included: (I) temperature at 20°C, (II) wavelength range from high = 245 nm to low = 195 nm and (III) wavelength interval at 0.2. In order to determine the spectrum of the sample buffer (background), 200 μl of Buffer C was aliquoted into a quartz cuvette (path length = 0.1 cm) and measured. For sample measurements, 200 μl of purified protein (protein of interest in Buffer C) at a concentration between 1 – 200 μM was aliquoted into a quartz

cuvette (path length = 0.1 cm). The circular dichroism spectra of the desired protein samples were collected in triplicates and averaged by using Chirascan software.

Protein Concentration Calculations

Concentrations of the purified proteins were determined spectrophotometrically using protein absorbance (A) measurements at 280 nm wavelength and extinction coefficient values (ε). The absorbance measurements were performed at 20°C using a Cary 60 UV-visible spectrophotometer (Varian). In order to calibrate the spectrophotometer to zero absorbance, 1 ml of Buffer C was transferred into a quartz cuvette (path length = 1cm) and measured. Then, 1 ml of purified protein (protein of interest in Buffer C) was aliquoted into a quartz cuvette (path length = 1cm) and the absorbance of the sample was recorded. The extinction coefficient of the protein of interest was calculated using the ProtParam tool (https://web.expasy.org/protparam). Finally, the protein concentration was determined using Beer-Lambert formula:

$$A = \varepsilon\, l\, c$$

A – absorbance (A_{280})

ε - extinction coefficient ($M^{-1}\, cm^{-1}$)

l – path (cm)

c – concentration (M)

FADD / Caspase-8 Protein Pull-Down Assay

Purified C-(His)$_6$-tagged FADD-FL (bait protein) and untagged ΔDEDs caspase-8 (C360A) (prey protein) were mixed at equimolar ratio of 10 μM in a total volume of 1 ml of the reaction buffer (50 mM Trizma base, 100 mM NaCl, [pH 7.4]) and incubated for 1 h at room temperature. The mixture was applied at 1 ml/min flow-rate onto the 5 ml Ni-

NTA column, pre-equilibrated with Buffer A. The column was attached to AKTA PrimePlus and 3-step washing was performed at 1-2 ml/min flow-rate by using: (I) 10 ml of Buffer A, (II) 30 ml of linear salt gradient (100% gradient; Buffers A and A*) and 10 ml of Buffer A**. Each wash step was collected as a separate fraction and concentrated at RCF=3739 at 4°C in Centricon tubes (Vivaspin 20, 10 kDa MWCO) to ~1 ml. Elution was performed with linear imidazole gradient (50 ml, 100% gradient) by using Buffers A** and B, which were applied at 1-2 ml/min. Protein eluates were collected as 10 ml fractions and concentrated in the same manner as wash fractions. Equal volumes (30 μl) of wash and elution fractions were loaded on 15% SDS-PAGE and analysed by Western blot.

As a control, purified C-(His)$_6$-GST tag (bait protein) and untagged ΔDEDs caspase-8 (C360A) (prey protein) were mixed at equimolar ratio of 10 μM in a total volume of 1 ml of the reaction buffer (50 mM Trizma base, 100 mM NaCl, [pH 7.4]) and incubated for 1 h at room temperature. The protein pull-down assay for the control mixture was performed in the same manner as for C-(His)$_6$-tagged FADD-FL and untagged ΔDEDs caspase-8 (C360A), followed by 15% SDS-PAGE and Western blot analysis.

The details of the protein pull-down assay and reagents used are summarised in Table 25.

Table 24. List of proteins and reagents used for FADD / caspase-8 protein pull-down assay.

Reaction mixture	• 10 µM C-(His)$_6$-tagged FADD-FL + 10 µM untagged ∆DEDs caspase-8 (C360A) • 10 µM C-(His)$_6$-tagged GST + 10 µM untagged ∆DEDs caspase-8 (C360A) – control
Reaction conditions	50 mM Tris, 100 mM NaCl, [pH 7.4], 1 h, room temperature
Column details	IMAC 5 ml His-trap FF nickel-nitrilotriacetic (Ni-NTA) acid-sepharose column, pre-equilibrated with Buffer A
Wash 1	10 ml of Buffer A (50 mM Trizma base, 500 mM NaCl, 20 mM imidazole, [pH 7.5]
Wash 2	30 ml linear salt gradient (100%) – Buffer A and A* (50 mM Trizma base, 1 M NaCl, 20 mM imidazole, [pH 7.5])
Wash 3	10 ml Buffer A** (50 mM Trizma base, 500 mM NaCl, 80 mM imidazole, [pH 7.5])
Elution	50 ml linear imidazole gradient – Buffers A** and B (50 mM Trizma base, 500 mM NaCl, 500 mM imidazole, [pH 7.5])

Caspase-10 / Caspase-8 Activity Assay

1 µM of purified untagged ∆DEDs caspase-10 (D415A) (enzyme) and 10 µM of purified untagged ∆DEDs caspase-8 (C360A) (substrate) were mixed in a total volume of 250 µl of the reaction buffer (50 mM Trizma base, 150 mM NaCl, 10% PEG, 0.1% CHAPS, [pH 7.4]) and incubated at room temperature. At noted timepoints, 30 µl of the reaction was aliquoted into the loading buffer, in order to stop the reaction and prepare samples for analysis by using 15% SDS-PAGE and Western blot.

In order to optimise the buffer and reaction conditions for the assay, 1 µM of purified untagged ∆DEDs caspase-10 (D415A) (enzyme) mixed with 10 µM of purified untagged ∆DEDs caspase-8 (C360A) (substrate) were tested at physiological conditions (50 mM Trizma base, 100 mM NaCl, [pH 7.4]. 10 µM of purified untagged ∆DEDs caspase-8 (C360A) alone was used as a control and tested at physiological conditions (50 mM Trizma base, 100 mM NaCl, [pH 7.4], stabilising conditions (50 mM Trizma base, 150

mM NaCl, 10% PEG, 0.1% CHAPS, [pH 7.4]) and in the presence of kosmotropic salts

(50 mM Trizma base, 150 mM NaCl and 1 M sodium citrate, [pH 7.4]). As previously, 30

μl of the reaction was aliquoted into the loading buffer at noted timepoints, followed by

analysis on 15% SDS-PAGE and Western blot.

The details of reactions and reagents used are summarised in Tables 26, 27 and 28.

Table 25. Conditions and timepoints list for ΔDEDs caspase-8 (C360A)/ΔDEDs caspase-10 (D415A) control assay.

Reaction	1 μM untagged ΔDEDs caspase-10 (D415A) + 10 μM untagged ΔDEDs caspase-8 (C360A)	Timepoints (minutes)
Physiological conditions	50 mM Trizma base, 150 mM NaCl, [pH 7.4]	• 0, 10, 40 160 (Fig. 48)

Table 26. Conditions and timepoints list for ΔDEDs caspase-8 (C360A) control assay.

Reaction	10 μM untagged ΔDEDs caspase-8 (C360A) – control	Timepoints (minutes)
Physiological conditions	50 mM Trizma base, 150 mM NaCl, [pH 7.4]	• 0, 10, 40 160 (Fig. 48) • 0, 0.5, 1, 1.5, 2, 3, 4, 5, 10 (Fig. 49A and B) • 0, 0.5, 1, 1.5, 2, 5, 10 (Fig. 50)
Stabilising conditions	50 mM Trizma base, 150 mM NaCl, 10% PEG, 0.1% CHAPS, [pH 7.4]	• 0, 0.5, 1, 1.5, 2, 5, 10 (Fig. 49B)
Addition of kosmotropic salts	50 mM Trizma base, 150 mM NaCl, 1 M sodium citrate, [pH 7.4]	• 0, 0.5, 1, 1.5, 2, 5, 10 (Fig. 50)

Table 27. Conditions and timepoints for ΔDEDs caspase-10 (D415A) / ΔDEDs caspase-8 (C360A) activity assay.

Reaction	1 μM untagged ΔDEDs caspase-10 (D415A) + 10 μM untagged ΔDEDs caspase-8 (C360A)	Timepoints (minutes)
Stabilising conditions	50 mM Trizma base, 150 mM NaCl, 10% PEG, 0.1% CHAPS, [pH 7.4]	• 0, 0.5, 1, 1.5, 2, 5, 10 (Fig. 43)

Statistical Analysis

Collected data sets were summarised in tables by using Microsoft Excel. The data were organised and presented based on various factors, such as cell line, cytotoxic drug type and dose, treatment duration and date of measurement. The statistical calculations, including mean, sum and standard deviation were then performed. Finally, experimental data were expressed as mean values ± standard error of mean (S.E.M.).

The following formula was used for calculation of the standard error bars:

$$S.E.M. = \pm \frac{SD}{\sqrt{n}}$$

SD - standard deviation

n – number of samples or datapoints

In order to perform significance analyses, the means between two or more groups of values were compared by using single-factor analysis of variance (single-factor ANOVA). In this analysis, the null hypothesis that "equal means of each sample" was tested. The significance was then assessed based on calculated p-values (probability values), which express the probability of obtaining a greater or equal mean difference between two groups, when compared with the observed values (assuming that the null

hypothesis it true). In this analysis, p<0.05 was considered as significant and p<0.001

as highly significant, meaning that the higher the p-value, the lower the significance.

CHAPTER 3

RESULTS – PART I

Functional Analysis of the Main Constituents of the

FADDosome Complex *In Vitro*

3.1. Design and Establishment of Protein Expression Constructs by Using pET-28a Vector

In order to reconstitute the FADDosome complex and to study the functional relationships and interactions of the main molecular constituents of the FADDosome *in vitro*, it was essential to express human caspase-10, caspase-8, cFLIP-L and FADD as recombinant proteins in *E. coli* and to purify them on chromatography columns.

In this study, as suggested by Stennicke and Salvesen (1999), and Denault and Salvesen (2002), the pET-expression system was used for recombinant production of the proteins of interest. The authors have demonstrated that using the pET vectors led to the successful expression of proteins and allowed to obtain very high yields. In this study, the pET-28a vector was used in this study due to the presence of N-terminal and optional C-terminal $(His)_6$-tags, which allows flexibility when designing and establishing expression constructs (Figure 14). In the pET-28a vector, the target genes are subcloned downstream of the T7 bacteriophage promoter and the lac operator (Figure 14). The vector containing the genes of interest is transformed into bacterial host, which contains the T7 polymerase gene controlled by the lacUV5 promoter. Synthesis of the T7 polymerase and the subsequent expression of genes under the T7 promoted is induced by addition of IPTG (Denault and Salvesen (2002).
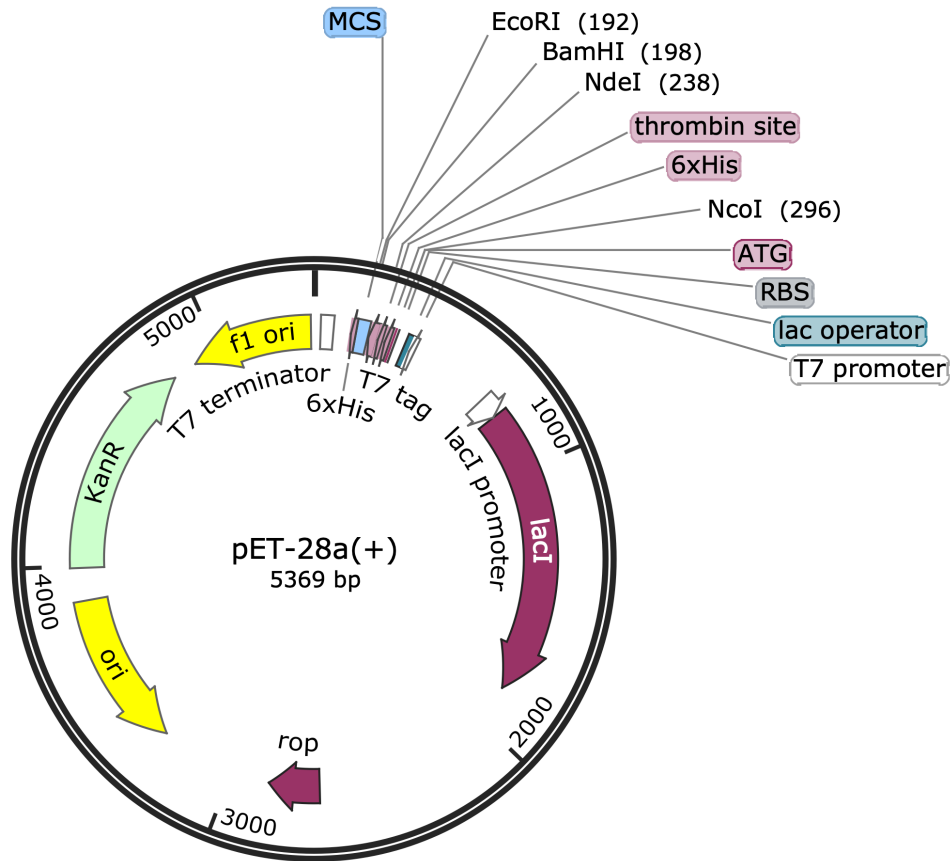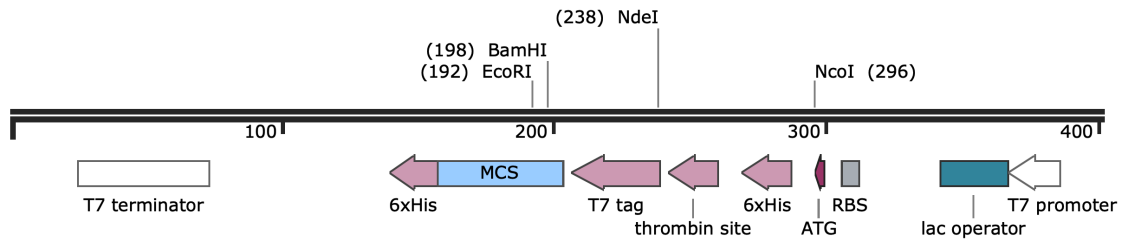
Figure 14. Schematics of an empty pET-28a vector.
A. Map of the vector with its main features **B.** Detailed schematics of the Multiple Cloning Site with indication of restrictions sites positions for enzymes used during cloning of desired DNA constructs.

Caspases and cFLIP-L proteins consist of domains, which include N-terminal death effector domains (DED1 and DED2) and active subunits: p18 and p10 for caspase-8, p18 and p12 for caspase-10 and caspase-like subunit for cFLIP-L. An adaptor protein FADD is composed of one DED domain and death domain (DD) (Figure 15 A, B, C and D). It is believed that the DED domains are necessary for interactions between these proteins (Carrington et al., 2006; Riley et al., 2015). Thus, in the present study, it was hypothesised that within the FADDosome, caspase-10, caspase-8, cFLIP-L and FADD would possibly associate in the DED-dependent manner. With respect to this, the initial aim was to express full-length recombinant proteins, containing their DED domains and active subunits. The recombinant expression of full-length caspase-10 and caspase-8 was successful and led to production of good levels of the desired proteins (data not shown). Nevertheless, purification of the proteins of interest resulted in obtaining very poor or no yields (data not shown). It was assumed that this was possibly caused by protein instability and/or degradation. With respect to this, a different strategy for recombinant protein production was needed.

Therefore, the death effector domains (DEDs) of caspase-10, caspase-8 and cFLIP-L were excluded in the DNA constructs (Figure 15A, B and C), similar to the recombinant proteins designed and produced by others (Stennicke and Salvesen, 1997; Garcia-Calvo et al., 1999; Boatright et al., 2004; Yu et al., 2009; Wachmann et al., 2010). The authors have shown that recombinant DED-truncated caspase-10, caspase-8 and cFLIP-L, which were expressed in *E. coli* and purified by liquid chromatography, can be functional without their DEDs *in vitro*. It was demonstrated that caspase-10 and caspase-8, which lacked their DEDs remained active and had the ability to process their substrates or other proteins *in vitro* (Stennicke and Salvesen, 1997; Garcia-Calvo et al., 1999; Boatright et al., 2004; Yu et al., 2009). Moreover, exclusion of DEDs in the caspase-10, caspas-8 and cFLIP-L constructs can be advantageous, as it might help facilitate the recombinant protein production. It was described that DEDs might undergo oligomerisation, which

greatly reduces solubility and increases toxicity levels of the proteins expressed in *E. coli* (Denault and Salvesen, 2002; Keller et al., 2009).

As the aim of this study was to analyse the functional relationships and interactions between caspase-10, caspase-8, cFLIP-L and FADD in terms of the FADDosome formation, it was crucial to express and purify different variants of the recombinant proteins. For this, the following variants were designed: ΔDEDs caspase-10 (wild type), ΔDEDs caspase-10 (C401A active site mutant), ΔDEDs caspase-10 (D415A linker mutant), ΔDEDs caspase-8 (wild type), ΔDEDs caspase-8 (C360A active site mutant), ΔDEDs caspase-8 (D374A/D384A linker mutant), ΔDEDs cFLIP-L (wild type), ΔDEDs cFLIP-L (D376A cleavage mutant) and FADD-FL (Figure 15A, B, C and D). Depending on experimental design, active site mutations allow to study the role of selected proteins as substrates in the reaction, whereas linker mutations allow to investigate biologic activity of selected proteins and their role as enzymes/activators in the reaction.

Mutation at C401A (active site mutation) abolishes the proteolytic activity of ΔDEDs caspase-10 and thus, prevents processing of other proteins and autocleavage. Mutation at D415A (linker mutation) prevents ΔDEDs caspase-10 from being cleaved by other proteins (Figure 15A). For ΔDEDs caspase-8, substitution at C360A (active site mutation) abolishes the proteolytic activity of the protein. This prevents processing of other proteins and autocleavage. Two substitutions at D374A/D384A (linker mutation) prevent ΔDEDs caspase-8 from being cleaved by other proteins (Figure 15B). In case of ΔDEDs cFLIP-L, mutation at D376A, which has been demonstrated to function as a preferred cleavage site for pro-caspase-8 (Yu et al*.,* 2009), it prevents cFLIP-L from being processed by caspase-8 (Figure 15C). The FADD-FL construct does not contain any mutations (Figure 15D), as they have not been reported to possess any (auto-) proteolytic activity.
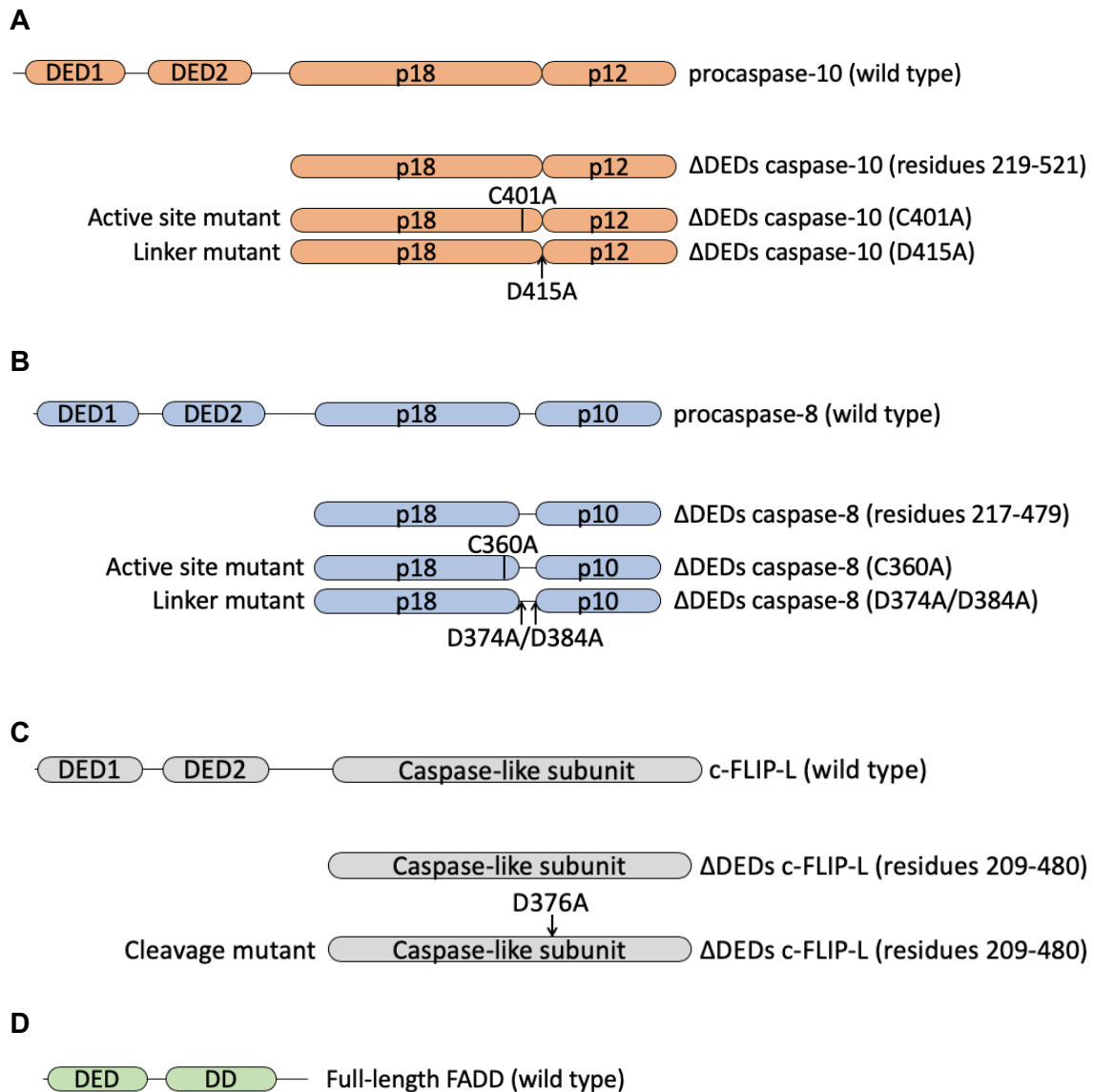
Figure 15. Schematic representation of human recombinant protein constructs used in this study.

A. The ΔDEDs caspase-10 construct without mutation and with single amino acid substitution at C401A (abolishes the proteolytic activity of ΔDEDs caspase-10 and therefore, prevents processing of other proteins and autocleavage) or at D415A (linker mutation, which prevents ΔDEDs caspase-10 from being cleaved by other proteins). All constructs are compared with wild type pro-caspase-10 variant. All subunits are defined as orange rectangles with rounded corners. **B.** The ΔDEDs caspase-8 construct without mutation and single amino acid substitutions at C360A or D374A/D384A. The substitution at C360A abolishes the proteolytic activity of ΔDEDs caspase-8 and therefore, prevents processing of other proteins and autocleavage. Two substitutions at D374A/D384A prevent ΔDEDs caspase-8 from being cleaved by other proteins. All subunits are defined as blue rectangles with rounded corners. **C.** The ΔDEDs cFLIP-L construct without mutation and with a single amino acid substitution at D376A. The substitution at D376A, which has been shown to be a preferred cleavage site for pro-caspase-8 (Yu et al.*,* 2009) prevents cFLIP-L from being processed by caspase-8. All subunits are defined as grey rectangles with rounded corners. **D.** The FADD-FL construct without mutation. All subunits are defined as green rectangles with rounded corners. *DED - death effector domain, DD - death domain.*

ΔDEDs caspase-10 (wild type) DNA fragment was cloned into *Nde1* and *BamH1* sites of the pET-28a vector. The construct was used to generate the ΔDEDs caspase-10 (C401A), ΔDEDs caspase-10 (D415A) variants by site-directed mutagenesis. As a result, the N-termini of all proteins were fused to a (His)$_6$ tag, which can be removed by thrombin treatment (Figure 16A and B).

A
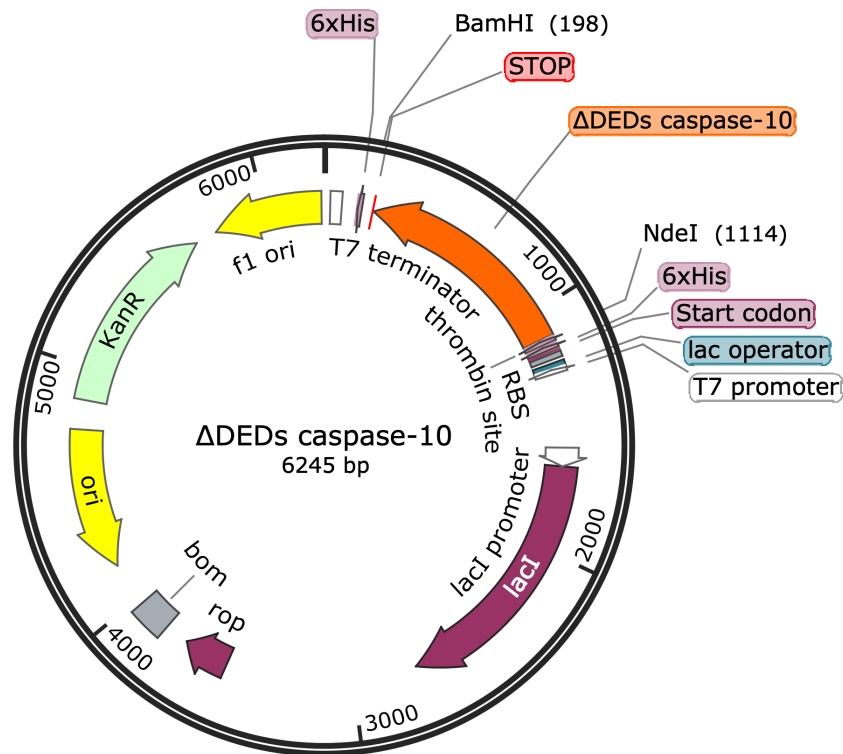
B
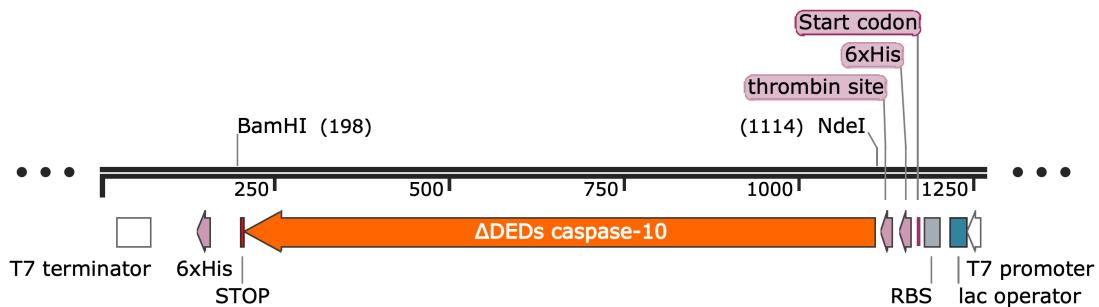
Figure 16. Map of the ΔDEDs caspase-10/pET-28a construct.
A. The ΔDEDs caspase-10 (wild type) gene was inserted into *Nde1* and *BamH1* sites of the pET-28a vector. The ΔDEDs caspase-10 (C401A), ΔDEDs caspase-10 (D415A) variants were generated by site-directed mutagenesis. **B.** Detailed schematics of the ΔDEDs caspase-10 insert with N-terminal (His)$_6$ tag and thrombin site for tag removal.

ΔDEDs caspase-8 (wild type) DNA segment was inserted into *Nde1* and *BamH1* sites of the pET-28a vector. Then, the ΔDEDs caspase-8 (C360A), ΔDEDs caspase-8 (C374A/D384A) variants were generated by site-directed mutagenesis. Thus, the N-termini of all proteins were fused to a $(His)_6$ tag, which can be removed by addition of thrombin (Figure 17A and B).

A
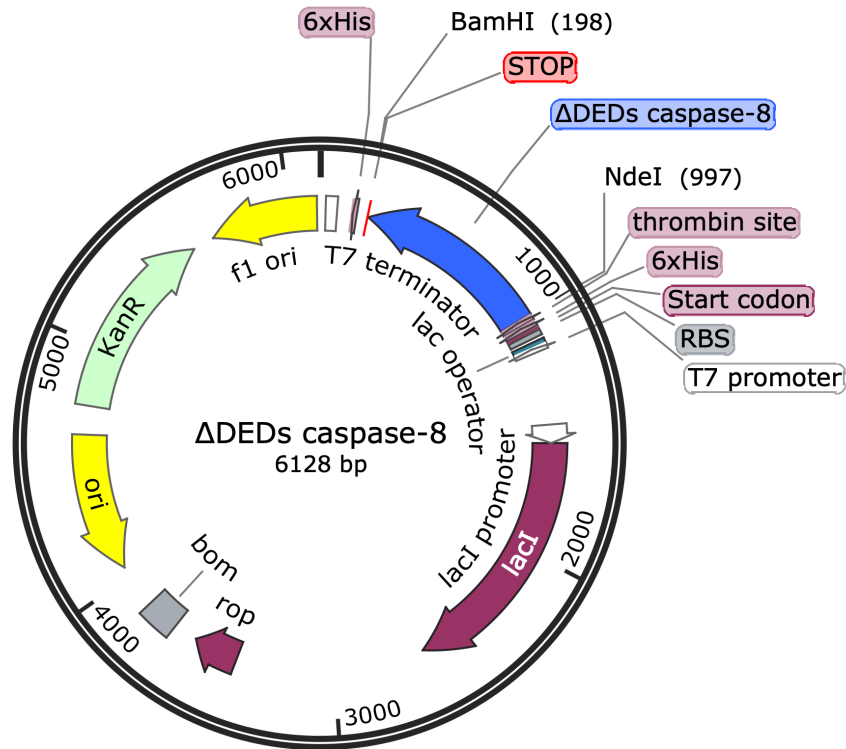
B
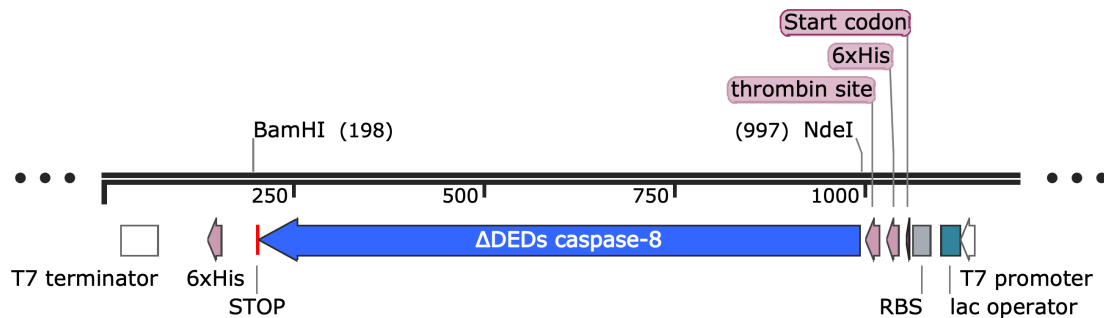
Figure 17. Map of the ΔDEDs caspase-8/pET-28a construct.
A. The ΔDEDs caspase-8 (wild type) gene was inserted into *Nde1* and *BamH1* sites of the pET-28a vector. The ΔDEDs caspase-8 (C360A), ΔDEDs caspase-8 (D374A/D384A) variants were generated by site-directed mutagenesis. **B.** Detailed schematics of the ΔDEDs caspase-8 insert with N-terminal $(His)_6$ tag and thrombin site for tag removal.

ΔDEDs cFLIP-L (wild type) DNA construct was cloned into *Nde1* and *BamH1* sites of the pET-28a vector. As a result, the N-terminus of the protein was fused to a (His)$_6$ tag, which can be cleaved off by using thrombin treatment (Figure 18A and B).

A
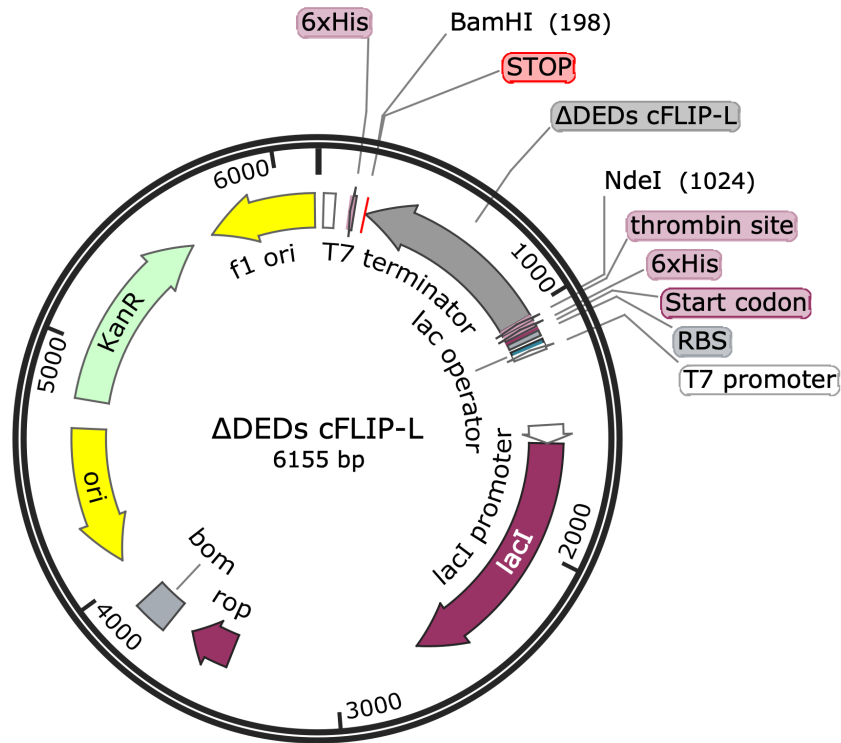
B
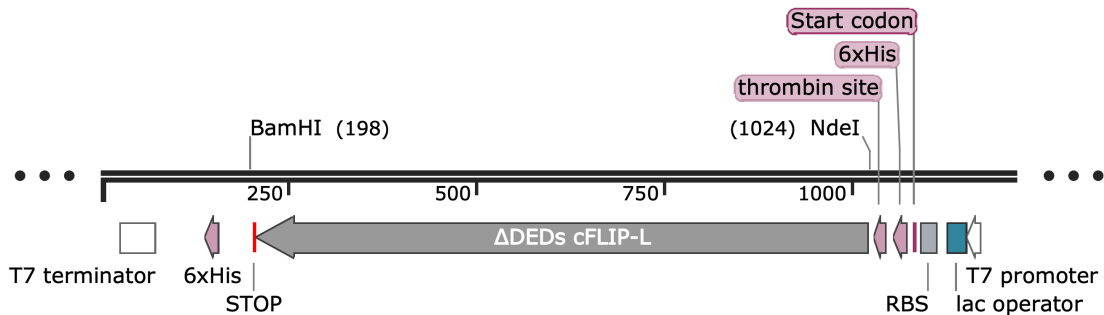
Figure 18. Map of the ΔDEDs cFLIP-L/pET-28a construct.
A. The ΔDEDs cFLIP-L gene (wild type) was inserted into *Nde1* and *BamH1* sites of the pET-28a vector. **B.** Detailed schematics of the ΔDEDs cFLIP-L insert with N-terminal (His)$_6$ tag and thrombin site for tag removal.

The FADD-FL gene (Figure 19) was cloned into *Nco1* and *EcoR1* sites of the pET-28a vector. In this construct, the C-terminus of the protein is fused to an uncleavable (His)$_6$ tag (Figure 19).

A
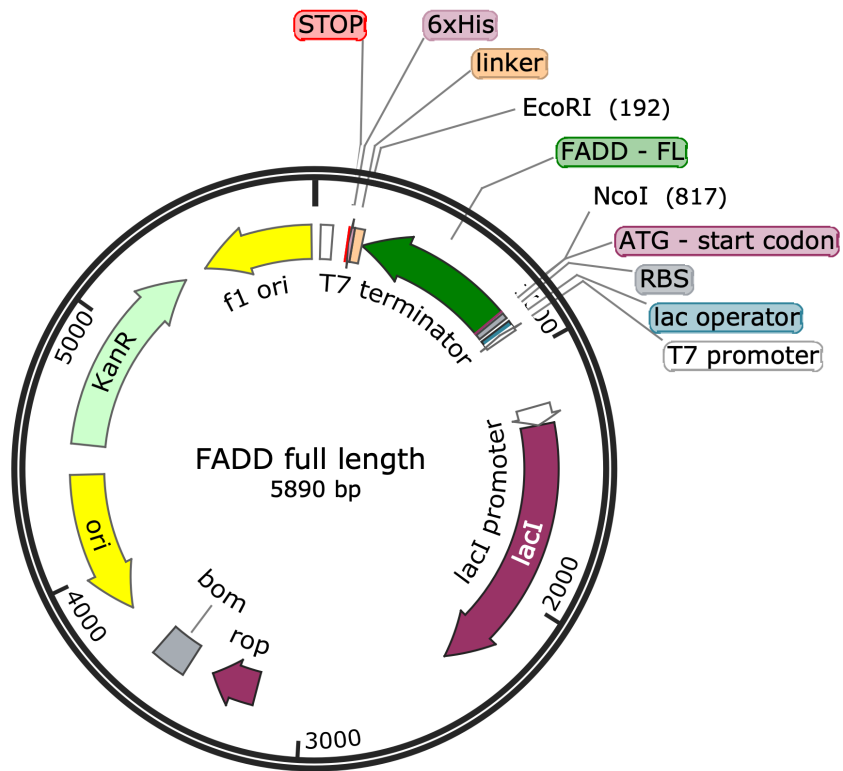
B
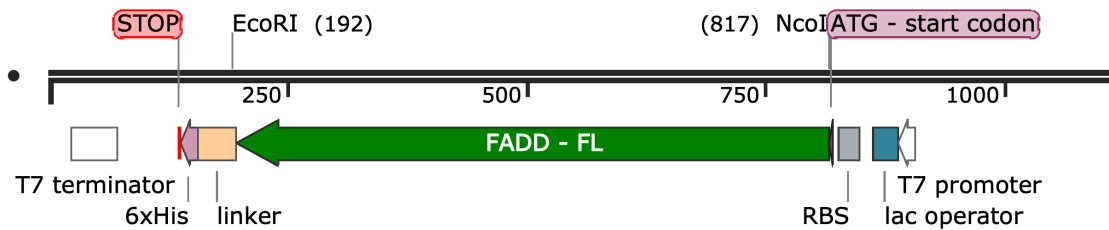
Figure 19. Map of the FADD-FL/pET-28a construct.
A. The FADD-FL gene was inserted into *Nco1* and *EcoR1* sites of the pET-28a vector **B.** Detailed schematics of the FADD-FL insert with C-terminal (His)$_6$ tag.

3.2. Expression of Human Recombinant ΔDEDs Caspase-10 (wild type), ΔDEDs Caspase-8 (wild type), ΔDEDs cFLIP-L (wild type) and FADD-FL

The main goals of the protein expression procedure are to obtain high yields of protein and maximum production of soluble protein per cell. Therefore, it was crucial to test and optimise expression conditions for each protein construct to achieve the most efficient production.

As a host for protein expression, *E. coli* strain BL21(DE3) was used. BL21(DE3) cells are known to allow an easy protein expression induction and are suitable for high-level protein expression. These bacteria are lysogens of the bacteriophage λDE3 and therefore, carry a DNA fragment containing the lacI gene, the lacUV5 promoter, and the T7 RNA polymerase gene. Transcription of the T7 RNA polymerase gene is controlled by the lacUV5 promoter, which is inducible by addition of IPTG. Initiation of T7 RNA polymerase expression leads to expression of recombinant genes inserted downstream of the T7 promoter in the pET-28a vector.

When selecting expression conditions for recombinant proteins production, the following parameters were considered: IPTG concentration, temperature and the time of expression. High IPTG concentrations (1 mM final concentration or above) and high temperature (37°C) allow rapid protein expression in a short period of time, however such conditions often lead to production of insoluble or misfolded proteins, which in turn aggregate in inclusion bodies. Therefore, induction with low IPTG concentrations and expression at lower temperatures for longer period of time (such as 15 h, overnight) are recommended in order to facilitate production of soluble proteins (Garcia-Calvo et al., 1999; Denault and Salvesen, 2002).

As a starting point, induction with 0.1 mM (final concentration) of IPTG, and expression at 18°C for 3h and 15 h were tested. The constructs that were tested for recombinant protein expression included: ΔDEDs caspase-10 (wild type), ΔDEDs caspase-8 (wild type), ΔDEDs cFLIP-L (wild type) and FADD-FL.

Tables 29-32 summarise the basic information regarding protein expression constructs and expected protein masses after expression and purification.

Table 29. Main features of the human recombinant ΔDEDs caspase-10 (wild type) construct with expected protein masses after expression.

Protein Details	
DNA Construct	ΔDEDs caspase-10 (aa residues 220-521; wild type) pET-28a, N-terminal (His)$_6$-tag
Host Cell Strain	BL21(DE3)
Tagged Protein MW (kDa)	35
Untagged Protein MW (kDa)	33

Table 30. Main features of the human recombinant ΔDEDs caspase-8 (wild type) construct with expected protein masses after expression.

Protein Details	
DNA Construct	ΔDEDs caspase-8 (aa residues 217-479; wild type) pET-28a, N-terminal (His)$_6$-tag
Host Cell Strain	BL21(DE3)
Tagged Protein MW (kDa)	31
Untagged Protein MW (kDa)	29

Table 31. Main features of the human recombinant ΔDEDs cFLIP-L (wild type) construct with expected protein masses after expression.

Protein Details	
DNA Construct	ΔDEDs cFLIP-L (aa residues 208-480; wild type), pET-28a, N-terminal (His)$_6$-tag
Host Cell Strain	BL21(DE3)
Tagged Protein MW (kDa)	30
Untagged Protein MW (kDa)	28

Table 32. Main features of the human recombinant FADD-FL construct with expected protein masses after expression.

Protein Details	
DNA Construct	FADD (aa residues 1-208; wild type), pET28a, C-terminal (His)$_6$-tag (non-cleavable)
Host Cell Strain	BL21(DE3)
Tagged Protein MW (kDa)	25
Untagged Protein MW (kDa)	N/A

The ΔDEDs caspase-10 (wild type), ΔDEDs caspase-8 (wild type), ΔDEDs cFLIP-L (wild type) and FADD-FL constructs were transformed into BL21(DE3) cells. After reaching the required OD (A_{600} = 0.6-0.8), small aliquots of whole cell extract (WCE) samples were taken before induction and saved for analysis. Recombinant protein expression was

induced with IPTG, followed by incubation with shaking overnight. In order to analyse the protein expression levels, WCE samples were taken 3 h and 15 h post-induction. The samples were run on 12% SDS-PAGE and stained with Coomassie Brilliant Blue. We observed that the N-(His)$_6$ ΔDEDs caspase-10 (wild type), N-(His)$_6$ ΔDEDs caspase-8 (wild type), N-(His)$_6$ ΔDEDs cFLIP-L (wild type) and C-(His)$_6$ FADD-FL were successfully expressed after 3 h and 15 h. The overnight expression allowed more efficient production, when compared to 3 h induction (Figure 20A, B, C and D).
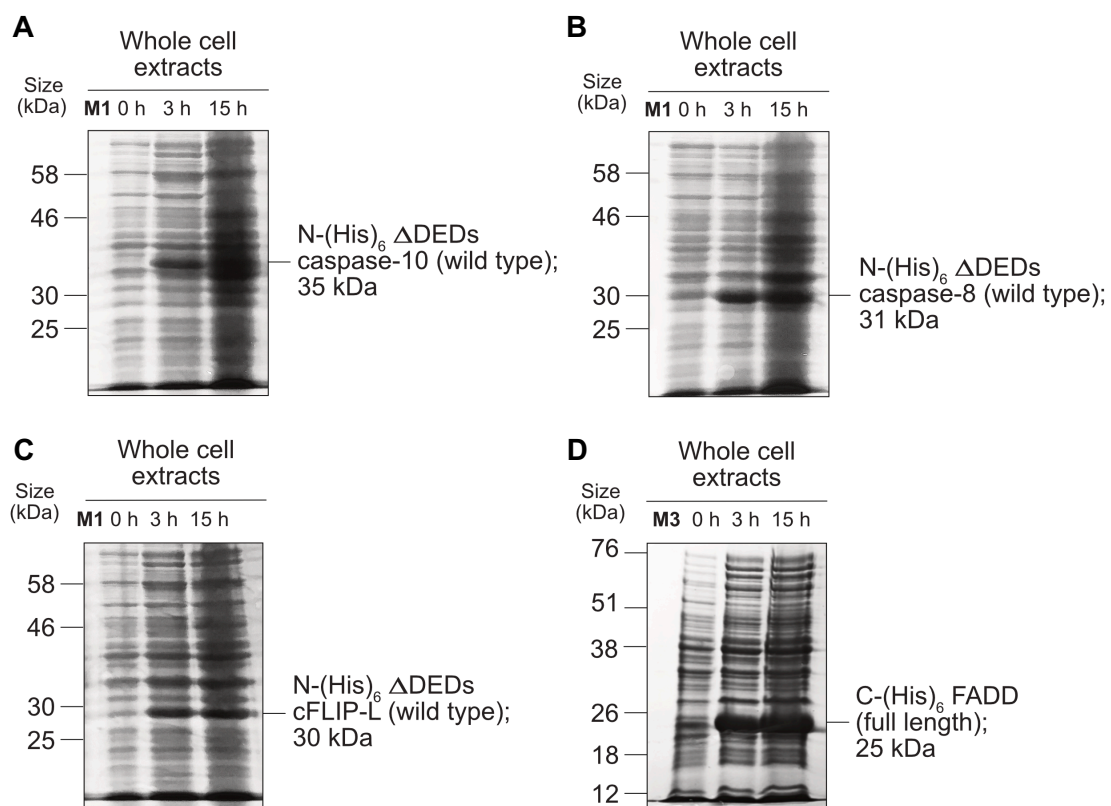
Figure 20. Expression levels of N-(His)$_6$ ΔDEDs caspase-10 (wild type), N-(His)$_6$ ΔDEDs caspase-8 (wild type), N-(His)$_6$ ΔDEDs cFLIP-L (wild type) and C-(His)$_6$ FADD-FL proteins.
A-D. The whole cell extract (WCE) samples were taken before induction as well as 3 h and 15 h post-induction for the analysis of the recombinant N-(His)$_6$ ΔDEDs caspase-10 (wild type), N-(His)$_6$ ΔDEDs caspase-8 (wild type), N-(His)$_6$ ΔDEDs cFLIP-L (wild type) and C-(His)$_6$ FADD-FL expression levels on 12% SDS-PAGE followed by staining with Coomassie Brilliant Blue.
M1 (Marker 1) and M3 (Marker 3) – protein ladders.

In order to assess solubility levels of the expressed proteins, 15 h after expression the bacteria were lysed by sonication. Soluble and insoluble fractions were separated by

centrifugation. Small aliquots of the lysate, supernatant and resuspended pellet fractions were taken for analysis. Our results showed that the highest levels of N-(His)$_6$ ΔDEDs caspase-10 (wild type), N-(His)$_6$ ΔDEDs caspase-8 (wild type), N-(His)$_6$ ΔDEDs cFLIP-L (wild type) and C-(His)$_6$ FADD-FL were found in the resuspended pellets (Figure 21A, B, C, and D), indicative of the formation of inclusion bodies in the bacteria. Therefore, it was essential to isolate and purify the recombination proteins from the inclusion bodies by solubilisation under denaturing conditions (Watt et al., 1999; Keller et al., 2009).
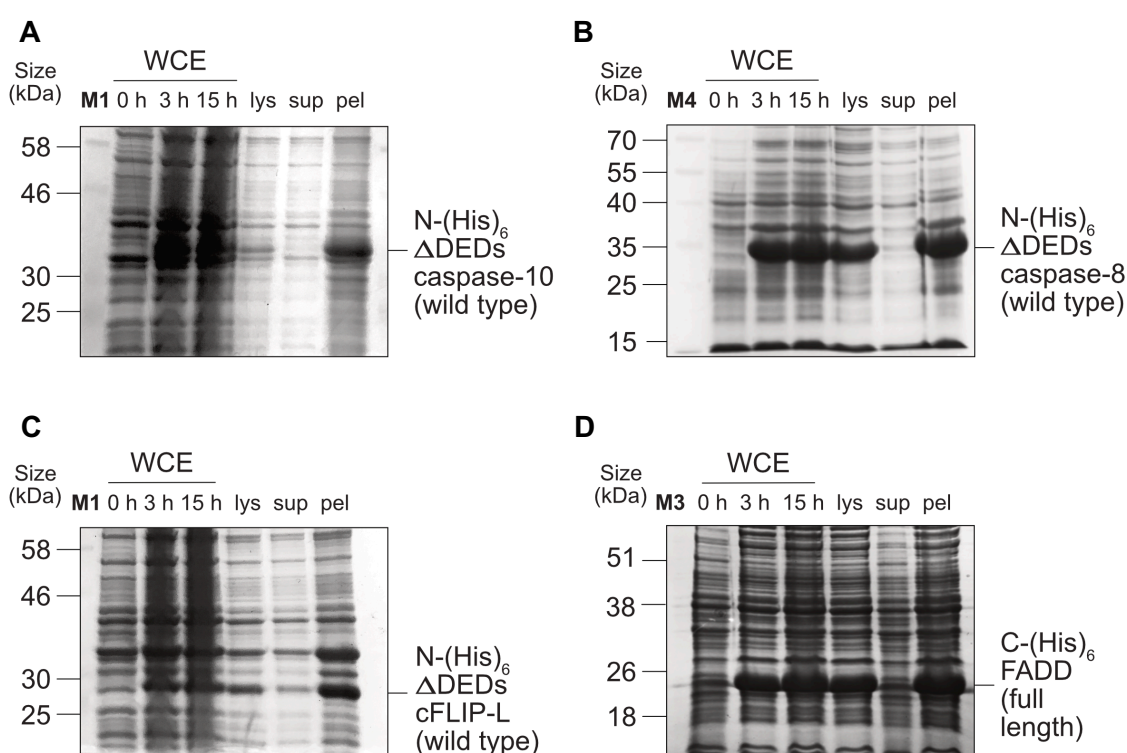
Figure 21. Solubility levels of N-(His)$_6$ ΔDEDs caspase-10 (wild type), N-(His)$_6$ ΔDEDs caspase-8 (wild type), N-(His)$_6$ ΔDEDs cFLIP-L (wild type) and C-(His)$_6$ FADD-FL proteins.
A. After 15 h of N-(His)$_6$ ΔDEDs caspase-10 (wild type) expression, lysate, supernatant and resuspended pellet samples were analysed on 12% SDS-PAGE and staining with Coomassie Brilliant Blue. WCE samples were used as control. **B.** After 15 h of N-(His)$_6$ ΔDEDs caspase-8 (wild type) expression lysate, supernatant and resuspended pellet samples were analysed on 12% SDS-PAGE and staining with Coomassie Brilliant Blue. WCE samples were used as control. **C.** After 15 h of N-(His)$_6$ ΔDEDs cFLIP-L (wild type) expression lysate, supernatant and resuspended pellet samples were analysed on 12% SDS-PAGE and staining with Coomassie Brilliant Blue. **D.** After 15 h of C-(His)$_6$ FADD-FL expression lysate, supernatant and resuspended pellet samples were analysed on 12% SDS-PAGE and staining with Coomassie Brilliant Blue.
M1 (Marker 1), M3 (Marker 3) and M4 (Marker 4) – protein ladders, WCE – whole cell extracts, Lys – lysed cells, Sup – supernatant, Pel – cell pellet.

3.3. Purification of N-(His)$_6$ ΔDEDs Caspase-10 (wild type), N-(His)$_6$ ΔDEDs Caspase-8 (wild type), N-(His)$_6$ ΔDEDs cFLIP-L (wild type) and C-(His)$_6$ FADD-FL

Following solubilisation of inclusion bodies under denaturing conditions, supernatants containing N-(His)$_6$ ΔDEDs caspase-10 (wild type), N-(His)$_6$ ΔDEDs Caspase-8 (wild type), N-(His)$_6$ ΔDEDs cFLIP-L (wild type) and C-(His)$_6$ FADD-FL were separated from cell debris and applied onto 5 ml IMAC (Ni-NTA) column. The immobilised proteins were then washed and refolded on the column by using linear urea gradient (8 M – 0 M urea), which was based on the methods described by Holzinger et al. (1996) and Ni-NTA column manufacturer's protocol. It was described that refolding of immobilised proteins might greatly limit the interactions between the protein molecules and therefore avoid their aggregation, which in contrast happens commonly during refolding in solution (Holzinger et al. 1996). Following the on-column refolding, the proteins of interest were eluted and selected fractions at the major elution peak at 280 nm were pooled and assessed for the protein purity. The samples were separated on 15% SDS-PAGE followed by staining with Coomassie Brilliant Blue.

We observed that N-(His)$_6$ ΔDEDs caspase-10 was successfully purified on the Ni-NTA column (Figure 22A and B). Interestingly, the analysis of elution fractions in the major elution peak unveiled the presence of two protein bands, 18 kDa and 12 kDa. The observation was different from the results obtained for the GuHCl supernatant, pellet and flow-through samples, which only showed a single narrow 35 kDa band (Figure 22A). Sizes of the eluted protein bands are 18 kDa and 12 kDa, what corresponds to the size of the active caspase-10 subunits p18 and p12. Such observation argues for self-

cleavage and activation of N-(His)$_6$ ΔDEDs caspase-10 (wild type) in the solution after purification.

A
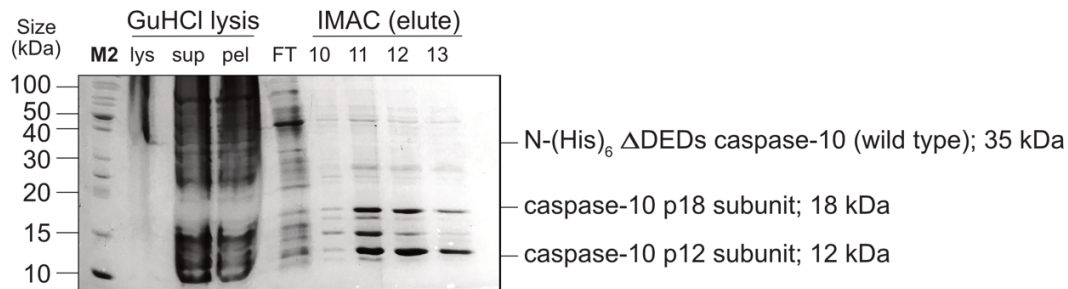
B
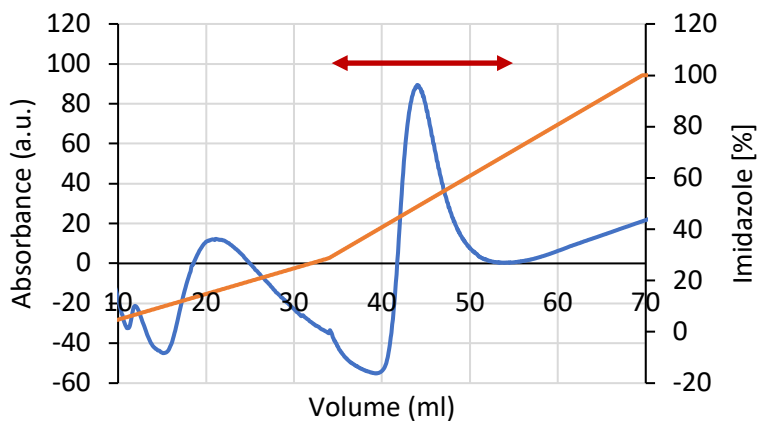
Figure 22. IMAC (Ni-NTA) purification of N-(His)$_6$ ΔDEDs caspase-10 (wild type).
A. Analysis of fractions after purification of N-(His)$_6$ ΔDEDs caspase-10 (wild type) on IMAC 5 ml His-trap FF nickel-nitrilotriacetic (Ni-NTA) column. The fractions show strong bands running at 18 kDa and 12 kDa. After purification, the following samples were taken for the analysis on SDS-PAGE: lysate, supernatant and pellet after GuHCl lysis of inclusion bodies containing the protein of interest, flow-through after IMAC purification as well as elution fractions number: 10, 11, 12 and 13. All samples were separated on 15% SDS-PAGE followed by staining with Coomassie Brilliant Blue. **B.** Elution profile of N-(His)$_6$ ΔDEDs caspase-10 (wild type) on IMAC 5 ml His-trap FF nickel-nitrilotriacetic (Ni-NTA) column; blue line represents protein absorbance; orange line represents imidazole gradient. Elution fractions taken for the SDS-PAGE analysis are indicated by the red arrow.
M2 (Marker 2) – protein ladder, GuHCl – guanidine hydrochloride, Lys – lysed cells, Sup – supernatant, Pel – cell pellet, FT – flow-through.

The 15% SDS-PAGE analysis for N-(His)$_6$ ΔDEDs caspase-8 (wild type) showed a successful protein purification (Figure 23A and B). In this case, analysis of elution fractions in the major elution peak at 280 nm also revealed the presence of two protein bands, 18 kDa and 10 kDa. The observation was in contrast to the results obtained for

the control (WCE) samples, which only showed a single 31 kDa band (Figure 23A). The molecular weights of both bands are consistent with the sizes of the active caspase-8 subunits p18 and p10. Similar to N-(His)$_6$ ∆DEDs caspase-10 (wild type), the result argues for self-activation of N-(His)$_6$ ∆DEDs caspase-8 (wild type) in the solution after purification.

A

B
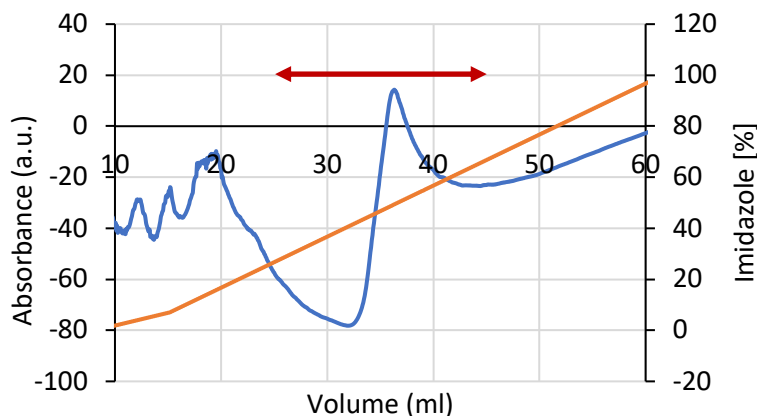
Figure 23. IMAC (Ni-NTA) purification of N-(His)$_6$ ∆DEDs caspase-8 (wild type).
A. Analysis of fractions after purification of N-(His)$_6$ ∆DEDs caspase-8 (wild type) on IMAC 5 ml His-trap FF nickel-nitrilotriacetic (Ni-NTA) column. The fractions reveal strong bands running at 18 kDa and 10 kDa. After purification, the following elution fractions were analysed on 15% SDS-PAGE: 10, 11, 12 and 13. WCE samples were used as controls. All samples were separated on 15% SDS-PAGE followed by staining with Coomassie Brilliant Blue. **B.** Elution profile of N-(His)$_6$ ∆DEDs caspase-8 (wild type) on IMAC 5 ml His-trap FF nickel-nitrilotriacetic (Ni-NTA) column; blue line represents protein absorbance; orange line represents imidazole gradient. Elution fractions taken for the SDS-PAGE analysis are indicated by the red arrow.
***M1** (marker 1) – protein ladder, WCE – whole cell extracts.*

Furthermore, we found that after elution of N-(His)$_6$ ΔDEDs cFLIP-L (wild type) from Ni-NTA column, the levels of purified protein were very low, when analysed on 15% SDS-PAGE and compared with control (WCE) samples (Figure 24A). However, we observed that the major elution peak at 280 nm was quite prominent, indicative of co-purification of other/host proteins (Figure 24B). Therefore, further processing and purification of the N-(His)$_6$ ΔDEDs cFLIP-L (wild type) sample was not continued.

A
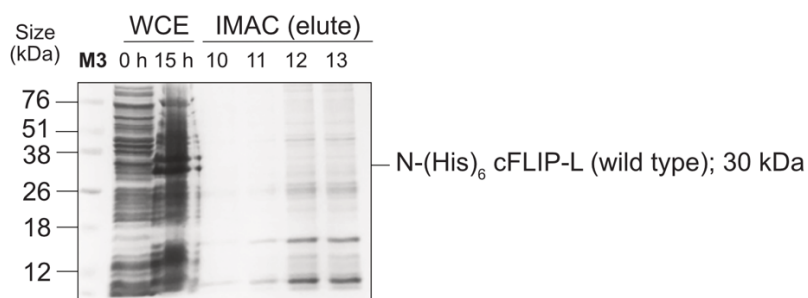
B
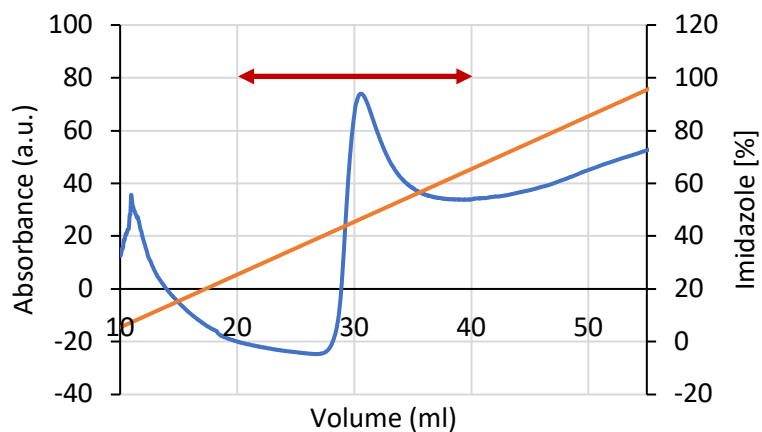
Figure 24. IMAC (Ni-NTA) purification of N-(His)$_6$ ΔDEDs cFLIP-L (wild type).
A. Fractions analysed after purification of N-(His)$_6$ ΔDEDs cFLIP-L (wild type) on IMAC 5 ml His-trap FF nickel-nitrilotriacetic (Ni-NTA) column. The fractions show very low levels of the purified protein at around 30 kDa. Following purification of the desired protein, the WCE (control) samples and Ni-NTA elution fractions number 10, 11, 12 and 13 were analysed by using 15% SDS-PAGE and subsequent staining with Coomassie Brilliant Blue. **B.** Elution profile of N-(His)$_6$ ΔDEDs cFLIP-L (wild type) on IMAC 5 ml His-trap FF nickel-nitrilotriacetic (Ni-NTA) column; blue line represents protein absorbance; orange line represents imidazole gradient. Elution fractions taken for the SDS-PAGE analysis are indicated by the red arrow.
M3 *(marker 3)* – protein ladder, WCE – whole cell extracts.

Analysis on 15% SDS-PAGE showed that C-(His)$_6$ FADD-FL was successfully expressed and purified on Ni-NTA column. Assessed elution fractions in the major elution peak at 280 nm (Figure 25A and B) revealed the presence of one major protein band. The observed 25 kDa band is consistent with the size of the (His)$_6$-tagged protein (Figure 25A). All elution fractions containing the protein of interest were combined into one sample, dialysed and concentrated to 2 ml. Small aliquots of the elute, dialysed and concentrated samples were run on 15% SDS-PAGE followed by staining with Coomassie Brilliant Blue (Figure 25C). Western blot analysis of the same samples confirmed the presence of purified C-(His)$_6$ FADD-FL (Figure 25D).

A

C-(His)$_6$ FADD (full length); 25 kDa

B

C

C-(His)$_6$ FADD (full length); 25 kDa

D

C-(His)$_6$ FADD (full length); 25 kDa
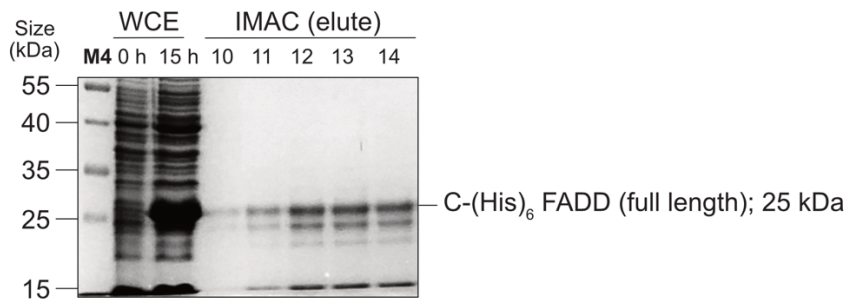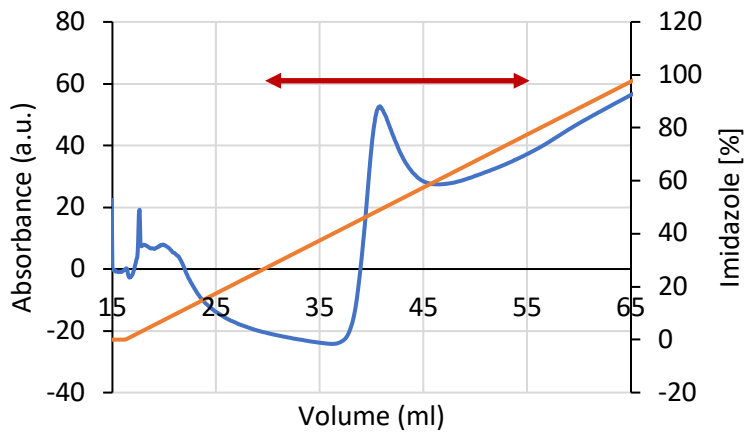
Western blot
(anti-FADD)
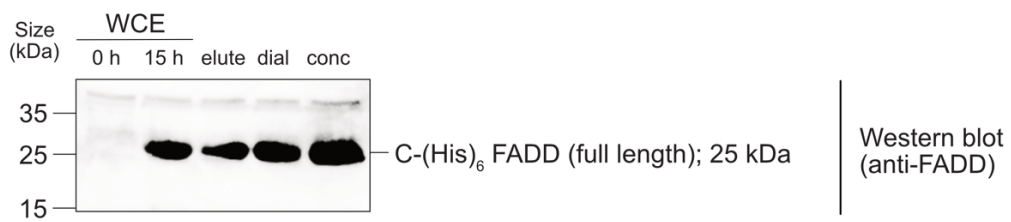
Figure 25. IMAC (Ni-NTA) purification of C-(His)₆ FADD-FL.
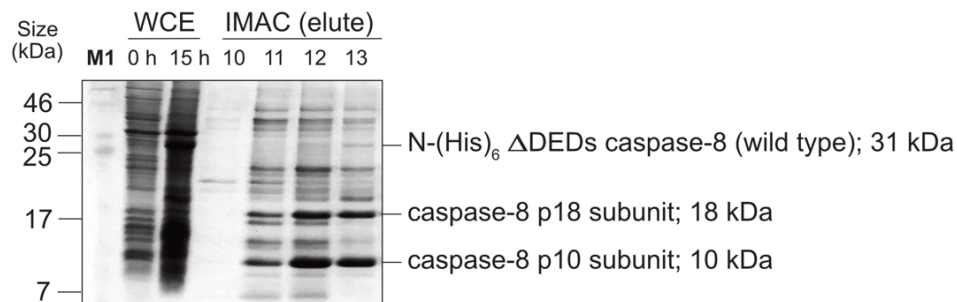**A.** Analysis of fractions after purification of C-(His)₆ FADD-FL on IMAC 5 ml His-trap FF nickel-nitrilotriacetic (Ni-NTA) column. The fractions reveal a strong band running at 25 kDa. Following purification of the protein of interest, the WCE (control) samples and Ni-NTA elution fractions number 10, 11, 12, 13 and 14 were analysed by using 15% SDS-PAGE and subsequent staining with Coomassie Brilliant Blue. **B.** Elution profile of C-(His)₆ FADD-FL on IMAC 5 ml His-trap FF nickel-nitrilotriacetic (Ni-NTA) column; blue line represents protein absorbance; orange line represents imidazole gradient. Elution fractions taken for the SDS-PAGE analysis are indicated by the red arrow. **C.** Ni-NTA fractions containing the desired protein were pooled, dialysed and concentrated for further processing. The elution, dialysed and concentrated protein samples were analysed on 15% SDS-PAGE and staining with Coomassie Brilliant Blue. **D.** The same samples were used for Western blot analysis and confirmation of successfully purified C-(His)₆ FADD-FL. WCE samples were used as controls. An antibody against FADD was used to confirm the presence of the desired protein.
***M4** (marker 4) – protein ladder, WCE – whole cell extracts, dial – dialysed, conc – concentrated.*

The concentrated (2 ml) sample containing C-(His)₆ FADD-FL was subjected to further purification by using SEC (Superdex 75) column. Protein eluates were collected as 2 ml fractions and assessed for purity by using 15% SDS-PAGE followed by staining with Coomassie Brilliant Blue (Figure 26A). Assessment of elution fractions in the major elution peak at 280 nm showed very high purity levels of C-(His)₆ FADD-FL (Figure 26A and B). The presence of the desired protein was also confirmed by Western blot (Figure 26C). Any host proteins that co-purified on Ni-NTA column and co-eluted within the C-(His)₆ FADD-FL peak were not separated by gel filtration and might be present in minimal amounts, acceptable for experimental purposes. Elution fractions containing the protein of interest were pooled, combined into one sample and concentrated in order to obtain 2 ml of the final pure protein sample.

In order to assess whether purified C-(His)₆ FADD-FL was folded, circular dichroism (CD) spectroscopy was carried out. The CD spectrum of the desired protein was obtained using 200 µl of purified protein sample (12 µM), which was transferred to an analytic cuvette and subjected to CD spectroscopy. The collected experimental spectrum of C-(His)₆ FADD-FL was then compared with a calculated spectrum of FADD, which was

obtained using the PDBMD2CD software (Mavridis and Janes, 2016) and the full-length human FADD structure (wild type; aa residues 1 – 191; PDB ID: 2GF5) (Figure 26D). The plotted CD data showed that the experimental spectrum of C-(His)$_6$ FADD-FL exhibited negative peaks from 205 to 225 nm, which was similar to the calculated spectrum of FADD (Figure 26D), indicating that the desired protein was folded and could be used for experimental purposes. It was also observed that in the experimental CD spectrum, the peak at around 208 nm was slightly greater than the peak at round 222 nm, whereas the calculated spectrum had both peaks of a similar value (Figure 26D). It was assumed that such observation was due to a few possible reasons: (I) the presence of C-terminal residues in purified C-(His)$_6$ FADD-FL (aa residues 192 – 208, which were excluded from human FADD, PDB ID: 2GF5) and/or (II) the possible presence of the minimal amounts of host *E. coli* proteins, which could be co-purified on Ni-NTA and SEC within the C-(His)$_6$ FADD-FL peak and affect the CD measurement. Additionally, it was considered, whether the presence of the C-terminal (His)$_6$ tag in the purified protein of interest could also influence its folding and the CD measurement. It was described that (His)$_6$ tag might have some effect on the structure of purified proteins. However, such effect is generally not significant and does not affect the functionality of the proteins (Carson et al., 2007).

A
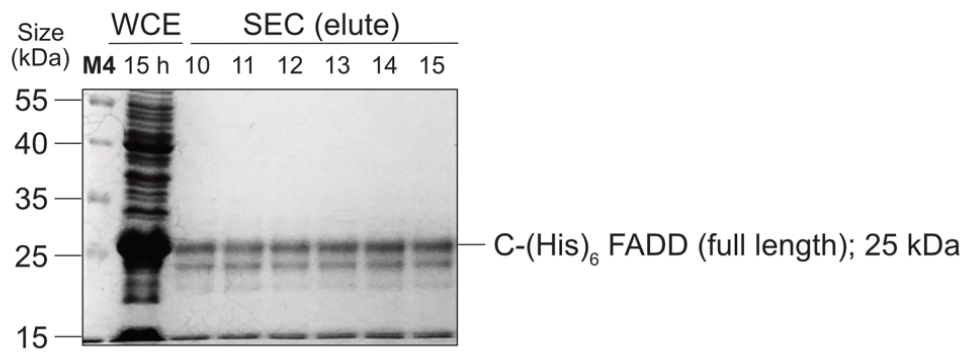
B
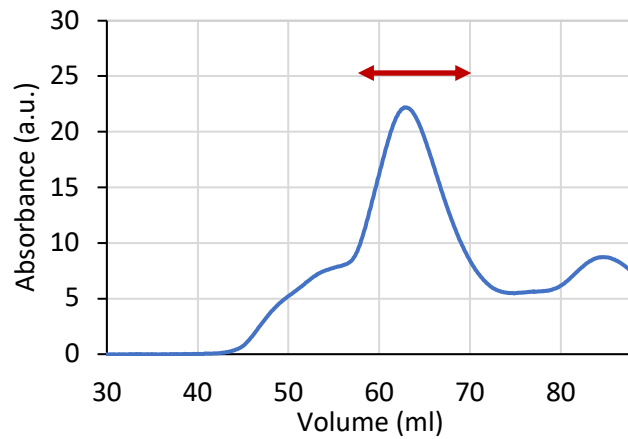
C
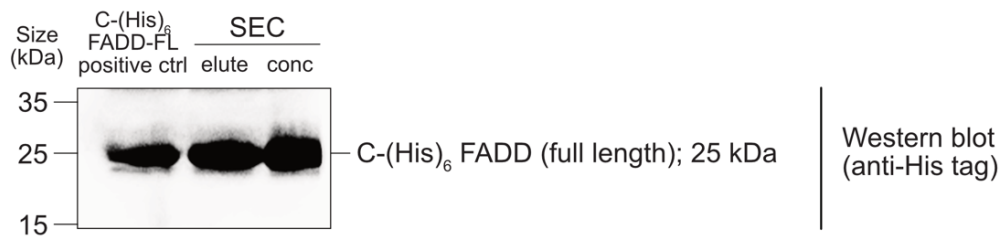
D
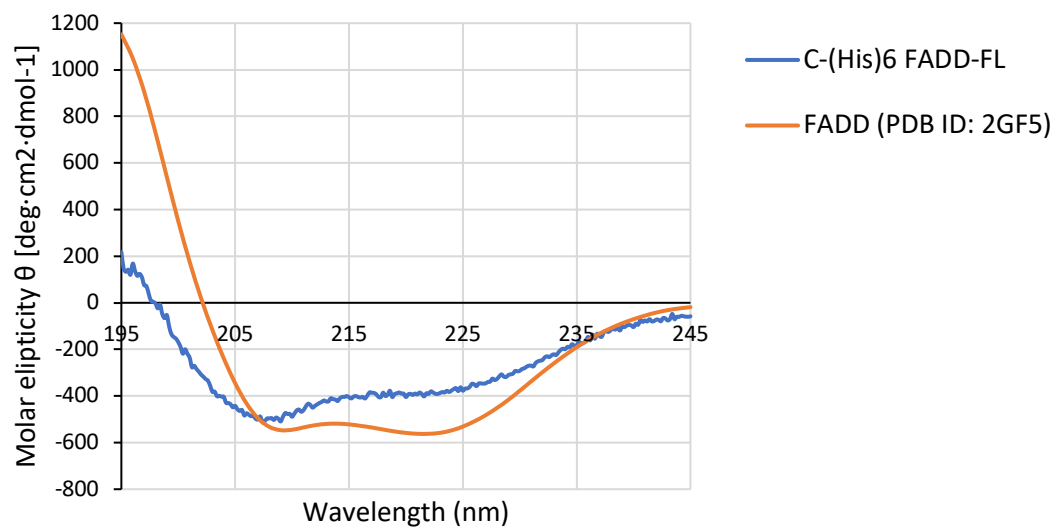
Figure 26. Purification of C-(His)$_6$ FADD-FL protein by using SEC.
A. Fractions analysed after purification of C-(His)$_6$ FADD-FL on SEC 120 ml HiLoad Superdex 75 16/60 column. The fractions show a strong band running at 25 kDa. After purification, the following elution fractions were taken for the analysis on SDS-PAGE: 10, 11, 12, 13, 14 and 15. WCE sample was used as control. All samples were separated on 15% SDS-PAGE followed by staining with Coomassie Brilliant Blue. **B.** Elution profile of C-(His)$_6$ FADD-FL on SEC 120 ml HiLoad Superdex 75 16/60 column; blue line represents protein absorbance. Elution fractions taken for the SDS-PAGE analysis are indicated by the red arrow. **C.** Fractions containing the desired pr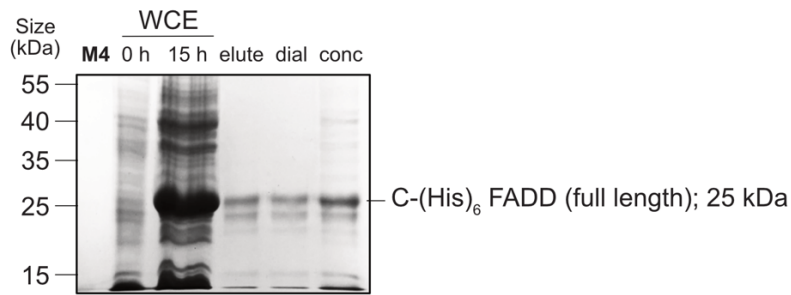otein were pooled, combined and concentrated. The combined elution and concentrated protein samples were subjected to Western blot analysis in order to confirm successful purification of FADD-FL. WCE sample was used as positive control. An antibody against FADD was used to confirm the presence of the desired protein. **D.** Comparison of calculated and experimental circular dichroism spectra for FADD. The calculated spectrum was obtained using the PDBMD2CD software (Mavridis and Janes, 2016) and the full-length human FADD structure (wild type; aa residues 1 – 191; PDB ID: 2GF5). The experimental spectrum was obtained using 200 µl of purified C-(His)$_6$ FADD-FL sample (12 µM), which was transferred to an analytic cuvette and subjected to circular dichroism spectroscopy. The orange curve represents the calculated CD spectrum of FADD, and the blue curve is the experimental spectrum of purified C-(His)$_6$ FADD-FL.
M4 (marker 4) – protein ladder, WCE – whole cell extracts, conc – concentrated.

The concentration of purified C-(His)$_6$ FADD-FL sample was calculated below by using Beer-Lambert formula, protein extinction coefficient and absorbance result measured by spectrophotometer.

Beer–Lambert formula: $A = \varepsilon\, l\, c$

Extinction coefficient (ε) = 18240
Path (l) = 1 cm
Absorbance at 280 (A) = 0.02232773 (1 ml, 1/10 dilution)
Concentration (c)

Calculation: $A = \varepsilon\, l\, c \rightarrow c = \frac{A}{\varepsilon} \rightarrow c = \frac{0.02232773}{18240} \times 10 = 0.00001224$ M = 12.24 µM

Next, the molar concentration of purified C-(His)$_6$ FADD-FL was converted into concentration in mg/ml as follows:

Formula: *concentration (mg/ml) = c (Molar) x MW (Daltons)*

Concentration (c) = 0.00001224 M

Molecular weight (MW) = 25000 Da

Calculation: concentration = 0.00001224 M x 25000 Da = 0.30602 mg/ml = 306.02 μg/ml

Finally, purified C-(His)$_6$ FADD-FL was aliquoted into 200 μl samples and stored at -20°C.

3.4. Expression of Human Recombinant ΔDEDs Caspase-10 (C401A), ΔDEDs Caspase-10 (D415A), ΔDEDs Caspase-8 (C360A) and ΔDEDs Caspase-8 (D374A/D384A)

Results obtained for ΔDEDs caspase-10 (wild type), ΔDEDs caspase-8 (wild type), ΔDEDs cFLIP-L (wild type) constructs showed successful expression and purification of the proteins of interest. Nevertheless, we observed, that purified N-(His)$_6$ ΔDEDs caspase-10 (wild type) and N-(His)$_6$ ΔDEDs caspase-8 (wild type) were cleaved into active subunits after purification.

Purification of the proteins of interest in their single-chained forms is of paramount importance for this study. In order to purify such proteins, the following mutated constructs were used: ΔDEDs caspase-10 (C401A), ΔDEDs caspase-10 (D415A), ΔDEDs caspase-8 (C360A) and ΔDEDs caspase-8 (D374A/D384A) (Figure 15A, B and C; p. 109). These variants were generated by using ΔDEDs caspase-10 (wild type) (Figure 16; p. 110) and ΔDEDs caspase-8 (wild type) (Figure 17; p. 112) constructs as a template and site-directed mutagenesis.

For protein production, induction with 0.1 mM (final concentration) of IPTG, and expression at 18°C for 3 h and 15 h were tested as a starting point. The constructs that were examined for recombinant protein expression included: ΔDEDs caspase-10 (C401A), ΔDEDs caspase-10 (D415A), ΔDEDs caspase-8 (C360A) and ΔDEDs caspase-8 (D374A/D384A).

Tables 33-34 summarise the basic information regarding protein expression constructs and expected protein masses after expression and purification.

Table 33. Main features of the human recombinant ΔDEDs caspase-10 constructs with expected protein masses after expression.

Protein Details	
DNA Construct	ΔDEDs caspase-10 (aa residues 220-521; C401A active site mutant; D415A linker mutant), pET-28a, N-terminal (His)$_6$-tag
Host Cell Strain	BL21(DE3)
Tagged Protein MW (kDa)	35
Untagged Protein MW (kDa)	33

Table 34. Main features of the human recombinant ΔDEDs caspase-8 constructs with expected protein masses after expression.

Protein Details	
DNA Construct	ΔDEDs caspase-8 (aa residues 217-479; C360A active site mutant; D374A/D384A linker mutant) pET-28a, N-terminal (His)$_6$-tag
Host Cell Strain	BL21(DE3)
Tagged Protein MW (kDa)	31
Untagged Protein MW (kDa)	29

The ΔDEDs caspase-10 (C401A), ΔDEDs caspase-10 (D415A), ΔDEDs caspase-8 (C360A) and ΔDEDs caspase-8 (D374A/D384A) constructs were transformed into BL21(DE3) cells. After the OD of the bacteria culture reached A_{600} = 0.6-0.8, small aliquots of whole cell extract (WCE) samples were taken and saved for analysis. Induction of recombinant protein expression was initiated by using IPTG, followed by incubation with shaking overnight. WCE samples were taken 3 h and 15 h after IPTG-induction, in order to assess the levels of the protein expression. Analysis of the WCE samples was performed on 12% SDS-PAGE and staining with Coomassie Brilliant Blue.

The results showed that the N-(His)$_6$ ΔDEDs caspase-10 (C401A), N-(His)$_6$ ΔDEDs caspase-10 (D415A), N-(His)$_6$ ΔDEDs caspase-8 (C360A) and N-(His)$_6$ ΔDEDs caspase-8 (D374A/D384A) were successfully expressed after 3 h and 15 h (Figure 27A, B, C and

D). Interestingly, we observed that the levels of N-(His)$_6$ ∆DEDs caspase-10 (C401A) and N-(His)$_6$ ∆DEDs caspase-10 (D415A) were very only slightly increased, when compared with uninduced cells. In contrast, the levels of N-(His)$_6$ ∆DEDs caspase-8 (C360A) and N-(His)$_6$ ∆DEDs caspase-8 (D374A/D384A) were markedly increased in comparison with the cells before induction.
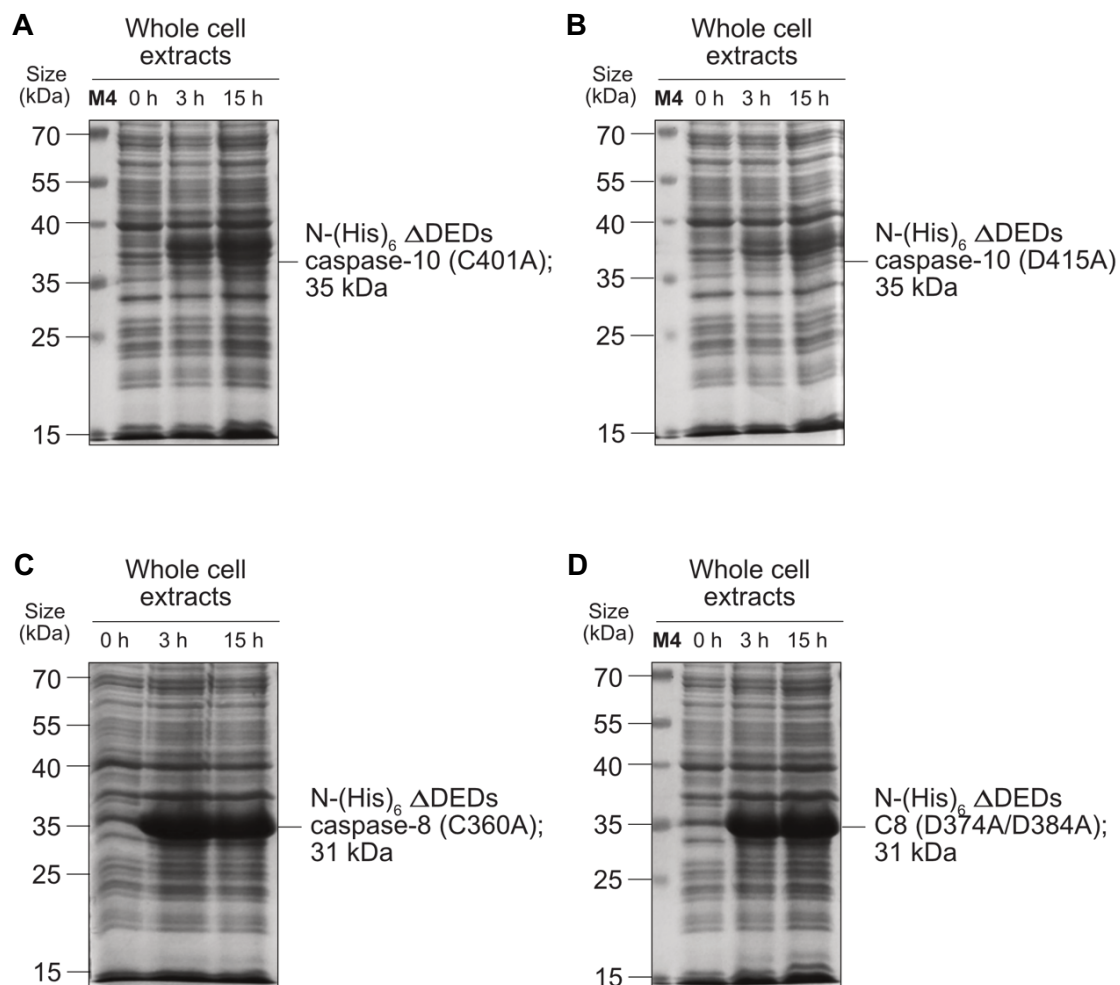
Figure 27. Expression levels of N-(His)$_6$ ∆DEDs caspase-10 (C401A), N-(His)$_6$ ∆DEDs caspase-10 (D415A), N-(His)$_6$ ∆DEDs caspase-8 (C360A) and N-(His)$_6$ ∆DEDs caspase-8 (D374A/D384A) proteins.
A-D. The whole cell extract (WCE) samples were taken before induction as well as 3 h and 15 h post-induction (IPTG at 0.1 mM final concentration) for the analysis of the recombinant N-(His)$_6$ ∆DEDs caspase-10 (C401A), N-(His)$_6$ ∆DEDs caspase-10 (D415A), N-(His)$_6$ ∆DEDs caspase-8 (C360A) and N-(His)$_6$ ∆DEDs caspase-8 (D374A/D384A) expression levels on 12% SDS-PAGE followed by staining with Coomassie Brilliant Blue.
M4 (marker 4) – protein ladder.

Due to the low levels of expressed N-(His)$_6$ ΔDEDs caspase-10 (C401A) and N-(His)$_6$ ΔDEDs caspase-10 (D415A), it was essential to further test and optimise conditions for recombinant protein production. For this, higher IPTG concentrations, such as 0.5 and 1 mM (final concentration) were used. The temperature and time of recombinant protein expression remained unchanged. ΔDEDs caspase-8 (C360A) construct was used as a control. WCE samples were taken before induction and saved for analysis. Transformation of the constructs and protein expression were performed as described previously. Bacteria cultures were incubated and shaken at 18° overnight. In order to analyse the levels of the protein expression, the WCE samples were taken 3 h and 15 h after IPTG-induction. The samples were run on 12% SDS-PAGE and stained with Coomassie Brilliant Blue.

The results obtained for N-(His)$_6$ ΔDEDs caspase-10 (C401A) (Figure 28A) and N-(His)$_6$ ΔDEDs caspase-10 (D415A) (Figure 28B) did not show any noticeable change nor increase of the protein expression after induction with both 0.5 and 1 mM final concentration of IPTG. The observation was comparable to the previous result (Figure 27A and B), where 0.1 mM final concentration of IPTG was used for induction. In contrast, the control N-(His)$_6$ ΔDEDs caspase-8 (C360A) production was very abundant after expression under the same conditions as for N-(His)$_6$ ΔDEDs caspase-10 (C401A) (Figure 28A) and N-(His)$_6$ ΔDEDs caspase-10 (D415A) (Figure 28B).
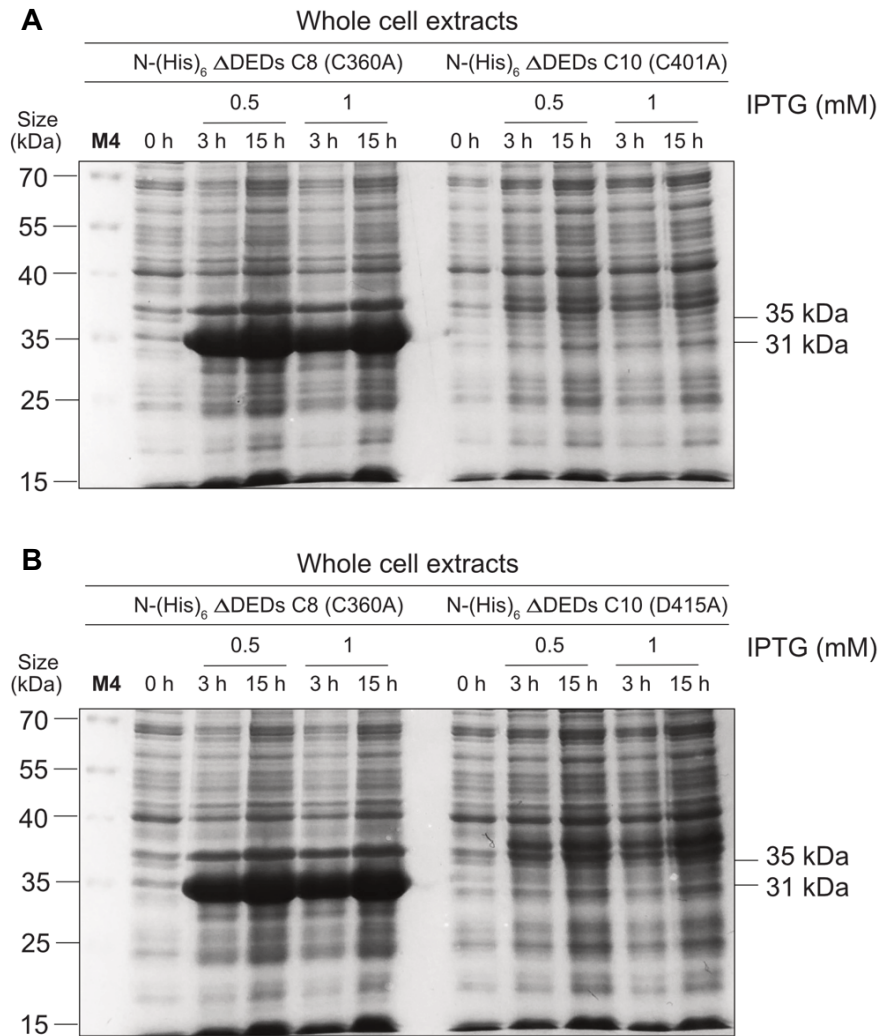
Figure 28. Expression levels of N-(His)$_6$ ΔDEDs caspase-10 (C401A) and N-(His)$_6$ ΔDEDs caspase-10 (D415A) proteins.
A. The whole cell extract samples were taken before induction as well as 3 h and 15 h post-induction (IPTG at 0.5 and 1 mM final concentration) for the analysis of the recombinant N-(His)$_6$ ΔDEDs caspase-10 (C401A) and the control N-(His)$_6$ ΔDEDs caspase-8 (C360A) expression levels on 12% SDS-PAGE followed by staining with Coomassie Brilliant Blue. **B.** The whole cell extract samples were taken before IPTG-induction (IPTG at 0.5 and 1 mM final concentration) as well as 3 h and 15 h after expression of the recombinant N-(His)$_6$ ΔDEDs caspase-10 (D415A) and the control N-(His)$_6$ ΔDEDs caspase-8 (C360A). The samples were analysed on 12% SDS-PAGE and stained with Coomassie Brilliant Blue.
M4 (marker 4) – protein ladder.

Lack of improvement of protein production efficiency after using higher IPTG concentrations led to assumption, that N-(His)$_6$ ΔDEDs caspase-10 (C401A) and N-(His)$_6$ ΔDEDs caspase-10 (D415A) were potentially too toxic, when expressed in *E. coli.* This could be caused by cAMP-mediated derepression of the lacUV5 promoter, which normally is regulated by the lacI repressor. However, it was demonstrated that expression of the lacUV5 promoter can be derepressed in the presence of cAMP, which in turn leads to the increase of the basal expression of T7 RNA polymerase (Grossman et al., 1998) and "leaky" expression of the inserted genes in their uninduced state. Derepression of the lacUV5 promoter can be effectively avoided by addition of 1% (w/v) of glucose to the bacteria growth medium and an overnight incubation of the liquid culture. Addition of glucose inhibits cAMP production in *E. coli.*

BL21(DE3) bacteria carrying the ΔDEDs caspase-10 (C401A), ΔDEDs caspase-10 (D415A) and ΔDEDs caspase-8 (C360A) constructs were grown in LB medium supplemented with glucose at 1% final concentration. After reaching the required OD (A_{600} = 0.6-0.8), small aliquots of WCE samples were taken before induction and saved for analysis. Recombinant protein expression was induced with 0.1 and 0.02 mM final concentration of IPTG, followed by incubation with shaking at 18° overnight.

In this experiment, 0.02 mM final concentration of IPTG was used, which is in line with other studies (Stennicke and Salvesen, 1999; Denault and Salvesen, 2002). It was suggested that lowering of the IPTG concentration might provide a more controlled, yet less stringent recombinant expression conditions, which as a result might lead to a successful production of toxic proteins in *E. coli*. The authors described that addition of 0.02 mM IPTG (final concentration) was optimal for expression of recombinant caspase-10 by using pET vectors and *E. coli* strain BL21(DE3) (Stennicke and Salvesen, 1999; Denault and Salvesen, 2002). Thus, it was tested, whether ΔDEDs caspase-10 (C401A)

and ΔDEDs caspase-10 (D415A) could be successfully expressed after induction with 0.02 mM IPTG (final concentration).

The WCE samples were taken 3 h and 15 h after induction with IPTG, in order to assess the levels of the protein expression. Analysis of the samples was carried out on 12% SDS-PAGE and followed by staining with Coomassie Brilliant Blue. We observed that the control N-(His)$_6$ ΔDEDs caspase-8 (C360A) was efficiently expressed, when induced with both 0.1 and 0.02 mM final concentration of IPTG in the presence of 1% (w/v) glucose (Figure 29A and B). The results obtained for N-(His)$_6$ ΔDEDs caspase-10 (C401A) (Figure 29A) and N-(His)$_6$ ΔDEDs caspase-10 (D415A) (Figure 29B) showed, that both proteins were also successfully expressed after supplementation with 1% (w/v) glucose and addition of 0.1 and 0.02 mM final concentration of IPTG. Induction with IPTG at the final concentration of 0.02 mM contributed to a slightly increased production of the recombinant proteins, when compared with the results obtained for proteins expressed with 0.1 mM final concentration of IPTG. Although the yield of N-(His)$_6$ ΔDEDs caspase-10 (C401A) and N-(His)$_6$ ΔDEDs caspase-10 (D415A) was reduced, when compared with the control N-(His)$_6$ ΔDEDs caspase-8 (C360A), it was acceptable for proceeding with protein purification.
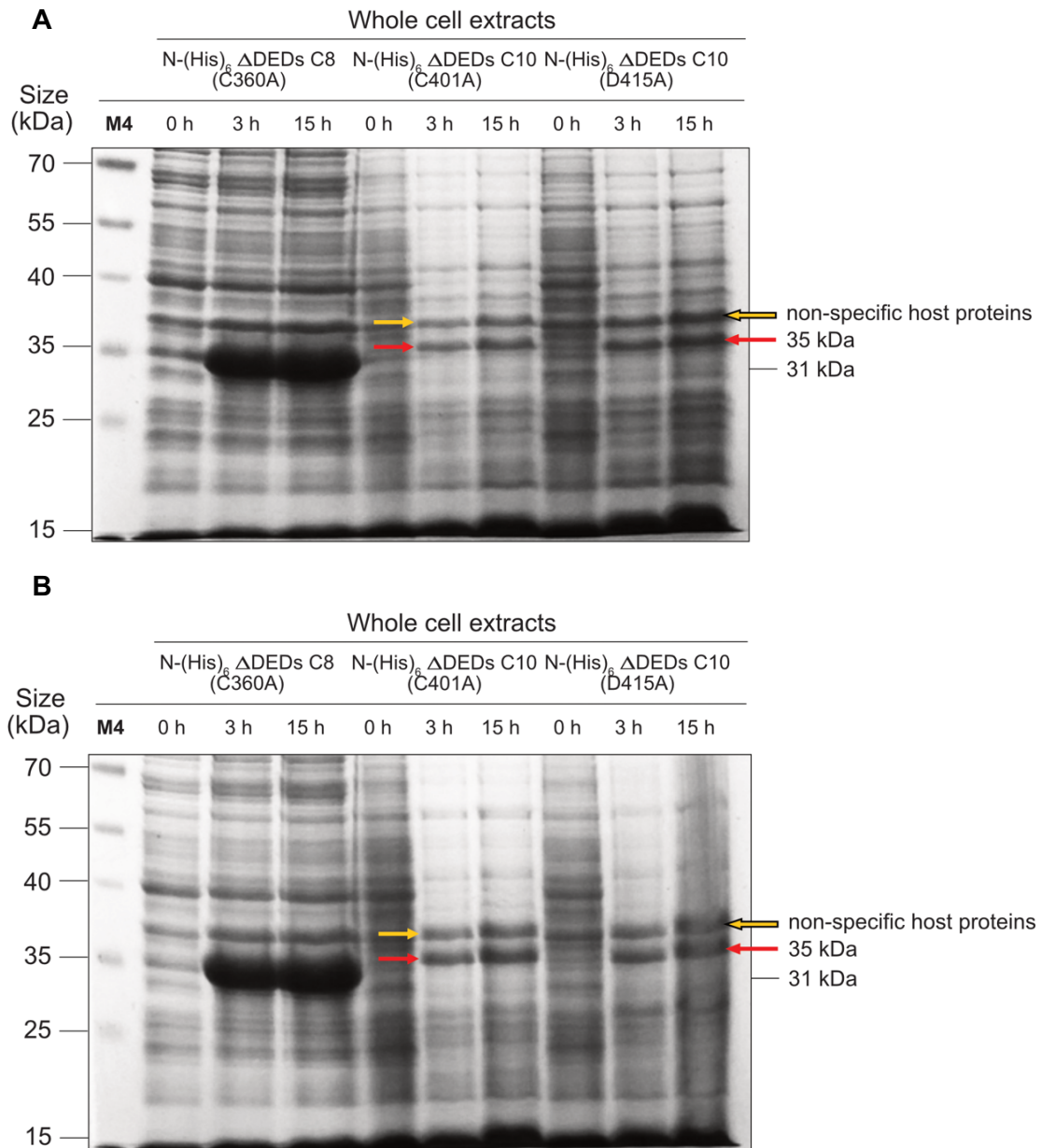
Figure 29. Expression levels of N-(His)₆ ΔDEDs caspase-10 (C401A) and N-(His)₆ ΔDEDs caspase-10 (D415A) proteins.

A. The proteins of interest were expressed in BL21(DE3) bacteria grown in LB medium supplemented with glucose at 1% (w/v) concentration. The whole cell extract samples were taken before induction as well as 3 h and 15 h post-induction (IPTG at 0.1 mM final concentration) for the analysis of the recombinant N-(His)₆ ΔDEDs caspase-10 (C401A), N-(His)₆ ΔDEDs caspase-10 (D415A) (both indicated by red arrows) and the control N-(His)₆ ΔDEDs caspase-8 (C360A) expression levels on 12% SDS-PAGE followed by staining with Coomassie Brilliant Blue. **B.** The proteins of interest were expressed in BL21(DE3) bacteria grown in LB medium supplemented with glucose at 1% (w/v) concentration. The whole cell extract samples were taken before IPTG-induction (IPTG at 0.02 mM final concentration) as well as 3 h and 15 h after expression of the recombinant N-(His)₆ ΔDEDs caspase-10 (C401A), N-(His)₆ ΔDEDs caspase-10 (D415A) (both indicated by red arrows) and the control N-(His)₆ ΔDEDs caspase-8 (C360A). The samples were analysed on 12% SDS-PAGE and stained with Coomassie Brilliant Blue.
*M4 (marker 4) – protein ladder.*

Following the successful expression, bacteria cells harbouring N-(His)$_6$ ΔDEDs caspase-8 (C360A), N-(His)$_6$ ΔDEDs caspase-10 (C401A) and N-(His)$_6$ ΔDEDs caspase-10 (D415A) were lysed by using sonication. Soluble and insoluble fractions of the lysates were separated by centrifugation. In order to assess the levels of solubility of the proteins, small aliquots of the lysate, supernatant and resuspended pellet fractions were analysed on 12% SDS-PAGE followed by Coomassie Brilliant Blue staining.

As shown in Figure 30, the highest amounts of N-(His)$_6$ ΔDEDs caspase-8 (C360A), N-(His)$_6$ ΔDEDs caspase-10 (C401A) and N-(His)$_6$ ΔDEDs caspase-10 (D415A) were found in the resuspended pellets, which suggests aggregation of the proteins of interest in bacterial inclusion bodies. Therefore, the recombination proteins were isolated from inclusion bodies by solubilisation under denaturing conditions.
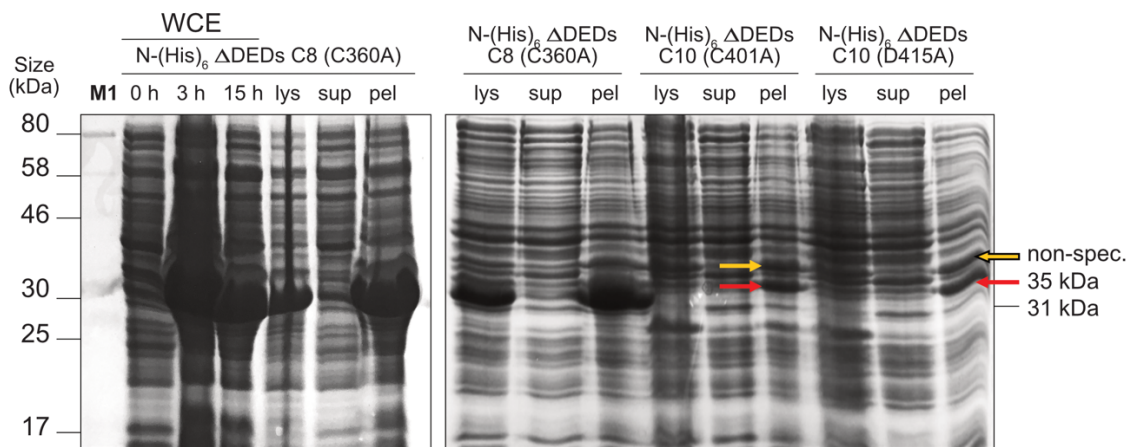
Figure 30. Solubility levels of the control N-(His)$_6$ ΔDEDs caspase-8 (C360A), N-(His)$_6$ ΔDEDs caspase-10 (C401A) and N-(His)$_6$ ΔDEDs caspase-10 (D415A).
After 15 h of N-(His)$_6$ ΔDEDs caspase-8 (C360A), N-(His)$_6$ ΔDEDs caspase-10 (C401A) and N-(His)$_6$ ΔDEDs caspase-10 (D415A) expression, lysate, supernatant and resuspended pellet samples were analysed on 12% SDS-PAGE followed by staining with Coomassie Brilliant Blue. WCE samples were used as controls. N-(His)$_6$ ΔDEDs caspase-10 (C401A) and N-(His)$_6$ ΔDEDs caspase-10 (D415A) are indicated by red arrows.
M1 (Marker 1) – protein ladder, WCE – whole cell extracts, Lys – lysed cells, Sup – supernatant, Pel – cell pellet.

3.5. Purification of N-(His)$_6$ ΔDEDs Caspase-10 (D415A) and N-(His)$_6$ ΔDEDs Caspase-8 (C360A)

In our previous report our group demonstrated that 5-FU-induced upregulation of caspase-10 provides a germ for subsequent FADDosome complex assembly. As a core driver of the FADDosome formation, upregulated caspase-10 acts as an apoptosis regulator, but not as a direct cell death initiator upon the treatment with 5-FU. At the FADDosome, caspase-8 is activated and initiates apoptosis (Mohr et al., 2018). Therefore, in the current study, the aim was to explore the role of caspase-10 as a constituent od the FADDosome and a potential caspase-8 activator.

For this, it was crucial to express and purify N-(His)$_6$ ΔDEDs Caspase-10 (D415A) – a linker mutant of ΔDEDs Caspase-10, which can act as an enzyme (activator) – and N-(His)$_6$ ΔDEDs Caspase-8 (C360A) – an active site mutant, that can play a role of a substrate.

After performing solubilisation under denaturing conditions, supernatants containing N-(His)$_6$ ΔDEDs Caspase-10 (D415A) and N-(His)$_6$ ΔDEDs Caspase-8 (C360A) were separated from cell debris and loaded onto 5 ml Ni-NTA column. Eluted proteins were collected as 5 ml fractions, which were taken for analysis. The samples were separated on 12% SDS-PAGE followed by staining with Coomassie Brilliant Blue.

We observed that N-(His)$_6$ ΔDEDs caspase-10 (D415A) was successfully purified during IMAC (Figure 31A). SDS-PAGE analysis and staining with Coomassie Brilliant Blue of the elution fractions at the major elution peak at 280 nm revealed the presence of a 35 kDa protein band, which corresponds to the expected size of the (His)$_6$-tagged protein after purification (Figure 31A). Additionally, we observed that the major elution peak was

quite prominent (Figure 31B), indicative of co-purification of other/host proteins, possibly due to the low levels of purified N-(His)$_6$ ΔDEDs caspase-10 (D415A).

Elution fractions containing N-(His)$_6$ ΔDEDs caspase-10 (D415A) were combined into one sample, dialysed and concentrated to ~10 ml. Small aliquots of the elute, dialysed and concentrated samples were analysed on 12% SDS-PAGE and stained with Coomassie Brilliant Blue (Figure 31C). The same samples were subjected to Western blot analysis, which confirmed the presence of purified N-(His)$_6$ ΔDEDs caspase-10 (D415A) (Figure 31C). Importantly, due to the low levels after purification, the protein was hardly detectable in the elution and dialysed fractions by using both Coomassie Brilliant Blue staining and Western blot. However, the concentrated fraction showed a decent N-(His)$_6$ ΔDEDs caspase-10 (D415A) band, acceptable for further processing.

After removal of the N-terminal (His)$_6$ tag by thrombin treatment, supernatant containing the untagged protein was then re-applied onto an IMAC column as described in the Methods Chapter. The flow-through fractions containing untagged ΔDEDs caspase-10 (D415A) were collected, combined and concentrated to 2 ml for further purification by using a SEC column. Small aliquots of the fractions before and after thrombin treatment as well as flow-through and concentrated samples after IMAC were run on 12% SDS-PAGE and stained with Coomassie Brilliant Blue. We observed a 33 kDa band, which confirmed the successful removal of the (His)$_6$ tag and separation of the untagged protein (Figure 31D).

A

N-(His)$_6$ ΔDEDs caspase-10 (D415A); 35 kDa

B

C

N-(His)$_6$ ΔDEDs caspase-10 (D415A); 35 kDa

N-(His)$_6$ ΔDEDs caspase-10 (D415A); 35 kDa

Western blot (anti-His tag)

D

N-(His)$_6$ ΔDEDs caspase-10 (D415A); 35 kDa
untagged ΔDEDs caspase-10 (D415A); 33 kDa
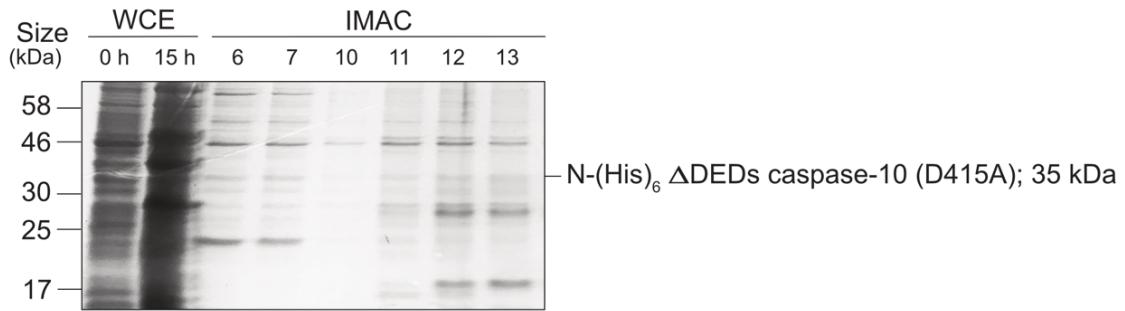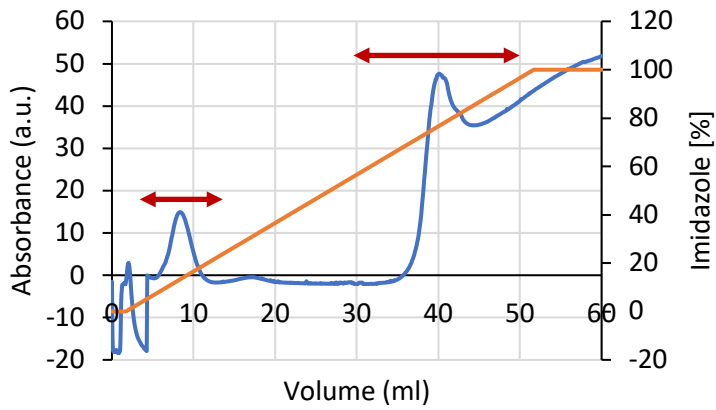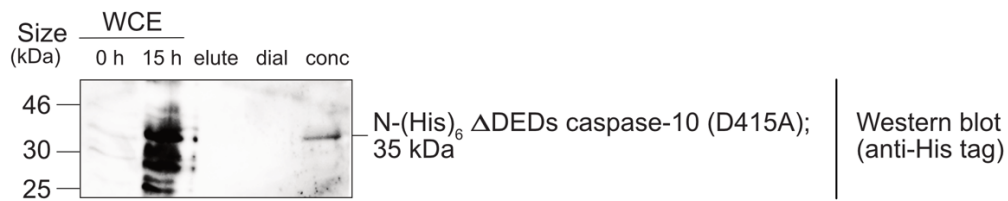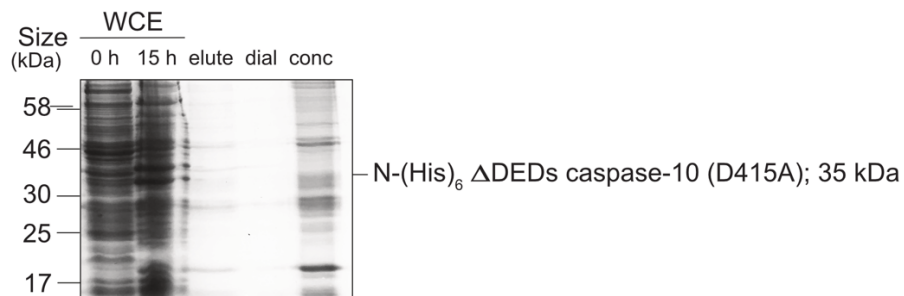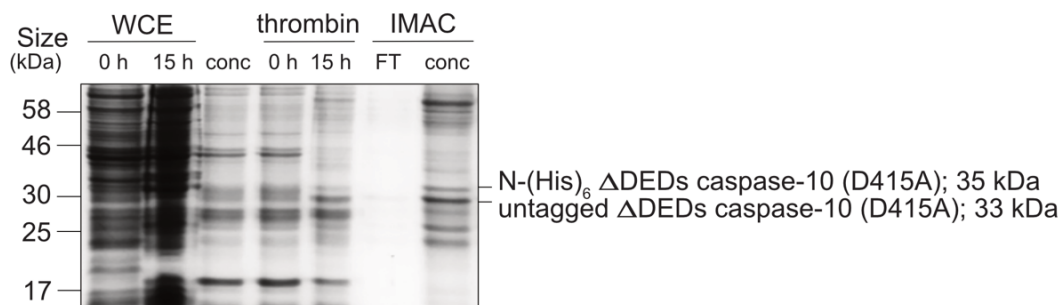
Figure 31. IMAC (Ni-NTA) purification of human recombinant N-(His)$_6$ ΔDEDs caspase-10 (D415A).
A. Analysis of fractions after purification of N-(His)$_6$ ΔDEDs caspase-10 (D415A) on IMAC 5 ml His-trap FF nickel-nitrilotriacetic (Ni-NTA) column. The fractions show a strong band running at 35 kDa. Following purification of the protein, the WCE (control) samples and Ni-NTA elution fractions number 6, 7, 10, 11, 12 and 13 were analysed by using 12% SDS-PAGE and subsequent staining with Coomassie Brilliant Blue. **B.** Elution profile of N-(His)$_6$ ΔDEDs caspase-10 (D415A) on IMAC 5 ml His-trap FF nickel-nitrilotriacetic (Ni-NTA) column; blue line represents protein absorbance; orange line represents imidazole gradient. Elution fractions taken for the SDS-PAGE analysis are indicated by the red arrow. **C.** Ni-NTA fractions containing the desired protein were pooled, dialysed and concentrated for further processing. The elution dialysed and concentrated protein samples were analysed on 12% SDS-PAGE and staining with Coomassie Brilliant Blue. The same samples were used for Western blot analysis and confirmation of successfully purified N-(His)$_6$ ΔDEDs caspase-10 (D415A). WCE samples were used as controls. An antibody against (His)$_6$ tag was used to confirm the presence of the desired protein. **D.** Cleavage of N-terminal (His)$_6$ tag. Supernatant containing N-(His)$_6$ ΔDEDs caspase-10 (D415A) was subjected to treatment with 125 units of thrombin, followed by gentle rotation at 4°C overnight and re-applied onto IMAC column. Fractions before and after thrombin treatment, as well as follow-through and concentrated samples after IMAC were analysed on 12% SDS-PAGE followed by staining with Coomassie Brilliant Blue. WCE and concentrated sample after first purification step were used as controls.
WCE – whole cell extracts, dial – dialysed, conc – concentrated, FT- flow-through.

Following further purification of untagged ΔDEDs caspase-10 (D415A) on SEC column, protein eluates were collected as 2 ml fractions and examined for purity on 12% SDS-PAGE and staining with Coomassie Brilliant Blue (Figure 32A). Assessment of elution fractions in the major elution peak at 280 nm showed very good purity levels of untagged ΔDEDs caspase-10 (D415A) (Figure 32A and B). Any host proteins that were co-purified and co-eluted within the untagged ΔDEDs caspase-10 (D415A) peak were not separated on SEC and may be present in minimal amounts, acceptable for experimental purposes.

The presence of the desired protein was confirmed by mass-spectrometry. The analysis identified two caspase-10 peptides, which were compared with the human caspase-10 sequence (Figure 32C). The protein sequence was retrieved from the National Centre for Biotechnology Information (NCBI) webpage by using the following search parameters: (I) database: "gene" and (II) keywords: "caspase-10 isoform 2 preproprotein [Homo sapiens] (accession number: NP_116756)".

SEC elution fractions containg untagged ΔDEDs caspase-10 (D415A) were pooled, combined into one sample and concentrated in order to obtain 2 ml of the final pure protein sample. Untagged ΔDEDs caspase-10 (D415A) was then subjected to circular dichroism (CD) spectroscopy in order to assess, whether it was folded after purification. The CD spectrum of the protein of interest was measured using 200 µl of purified protein sample (1.4 µM). The obtained CD spectrum of untagged ΔDEDs caspase-10 (D415A) was then compared with a calculated spectrum of ΔDEDs caspase-8 (wild type) (Figure 32D). The calculation of the spectrum was performed using the PDBMD2CD software (Mavridis and Janes, 2016) and the ΔDEDs human caspase-8 structure (wild type; aa residues 217 – 479; PDB ID: 4PRZ). It is noteworthy, that the experimental CD spectrum of untagged ΔDEDs caspase-10 (D415A) was compared to the calculated CD spectrum of ΔDEDs caspase-8 (wild type) due to the lack of the crystal structure of caspase-10 and the fact that caspase-8 and caspase-10 are closely related and their amino acid sequences share similarity in 46% (Wachmann et al., 2010).

Due to low levels of the purified untagged ΔDEDs caspase-10 (D415A), obtained CD spectrum was slightly noisy, but clear enough for analysis and interpretation. The plotted CD data revealed that the experimental spectrum of untagged ΔDEDs caspase-10 (D415A) and the calculated spectrum of ΔDEDs caspase-8 (wild type) showed negative minima from 205 to 225 nm (Figure 32D). The observed results suggested that purified untagged ΔDEDs caspase-10 (D415A) was folded following purification and it could be used for further experiments. However, it is noteworthy that the minima of the calculated spectrum were slightly more distinct and negative than the experimental one (Figure 32D). Such marginal differences were not unexpected, considering that the experimental and calculated CD spectra were determined for two closely related, yet different proteins.

A

Size (kDa)	WCE		SEC (elute)							
	0 h	15 h	10	11	12	13	14	15	16	17
58										
46										
30										
25										
17										

N-(His)$_6$ ΔDEDs caspase-10 (D415A); 35 kDa
untagged ΔDEDs caspase-10 (D415A); 33 kDa
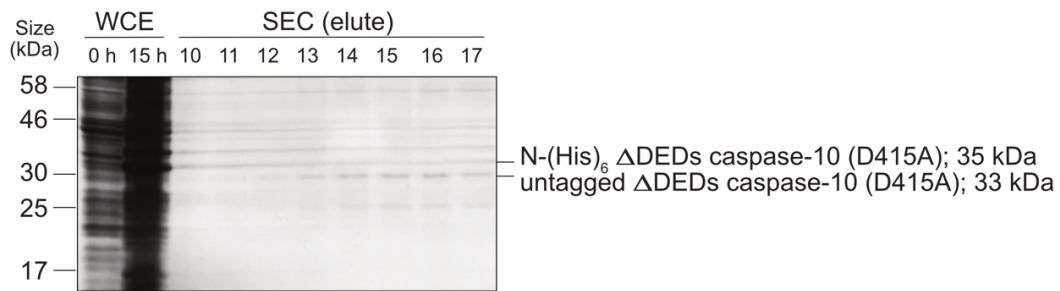
B
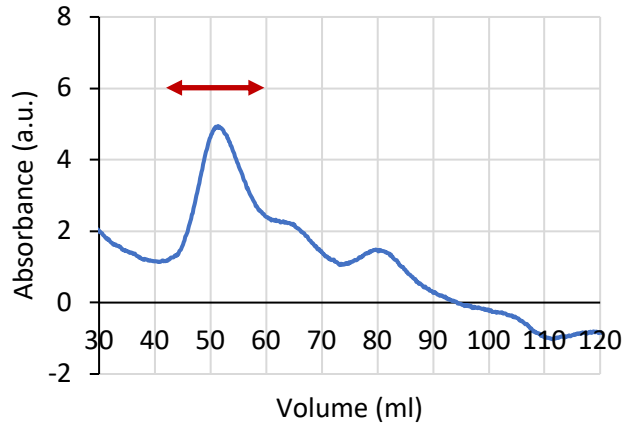
C

```
  1 MKSQGQHWYS SSDKNCKVSF REKLLIIDSN LGVQDVENLK FLCIGLVPNK
 51 KLEKSSSASD VFEHLLAEDL LSEEDPFFLA ELLYIIRQKK LLQHLNCTKE
101 EVERLLPTRQ RVSLFRNLLY ELSEGIDSEN LKDMIFLLKD SLPKTEMTSL
151 SFLAFLEKQG KIDEDNLTCL EDLCKTVVPK LLRNIEKYKR EKAIQIVTPP
201 VDKEAESYQG EEELVSQTDV KTFLEALPQE SWQNKHAGSN GNRATNGAPS
251 LVSRGMQGAS ANTLNSETST KRAAVYRMNR NHRGLCVIVN NHSFTSLKDR
301 QGTHKDAEIL SHVFQWLGFT VHIHNNVTKV EMEMVLQKQK CNPAHADGDC
351 FVFCILTHGR FGAVYSSDEA LIPIREIMSH FTALQCPRLA EKPKLFFIQA
401 CQGEEIQPSV SIEADALNPE QAPTSLQDSI PAEADFLLGL ATVPGYVSFR
451 HVEEGSWYIQ SLCNHLKKLV PRMLKFLEKT MEIRGRKRTV WGAKQISATS
501 LPTAISAQTP RPPMRRWSSV S*
```

D

untagged ΔDEDs caspase-10 (D415A)

ΔDEDs caspase-8 (wild type; PDB ID: 4PRZ)
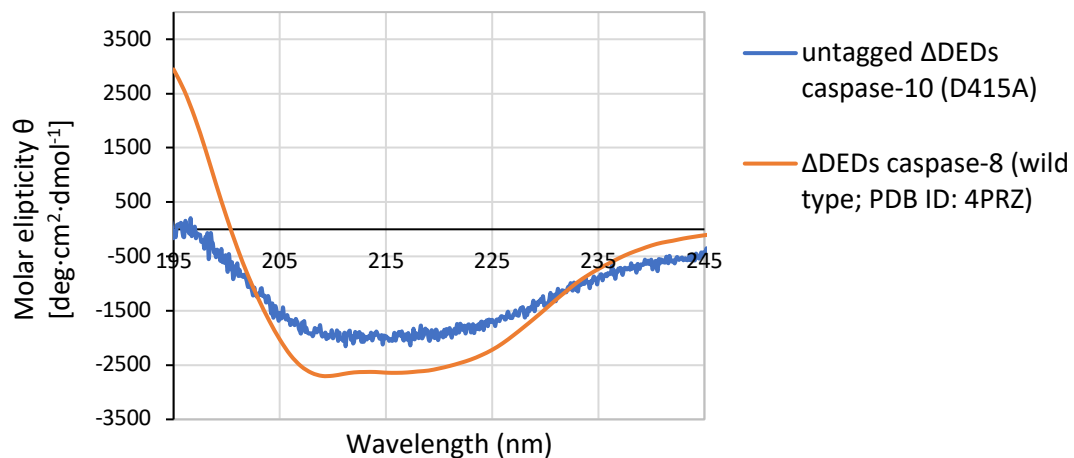
Figure 32. Purification of untagged ΔDEDs caspase-10 (D415A) by using SEC.
A. Fractions analysed after purification of untagged ΔDEDs caspase-10 (D415A) on SEC 120 ml HiLoad Superdex 75 16/60 column. The fractions show good levels of the protein of interest at around 33 kDa. After purification, the following elution fractions were taken for the analysis on SDS-PAGE: 10, 11, 12, 13, 14, 15, 16 and 17. WCE samples were used as controls. All samples were separated on 12% SDS-PAGE followed by staining with Coomassie Brilliant Blue. **B.** Elution profile of untagged ΔDEDs caspase-10 (D415A) on SEC 120 ml HiLoad Superdex 75 16/60 column; blue line represents protein absorbance. Elution fractions taken for the SDS-PAGE analysis are indicated by the red arrow. **C.** Fractions containing the desired protein were pooled, combined and concentrated. The purified protein sample was subjected to mass-spectrometry analysis in order to confirm successful purification of untagged ΔDEDs caspase-10 (D415A). Caspase-10 isoform 2 preproprotein [Homo sapiens] (accession number: NP_116756) was retrieved from NCBI website and used to compare two peptides found by mass-spectrometry. Peptides identified by mass spectrometry are in blue and red. **D.** Comparison of calculated and experimental circular dichroism spectra for ΔDEDs caspase-8 (wild type) and untagged ΔDEDs caspase-10 (D415A), respectively. The calculated spectrum was obtained using the PDBMD2CD software (Mavridis and Janes, 2016) and the human ΔDEDs caspase-8 structure (wild type; aa residues 217 – 479; PDB ID: 4PRZ). The experimental spectrum was obtained using 200 μl of purified untagged ΔDEDs caspase-10 (D415A) sample (1.4 μM), which was transferred to an analytic cuvette and subjected to circular dichroism spectroscopy. The orange curve represents the calculated CD spectrum of ΔDEDs caspase-8 (wild type), and the blue curve is the experimental spectrum of purified untagged ΔDEDs caspase-10 (D415A).

The concentration of the purified sample was calculated below by using Beer-Lambert formula, protein extinction coefficient and absorbance result measured by spectrophotometer.

Beer–Lambert formula: $A = \varepsilon\, l\, c$

Extinction coefficient (ε) = 33460
Path (l) = 1 cm
A$_{280}$ = 0.00459131 (1 ml, 1/10 dilution)
Concentration (c)

Calculation: $A = \varepsilon\, l\, c \rightarrow c = \frac{A}{\varepsilon} \rightarrow c = \frac{0.00459131}{33460} \times 10 = 0.000001372$ M = 1.37 μM

Next, the molar concentration of purified untagged ΔDEDs caspase-10 (D415A) was converted into concentration in mg/ml as follows:

Formula: *concentration (mg/ml) = c (Molar) x MW (Daltons)*

Concentration (c) = 0.000001372 M
Molecular weight (MW) = 35000 Da

Calculation: concentration = 0.000001372 M x 35000 Da = 0.04802 mg/ml = 48 μg/ml

Finally, purified untagged ΔDEDs caspase-10 (D415A) was dispensed into 200 μl aliquots and stored at -20°C.

Furthermore, results for N-(His)$_6$ ΔDEDs caspase-8 (C360A) showed that the protein was successfully purified during IMAC (Figure 33A and B). Elution fractions at the major elution peak at 280 nm were run on 12% SDS-PAGE and stained with Coomassie Brilliant Blue. We observed a 31 kDa protein band, which corresponds to the expected size of purified N-(His)$_6$ ΔDEDs caspase-8 (C360A) (Figure 33A).

Elution fractions containing the protein of interest were combined into one sample, dialysed and concentrated to ~10 ml. For removal of the N-terminal (His)$_6$ tag, the protein of interest was treated with 125 units of thrombin. The sample was rotated at 4°C overnight and re-applied onto an IMAC column in the same manner as previously described. The flow-through fractions containing N-(His)$_6$ ΔDEDs caspase-8 (C360A) were collected, combined and concentrated to 2 ml for further purification on a SEC column. Small aliquots of the following samples: eluted, dialysed, concentrated, fractions before and after thrombin treatment as well as flow-through and concentrated flow-through after IMAC were run on 12% SDS-PAGE and stained with Coomassie Brilliant Blue. The analysis showed a 29 kDa, indicating a successful removal of the (His)$_6$ tag and separation of the untagged protein (Figure 33C).

The same samples were examined for the presence of the desired protein by Western blot. First, an antibody against (His)$_6$-tag was used. The analysis confirmed the successful purification of N-(His)$_6$ ΔDEDs caspase-8 (C360A). As expected, no protein bands were detected in the following samples: after treatment with thrombin and after second IMAC purification (Figure 33D). The Western blot membrane was then re-probed by using an antibody against caspase-8/p18 subunit. The result revealed the presence of caspase-8 in all analysed samples and confirmed successful removal of the N-terminal (His)$_6$ tag (Figure 33D).

A
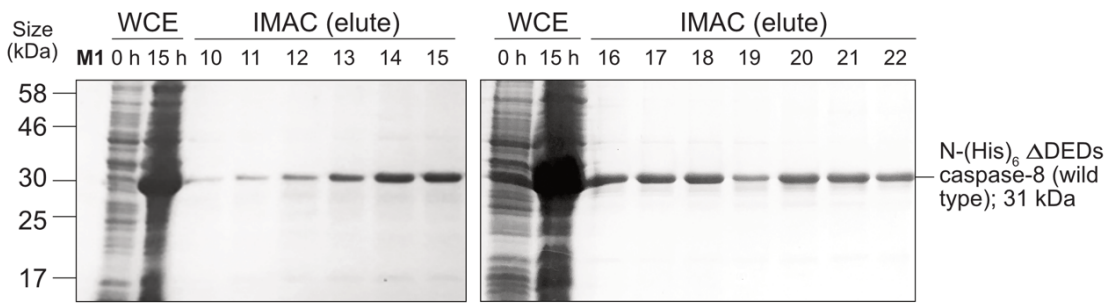
B
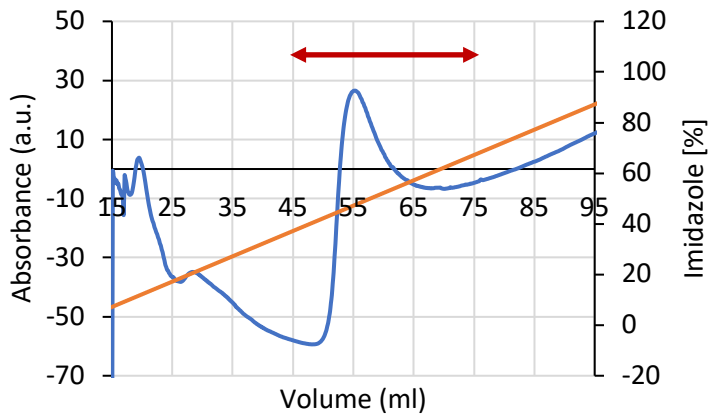
C
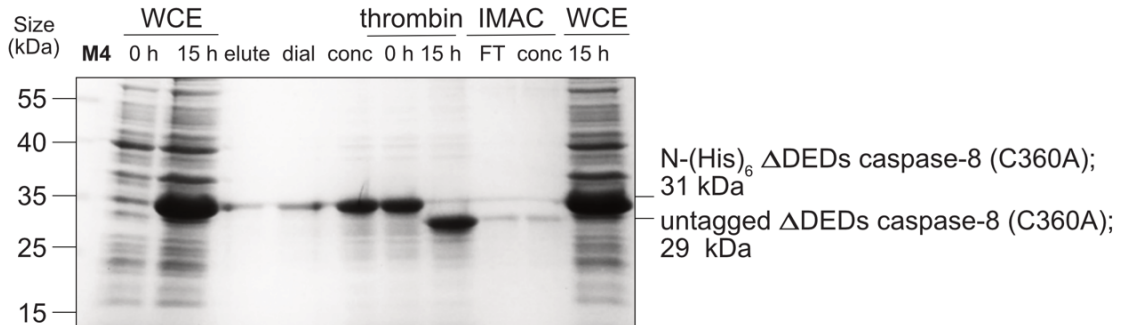
D
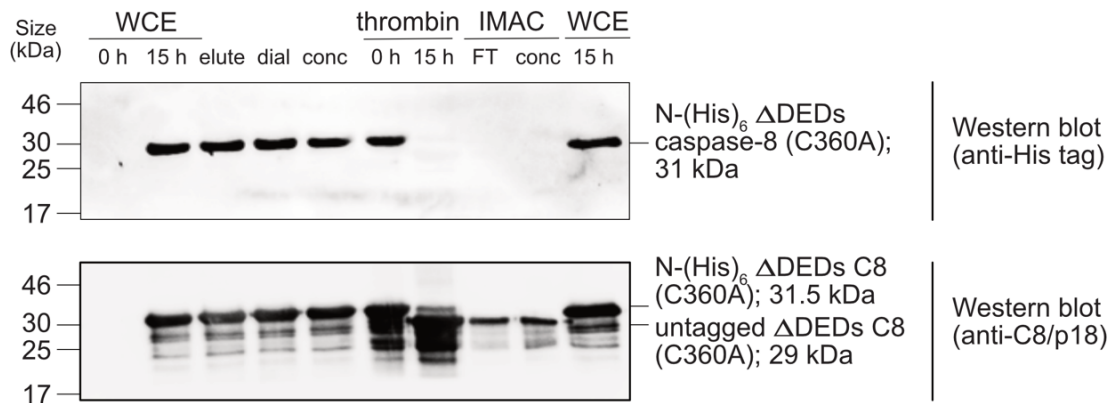
Figure 33. IMAC (Ni-NTA) purification of human recombinant N-(His)₆ ΔDEDs caspase-8 (C360A).
A. Fractions analysed after purification of N-(His)₆ ΔDEDs caspase-8 (C360A) on IMAC 5 ml His-trap FF nickel-nitrilotriacetic (Ni-NTA) column. The fractions reveal a strong band running at 31 kDa**.** Following purification of the desired protein, the WCE (control) samples and Ni-NTA elution fractions from 10-22 were examined by using 12% SDS-PAGE and stained with Coomassie Brilliant Blue. **B.** Elution profile of N-(His)₆ ΔDEDs caspase-8 (C360A) on IMAC 5 ml His-trap FF nickel-nitrilotriacetic (Ni-NTA) column; blue line represents protein absorbance; orange line represents imidazole gradient. Elution fractions taken for the SDS-PAGE analysis are indicated by the red arrow. **C.** Cleavage of N-terminal (His)₆ tag. Ni-NTA fractions containing the desired protein were pooled, dialysed and concentrated for further processing. Supernatant containing N-(His)₆ ΔDEDs caspase-8 (C360A) was subjected to treatment with 125 units of thrombin, followed by gentle rotation at 4°C overnight and re-applied onto IMAC column. The elution, dialysed, concentrated, before and after thrombin treatment samples, as well as follow-through and concentrated flow-through samples after IMAC were analysed on 12% SDS-PAGE and staining with Coomassie Brilliant Blue. **D.** The same samples were used for Western blot analysis, in order to confirm the successful purification of N-(His)₆ ΔDEDs caspase-8 (C360A) and subsequent removal of the (His)₆ tag. WCE samples were used as controls. An antibody against (His)₆-tag and caspase-8/p18 subunit were used to confirm the presence of the desired protein.
*M1 (Marker 1) and **M4** (marker 4) – protein ladder, WCE – whole cell extracts, dial – dialysed, conc – concentrated, FT- flow-through.*

Supernatant containing untagged ΔDEDs caspase-8 (C360A) was further fractionated on SEC column. Eluted protein samples were collected as 2 ml fractions and tested for purity by using 12% SDS-PAGE and staining with Coomassie Brilliant Blue (Figure 34A and B). The results obtained for the fractions in the major elution peak at 280 nm revealed very high purity levels of untagged ΔDEDs caspase-8 (C360A) (Figure 34A and B). Any host proteins that co-purified and co-eluted within the untagged ΔDEDs caspase-8 (C360A) peak were not separated on SEC and are present in minimal amounts, acceptable for experimental purposes.

SEC eluates containing untagged ΔDEDs caspase-8 (C360A) were pooled, combined into one sample and concentrated to 2 ml. A single SEC eluate and concentrated SEC eluates were subjected to Western blot analysis. First, the sampes were examined by using an antibody against (His)₆-tag. As expected, no protein was detectable in the eluate samples, when compared with the control N-(His)₆ ΔDEDs caspase-8 (C360A). Re-probing with an antibody against caspase-8/p18 subunit showed, that caspase-8 was

present in all analysed samples, confirming successful purification on SEC column. (Figure 34C).

In order to check whether untagged ΔDEDs caspase-8 (C360A) was folded after purification, circular dichroism (CD) spectroscopy was performed. The CD spectrum of the protein of interest was collected using 200 μl of purified protein sample (48 μM), subjected to CD spectroscopy analysis. The collected experimental spectrum of untagged ΔDEDs caspase-8 (C360A) was then compared with a calculated spectrum of ΔDEDs caspase-8 (wild type) (Figure 34D). The calculated spectrum was obtained using the PDBMD2CD software (Mavridis and Janes, 2016) and the ΔDEDs human caspase-8 structure (wild type; aa residues 217 – 479; PDB ID: 2K7Z).

After plotting the CD data, it was observed that the experimental spectrum of untagged ΔDEDs caspase-8 (C360A) showed negative peaks from 205 to 225 nm. This observation was comparable to the calculated spectrum of ΔDEDs caspase-8 (wild type) (Figure 34D), which suggested that purified untagged ΔDEDs caspase-8 (C360A) was folded and could be used for experimental purposes. The result also showed that the peaks in the experimental CD spectrum were slightly more negative than the peaks in the calculated spectrum (Figure 34D). This could be possibly caused by the presence of the point mutation, C360A, in the ΔDEDs caspase-8 protein, which would be in line with the observations described by others, as it was demonstrated that mutations might affect protein folding to some extent (Hwang et al., 2014). The authors observed that the mutated proteins would exhibit less negative CD spectra than the wild type ones. Importantly, it was shown that despite the conformational changes, the mutated proteins were still functional (Hwang et al., 2014). The slight difference in the values of the experimental and calculated peaks could be also possibly caused by host *E. coli* proteins, which could be co-eluted on Ni-NTA and SEC within the untagged ΔDEDs

caspase-8 (C360A) peak and present in minimal amounts in the protein sample measure

by CD spectroscopy.

A

N-(His)₆ ΔDEDs caspase-8 (C360A); 31 kDa
untagged ΔDEDs caspase-8 (C360A); 29 kDa

B

C

N-(His)₆ ΔDEDs caspase-8 (C360A); 31 kDa — Western blot (anti-His tag)

N-(His)₆ ΔDEDs caspase-8 (C360A); 31.5 kDa
untagged ΔDEDs caspase-8 (C360A); 29 kDa — Western blot (anti-C8/p18)

D

untagged ΔDEDs caspase-8 (C360A)

ΔDEDs caspase-8 (wild type; PDB ID: 2K7Z)
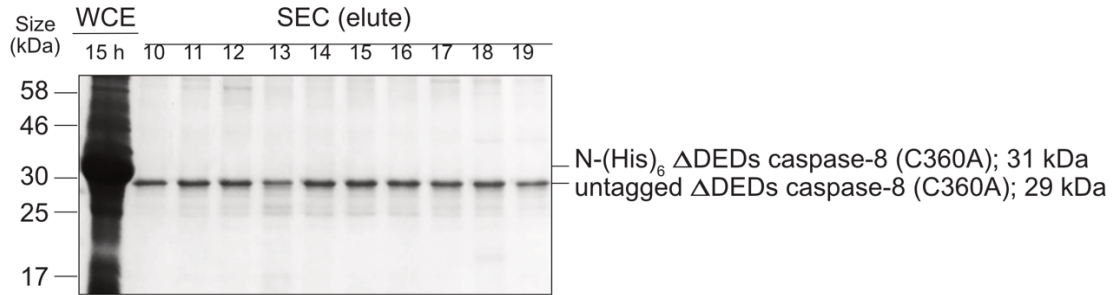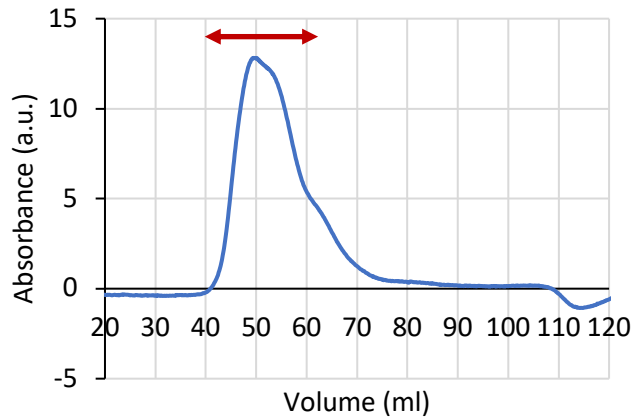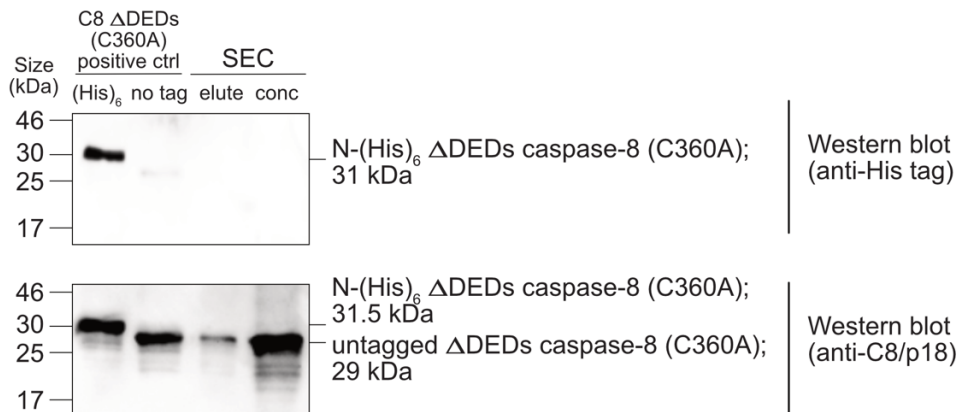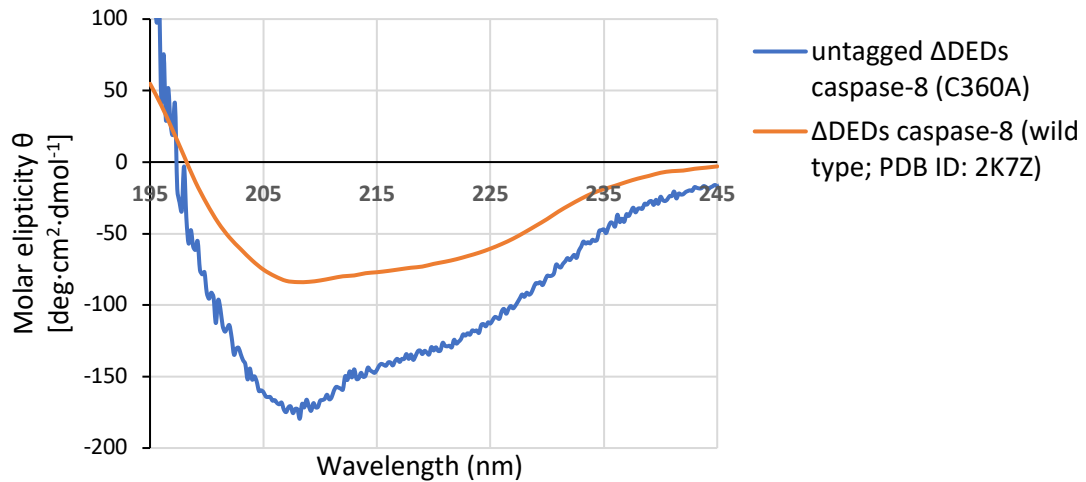
Figure 34. Purification of untagged ∆DEDs caspase-8 (C360A) by using SEC.
A. Fractions analysed after purification of untagged ∆DEDs caspase-8 (C360A) on SEC 120 ml HiLoad Superdex 75 16/60 column. The fractions show a strong band running at 29 kDa. After purification of the desired protein, the following elution fractions were taken for the analysis on SDS-PAGE: 10, 11, 12, 13, 14, 15, 16, 17, 18 and 19. WCE sample was used as control. All samples were separated on 12% SDS-PAGE followed by staining with Coomassie Brilliant Blue. **B.** Elution profile of untagged ∆DEDs caspase-8 (C360A) on SEC 120 ml HiLoad Superdex 75 16/60 column; blue line represents protein absorbance. Elution fractions taken for the SDS-PAGE analysis are indicated by the red arrow. **C.** Fractions containing the desired protein were pooled, combined and concentrated. The elution and concentrated protein samples after SEC were subjected to Western blot analysis. An antibody against (His)$_6$-tag and caspase-8/p18 subunit were used in order to confirm successful purification of untagged ∆DEDs caspase-8 (C360A). **D.** Comparison of calculated and experimental circular dichroism spectra for ∆DEDs caspase-8. The calculated spectrum was obtained using the PDBMD2CD software (Mavridis and Janes, 2016) and the human ∆DEDs caspase-8 structure (wild type; aa residues 217 – 479; PDB ID: 2K7Z). The experimental spectrum was obtained using 200 µl of purified untagged ∆DEDs caspase-8 (C360A) sample (48 µM), which was transferred to an analytic cuvette and subjected to circular dichroism spectroscopy. The orange curve represents the calculated CD spectrum of ∆DEDs caspase-8 (wild type), and the blue curve is the experimental spectrum of purified untagged ∆DEDs caspase-8 (C360A).

The concentration of the purified sample was calculated below by using Beer-Lambert formula, protein extinction coefficient and absorbance result measured by spectrophotometer.

Beer–Lambert formula: $A = \varepsilon\, l\, c$

Extinction coefficient (ε) = 24005
Path (l) = 1 cm
A$_{280}$ = 0.1167048 (1 ml, 1/10 dilution)
Concentration (c)

Calculation: $A = \varepsilon\, l\, c \rightarrow c = \frac{A}{\varepsilon} \rightarrow c = \frac{0.1167048}{24005} \times 10 = 0.00004862$ M =
48.62 µM

Next, the molar concentration of purified untagged ∆DEDs caspase-8 (C360A) was converted into concentration in mg/ml as follows:

Formula: *concentration (mg/ml) = c (Molar) x MW (Daltons)*

Concentration (c) = 0.00004862 M
Molecular weight (MW) = 31000 Da

Calculation: concentration = 0.00004862 M x 31000 Da = 1.507 mg/ml

Finally, purified untagged ΔDEDs caspase-8 (C360A) was aliquoted into 200 μl samples and stored at -20°C.

3.6. Design and Establishment of Alternative Protein Expression Constructs by Using pGEX-4T-3 System

By using pET-28a system, we have successfully expressed and purified C-(His)$_6$ FADD-FL, untagged ΔDEDs caspase-8 (C360A) and untagged ΔDEDs caspase-10 (D415A). The yield obtained after purification of the first two proteins was good and satisfactory, whereas the yield of the third protein was low and only enough for selected experiments. Moreover, purification of N-(His)$_6$ ΔDEDs cFLIP-L was unsuccessful, when using the pET-28a system. Such results suggested two possible scenarios: (I) protein expression levels were too low and/or (II) only small parts of proteins were solubilised and isolated from inclusion bodies. Upscaling the recombinant protein production and optimisation of solubilisation under denaturing conditions did not increase the yield after purification (data not shown).

Therefore, it was essential to consider using a different protein production system, which could allow higher and more efficient expression as well as increase the level of protein solubility, when expressed in *E. coli*. Aside testing and monitoring different induction and expression parameters (such as various IPTG concertation, time and temperature), it is common to use a fusion protein technology, which recommends utilising fusion partners or tags, also known as solubility enhancer tags (Costa et al., 2014). A wide range of such tags is available and one of the most common and well-known ones is glutathione-S-transferase (GST), which was selected in this study.

pGEX plasmid vectors function as a well-established known expression system, which allows production of proteins fused to the GST tag. In this system, protein expression is controlled by the IPTG-inducible tac promoter. Expression of the insert is tightly regulated by the presence of the product of the lacI^q gene and lac operator, which are

also engineered in the vector (Figure 35A). The lacI^q gene product functions as the tac repressor, which can be outcompeted by addition of IPTG, leading to expression of an inserted gene.

In this study, the pGEX-4T-3 vector was used for establishment of the protein expression constructs (Figure 35A and B).

A
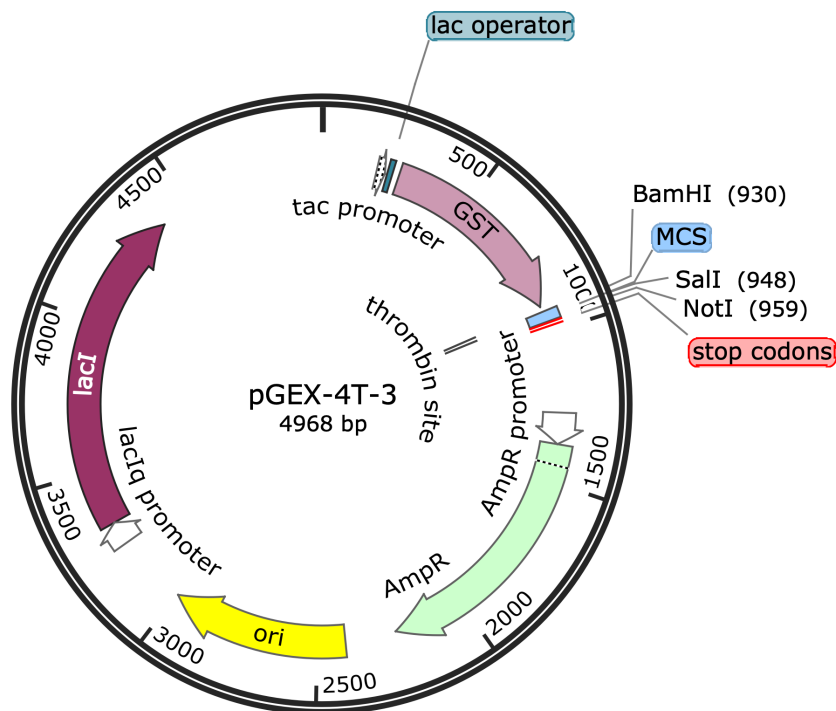
B
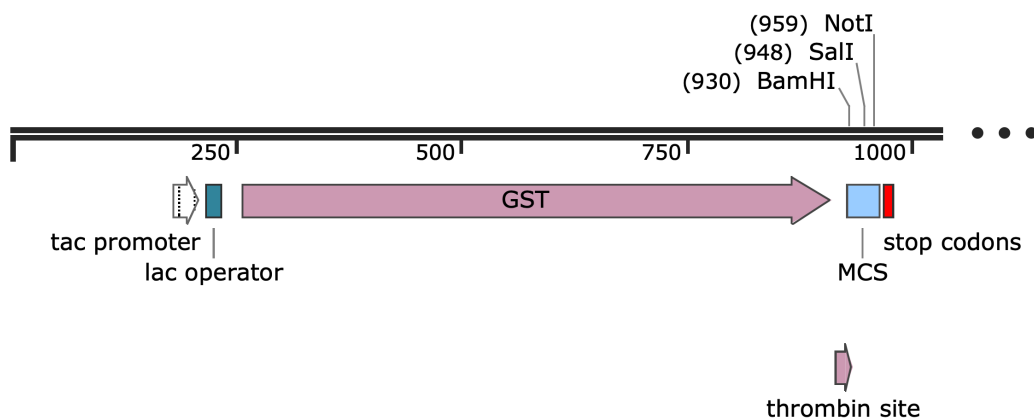
Figure 35. Schematics of an empty pGEX-4T-3 vector.
A. Map of the vector with its main features **B.** Detailed schematics of the Multiple Cloning Site with N-terminal GST tag and indication of restrictions sites positions for enzymes used during cloning of desired constructs.

The first step was to modify the pGEX-4T-3 vector, in order to add the (His)$_6$ tag downstream of the Multiple Cloning Site (MCS) (Figure 36A and 37A). This would result in expression of the proteins with the N-terminal GST and C-terminal (His)$_6$ tag. The second tag was added to facilitate purification on the Ni-NTA column and to utilise an already established protocol from the pET-28a system, so only minor optimisations to the protein expression conditions would need to be made for the new system.

Empty pGEX-4T-3 vector was modified by cloning of DNA inserts containing C-terminal (His)$_6$ tag with thrombin or TEV cleavage site into the *Sal1* and *Not1* sites of the plasmid (Figure 36A and B; Figure 37A and B). Usage of the pGEX-4T-3 / thrombin-(His)$_6$ requires only one treatment with thrombin in order to remove both N-GST and C-(His)$_6$ tags, whereas usage of pGEX-4T-3 / TEV-(His)$_6$ allows to remove N-GST and to leave C-(His)$_6$ tag after the thrombin treatment. When necessary, C-(His)$_6$ tag can be cut off with TEV protease.
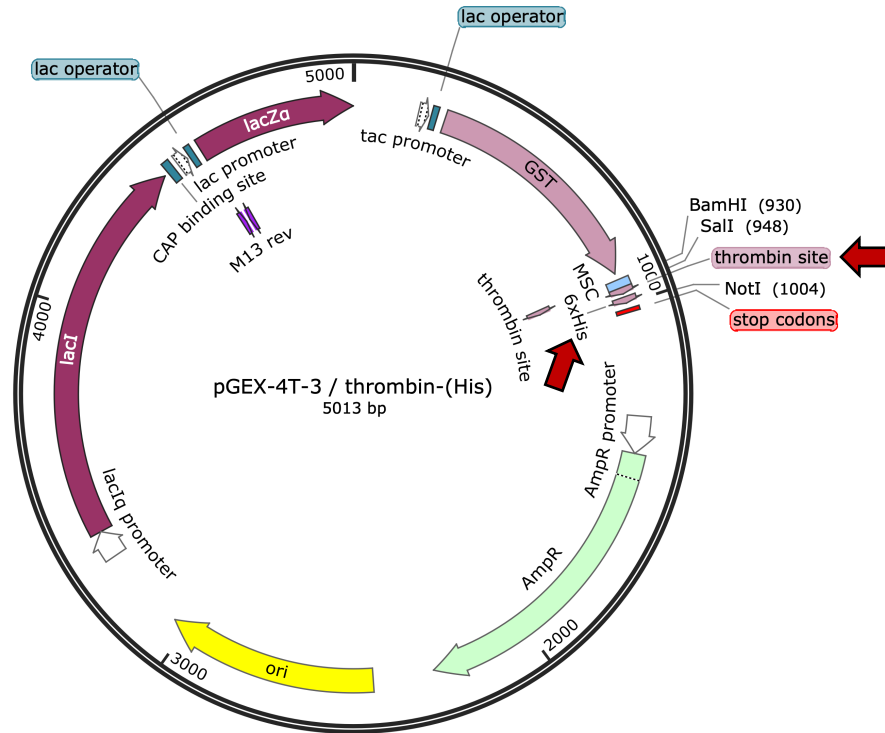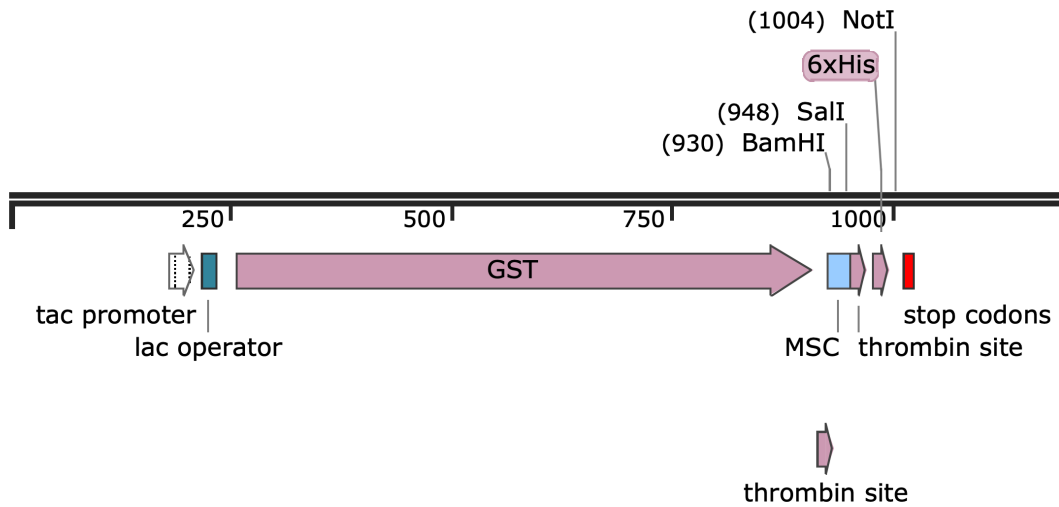
Figure 36. Schematics of the pGEX-4T-3 vector with additional (His)$_6$ tag and thrombin site.
A. Map of the vector with its main features. Additional (His)$_6$ tag with thrombin site (indicated by the red arrow) for tag removal was inserted into *Sal1* and *Not1* sites of the pGEX-4T-3 vector. **B.** Detailed schematics of the Multiple Cloning Site with N-terminal GST, C-terminal (His)$_6$ tag and indication of restriction sites positions for enzymes used during cloning of desired constructs.
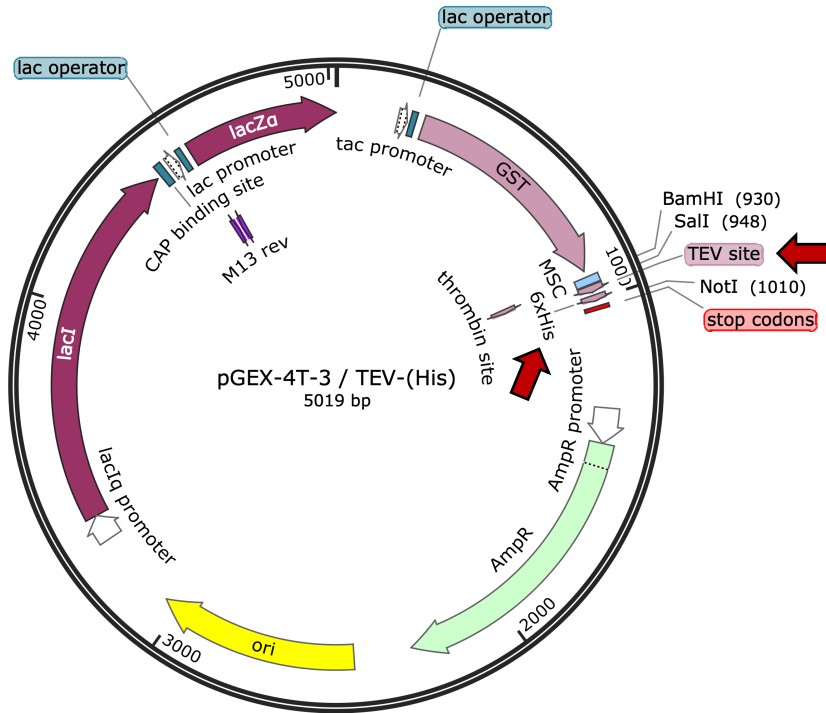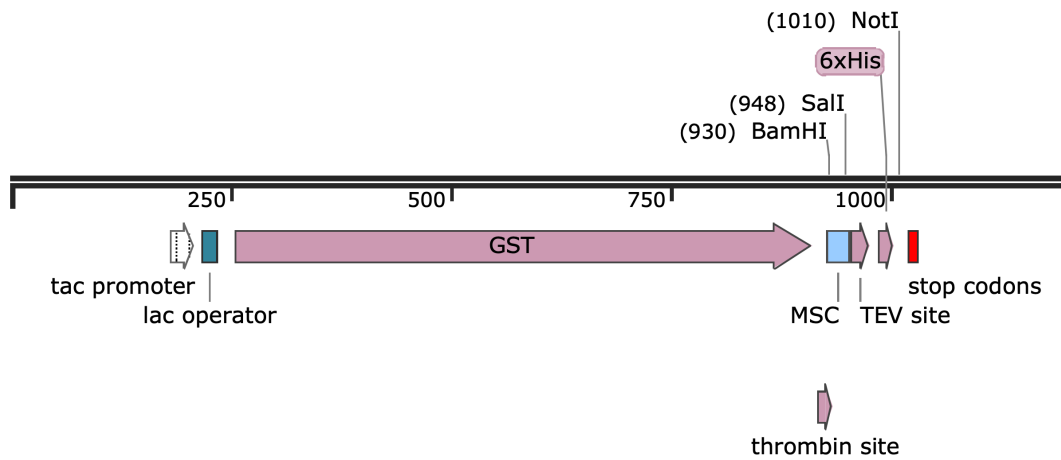
Figure 37. Schematics of the pGEX-4T-3 vector with additional (His)₆ tag and TEV site.
A. Map of the vector with its main features. Additional (His)₆ tag with TEV site (indicated by the red arrow) for tag removal was inserted into *Sal1* and *Not1* sites of the pGEX-4T-3 vector. **B.** Detailed schematics of the Multiple Cloning Site with N-terminal GST, C-terminal (His)₆ tag and indication of restriction sites positions for enzymes used during cloning of desired constructs.

For establishment of the pGEX-4T-3-based protein expression constructs, the same DNA fragments were used as for the pET-28a system and were described in detail on p. 88-89. The schematics of the constructs is shown in Figure 15A, B and C (p. 109). Additionally, a construct containing the cleavage mutant of cFLIP-L with a single amino acid substitution at D376A was generated (Figure 15C, p. 109). Mutation at this site, which has been described as a preferred cleavage site for pro-caspase-8 (Yu et al., 2009), prevents cFLIP-L from being processed by caspase-8.

ΔDEDs caspase-8 (C360A) DNA fragment was cloned into *BamH1* and *Sal1* sites of the pGEX-4T-3/thrombin-(His)$_6$ vector. As a result, the N-terminus and C-terminus of the protein were fused to the GST tag and the (His)$_6$ tag, respectively. Both tags can be removed by thrombin treatment (Figure 38A and B).
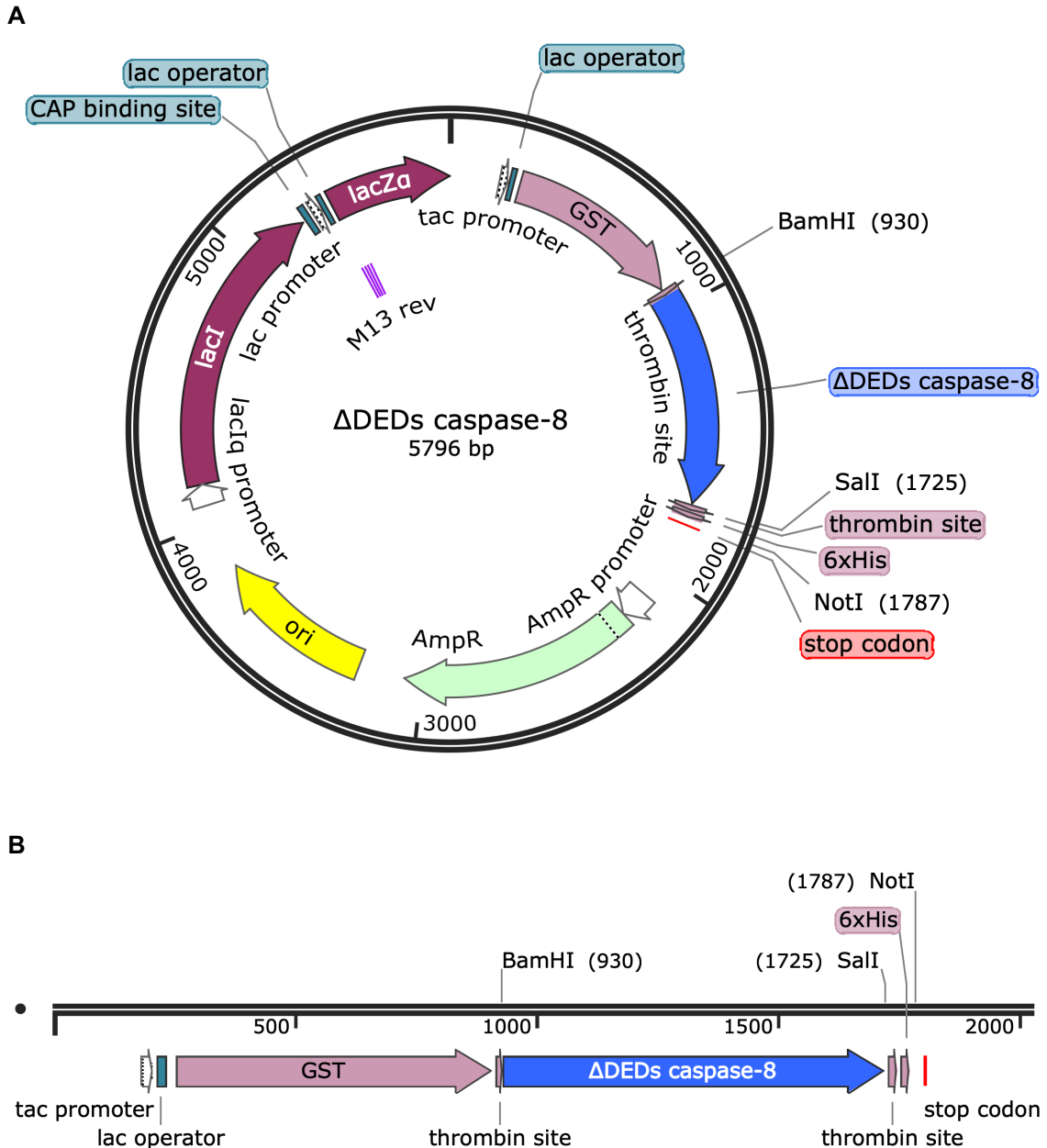
Figure 38. Map of the ΔDEDs caspase-8 (C360A) pGEX-4T-3/thrombin-(His)$_6$ construct.
A. The ΔDEDs caspase-8 gene (C360A) was inserted into *BamH1* and *Sal1* sites of the pGEX-4T-3/thrombin-(His)$_6$ vector **B.** Detailed schematics of the ΔDEDs caspase-8 (C360A) insert with N-terminal GST and C-terminal (His)$_6$ tag with thrombin sites for tags removal.

ΔDEDs caspase-10 (C401A) and ΔDEDs caspase-10 (D415A) DNA segments were inserted into *BamH1* and *Sal1* sites of the pGEX-4T-3/thrombin-(His)$_6$ vector. Therefore, the N-termini and C-termini of the proteins were fused to the GST tag and the (His)$_6$ tag, respectively. Both tags can be removed by addition of thrombin (Figure 39A and B).

A
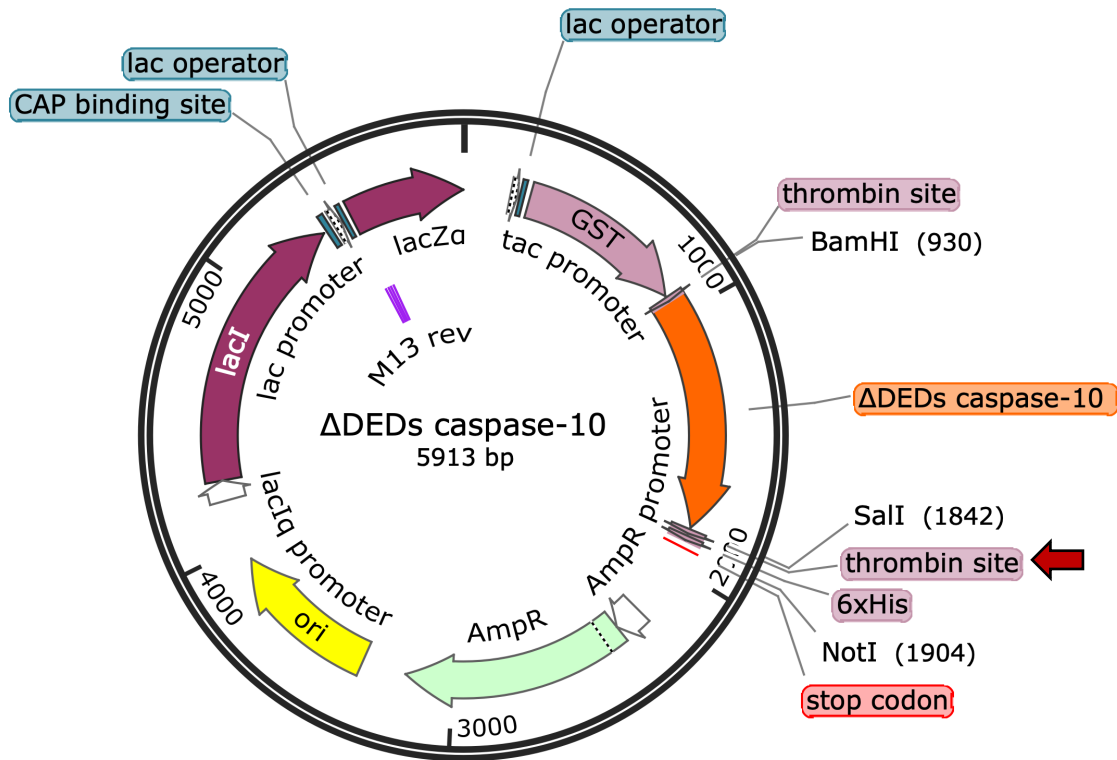
B
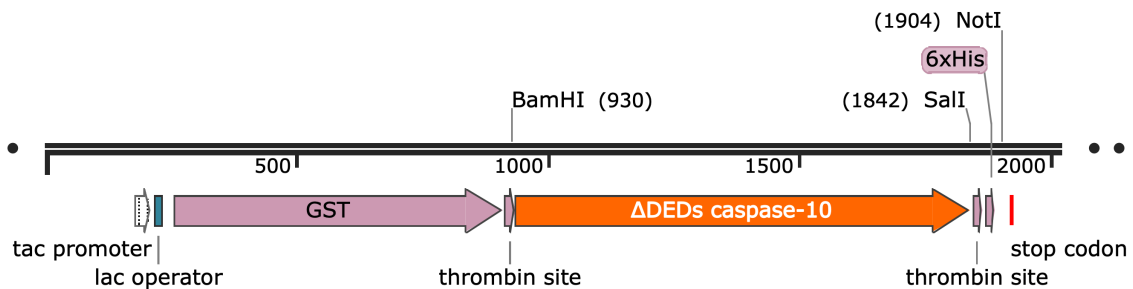
Figure 39. Map of the ΔDEDs caspase-10/pGEX-4T-3/thrombin-(His)$_6$ construct.
A. The ΔDEDs caspase-10 gene (containing either C401A or D415A mutation) was inserted into *BamH1* and *Sal1* sites of the pGEX-4T-3/thrombin-(His)$_6$ vector. **B.** Detailed schematics of the ΔDEDs caspase-10 insert with N-terminal GST and C-terminal (His)$_6$ tag with thrombin sites for tags removal.

ΔDEDs caspase-10 (C401A) and ΔDEDs caspase-10 (D415A) DNA genes were engineered into *BamH1* and *Sal1* sites of the pGEX-4T-3/TEV-(His)₆ plasmid. This resulted in fusion of the N-termini and C-termini of the proteins to the GST tag and the (His)₆ tag, respectively. The N-GST tag can be removed by thrombin treatment, whereas the C-(His)₆ can be cut off with TEV (Figure 40A and B).

A
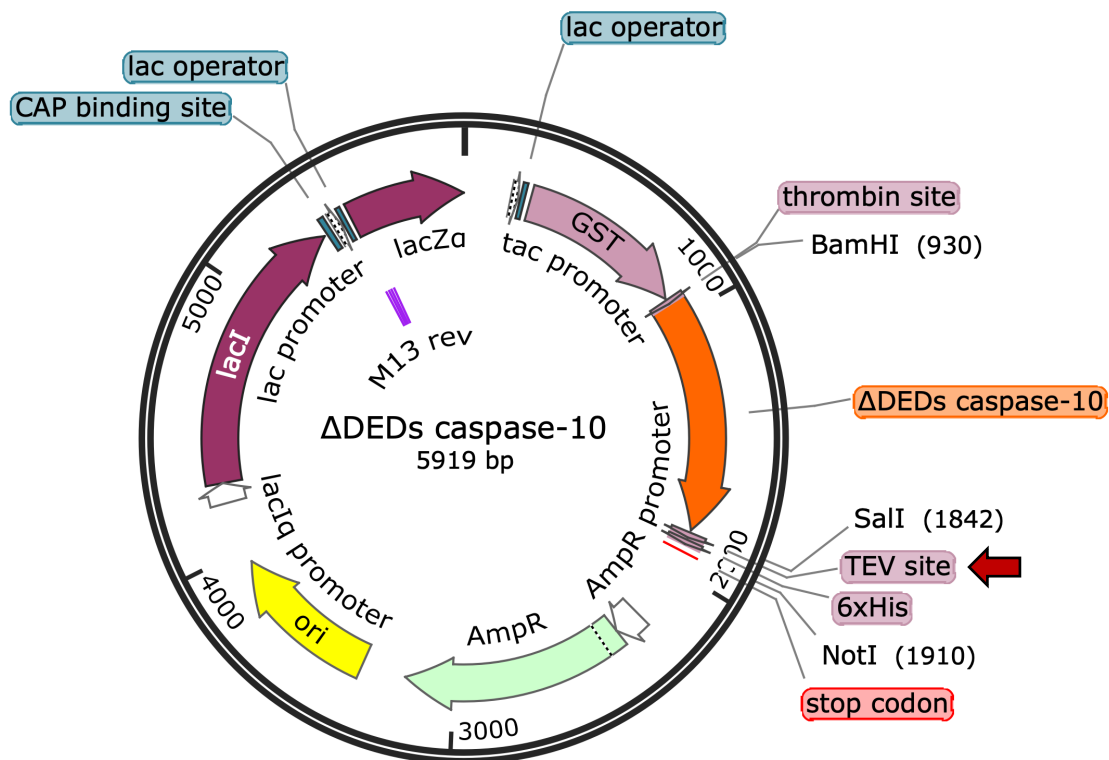
B
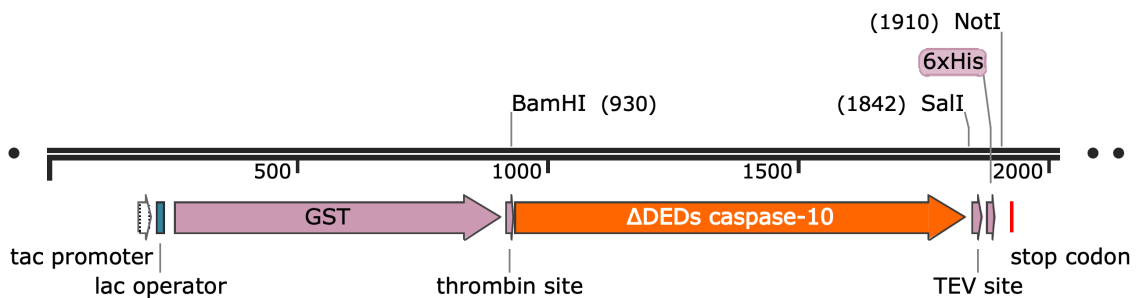
Figure 40. Map of the caspase-10/pGEX-4T-3/TEV-(His)₆ construct.
A. The ΔDEDs caspase-10 gene (containing either C401A or D415A mutation) was inserted into *BamH1* and *Sal1* sites of the pGEX-4T-3/TEV-(His)₆ vector. **B.** Detailed schematics of the ΔDEDs caspase-10 insert with N-terminal GST with thrombin site and C-terminal (His)₆ tag with TEV site for tags removal.

ΔDEDs cFLIP-L (wild type) and ΔDEDs cFLIP-L (D376A) DNA fragments were cloned into *BamH1* and *Sal1* sites of the pGEX-4T-3/thrombin-(His)₆ vector. In these constructs, the N-termini and C-termini of the proteins were fused to the GST tag and the (His)₆ tag, respectively. Both tags can be cut off by using thrombin (Figure 41A and B).

A
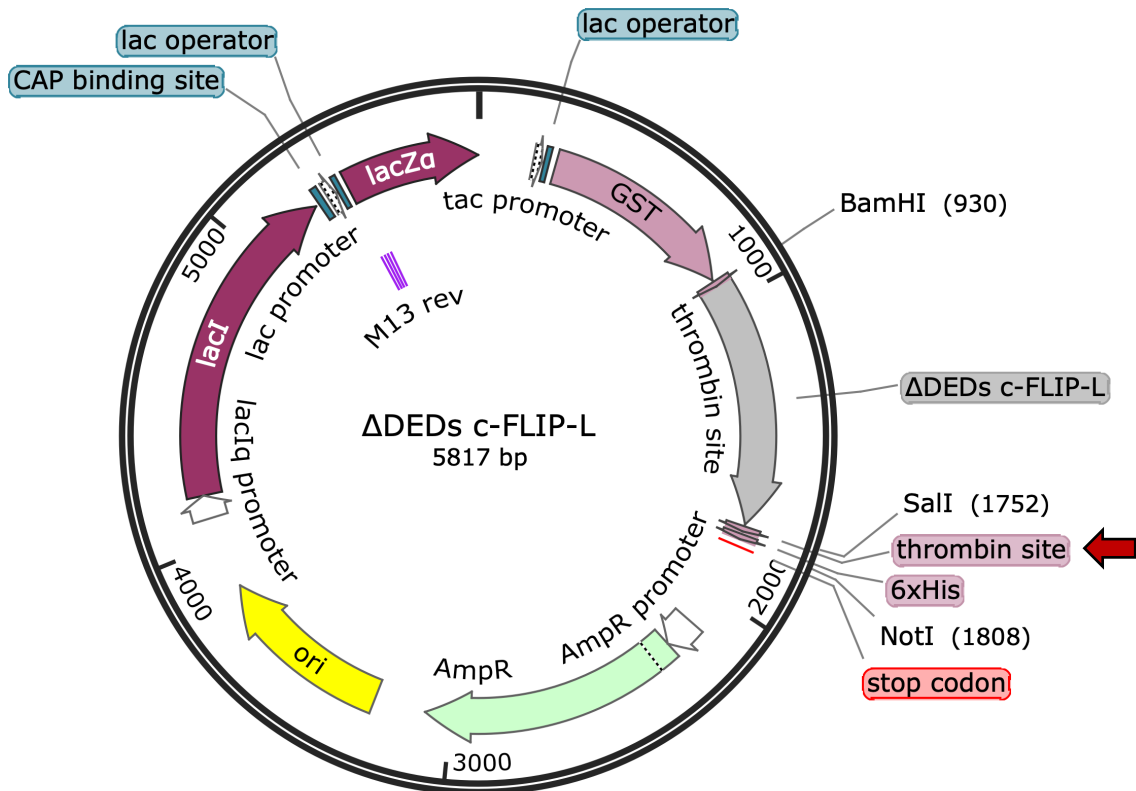
B
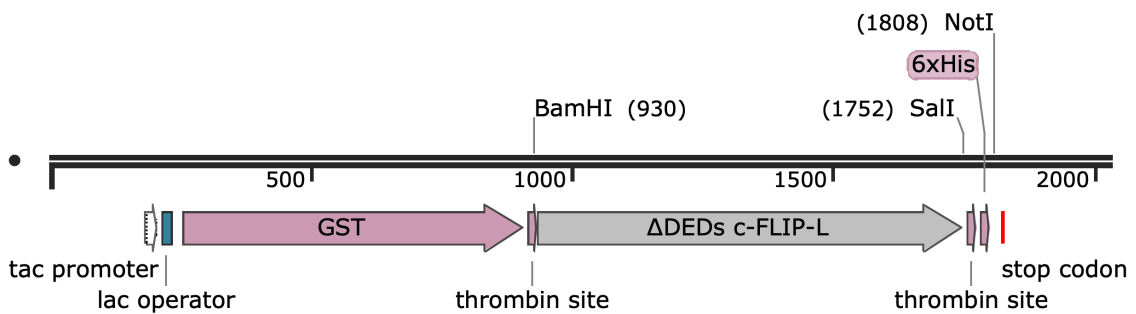
Figure 41. Map of the ΔDEDs cFLIP-L/pGEX-4T-3/thrombin-(His)₆ construct.
A. The ΔDEDs cFLIP-L gene (wild type or D376A mutant) was inserted into *BamH1* and *Sal1* sites of the pGEX-4T-3/thrombin-(His)₆ vector **B.** Detailed schematics of the ΔDEDs cFLIP-L insert with N-terminal GST and C-terminal (His)₆ tag with thrombin sites for tags removal.

ΔDEDs cFLIP-L (wild type) and ΔDEDs cFLIP-L (D376A) DNA segments were engineered into *BamH1* and *Sal1* sites of the pGEX-4T-3/TEV-(His)₆ vector. As a result, the N-termini and C-termini of the proteins were fused to the GST tag and the (His)₆ tag, respectively. The N-GST tag can cut off by thrombin treatment, whereas C-(His)₆ can be removed with TEV (Figure 42A and B).

A
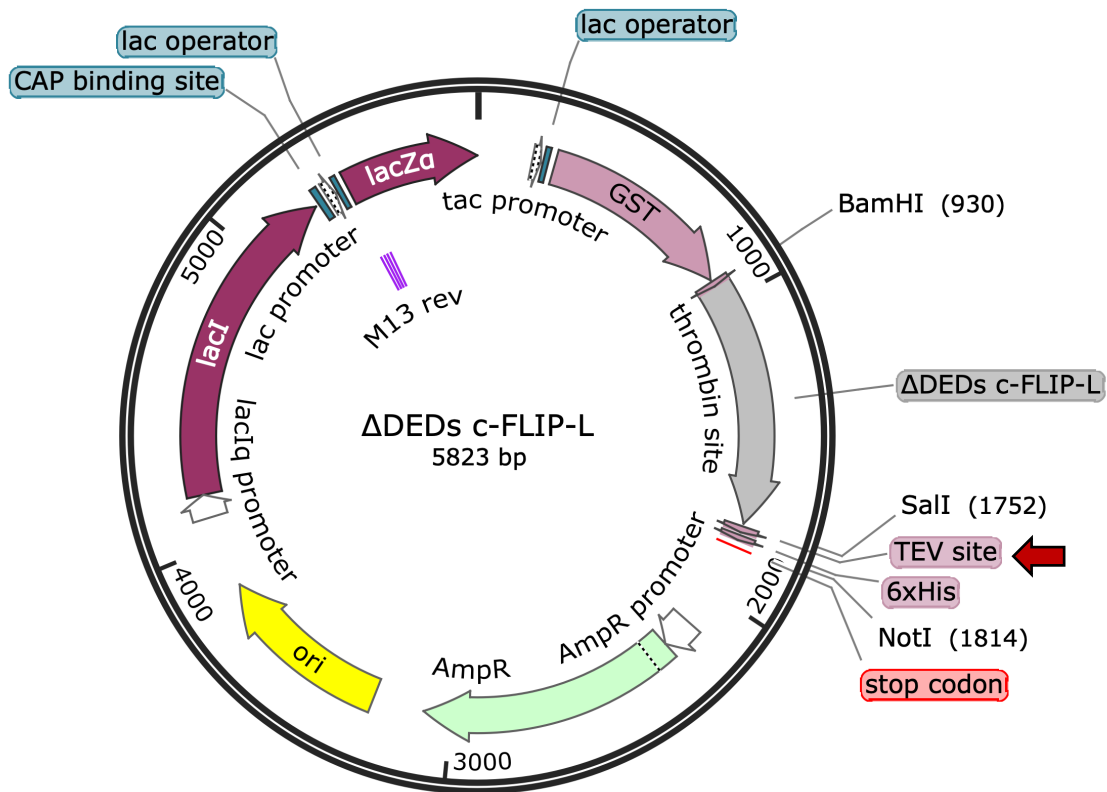
B
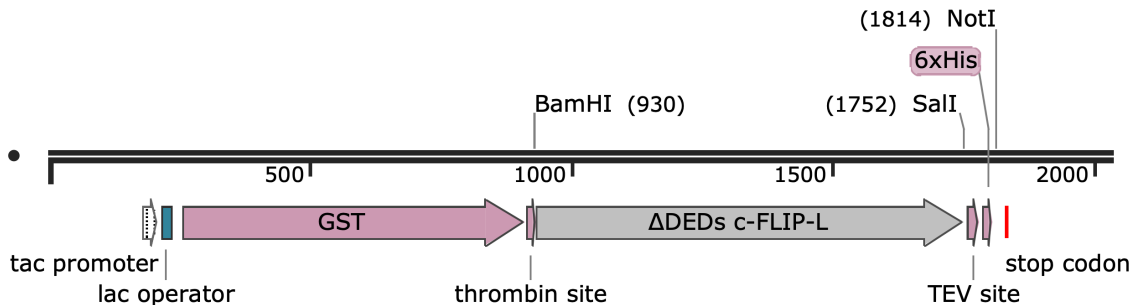
Figure 42. Map of the ΔDEDs cFLIP-L/pGEX-4T-3/TEV-(His)₆ construct.
A. The ΔDEDs cFLIP-L gene (wild type or D376A mutant) was inserted into *BamH1* and *Sal1* sites of the pGEX-4T-3/TEV-(His)₆ vector **B.** Detailed schematics of the ΔDEDs cFLIP-L insert with N-terminal GST and C-terminal (His)₆ tag with TEV site for tag removal.

As a host for protein expression, *E. coli* strain BL21-RIL was used. These bacteria are derivatives of the BL21 *E. coli* strain, which is known to enable high-level protein expression, as they are engineered to contain genes encoding for rare tRNAs. BL21-RIL cells were selected due to the fact, that the protein expression with the pGEX-4T-3 plasmid is driven by the tac promoter, therefore it was not necessary to employ a DE3 lysogen as host.

As a starting point, induction with 0.1 mM (final concentration) of IPTG, and expression at 30°C for 3h and 15 h were tested. The constructs that were assessed for recombinant protein expression included: empty pGEX-4T-3/thrombin-C-(His)$_6$ vector (used to express GST as a control for protein assays), ΔDEDs caspase-8 (C360A)/thrombin-(His)$_6$ (control for expression conditions) as well as ΔDEDs caspase-10 (C401A), ΔDEDs caspase-10 (D415A), ΔDEDs cFLIP-L (wild type) and ΔDEDs cFLIP-L (D376A) constructs with both thrombin-(His)$_6$ and TEV-(His)$_6$ tags.

Tables 35-38 summarise the basic information regarding protein expression constructs and expected protein masses after expression and purification.

Table 35. Main features of the pGEX-4T-3/thrombin-(His)$_6$ control construct with expected protein masses after expression

Protein Details	
DNA Construct	None; the expression product is the N-terminal GST tag fused with C-terminal (His)$_6$-tag
Host Cell Strain	BL21-RIL
Tagged Protein MW (kDa)	26

Table 36. Main features of the human recombinant ΔDEDs caspase-8 constructs with expected protein masses after expression.

Protein Details	
DNA Construct	ΔDEDs caspase-8 (aa residues 217-479; C360A active site mutant), pGEX-4T-3, N-terminal GST tag and C-terminal (His)$_6$-tag
Host Cell Strain	BL21-RIL
Tagged Protein MW (kDa)	58
Untagged Protein MW (kDa)	29

Table 37. Main features of the human recombinant ΔDEDs caspase-10 constructs with expected protein masses after expression.

Protein Details	
DNA Construct	ΔDEDs caspase-10 (aa residues 219-521, C401A active site mutant; D415A linker mutant), pGEX-4T-3, N-terminal GST tag and C-terminal (His)$_6$-tag
Host Cell Strain	BL21-RIL
Tagged Protein MW (kDa)	62
Untagged Protein MW (kDa)	33

Table 38. Main features of the human recombinant ΔDEDs cFLIP-L constructs with expected protein masses after expression.

Protein Details	
DNA Construct	ΔDEDs cFLIP-L (aa residues 208-480; wild type and D376A cleavage mutant), pGEX-4T-3, N-terminal GST tag and C-terminal (His)$_6$-tag
Host Cell Strain	BL21-RIL
Tagged Protein MW (kDa)	57
Untagged Protein MW (kDa)	28

3.7. Expression of Human Recombinant ΔDEDs Caspase-10 (C401A), ΔDEDs Caspase-10 (D415A) and ΔDEDs cFLIP-L (wild type and D376A) Constructs

The constructs were transformed into BL21-RIL cells. After reaching the required OD (A_{600} = 0.6-0.8), small aliquots of whole cell extract (WCE) samples were taken before induction and saved for analysis. Recombinant protein expression was induced with IPTG, followed by incubation with shaking overnight. In order to analyse the protein expression levels, WCE samples were taken 3 h and 15 h post-induction. The samples were run on 12% SDS-PAGE and stained with Coomassie Brilliant Blue.

As shown in Figure 35A, B, C, D, E and F, GST/thrombin-C-(His)$_6$, N-GST ΔDEDs caspase-8 (C360A)/thrombin-C-(His)$_6$ as well as N-GST ΔDEDs caspase-10 (C401A), N-GST ΔDEDs caspase-10 (D415A), N-GST ΔDEDs cFLIP-L (wild type) and N-GST ΔDEDs cFLIP-L (D376A) with both thrombin-(His)$_6$ and TEV-(His)$_6$ tags were successfully expressed after 3 h and 15 h. The 3h expression enabled more efficient production, when compared to 15 h induction (Figure 43A, B, C, D, E and F).

The levels of N-GST ΔDEDs caspase-10 (C401A), N-GST ΔDEDs caspase-10 (D415A), N-GST ΔDEDs cFLIP-L (wild type) and N-GST ΔDEDs cFLIP-L (D376A) with both thrombin-(His)$_6$ and TEV-(His)$_6$ tags (Figure 35C, D, E and F) were comparable with the results obtained for the control GST/thrombin-C-(His)$_6$, N-GST and ΔDEDs caspase-8 (C360A)/thrombin-C-(His)$_6$ (Figure 35A and B).
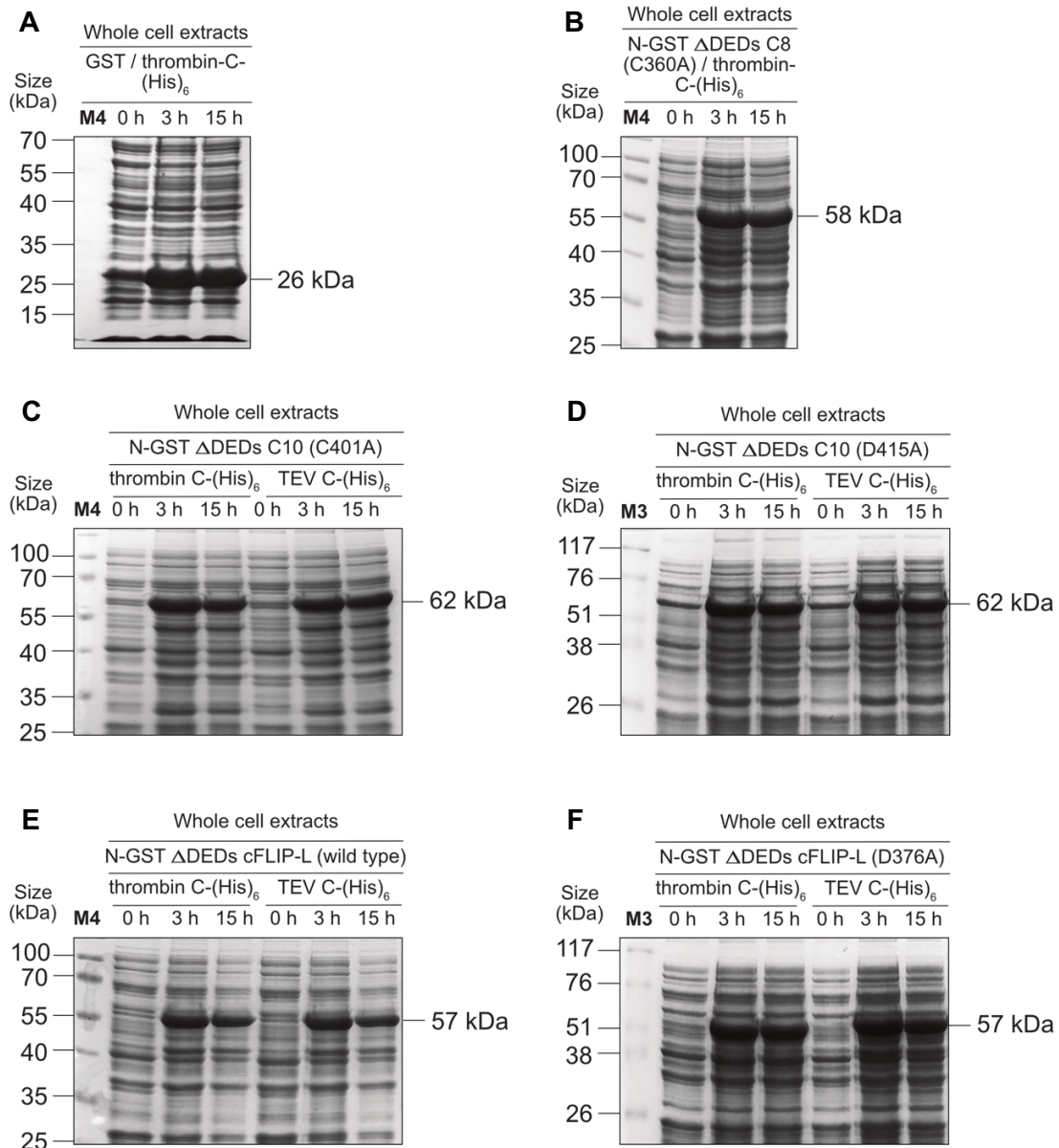
Figure 43. Expression levels of the proteins produced by using the pGEX-4T-3 system.
A-F. The whole cell extract (WCE) samples were taken before induction as well as 3 h and 15 h post-induction (IPTG at 0.1 mM final concentration) for the analysis of the expression levels of the following proteins: N-GST ΔDEDs caspase-10 (C401A), N-GST ΔDEDs caspase-10 (D415A), N-GST ΔDEDs cFLIP-L (wild type) and N-GST ΔDEDs cFLIP-L (D376A) with both thrombin-(His)$_6$ and TEV-(His)$_6$. GST/thrombin-C-(His)$_6$ and N-GST ΔDEDs caspase-8 (C360A)/thrombin-C-(His)$_6$ were used as controls. The samples were analysed on 12% SDS-PAGE followed by staining with Coomassie Brilliant Blue.
M3 (Marker 3) and M4 (marker 4) – protein ladders.

In order to examine solubility levels of the expressed proteins, 3 h after expression the bacteria were harvested and lysed by sonication. Supernatants and insoluble fractions were separated by centrifugation. The lysate, supernatant and resuspended pellet fractions were aliquoted and taken for analysis by using 12% SDS-PAGE and staining with Coomassie Brilliant Blue.

We observed that the highest levels of N-GST ΔDEDs caspase-10 (C401A), N-GST ΔDEDs caspase-10 (D415A), N-GST ΔDEDs cFLIP-L (wild type) and N-GST ΔDEDs cFLIP-L (D376A) with both thrombin-$(His)_6$ and TEV-$(His)_6$ tags were found in the resuspended pellets (Figure 44A, C, D, E and F). As previously, the expressed proteins were aggregated in inclusion bodies. The observation was comparable with the result obtained for the control N-GST ΔDEDs caspase-8 (C360A)/thrombin-C-$(His)_6$, which was also most abundant in the resuspended pellet fraction. In contrast and as expected, the control GST/thrombin-C-$(His)_6$ was mostly found in the supernatant.

As previously, solubilisation under denaturing conditions was used to isolate and purify the recombination proteins from the inclusion bodies. The solubilisation was performed in the same manner, as described for the pET-28a system.

A

WCE

GST / thrombin-C-(His)$_6$

Size (kDa) — M4 0 h 3 h lys sup pel

70 — , 55 —, 40 —, 35 —, 25 —, 15 — — 26 kDa

B

WCE

N-GST ΔDEDs C8 (C360A)/
thrombin-C-(His)$_6$

Size (kDa) — M4 0 h 3 h lys sup pel

100 —, 70 —, 55 —, 40 —, 35 —, 25 — — 58 kDa

C

WCE   WCE

N-GST ΔDEDs caspase-10 (C401A)

thrombin-C-(His)$_6$ TEV-C-(His)$_6$

Size (kDa) — M4 0 h 3 h lys sup pel   M4 0 h 3 h lys sup pel

100 —, 70 —, 55 —, 40 —, 35 —, 25 — — 62 kDa

D

WCE   WCE

N-GST ΔDEDs caspase-10 (D415A)

thrombin-C-(His)$_6$ TEV-C-(His)$_6$

Size (kDa) — M4 0 h 3 h lys sup pel   M4 0 h 3 h lys sup pel

100 —, 70 —, 55 —, 40 —, 35 —, 25 — — 62 kDa

E

WCE   WCE

N-GST ΔDEDs c-FLIP-L (wild type)

thrombin-C-(His)$_6$ TEV-C-(His)$_6$

Size (kDa) — M4 0 h 3 h lys sup pel   M4 0 h 3 h lys sup pel

100 —, 70 —, 55 —, 40 —, 35 —, 25 — — 57 kDa

F

WCE   WCE

N-GST ΔDEDs c-FLIP-L (D376A)

thrombin-C-(His)$_6$ TEV-C-(His)$_6$

Size (kDa) — M4 0 h 3 h lys sup pel   M4 0 h 3 h lys sup pel

100 —, 70 —, 55 —, 40 —, 35 —, 25 — — 57 kDa

Figure 44. Solubility levels of the proteins expressed by using the pGEX-4T-3 system.
A. After 3 h of GST/thrombin-C-(His)$_6$ expression, the lysate, supernatant and resuspended pellet samples were analysed on 12% SDS-PAGE and stained with Coomassie Brilliant Blue. WCE samples were used as control. **B.** After 3 h of N-GST ΔDEDs caspase-8 (C360A)/thrombin-C-(His)$_6$ expression, the lysate, supernatant and resuspended pellet samples were analysed on 12% SDS-PAGE followed by staining with Coomassie Brilliant Blue. WCE samples served as controls. **C.** After 3 h expression of N-GST ΔDEDs caspase-10 (C401A) with both thrombin-(His)$_6$ and TEV-(His)$_6$ tags, the lysate, supernatant and resuspended pellet samples were analysed on 12% SDS-PAGE and stained with Coomassie Brilliant Blue. WCE samples were utilised as controls. **D.** After 3 h expression of N-GST ΔDEDs caspase-10 (D415A) with both thrombin-(His)$_6$ and TEV-(His)$_6$ tags, the lysate, supernatant and resuspended pellet samples were analysed on 12% SDS-PAGE followed by staining with Coomassie Brilliant Blue. **E.** After 15 h expression of N-GST ΔDEDs cFLIP-L (wild type) with both thrombin-(His)$_6$ and TEV-(His)$_6$ tags, the lysate, supernatant and resuspended pellet samples were analysed on 12% SDS-PAGE and stained with Coomassie Brilliant Blue. WCE samples were used as controls. **F.** After 15 h expression of N-GST ΔDEDs cFLIP-L (D376A) with both thrombin-(His)$_6$ and TEV-(His)$_6$ tags, the lysate, supernatant and resuspended pellet samples were analysed on 12% SDS-PAGE and stained with Coomassie Brilliant Blue. WCE samples served as controls.
M4 (marker 4) – protein ladder, WCE – whole cell extracts, Lys – lysed cells, Sup – supernatant, Pel – cell pellet.

3.8. Purification of the Control GST/thrombin-C-(His)$_6$ Protein

Soluble (His)$_6$-tagged GST was purified on IMAC column by following the manufacturer's protocol. Analysis on 15% SDS-PAGE and subsequent staining with Coomassie Brilliant Blue showed that the protein was successfully purified. Assessed elution fractions in the major elution peak at 280 nm (Figure 45A and B) revealed the presence of one major protein band. The observed 26 kDa band is consistent with the size of the (His)$_6$-tagged GST (Figure 45A). All elution fractions containing the protein of interest were combined into one sample, dialysed and concentrated to 2 ml. Small aliquots of the elute, dialysed and concentrated samples were run on 15% SDS-PAGE followed by staining with Coomassie Brilliant Blue. The analysis further confirmed the presence of the purified protein (Figure 45C).

A

B

C
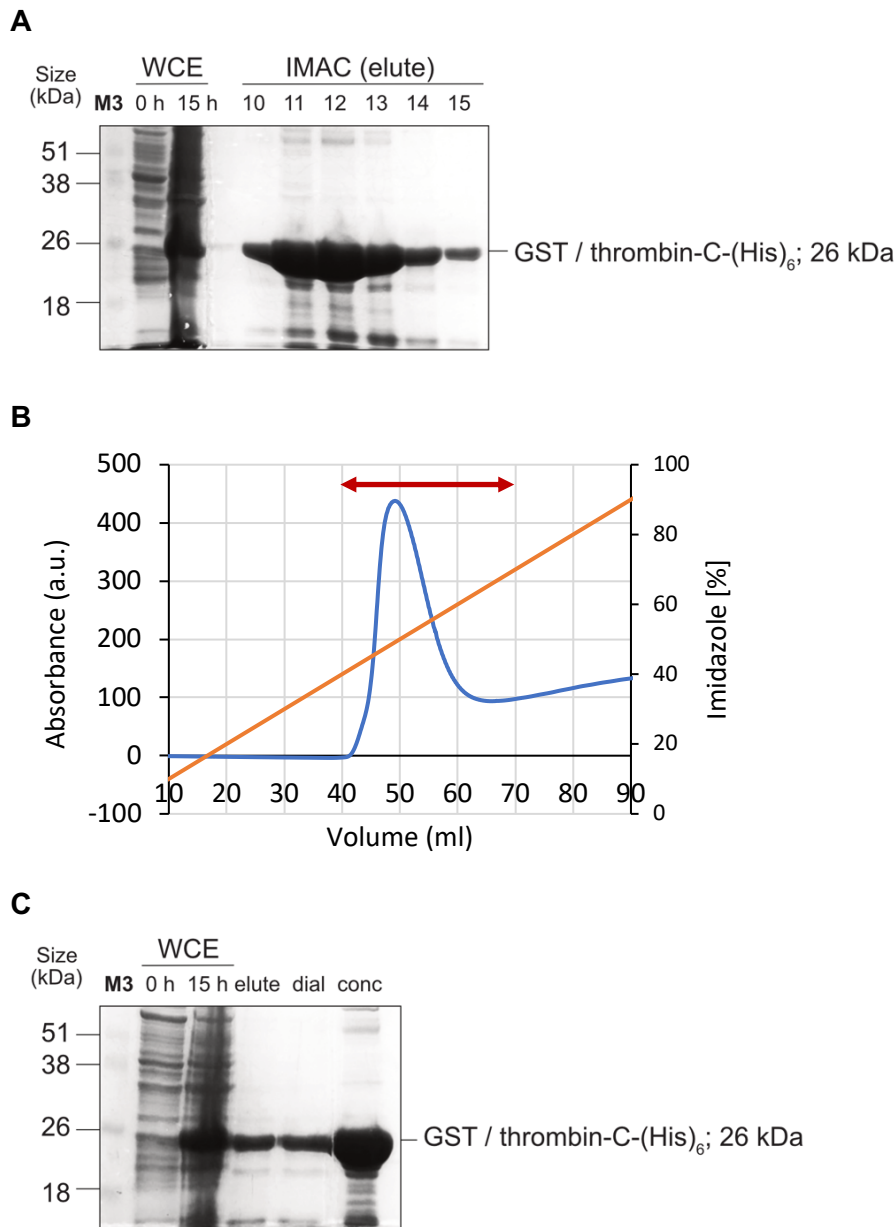
Figure 45. IMAC (Ni-NTA) purification of GST/thrombin-C-(His)$_6$.
A. Analysis of fractions after purification of GST/thrombin-C-(His)$_6$ on IMAC 5 ml His-trap FF nickel-nitrilotriacetic (Ni-NTA) column. The fractions reveal a strong band running at 26 kDa. Following purification of the protein, the WCE (control) samples and Ni-NTA elution fractions number 10, 11, 12, 13, 14 and 15 were analysed by using 15% SDS-PAGE and subsequent staining with Coomassie Brilliant Blue. **B.** Elution profile of GST/thrombin-C-(His)$_6$ on IMAC 5 ml His-trap FF nickel-nitrilotriacetic (Ni-NTA) column; blue line represents protein absorbance; orange line represents imidazole gradient. Elution fractions taken for the SDS-PAGE analysis are indicated by the red arrow. **C.** Fractions containing the desired protein were pooled, dialysed and concentrated for further processing. The elution dialysed and concentrated protein samples were analysed on 15% SDS-PAGE and staining with Coomassie Brilliant Blue. WCE samples were used as controls.
M3 (Marker 3) – protein ladder, WCE – whole cell extracts, dial – dialysed, conc – concentrated.

The concentrated (2 ml) sample containing (His)$_6$-tagged GST was further purified on SEC column. Protein eluates were collected as 2 ml fractions and examined for purity by using 15% SDS-PAGE followed by staining with Coomassie Brilliant Blue (Figure 46A and B). Analysis of elution fractions in the major elution peak at 280 nm showed very high purity levels of (His)$_6$-tagged GST (Figure 46A). Any host proteins that co-purified on IMAC column and co-eluted within the (His)$_6$-tagged GST peak were not separated by SEC and were present in minimal amounts, acceptable for experimental purposes.

A

B
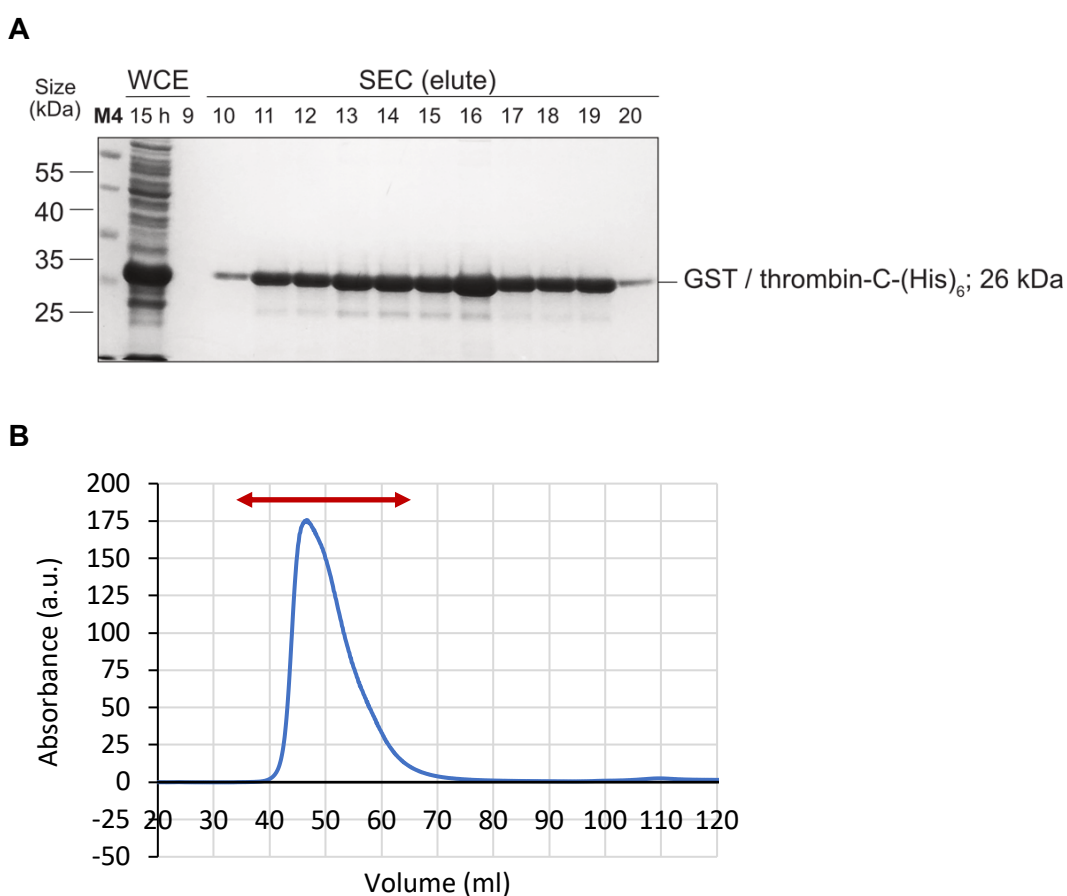
Figure 46. Purification of (His)$_6$-tagged GST protein by using SEC.
A. Analysis of fractions after purification of (His)$_6$-tagged GST on SEC 120 ml HiLoad Superdex 75 16/60 column. The fractions reveal a strong band running at 26 kDa. After purification, the SEC elution fractions from 9 to 20 were taken for analysis. WCE sample was used as control. All samples were separated on 15% SDS-PAGE followed by staining with Coomassie Brilliant Blue.
B. Elution profile of (His)$_6$-tagged GST on SEC 120 ml HiLoad Superdex 75 16/60 column; blue line represents protein absorbance. Elution fractions taken for the SDS-PAGE analysis are indicated by the red arrow.
***M4** (Marker 4) – protein ladder.*

Elution fractions containg the protein of interest were pooled, combined into one sample and concentrated in order to obtain 2 ml of the final pure protein sample. The concentration of purified (His)$_6$-tagged GST sample was calculated below by using Beer-Lambert formula, protein extinction coefficient and absorbance result measured by spectrophotometer.

Beer–Lambert formula: $A = \varepsilon\,l\,c$

Extinction coefficient (ε) = 42860
Path (l) = 1 cm
A$_{280}$ = 0.08838008 (1 ml, 1/100 dilution)
Concentration (c)

Calculation: $A = \varepsilon\,l\,c \rightarrow c = \frac{A}{\varepsilon} \rightarrow c = \frac{0.08838008}{42860} \times 100 = 0.00020621$ M = 206.21 μM

Next, the molar concentration of purified untagged ΔDEDs caspase-8 (C360A) was converted into concentration in mg/ml as follows:

Formula: *concentration (mg/ml) = c (Molar) x MW (Daltons)*

Concentration (c) = 0. 00020621 M
Molecular weight (MW) = 26000 Da

Calculation: concentration = 0.00020621 M x 26000 Da = 5.361 mg/ml

Finally, purified (His)$_6$-tagged GST was separated into 200 μl aliquots and prepared for storage at -20°C.

3.9. Purification of N-GST ΔDEDs Caspase-10 (D415A)/thrombin-C-(His)$_6$

Following solubilisation under denaturing conditions, supernatant containing N-GST ΔDEDs aspase-10 (D415A)/thrombin-C-(His)$_6$ was applied onto IMAC column and purified as described for the pET-28a system.

The results obtained for N-GST ΔDEDs caspase-10 (D415A)/thrombin-C-(His)$_6$ showed that the protein was successfully purified (Figure 47A and B). The fractions at the major elution peak at 280 nm were analysed on 12% SDS-PAGE and stained with Coomassie Brilliant Blue. We observed a 62 kDa protein band, which corresponds to the expected size of the purified protein (Figure 47).

Elution fractions containing the protein of interest were combined into one sample, dialysed and concentrated to ~10 ml. in order to remove the N-terminal GST and C-terminal (His)$_6$ tag, the protein of interest was treated with 125 units of thrombin. The sample was rotated at 4°C overnight and re-applied onto IMAC column in the same manner as previously described. The flow-through fractions containing N-GST ΔDEDs caspase-10 (D415A)/thrombin-C-(His)$_6$ were collected, combined and concentrated to 2 ml for further purification on SEC column. Small aliquots of the following samples: eluted, dialysed and concentrated as well as flow-through, wash and concentrated flow-through after IMAC were run on 12% SDS-PAGE and stained with Coomassie Brilliant Blue (Figure 47C). The analysis revealed the presence of two protein bands, 33 kDa and 26 kDa, in the concentrated fraction after tags removal and second IMAC purification (Figure 47C). The 33 kDa and 26 kDa bands corresponded to the sizes of untagged ΔDEDs caspase-10 (D415A) and GST, respectively, indicating a successful removal of the GST and (His)$_6$ tags as well as separation of the untagged protein. Surprisingly, the

levels of untagged ΔDEDs caspase-10 (D415A) in the concentrated fraction after second IMAC purification were considerably reduced, when compared with the fraction obtained and concentrated after the first purification step (Figure 47C).

Moreover, further purification on the SEC column showed that the protein of interest eluted at the end of the purification process (indicated by the red arrow in Figure 47D), which was not in line with the expected elution at 45 ml, observed previously for untagged ΔDEDs caspase-10 (D415A) (Figure 32A, p. 144). Therefore, it was assumed, that the protein of interest was not stable and could not be used for experimental purposes.

A

WCE — IMAC (elute)

N-GST ΔDEDs caspase-10 (D415A) / thrombin-C-(His)$_6$; 62 kDa

B

C

WCE — IMAC

N-GST ΔDEDs caspase-10 (D415A) / thrombin-C-(His)$_6$; 62 kDa

← untagged caspase-10 (D415A); 33 kDa
← cleaved off GST tag; 26 kDa
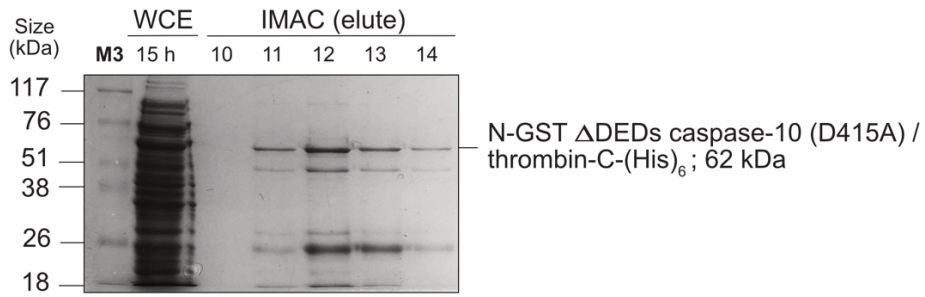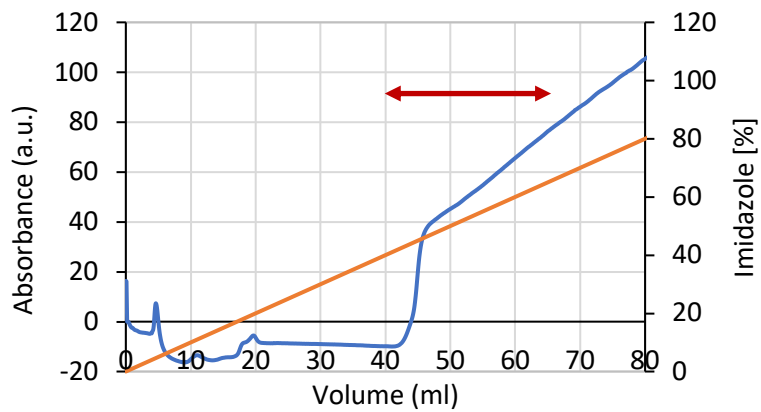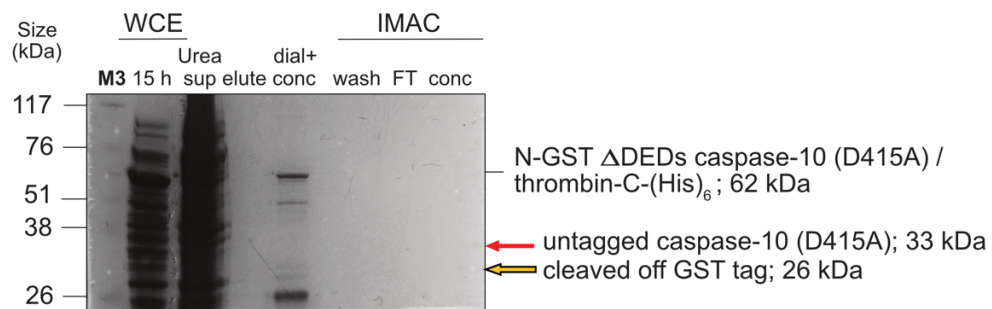
D
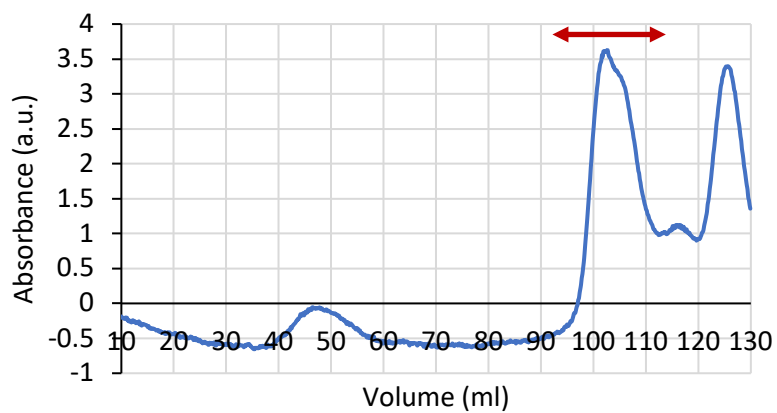
Figure 47. IMAC (Ni-NTA) and SEC purification of N-GST ∆DEDs caspase-10 (D415A)/thrombin-C-(His)$_6$.

A. Analysis of fractions after purification of N-GST ∆DEDs caspase-10 (D415A)/thrombin-C-(His)$_6$ on IMAC 5 ml His-trap FF nickel-nitrilotriacetic (Ni-NTA) column. The fractions show a strong band running at 62 kDa. Following purification of the protein of interest, the WCE (control) sample and Ni-NTA elution fractions number 10, 11, 12, 13 and 14 were analysed by using 12% SDS-PAGE and subsequent staining with Coomassie Brilliant Blue. **B.** Elution profile of N-GST ∆DEDs caspase-10 (D415A)/thrombin-C-(His)$_6$ on IMAC 5 ml His-trap FF nickel-nitrilotriacetic (Ni-NTA) column; blue line represents protein absorbance; orange line represents imidazole gradient. Elution fractions taken for the SDS-PAGE analysis are indicated by the red arrow. **C**. Cleavage of C-terminal (His)$_6$. Fractions containing the desired protein were pooled, dialysed and concentrated for thrombin treatment. The elution dialysed and concentrated protein samples as well as flow-through, wash and concentrated flow-through after addition of thrombin and second IMAC purification were analysed on 12% SDS-PAGE and staining with Coomassie Brilliant Blue. WCE sample and supernatant after urea lysis were used as controls. The fractions show very low levels of the desired protein at around 33 kDa. **D.** Elution profile of N-GST ∆DEDs caspase-10 (D415A)/thrombin-C-(His)$_6$ on SEC 120 ml HiLoad Superdex 75 16/60 column; blue line represents protein absorbance. Fractions that possibly contain the protein of interest are indicated by the red arrow.

M3 (Marker 3) – protein ladder, WCE – whole cell extracts, sup – supernatant, dial – dialysed, conc – concentrated.

3.10. Investigation of Caspase-10-Mediated Processing of Caspase-8 *in Vitro*

As mentioned, in the current study we were interested in investigation of the role of caspase-10 as a component of the FADDosome and a potential caspase-8 activator. In order to assess, whether caspase-10 has the ability to activate caspase-8 *in vitro*, we performed an activity assay for purified untagged ΔDEDs caspase-10 (D415A) and untagged ΔDEDs caspase-8 (C360A), which were expressed by using the pET-28a system followed by purification on the IMAC and SEC columns, as described earlier in this Chapter. The roles of untagged ΔDEDs caspase-10 (D415A) and untagged ΔDEDs caspase-8 (C360A) in the reaction was to act as an enzyme and substrate, respectively.

First, the purified untagged ΔDEDs caspase-10 (D415A) and untagged ΔDEDs caspase-8 (C360A) were mixed at the concentrations of 1 μM and 10 μM, respectively, and incubated at physiological conditions (50 mM Trizma base, 150 mM NaCl [pH 7.4]) in a total volume of 250 μl of the reaction buffer. The mixture was incubated at room temperature. At the 0, 10, 40 and 160 minutes, 30 μl of the reaction was aliquoted into the loading buffer. As a control, 10 μM of untagged ΔDEDs caspase-8 (C360A) alone was used and subjected to the same conditions as the mixture. At the 0, 10, 40 and 160 minutes, 30 μl of samples were aliquoted into the loading buffer. The control and assay samples were run on 15% SDS-PAGE and analysed by Western Blot.

As shown in Figure 46, after performing the ΔDEDs caspase-10 (D415A) and ΔDEDs caspase-8 (C360A) assay, the levels of the single-chained ΔDEDs caspase-8 (C360A) decreased slightly and gradually after 10 and 40. After 160 minutes, the levels of the

protein were markedly decreased. However, we observed the same phenomenon for the control ΔDEDs caspase-8 (C360A).
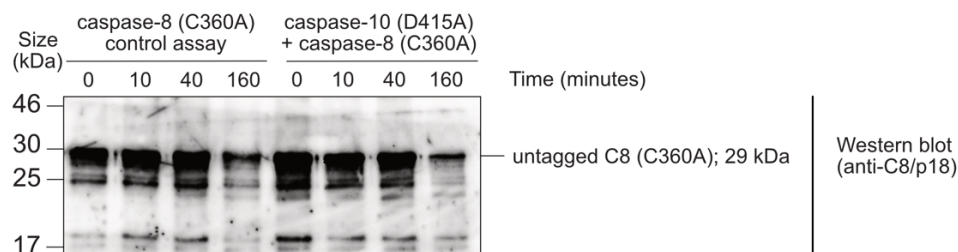
Figure 48. Caspase-10 / caspase-8 activity assay in physiological conditions.
1 μM of untagged ΔDEDs caspase-10 (D415A) (enzyme) and 10 μM of purified untagged ΔDEDs caspase-8 (C360A) (substrate) were mixed in a total volume of 250 μl of the reaction buffer (50 mM Trizma base, 150 mM NaCl, [pH 7.4]) and incubated at room temperature. 10 μM of purified untagged ΔDEDs caspase-8 (C360A) was used as a control and subjected to the same reaction conditions. At noted timepoints, 30 μl of the control and reaction were aliquoted into the loading buffer. The samples were analysed by 15% SDS-PAGE and Western blot. An antibody against caspase-8/p18 subunit was used to detect the protein of interest.

It was assumed, that the observed decrease of the control ΔDEDs caspase-8 (C360A) was caused by one of the following possible scenarios: (I) instability or (II) self-cleavage of the protein into smaller fragments, which increased proportionally to the time of incubation. In order to examine the stability of ΔDEDs caspase-8 (C360A), we used 10 μM of untagged ΔDEDs caspase-8 (C360A) alone, which was incubated at room temperature and at physiological conditions. To test the ΔDEDs caspase-8 (C360A) stability in more detail, the samples were taken after 0, 0.5, 1, 1.5, 2, 3, 4, 5 and 10 minutes of incubation and aliquoted into the loading buffer. The Western blot result showed, that the levels of single-chained ΔDEDs caspase-8 (C360A) were gradually reduced, proportionally to the time of incubation (Figure 49A). This indicated that the protein becomes unstable or cleaves itself after a short period of time. Therefore, it was essential to optimise buffer and reaction conditions for the assay.

For this, 10 μM of purified untagged ΔDEDs caspase-8 (C360A) alone was used and assessed for its stability by using 50 mM Trizma base, 150 mM NaCl, 10% PEG, 0.1%

CHAPS [pH 7.4] buffer, which provided stabilising conditions for caspases reactions. As previously, 10 μM of untagged ΔDEDs caspase-8 (C360A) alone at physiological conditions was used as a control. The samples were taken and aliquoted into the loading buffer after 0, 0.5, 1 1.5, 2, 5 and 10 minutes and analysed by Western blot. As expected, the levels of control ΔDEDs caspase-8 (C360A) were gradually decreasing with time (Figure 49B). In contrast, at stabilising conditions, the levels of single-chained ΔDEDs caspase-8 (C360A) were not reduced, indicating that the protein remained stable in the tested conditions (Figure 49B).

A
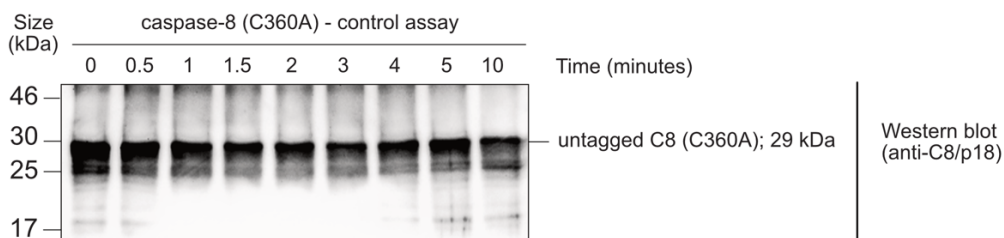
B
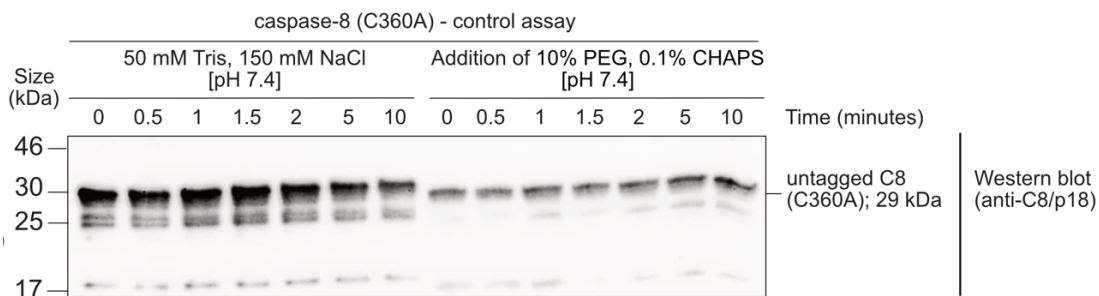
Figure 49. Stability test for ΔDEDs caspase-8 (C360A).
A. 10 μM of purified untagged ΔDEDs caspase-8 (C360A) was incubated at room temperature in a total volume of 250 μl of the physiological buffer (50 mM Trizma base, 150 mM NaCl, [pH 7.4]). At noted timepoints, 30 μl of the control and reaction were aliquoted into the loading buffer. The samples were analysed 15% SDS-PAGE and Western blot. An antibody against casapase-8 p18 subunit was used, in order to assess the levels of ΔDEDs caspase-8 (C360A). **B.** 10 μM of purified untagged ΔDEDs caspase-8 (C360A) was incubated at room temperature in a total volume of 250 μl of the stabilising buffer (50 mM Trizma base, 150 mM NaCl, 10% PEG, 0.1% CHAPS, [pH 7.4]). 10 μM of purified untagged ΔDEDs caspase-8 (C360A) incubated at physiological conditions was used as control. At noted timepoints, 30 μl of the control and reaction were aliquoted into the loading buffer. The samples were run on 15% SDS-PAGE and examined for ΔDEDs caspase-8 (C360A) stability by Western blot. An antibody against casapase-8 p18 subunit was used, in order to assess the levels of ΔDEDs caspase-8 (C360A).

In order to assess, whether ΔDEDs caspase-8 (C360A) has the ability to cleave itself, we performed an assay in the presence of kosmotropic salts, which are known to accelerate dimerization and subsequently, proteolysis and activation of proteins (Boatright et al., 2004). For this, we used 10 μM of purified untagged ΔDEDs caspase-8 (C360A) alone, which was incubated in the reaction buffer containing kosmotropic salts (50 mM Trizma base, 150 mM NaCl, 1 M sodium citrate, [pH 7.4]) As previously, 10 μM of untagged ΔDEDs caspase-8 (C360A) alone was incubated at physiological conditions was used as a control.

The control and tested samples were aliquoted into the loading buffer after 0, 0.5, 1, 1.5, 2, 5 and 10 minutes and analysed on 15% SDS-PAGE followed by Western blot. As shown in Figure 50 (right), the levels single-chained of ΔDEDs caspase-8 (C360A) were not decreased in the presence of 1 M sodium citrate after 0.5, 1, 1.5, 2, 5 and 10 minutes and were comparable with the results obtained for the control (Figure 50; left), ruling out the ability of ΔDEDs caspase-8 (C360A) to cleave itself.
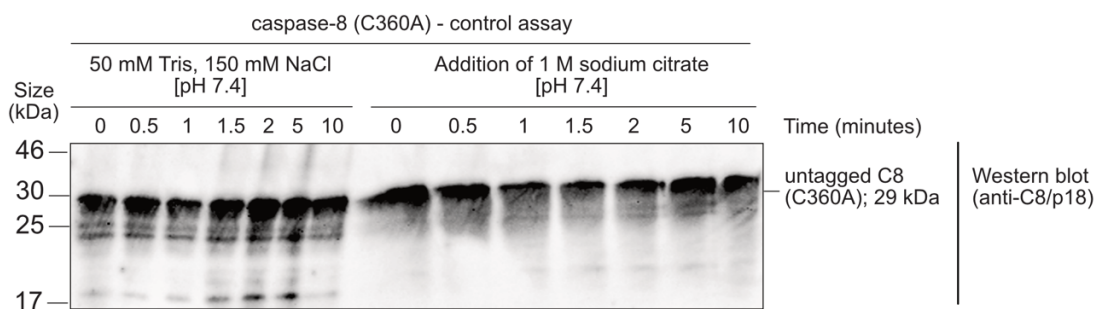
Figure 50. Self-cleavage test for ΔDEDs caspase-8 (C360A) in the presence of kosmotropic salts.
10 μM of purified untagged ΔDEDs caspase-8 (C360A) alone was incubated at room temperature in a total volume of 250 μl of the buffer containing kosmotropic salts (50 mM Trizma base, 150 mM NaCl, 1 M sodium citrate, [pH 7.4]). 10 μM of purified untagged ΔDEDs caspase-8 (C360A) incubated in physiological conditions was used as a control. At noted timepoints, 30 μl of the control and reaction were aliquoted into the loading buffer. The samples were run on 15% SDS-PAGE and examined for ΔDEDs caspase-8 (C360A) stability by Western blot. An antibody against casapase-8 p18 subunit was used, in order to assess the levels of ΔDEDs caspase-8 (C360A).

Next, we performed the caspase-10 / caspase-8 activity assay by using the stabilising conditions. For this, we mixed 1 μM of purified untagged ΔDEDs caspase-10 (D415A) and 10 μM of purified untagged ΔDEDs caspase-8 (C360A) and incubated in the stabilising reaction buffer (50 mM Trizma base, 150 mM NaCl, 10% PEG, 0.1% CHAPS, [pH 7.4]) for 0, 0.5, 1 1.5, 2, 5 and 10 minutes. As a control we used 10 μM of untagged ΔDEDs caspase-8 (C360A) alone incubated at stabilising conditions. At indicated timepoints, 30 μl of the control and mixture were aliquoted and analysed by 15% SDS-PAGE and Western blot. We observed that the levels of single chained ΔDEDs caspase-8 (C360A) were decreasing gradually and proportionally to the time of incubation and were markedly reduced, when compared with the control samples taken at compared timepoints (Figure 51). Thus, our data indicated that ΔDEDs caspase-10 (D415A) could proteolytically process ΔDEDs caspase-8 (C360A) *in vitro*.
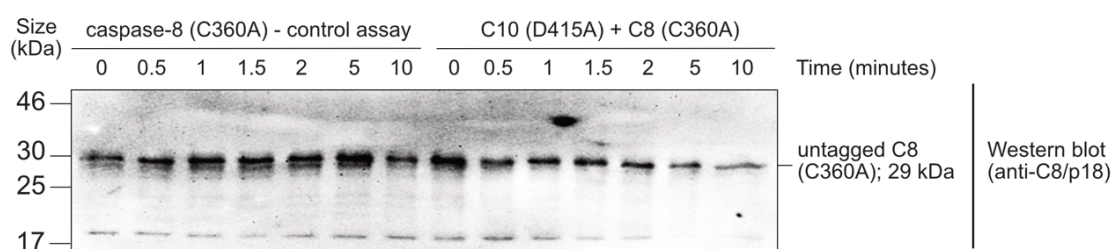
Figure 51. Caspase-10 / caspase-8 activity assay in stabilising conditions.
1 μM of untagged ΔDEDs caspase-10 (D415A) (enzyme) and 10 μM of purified untagged ΔDEDs caspase-8 (C360A) (substrate) were mixed in a total volume of 250 μl of the reaction buffer (50 mM Trizma base, 150 mM NaCl, 10% PEG, 0.1% CHAPS [pH 7.4]) and incubated at room temperature. 10 μM of purified untagged ΔDEDs caspase-8 (C360A) was used as a control and subjected to the same reaction conditions. At noted timepoints, 30 μl of the control and reaction were aliquoted into the loading buffer. The samples were analysed by 15% SDS-PAGE and Western blot. An antibody against caspase-8/p18 subunit was used to detect the protein of interest.

3.11. Investigation of Interaction Relationship Between Caspase-8 and FADD *in Vitro*

Conventionally, FADD is known to be involved in formation of the DISC complex, which initiates the extrinsic apoptotic pathway. As an adaptor molecule, FADD binds to a death receptor and recruits caspase-8, which is cleaved and activated at the DISC, leading to induction of apoptosis. It is believed that FADD and caspase-8 interact via homotypic interaction between the DEDs, which are present in the structure of both proteins. Currently, there is only one report describing the molecular mechanism responsible for such interaction, which is based on investigation of the FADD/pro-caspase-8 binding in the context of the DISC assembly (Carrington et al., 2006). The authors also proposed a model for such interaction by studying the crystal structure of MC159, also known as vFLIP. DEDs of this protein are structurally similar to DEDs of FADD and caspase-8. Therefore, the evidence of the FADD/caspase-8 interaction in the context of formation of the intracellular apoptosis-inducing protein complexes, such as FADDosome, which do not require involvement of the death receptors, is still missing.

Furthermore, in the previous report our group has demonstrated that FADD plays a central role in the FADDosome formation and acts as a functional partner in caspase-8 activation at the complex. The FADD-dependent caspase-8 activation was confirmed by examination of FADD-silenced HCT116 cells. Upon 5-FU treatment, both apoptosis and caspase-8 activation were inhibited in HCT.shFADD cells (Mohr et al., 2018).

Thus, we examined the interaction between FADD and caspase-8 by performing an pull-down assay (Figure 52). C-(His)$_6$ FADD-FL (bait protein) and untagged ΔDEDs caspase-8 (C360A) (prey protein) were expressed by using pET-28a system and purified on the IMAC and SEC columns, as shown earlier in this Chapter. The purified proteins were

mixed at equimolar ratio of 10 μM and incubated in the reaction buffer (50 mM Trizma base, 100 mM NaCl, [pH 7.4]) at room temperature. The mixture was applied onto the 5 ml IMAC (Ni-NTA) column followed by the washing and protein elution steps as described in the Methods Chapter. The wash and elution fraction were collected, concentrated to ~ 1ml and analysed for the presence of FADD-FL and ΔDEDs caspase-8 (C360A) by using 15% SDS-PAGE and Western blot.

Additionally, a pull-down assay was performed for the control GST/thrombin-C-(His)$_6$ and untagged ΔDEDs caspase-8 (C360A). The control protein was expressed by using the pGEX-4T-3 system followed by purification on the IMAC and SEC columns, as described earlier in this Chapter. In principle, the assay was carried out in the same manner as for C-(His)$_6$-tagged FADD-FL and untagged ΔDEDs caspase-8 (C360A), followed by 15% SDS-PAGE and Western blot analysis (Figure 52).
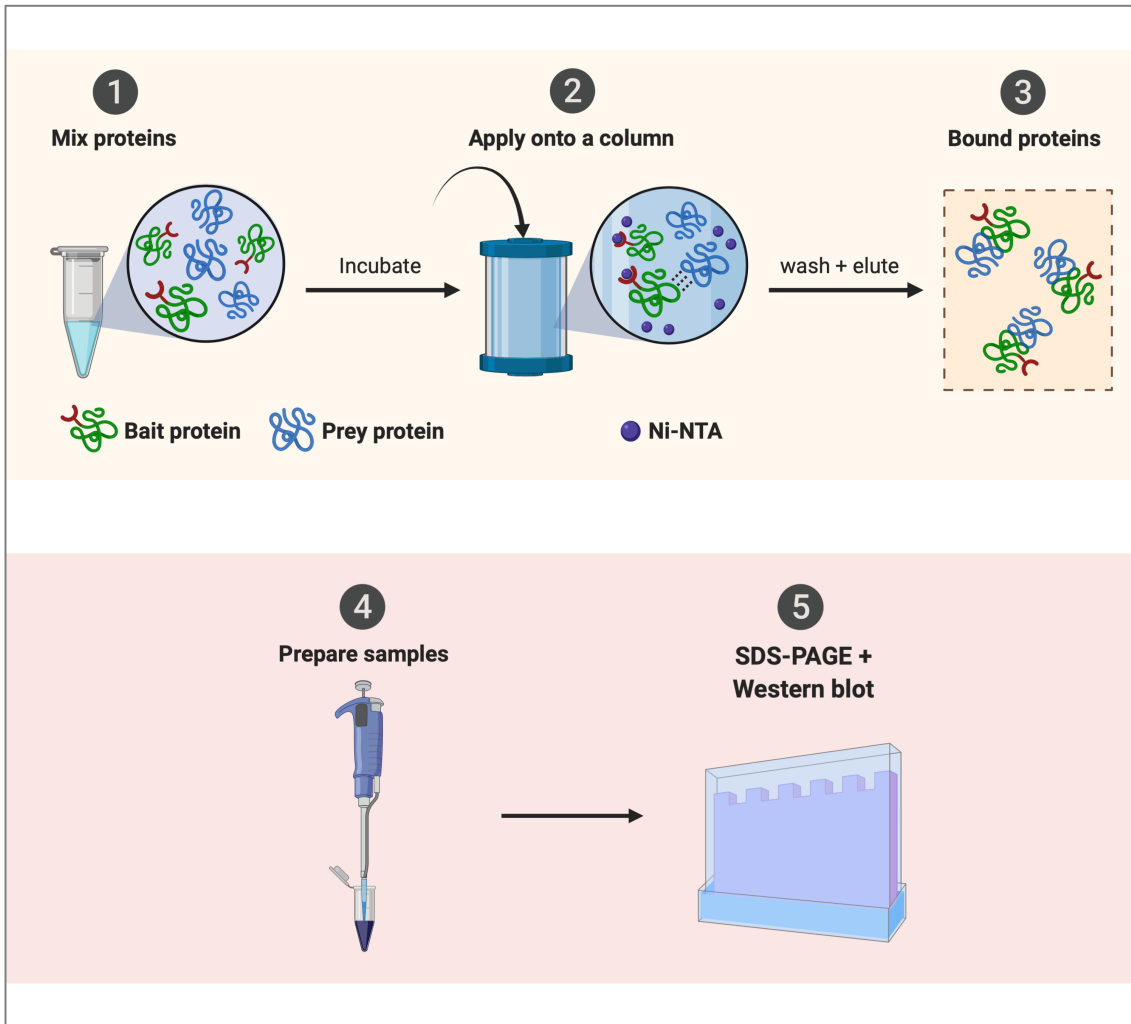
Figure 52. The principle and steps of the FADD / caspase-8 pull-down assay.

For this assay, C-(His)$_6$ FADD-FL (bait protein) and untagged ΔDEDs caspase-8 (C360A) (prey protein) were used. The bait protein contains the C-terminal (His)$_6$ tag, which can bind to the Ni-NTA resin. The prey protein remains untagged, thus it can only bind to the bait protein, if an interaction between the proteins of interest occurs. C-(His)$_6$ FADD-FL and untagged ΔDEDs caspase-8 (C360A) were mixed at equimolar ratio of 10 μM and incubated in the reaction buffer (50 mM Trizma base, 100 mM NaCl, [pH 7.4]) at room temperature. The mixture was applied onto the IMAC (Ni-NTA) column. Next, the column was washed in order to remove any excess or unbound proteins. Then, the bound proteins of interest were eluted from the column. The wash fractions and protein eluates were collected separately and concentrated. Equal volumes (30 μl) of the wash and elution fractions were loaded onto 15% SDS-PAGE and analysed by Western blot.[14]

As shown in Figure 53A, C-(His)$_6$-tagged FADD-FL eluted in fraction 2 and 3, whereas untagged ΔDEDs caspase-8 (C360A) eluted in fraction 2. The levels of the eluted proteins were similar to the levels of their controls. Interestingly, the amount of untagged

---

[14] Image created with BioRender.com

ΔDEDs caspase-8 (C360A) that eluted in fraction 2 was comparable with the amount of C-(His)$_6$-tagged FADD-FL, which eluted in the same fraction. The proteins of interest were not detected in the wash fractions. The results obtained for the control assay showed that C-(His)$_6$ GST and untagged ΔDEDs caspase-8 (C360A) eluted in fraction 2 (Figure 53B). The levels of C-(His)$_6$ GST were similar to the amount of the controls in lanes 1 and 2. Importantly, the levels of eluted untagged ΔDEDs caspase-8 (C360A) were decreased, when compared with the controls in lanes 2 and 3, as well as control C-(His)$_6$ GST (Figure 53B). the proteins of interest were not detected in the wash fractions.

Additionally, we performed the Western blot analysis for elution fractions obtained from both assays, which were run on one SDS-PAGE. The analysis was carried out in order to compare the levels of eluted untagged ΔDEDs caspase-8 (C360A) during both assays (Figure 53C) and to confirm the reliability of the C-(His)$_6$ FADD-FL / untagged ΔDEDs caspase-8 (C360A) experiment. We observed that amount of eluted protein (indicated by the red arrow) during the control C-(His)$_6$ GST / untagged ΔDEDs caspase-8 (C360A) assay was markedly reduced, when compared with the protein levels eluted during the C-(His)$_6$ FADD-FL / untagged ΔDEDs caspase-8 (C360A) pull-down assay and the controls in lanes 1, 2 and 3 (Figure 53C). Thus, our data suggest that C-(His)$_6$ FADD-FL and ΔDEDs caspase-8 (C360A) were capable to bind *in vitro*.
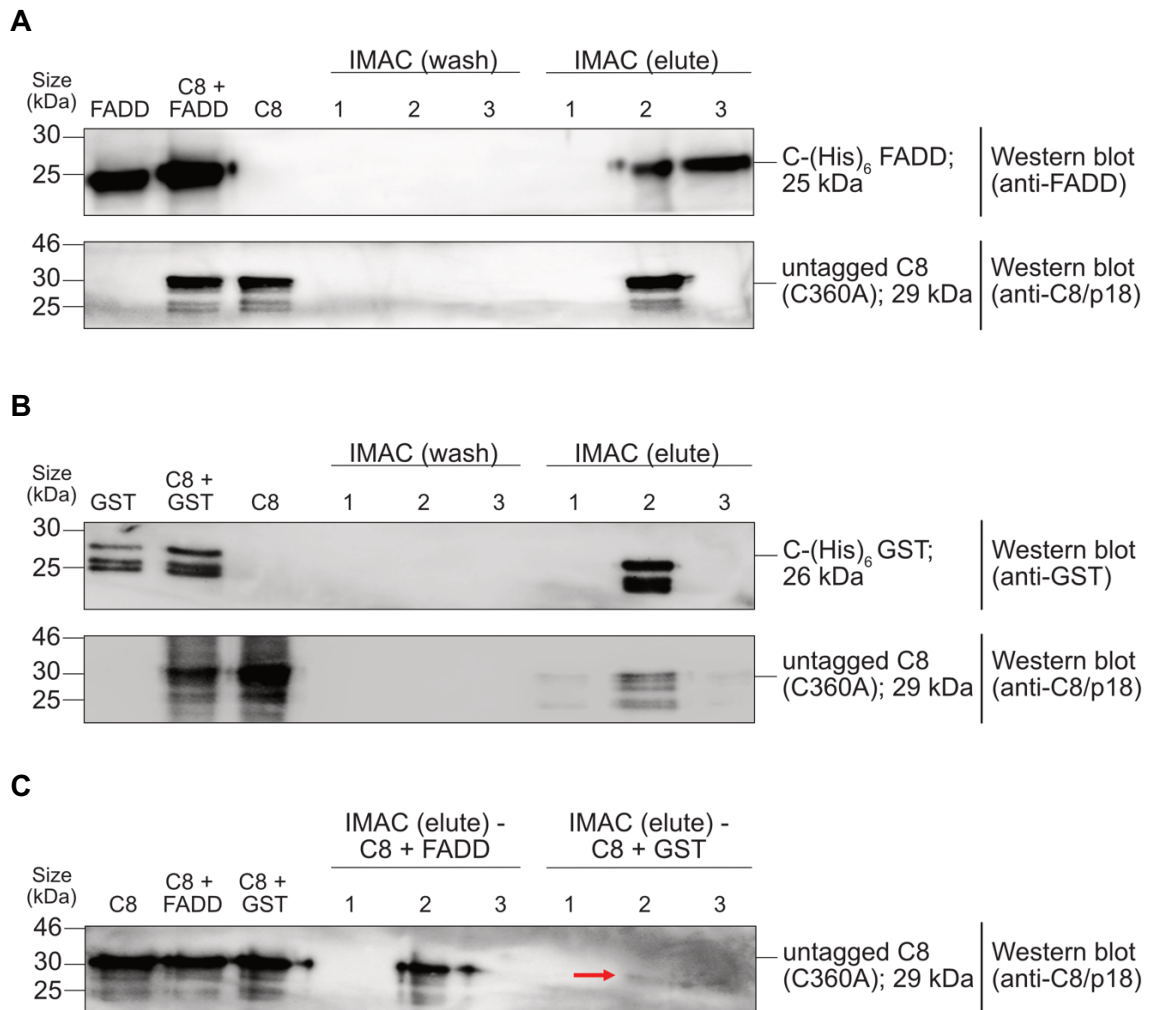
Figure 53. FADD / caspase-8 pull-down assay with controls and comparison blot.
A. Purified C-(His)$_6$-tagged FADD-FL (bait protein) and untagged ΔDEDs caspase-8 (C360A) (prey protein) were mixed at equimolar ratio of 10 μM and incubated in the reaction buffer (50 mM Trizma base, 100 mM NaCl, [pH 7.4]) at room temperature. The mixture was applied onto the 5 ml IMAC (Ni-NTA) column, which was then attached to AKTA PrimePlus. The column was washed, and the proteins were eluted. The wash and elution fraction were collected, concentrated and analysed for the presence of FADD and ΔDEDs caspase-8 (C360A) by using 15% SDS-PAGE and Western blot. The antibodies against FADD and aspase-8 p18 subunit were used in order to detect the proteins of interest. **B.** The control GST/thrombin-C-(His)$_6$ and untagged ΔDEDs caspase-8 (C360A) assay and analysis were carried out in the same manner as for C-(His)$_6$-tagged FADD-FL and untagged ΔDEDs caspase-8 (C360A). The antibodies against GST tag and aspase-8 p18 subunit were used in order to detect the proteins of interest. **C.** Comparison blot for elution fractions obtained during both C-(His)$_6$-tagged FADD-FL / untagged ΔDEDs caspase-8 (C360A) (middle), and GST/thrombin-C-(His)$_6$ / untagged ΔDEDs caspase-8 (C360A) (right; elution fraction 2 indicated by the red arrow) assays. The eluates were analysed for the levels of caspase-8. An antibody against caspase-8/p18 subunit was used to detect the protein.

CHAPTER 4

RESULTS – PART II

Regulation of the FADDosome Formation in

Response to Chemotherapeutic Drugs[15]

4.1 ATR But Not ATM is Phosphorylated in HCT.shctrl Cells Exposed to 5-FU

The ATR and ATM kinases play a crucial role in the conventional DNA damage response machinery. Induction of the DNA lesions contributes to autocatalytic phosphorylation of ATR and ATM, which is a hallmark of their active state. Activation of these kinases leads to phosphorylation of a wide range of proteins involved in the DNA damage response signalling. Thus, we wondered, whether these kinases could be involved in translation of the 5-FU-induced DNA damage into apoptotic signals and the subsequent FADDosome formation. With respect to this, our first aim was to test, whether ATR and ATM were phosphorylated in response to 5-FU in cancer cells.

To examine this, we used HCT.shctrl cells, a stable control knockdown, derived from HCT116 human colorectal cancer cells. This derivative was generated with an empty knockdown plasmid and was subjected to the same experimental procedure, that was used for generation of the other stable knockdowns used in this study. In principle, HCT.shctrl and HCT116 cells respond in the same way to treatment with 5-FU. HCT.shctrl cells were exposed to 5-FU for 2 h, 4 h, 8 h, 15 h and 24 h. The untreated cells (0 h) serves as a control. The cells were analysed for ATR and ATM activation by using antibodies against the Thr1989 and Ser1981 phosphorylation sites, respectively. Moreover, the cells were assessed for the endogenous levels of ATR and ATM using the total ATR and ATM antibodies, respectively.

The results obtained by Western blot revealed that ATR was phosphorylated in HCT.shctrl cells in response to 5-FU. We observed that the ATR phosphorylation levels were gradually increasing after 2 h, 4 h and 8 h treatment with 5-FU and slightly decreasing after 15 h and 24 h exposure to the drug. it was also found that

phosphorylation of ATM was not elevated in HCT.shctrl cells subjected to the anti-tumour drug. Furthermore, the levels of total ATR and ATM were increased in HCT.shctrl cells untreated and treaded with 5-FU.

The chemotherapeutic drug-induced cytotoxic stress typically contributes to accumulation of proteins involved in regulation of the cell cycle, such as p53. Thus, HCT.shctrl cells were examined for the levels of p53 in response to 5-FU. As expected, p53 levels were gradually increasing after exposure to 5-FU (Figure 54).

The obtained results indicate that ATR, but not ATM, undergoes phosphorylation after the treatment with 5-FU, which suggest that this kinase acts as the key sensor of the DNA damage cause by 5-FU in HCT.shctrl cells. Moreover, the results showed that p53 was accumulated in response to 5-FU, which indicated that HCT.shctrl cells were able to respond to 5-FU-inflicted DNA damage.
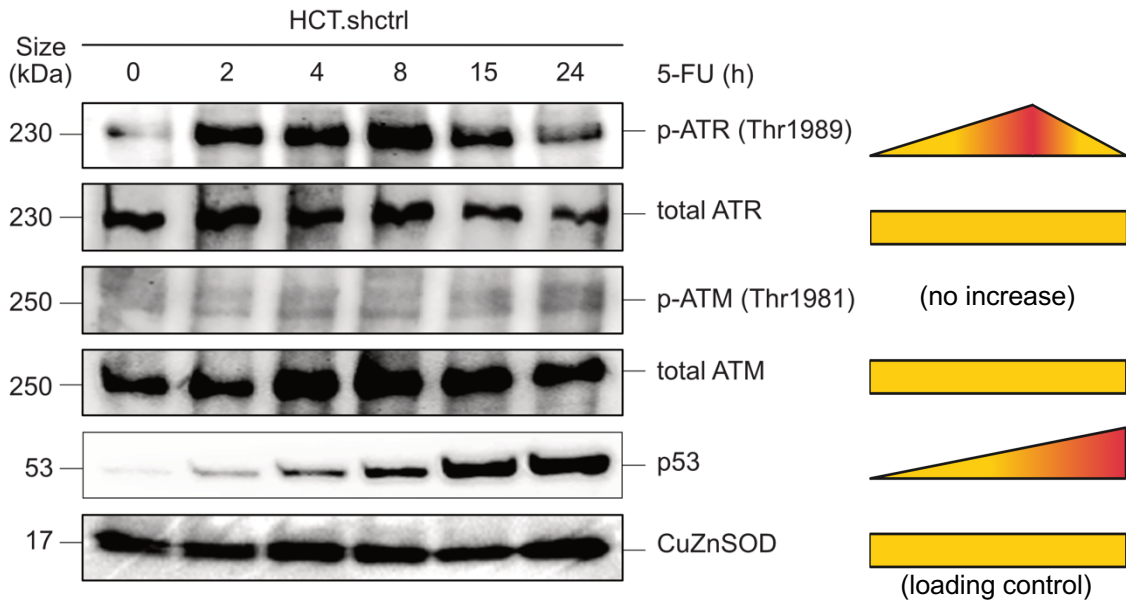
Figure 54. Treatment with 5-FU promotes ATR phosphorylation in HCT.shctrl cells.
Exposure to 5-FU causes an increase of ATR phosphorylation after 2 h, 4 h and 8 h and its slight decrease after 15 h and 24 h, whereas ATM phosphorylation was not elevated in response to the anti-tumour drug. Upon treatment with 5-FU, the levels of p53 induction were gradually elevating and proportionally to the time of incubation. Moreover, the levels of total ATR and ATM were elevated in HCT.shctrl cells untreated and treated with 5-FU. The protein extracts of HCT.shctrl cells untreated and treated with 5-FU (200 μM) for 0, 2, 4, 8, 15 and 24 h were subjected to Western blot analysis and assessed for the phosphorylation status of ATR and ATM. Additionally, the cells were examined for the p53 levels in response to the same treatment. Total ATR, total ATM and CuZnSOD were used as loading controls.

4.2 Inhibition and Silencing of ATR Strongly Decreases Chk1 and Chk2 Phosphorylation Levels in Response to 5-FU

Activation of Chk1 and Chk2 kinases via ATR- and ATM-mediated phosphorylation, respectively, has been widely described in the context of the conventional DNA damage response model and DNA repair. Similar to ATR and ATM, our knowledge of the roles of Chk1 and Chk2 in the genotoxic stress-induced apoptosis remains sparse. Moreover, it remains unknown, whether activation of Chk1 and Chk2 is regulated by ATR and/or ATM, respectively, in response to chemotherapeutic drug-induced apoptosis. In order to clarify this, we used HCT.shctrl cells, which were pre-treated with ATR kinase inhibitor (AZD6738) or/and ATM kinase inhibitor (KU55933) 30 min prior to the addition of 5-FU. The HCT.shctrl cells, that were exposed to DMSO only or DMSO plus 5-FU served as a control. The cells were then incubated for 24 h and analysed by Western blot for Chk1 and Chk2 activation using antibodies against the Ser317 and Thr68 phosphorylation sites, respectively. Antibodies against total Chk1 and Chk2 were used to assess the endogenous levels of Chk1 and Chk2, respectively.

The results showed that upon exposure to 5-FU, the Chk1 and Chk2 phosphorylation levels were strongly increased in HCT.shctrl cells. Moreover, we observed that in the presence of ATR inhibitor the levels of phosphorylated Chk1 and Chk2 were considerably reduced in HCT.shctrl cells after treatment with 5-FU, when compared to HCT.shctrl cells subjected to the anti-tumour drug alone. Moreover, after application of the ATM inhibitor, the levels of phosphorylated Chk1 were increased to the same degree in response to 5-FU as in HCT.shctrl cells exposed to the chemotherapeutic alone. Interestingly, we observed that Chk2 phosphorylation was elevated in the HCT.shctrl

cells treated with 5-FU alone, whereas it was strongly reduced in the cells exposed to ATR or ATM inhibitor combined with 5-FU (Figure 55).

As expected, we observed that application of both ATR and ATM inhibitors lead to reduction of Chk1 and Chk2 phosphorylation levels in HCT.shctrl cells treated with 5-FU. These results showed that ATM was dispensable for 5-FU-induced phosphorylation of Chk1, however both ATR and ATM were required for Chk2 phosphorylation in response to 5-FU. Interestingly, the levels of total Chk1 and total Chk2 were markedly reduced in response to treatment with 5-FU plus ATR and ATM inhibitors (Figure 55).

As previously, the cells were examined for the levels of p53. As shown in Figure 55, inhibition of ATR, but not ATM blocked the 5-FU-induced increase in p53. The same event was observed in response to exposure to 5-FU combined with ATR and ATM inhibitors. Thus, the results indicate, that activation of Chk1 and induction of p53 are ATR-dependent, whereas activation of Chk2 is mediated by both ATR and ATM.
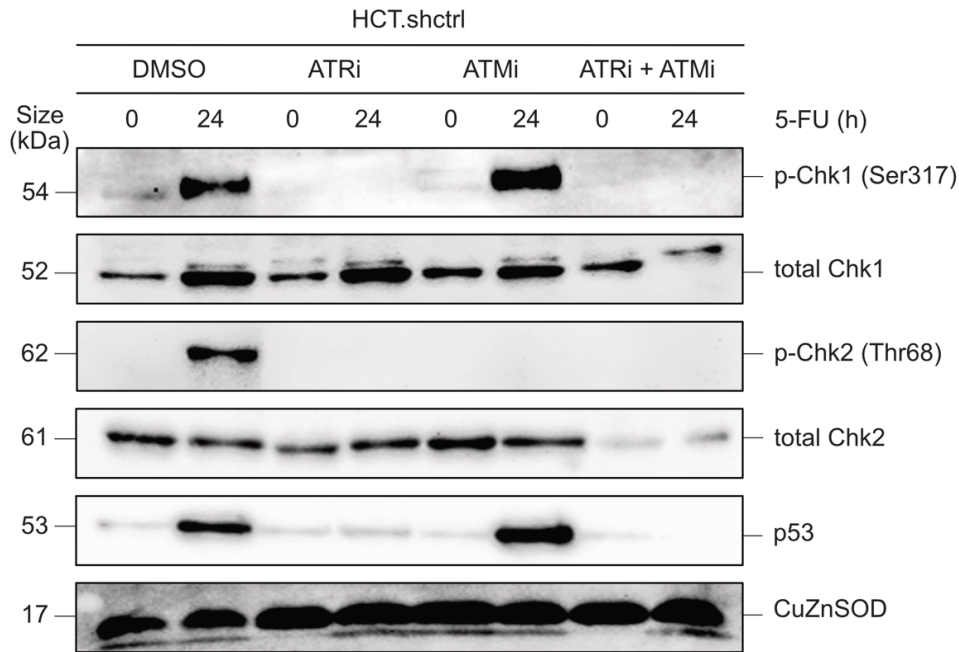
Figure 55. Chk1 and Chk2 phosphorylation status in HCT.shctrl cells exposed to 5-FU alone or 5-FU plus ATR inhibitor or/and ATM inhibitor.
Treatment with 5-FU caused a strong increase of Chk1 and Chk2 phosphorylation in the control (HCT.shctrl plus DMSO) cells. Addition of the ATR inhibitor AZD6738 led to considerable decrease of the Chk1 and Chk2 phosphorylation in response to 5-FU. Exposure to the ATM inhibitor KU55933 caused a strong reduction of Chk2, but not Chk1 phosphorylation after treatment with 5-FU. Application of both ATR and ATM inhibitors led to decrease of the Chk1 and Chk2 phosphorylation as well as total Chk1 and Chk2 levels in response to 5-FU. Moreover, the levels of p53 induction were markedly increased in the 5-FU-induced control cells. Application of the ATR inhibitor alone or ATR and ATM inhibitors blocked the p53 induction in response to 5-FU. In contrast, addition of the ATM inhibitor alone did not block the p53 induction after treatment with 5-FU. HCT.shctrl cells were exposed to ATR inhibitor AZD6738 (2 μM) or/and ATM inhibitor KU55933 (2 μM) and then untreated or treated with 5-FU followed by incubation for 24 h. The HCT.shctrl cells, that were exposed to DMSO only or DMSO plus 5-FU served as a control. The cells were checked for Chk1 and Chk2 phosphorylation by using Western blot. Additionally, the cells were assessed for the levels of p53 protein. Total Chk1, total Chk2 and CuZnSOD served as loading controls.

To further examine the role of ATR in phosphorylation of its downstream targets in 5-FU-induced cell death, we generated a stable ATR knockdown clone of HCT116 cells named HCT.shATR. It was confirmed by Western blot that HCT.shATR cells harboured no detectable ATR levels (Figure 56A).

After being treated with 5-FU, HCT.shctrl and HCT.shATR cells were subjected to Western blot and analysed for the levels of phosphorylated Chk1 and Chk2. Our results

showed that Chk1 phosphorylation was strongly increased in HCT.shctrl cells treated with 5-FU. In contrast, we observed an almost complete inhibition of Chk1 phosphorylation in HCT.shATR cells in response to the anti-tumour drug (Figure 56B). Moreover, while the chemotherapeutic drug-induced phosphorylation of Chk2 was slightly increased in HCT.shctrl cells, HCT.shATR cells showed almost no detectable phosphorylated Chk2. As expected, p53 levels were strongly decreased in 5-FU-treated cells with knocked down ATR. These results further confirm the requirement of ATR for phosphorylation of both Chk1 and Chk2 as well as induction of p53 in response to 5-FU. (Figure 56B).

Therefore, the obtained results indicate that, similar to ATR, the Chk1 and Chk2 kinases undergoes phosphorylation upon exposure to 5-FU and play a role in the DNA damage signalling in 5-FU-induced apoptosis in HCT.shctrl cells. Moreover, these findings indicate that Chk1 activation and p53 accumulation are regulated by ATR, whereas Chk2 activation is mediated by both ATR and ATM in response to 5-FU. Thus, the above observations suggest that upon the 5-FU-induced DNA damage, activated ATR signals towards its downstream targets, Chk1/Chk2 and p53, leading to their subsequent activation and accumulation, respectively.
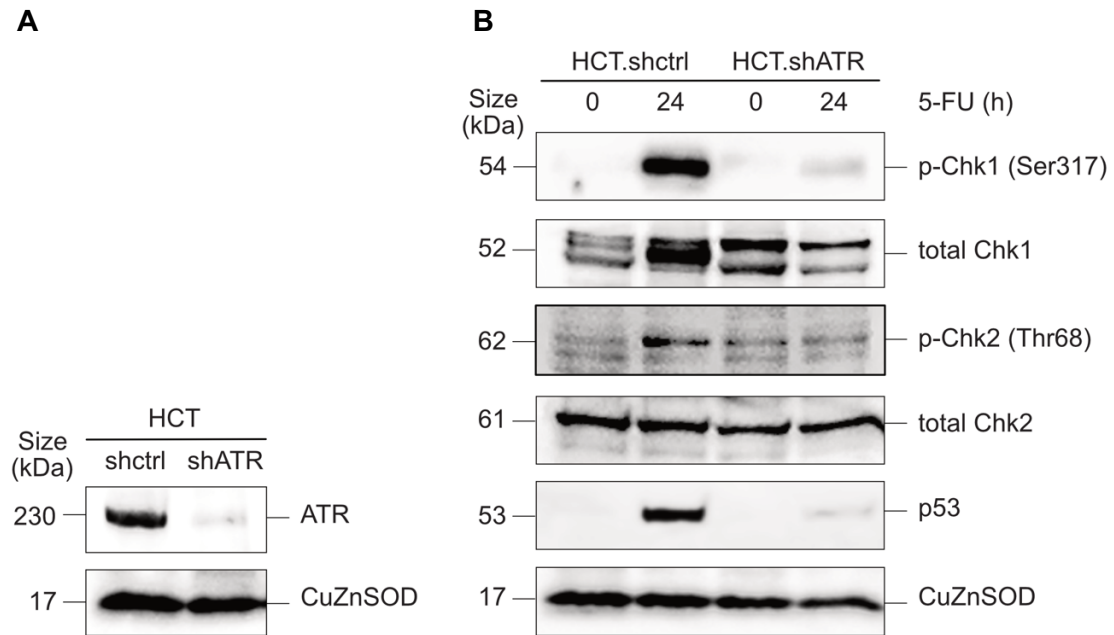
Figure 56. Levels of 5-FU-induced Chk1 and Chk2 phosphorylation in HCT.shATR cells.
A. HCT.shATR cells are unable to express ATR protein, when compared to HCT.shctrl cells. The cell extracts were subjected to Western blot analysis and assessed for the levels of ATR. CuZnSOD served as a loading control. **B.** Treatment with 5-FU led to considerable increase of Chk1 and Chk2 phosphorylation as well as p53 induction in HCT.shctrl cells. On the contrary, knocking down of ATR caused an almost complete inhibition of Chk1 and Chk2 phosphorylation as well as p53 induction in 5-FU-treated HCT.shATR cells. The HCT.shctrl (control) and HCT.shATR cells were untreated or treated with 5-FU for 24 h followed by Western blot analysis. The blots were assessed for the levels of phosphorylated Chk1 and Chk2. Additionally, the cells were examined for the p53 levels in response to the same treatment. Total Chk1, total Chk2 and CuZnSOD were used as loading controls.

4.3 Inhibition and Silencing of ATR Lead to a Strong Reduction of Caspase-10 Upregulation Levels After the 5-FU Treatment

Next, we wondered, whether ATR and/or ATM could regulate the 5-FU-induced upregulation of caspase-10 and subsequent FADDosome formation. In order to elucidate that, we used HCT.shctrl cells, which were pre-treated with ATR inhibitor (AZD6738) or/and ATM inhibitor (KU55933) for 30 min and then incubated with or without 5-FU for 24 h. The HCT.shctrl cells, that were exposed to DMSO only or DMSO plus 5-FU were utilised as a control. The cells were analysed by Western blot and assessed for capsase-10 upregulation levels.

The results showed that caspase-10 upregulation was strongly elevated in the control (HCT.shctrl plus DMSO) cells in response to 5-FU. Interestingly, we found that blocking of ATR led to a complete abrogation of caspase-10 upregulation after treatment with 5-FU. Moreover, the results unveiled, that in the presence of ATM inhibitor, caspase-10 was upregulated to a similar degree as in the HCT.shctrl cells. Additionally, like the result obtained for the ATR inhibitor plus 5-FU treatment, blocking of both ATR and ATM contributed to a strong reduction of caspase-10 upregulation in response to 5-FU (Figure 57). Our data indicate that 5-FU-induced caspase-10 upregulation is ATR-dependent and ATM-independent in apoptosis triggered by 5-FU.
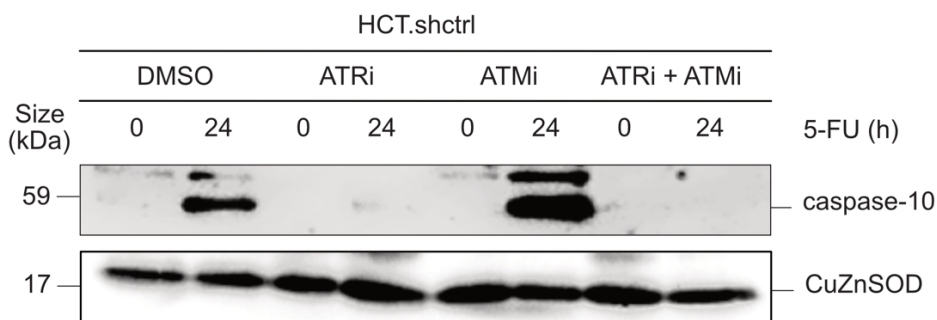
Figure 57. Levels of upregulated caspase-10 in HCT.shctrl cells treated with 5-FU alone or 5-FU plus ATR inhibitor or/and ATM inhibitor.
Upon treatment with 5-FU, upregulation of caspase-10 was strongly increased in the control (HCT.shctrl plus DMSO) cells. Exposure to the ATR inhibitor alone or ATR and ATM inhibitors markedly reduced the caspase-10 upregulation levels in response to 5-FU. In contrast, addition of the ATM inhibitor alone did not decrease the caspase-10 upregulation after treatment with 5-FU. HCT.shctrl cells were exposed to ATR inhibitor AZD6738 (2 μM) or/and ATM inhibitor KU55933 (2 μM) with or without 5-FU and then incubated for 24 h. The HCT.shctrl cells, that were exposed to DMSO only or DMSO plus 5-FU were utilised as a control. The cells were assessed for the levels of upregulated caspase-10 by using Western blot. CuZnSOD was used as a loading control.

In order to further elucidate the role of ATR in anti-cancer drug-induced caspase-10 upregulation, we used HCT.shATR cells and assessed them for the caspase-10 levels in response to 5-FU. The results obtained by Western blot showed that caspase-10 was no longer upregulated in HCT.shATR cells subjected to the chemotherapeutic drug treatment (Figure 58). Such observation confirmed the results obtained for HCT.shctrl cells treated with combination of 5-FU and ATR inhibitor (Figure 57). Thus, these findings further confirm the requirement of ATR for caspase-10 upregulation in 5-FU-induced apoptosis.

The obtained results demonstrate that the signal form the 5-FU-induced DNA damage is transduced by activated ATR towards caspase-10, leading to its upregulation and subsequent apoptosis-inducing FADDosome complex formation.
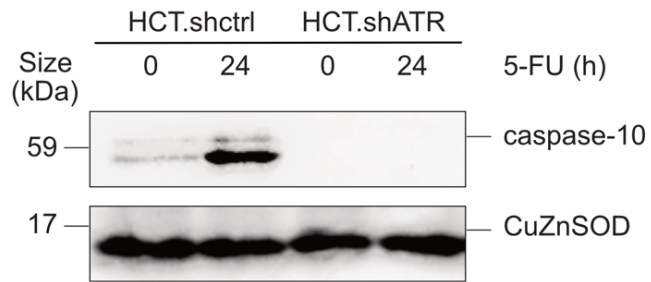
Figure 58. Induction of caspase-10 upregulation by ATR kinase in response to 5-FU.
Treatment with was 5-FU contributed to elevation of caspase-10 upregulation in HCT.shctrl cells. In contrast, caspase-10 was no longer upregulated in cells with knocked down ATR, namely HCT.shATR, after treatment with 5-FU. The HCT.shctrl (control) and HCT.shATR cells were untreated or treated with 5-FU. After incubation for 24 h, the cells were analysed for caspase-10 upregulation levels by Western blot. CuZnSOD was used as a loading control.

4.4 Loss of p53 and Caspase-10 Does Not affect Chk1 and Chk2 Phosphorylation Levels in Response to 5-FU

In this study, it was found that when ATR was inhibited or silenced, phosphorylation of Chk1 and Chk2, induction of p53 and upregulation of caspase-10 were strongly reduced in response to 5-FU. In order to explore the DNA-damage initiated signalling pathway and examine the order of molecular events downstream of ATR in more detail, the cells that were knocked out for p53 (HCT.p53-/-) and knocked down for caspase-10 (HCT.shC10) were used. The HCT.p53-/- cells were a gift from Bert Vogelstein, whereas the HCT.shCaspase-10 cells were generated using RNA interference (RNAi), as described in the Methods. It was confirmed by Western blot that HCT.p53-/- and HCT.shCaspase-10 cells harboured no detectable p53 and caspase-10, respectively (Figure 59A and B).
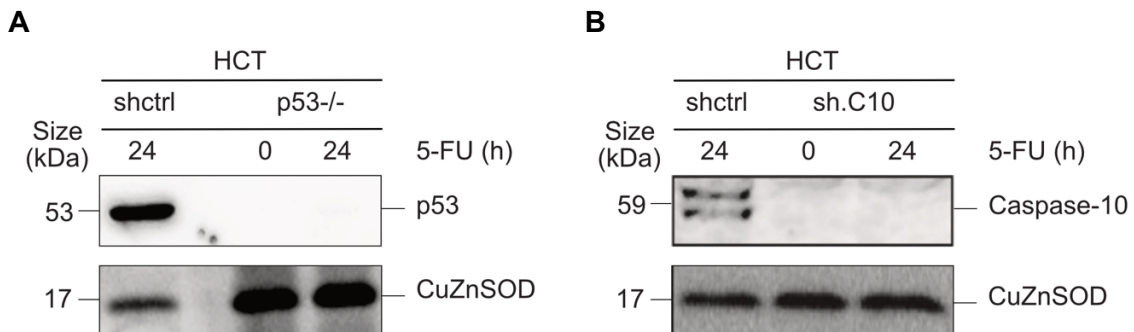
Figure 59. Validation of the p53 knockout (HCT.p53-/-) and caspase-10 knockdown (HCT.shC10) cells.
A. The levels of p53 are considerably increased HCT.shctrl (control cells) in response to 5-FU. Untreated and 5-FU-treated HCT.p53-/- cells are unable to express p53 protein, when compared to HCT.shctrl cells. The cell extracts were subjected to Western blot analysis and assessed for the levels of p53. CuZnSOD served as a loading control. B. Upregulation of caspase-10 is markedly elevated HCT.shctrl (control cells) after exposure to 5-FU. Untreated and 5-FU-treated HCT.shC10 cells are unable to express caspase-10, when compared to HCT.shctrl cells. The cell extracts were analysed using Western blot and assessed for the levels of caspase-10. CuZnSOD was utilised as a loading control.
C10 – caspase-10.

The HCT.shctrl, HCT.p53-/- and HCT.shC10 cells were untreated and treated with 5-FU

for 24 h and subjected to Western blot analysis, in order to assess the Chk1 and Chk2

phosphorylation levels in response to 5-FU. As illustrated in Figure 58, the Chk1 and

Chk2 phosphorylation levels were not increased in the untreated HCT.p53-/- cells. In

contrast, exposure to 5-FU led to considerable elevation of the Chk1 and Chk2

phosphorylation in HCT.p53-/- cells (Figure 60). These observations were comparable

with the results obtained for HCT.shctrl cells untreated and treated with the anti-cancer

drug. The obtained results suggest that in 5-FU-induced apoptosis Chk1 and Chk2

activation is triggered in the p53-dependent manner.
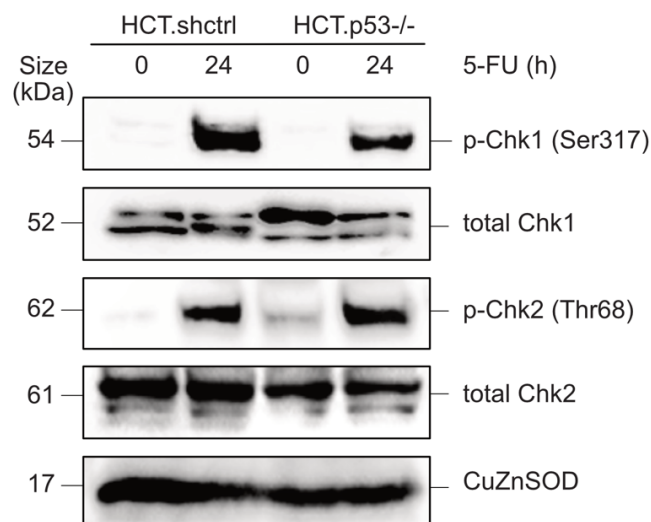
Figure 60. Levels of 5-FU-induced Chk1 and Chk2 phosphorylation in HCT.p53-/- cells.
In untreated HCT.shctrl and HCTp53-/- cells, the levels of Chk1 and Chk2 phosphorylation were
not increased, whereas treatment with 5-FU contributed to a strong elevation of phosphorylated
Chk1 and Chk2 in these cell lines. The HCT.shctrl (control) and HCT.p53-/- cells were untreated
and treated with 5-FU for 24 h followed by Western blot analysis. The blots were assessed for
the levels of phosphorylated Chk1 and Chk2. Total Chk1, total Chk2 and CuZnSOD served as
loading controls.

Moreover, it was observed that the phosphorylation of Chk1 and Chk2 was not elevated

in untreated HCT.shC10 cells. In contrast, it was found that both Chk1 and Chk2 were

phosphorylated in HCT.shC10 cells in response to 5-FU. Importantly, the levels of Chk1

and Chk2 phosphorylation in the absence of caspase-10 were increased to the same

degree as in HCT.shctrl cells subjected to treatment with the chemotherapeutic drug. (Figure 61). This suggest that Chk1 and Chk2 activation occurs upstream of caspase-10.

In order to check, whether HCT.shC10 cells mounted the same response to treatment with 5-FU as the HCT.shctrl cells, the cells were assessed for the levels of p53 and p21. We observed that induction of p53 and p21 was strongly increased in HCT.shC10 cells exposed to 5-FU. The observation was comparable to the results obtained for HCT.shctrl cells subjected to the same treatment (Figure 61). This suggests that there is no fundamental difference in the action of 5-FU in parental and caspase-10-silenced cells, i.e. p53 upregulation is not caspase-10-dependent.
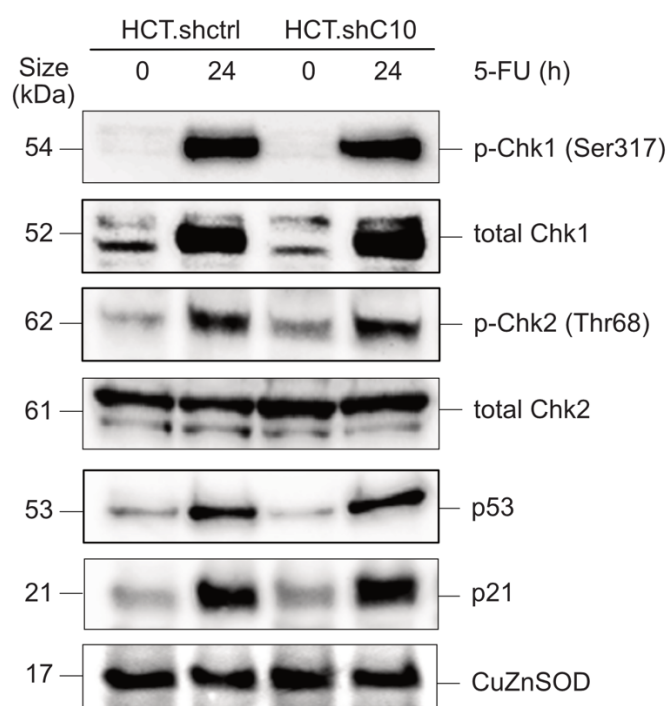
Figure 61. Levels of Chk1 and Chk2 phosphorylation in 5-FU-treated HCT.shC10 cells.
In untreated HCT.shctrl and HCT.shC10, the levels of Chk1 and Chk2 phosphorylation were not increased, whereas treatment with 5-FU contributed to a strong elevation of phosphorylated Chk1 and Chk2 in these cell lines. The HCT.shctrl (control) and HCT.shC10 cells were untreated and treated with 5-FU for 24 h. The whole cell extracts were analysed for Chk1 and Chk2 phosphorylation levels by Western blot. The cells were also assessed or the levels of 5-FU-iduced p53 and p21. Total Chk1, total Chk2 and CuZnSOD were utilised as loading controls.
C10 – caspase-10.

The above findings suggest that upon the 5-FU-induced DNA damage, activation of Chk1 and Chk2 occurs independently of p53 and upstream of caspase-10. Moreover, it was found that caspase-10 was dispensable for induction of p53 in 5-FU-induced apoptosis. Taken these and our previous results showing that caspase-10 upregulation and FADDosome formation were p53-independent (Mohr et al., 2018), it appears that p53 possibly regulates a different pathway of apoptosis in HCT.shctrl cells treated with 5-FU.

4.5 Treatment with the Chk Inhibitor, CHIR-124, Blocks Chk1 and Chk2 Phosphorylation After Exposure to 5-FU or Etoposide

Next, it was asked, whether Chk1 and Chk2 play a role in the anti-cancer drug-induced apoptosis. To be more specific, the question arised, whether these kinases could act downstream of ATR to signal to caspase-10 and FADDosome-mediated cell death and whether they could be involved in determining the mode of apoptosis (FADDosome vs. FLIPosome).

In order to find out, HCT.shctrl cells were used and treated with 5-FU or etoposide alone as well as the combination of CHIR-124 and 5-FU or etoposide. The HCT.shctrl cells, that were exposed to DMSO only or DMSO plus 5-FU or etoposide were used as a control. The cells were incubated for 24 h and analysed by Western blot for Chk1 and Chk2 phosphorylation levels in order to validate the action of the kinase inhibitor.

The Western blot analysis showed that in response to CHIR-124 plus 5-FU the levels of phosphorylated Chk1 and Chk2 were markedly decreased in HCT.shctrl cells, when compared to the control (HCT.shctrl plus DMSO) cells exposed to the chemotherapeutic drug. The observation was comparable to the results obtained for HCT.shctrl cells subjected to the CHIR-124 plus etoposide treatment, which also showed a considerable reduction of Chk1 and Chk2 phosphorylation levels (Figure 62). These findings indicate that CHIR-124 can block phosphorylation of both Chk1 and Chk2.

Additionally, it was checked, whether the HCT.shctrl cells stimulated with CHIR-124 plus 5-FU or etoposide mount the same response to the treatment as the HCT.shctrl cells exposed to 5-FU or etoposide alone. We observed that induction of p53 and p21 was

highly elevated in HCT.shctrl cells treated with CHIR-124 plus 5-FU or etoposide. The observation was comparable to the results obtained for HCT.shctrl cells subjected to the 5-FU or etoposide treatment alone (Figure 62). This indicates that there is no fundamental difference in the action between CHIR-124 combined with 5-FU or etoposide and 5-FU or etoposide alone.

Therefore, these results demonstrate the functionality of the CHIR-124 inhibitor, which effectively blocked Chk1 and Chk2 phosphorylation upon exposure to 5-FU or etoposide.
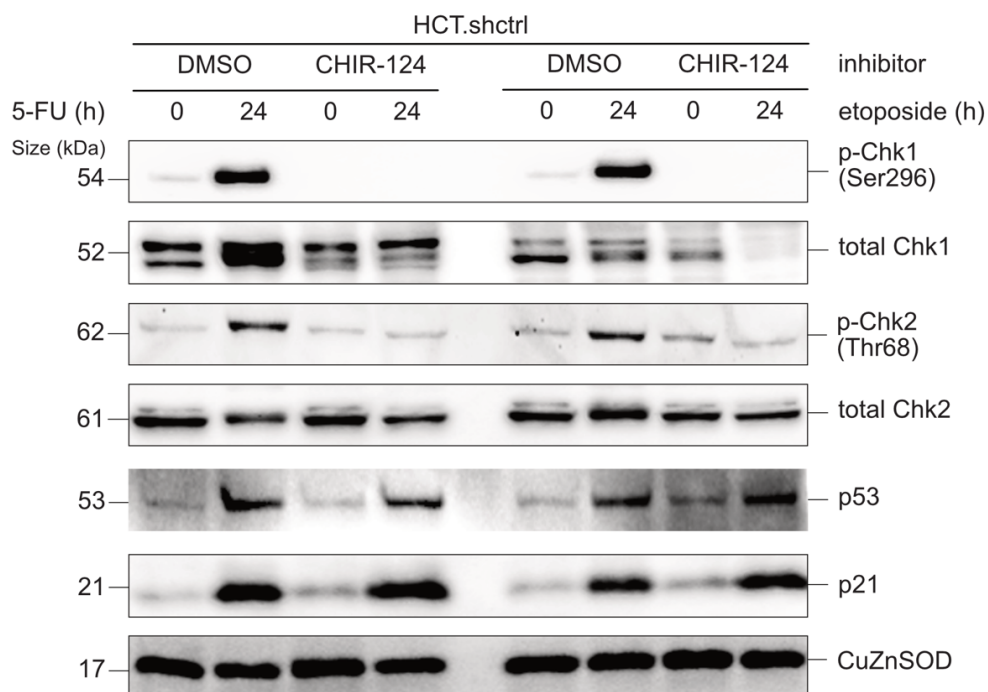
Figure 62. . Levels of phosphorylated Chk1 and Chk2 in HCT.shctrl cells exposed to 5-FU or etoposide alone and CHIR-124 plus 5-FU or etoposide.
Upon treatment with 5-FU or etoposide, Chk1 and Chk2 undergo phosphorylation in HCT.shctrl cells. Application of CHIR-124 blocked the Chk1 and Chk2 phosphorylation in HCT.shctrl cells exposed to 5-FU or etoposide. HCT.shctrl cells were treated with the combination of Chk1/Chk2 inhibitor CHIR-124 (250 nM) plus 5-FU or etoposide. HCT.shctrl cells exposed to DMSO only or DMSO plus 5-FU or etoposide were utilised as a control. The cells were incubated for 24 h and tested for Chk1 and Chk2 phosphorylation by using Western blot. Additionally, the cells were assessed for the levels of induced p53 and p21 in response to the treatments. Total Chk1, total Chk2 and CuZnSOD served as loading controls.

4.6 Inhibition with CHIR-124 Reduces Caspase-10 Upregulation Levels After the Treatment with 5-FU

To examine, whether Chk1 and Chk2 kinases could be involved in signal transduction leading to caspase-10 upregulation and FADDosome-mediated apoptosis, HCT.shctrl cells were used and stimulated with 5-FU or etoposide alone as well as the combination of CHIR-124 and 5-FU or etoposide. The HCT.shctrl cells exposed to DMSO only or DMSO plus 5-FU or etoposide served as a control. It was necessary to examine the roles of Chk1 and Chk2 in caspase-10 upregulation in HCT.shctrl cells treated with both chemotherapeutic drugs, as the aim was to determine, whether these kinases could be involved in caspase-10 upregulation specifically in response to 5-FU or whether such molecular event was important for apoptosis induced by other anti-tumour drugs as well. Etoposide is described as a topoisomerase inhibitor, forming a complex with topoisomerase II, which leads to DNA damage and gives rise to DNA double strand breaks. In contrast, 5-FU is believed to cause DNA damage by giving rise to single-strand breaks.

The HCT.shctrl cells subjected to the respective treatments were incubated for 24 h and assessed for the levels of upregulated caspase-10 by using Western blot. As illustrated in Figure 54, caspase-10 upregulation was markedly increased in the control (HCT.shctrl plus DMSO) cells treated with 5-FU (Figure 63). Importantly, the results showed that application of CHIR-124 led to a considerable reduction of caspase-10 upregulation in response to 5-FU (Figure 63). Furthermore, it was observed observed that caspase-10 upregulation levels were not elevated in response to etoposide (Figure 63). In this context, treatment with CHIR-124 and etoposide did not affect the caspase-10 levels. These findings indicate that caspase-10 upregulation is Chk1/Chk2-dependent in 5-FU-induced apoptosis and that this molecular event is specific for 5-FU.

Therefore, the obtained results suggest that, similar to ATR, activated Chk1 and Chk2 are responsible for signal transduction from the 5-FU-induced DNA damage site towards upregulation of caspase-10 and thereby acts as regulators of the FADDosome formation in HCT.shctrl cells.
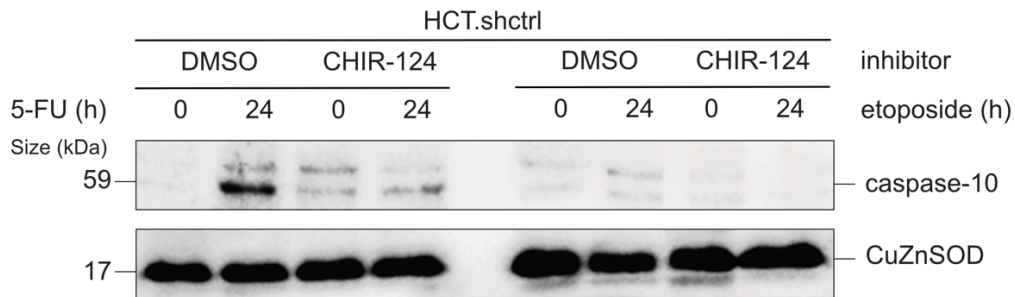
Figure 63. Caspase-10 upregulation status in HCT.shctrl cells exposed to 5-FU or etoposide alone and CHIR-124 plus 5-FU or etoposide.
In the control HCT.shctrl cells exposed to DMSO, caspase-10 upregulation was strongly increased in response to treatment with 5-FU, but not etoposide. Treatment with Chk1/Chk2 inhibitor CHIR-124 considerably reduced the caspase-10 upregulation levels after stimulation with 5-FU. Exposure to CHIR-124 and etoposide did not affect the caspase-10upregulation levels in HCT.shctrl cells. HCT.shctrl cells were stimulated with Chk1/Chk2 inhibitor CHIR-124 (250 nM) plus 5-FU or etoposide. The HCT.shctrl cells exposed to DMSO only or DMSO plus 5-FU or etoposide served as a control. After incubation for 24 h, the cell lysates were examined for the levels of caspase-10 by using Western blot. CuZnSOD was utilised as a loading control.

4.7 Inhibition with CHIR-124 Significantly Increases Apoptosis Levels in Response to 5-FU

In order to assess the role of Chk1 and Chk2 in the regulation anti-cancer drug-induced apoptosis, HCT.shctrl cells were used and treated with 5-FU alone and the 5-FU/CHIR-124 combination. The cells were incubated for 24 and 48 h and analysed by DNA hypodiploidy assay for apoptosis measurement. The obtained measurement data were plotted as average apoptosis and specific apoptosis results. The average apoptosis is represented by absolute cell death levels of untreated and treated cells. The specific apoptosis was obtained by subtraction of the basal cell death values from the apoptosis levels of cells exposed to treatments. Both average and specific apoptosis are expressed as mean values.

As illustrated in Figure 55A, the levels of average apoptosis in HCT.shctrl cells treated with 5-FU alone and HCT.shctrl cells exposed to CHIR-124 inhibitor plus 5-FU were about 10.3% and 25.8%, respectively, after 24 h treatment. The levels of average apoptosis in 5-FU-treated HCT.shctrl cells and HCT.shctrl cells subjected to CHIR-124 inhibitor plus 5-FU treatment were about 36.8% and 42.5%, respectively after 48 h treatment. The specific apoptosis results showed that for HCT.shctrl cells treated with 5-FU alone and HCT.shctrl cells exposed to 5-FU plus CHIR-124 inhibitor, the levels of cell death were about 5.4% and 19.6%, respectively, after 24 h treatment. Moreover, for 5-FU-treated HCT.shctrl cells and HCT.shctrl cells subjected to 5-FU plus CHIR-124 inhibitor treatment, the specific apoptosis values were about 31.6% and 36.3% (Figure 64B).

These results indicate that application of CHIR-124 plus 5-FU led to a significant increase of cell death after 24 h, when compared with the 5-FU treatment alone (Figure 64A and

B). Following 48 h exposure to the CHIR-124/5-FU combination, the levels of apoptosis in HCT.shctrl cells were also strongly elevated, however such observation was comparable with the results obtained for HCT.shctrl cells stimulated with 5-FU alone (Figure 64A and B). We observed the same phenomenon in HCT116 cells, that were knocked down for ATR, caspase-10, RIP1, and TRAF2 and treated with 5-FU (Mohr et al., 2018). Further analysis revealed that these cells were able to switch to an alternative cell death mechanism, which required assembly of the FLIPosome platform (Mohr et al., 2018).

Thus, similar to our previous findings, the results obtained for HCT.shctrl cells exposed to CHIR-124 plus 5-FU suggest that the cells are might be able to switch to an alternative mode of apoptosis.
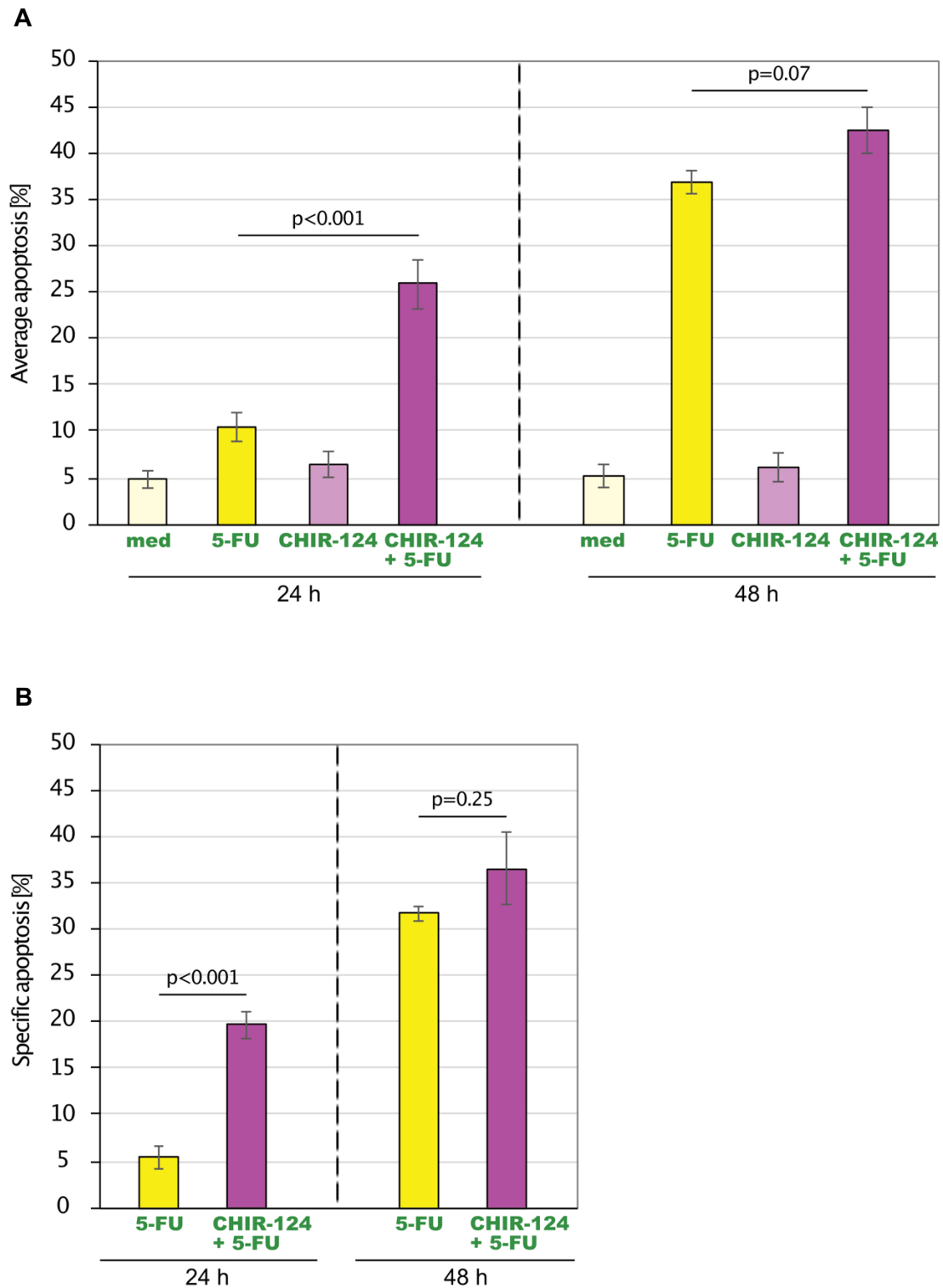
Figure 64. Levels of the average and specific apoptosis in HCT.shctrl cells treated with combination of CHIR-124 and 5-FU after 24 h and 48 h.
A. Average apoptosis levels in HCT.shctrl cells after treatment with 5-FU only and CHIR-124 plus 5-FU. The cells were exposed to the treatments for 24 and 48 h. The cell death was measured by using flow cytometry. Data are shown as mean values ± S.E.M, n=6. **B.** Levels of specific apoptosis in HCT.shctrl cells stimulated with 5-FU only and CHIR-124 plus 5-FU. The cells were subjected to the treatments for 24 and 48 h. The cell death measurements were performed by using flow cytometry. Data are shown as mean values ± S.E.M, n=6.

4.8 Inhibition with CHIR-124 Leads to Degradation of cIAP1 in Response to 5-FU

Our group demonstrated previously that in the absence of ATR, caspase-10, RIP1 or TRAF2, the cells were able to switch to the FLIPosome-mediated apoptosis, of which one of the key features was the degradation of cIAP1 (Mohr et al., 2018). Moreover, the results obtained in this study have shown that apoptosis was significantly increased in the cells treated with CHIR-124/5-FU combination, suggesting an initiation of the FLIPosome-mediated cell death. In order to confirm that the cells were indeed able to switch to the FLIPosome, it was assessed, whether cIAP1 was degraded in response to Chk1/Chk2 inhibition.

In order to test this hypothesis, HCT.shctrl cells were used and treated with a combination of CHIR-124 plus 5-FU. The HCT.shctrl cells exposed to DMSO only or DMSO plus 5-FU were used as a control. The cells were incubated for 24 h and checked for the levels of cIAP1 by Western blot. It was observed that the levels of cIAP1 were slightly decreased and almost completely lost in the cells treated with CHIR-124 alone and with CHIR-124 plus 5-FU, respectively, which was in contrast to the result obtained for HCT.shctrl cells treated with 5-FU (Figure 65). These observations confirmed that blocking of Chk1/Chk2 contributed to cIAP1 degradation in response to the 5-FU and indicated that the cells were able to switch to the FLIPosome-mediated mode of apoptosis in the absence of Chk1 and Chk2.

Therefore, the described findings indicate that HCT.shctrl cells can switch to the alternative mechanisms of apoptosis, the FLIPosome, upon inhibition of Chk1 and Chk2 activation and 5-FU treatment. Moreover, similar to the results obtained for the cells lacking caspase-10, ATR, RIP1 or TRAF2 (Mohr et al., 2018), the hallmark of the

FLIPosome mode of apoptosis in HCT.shctrl cells with blocked Chk1 and Chk2 is that cIAP1 undergoes degradation in response to 5-FU.
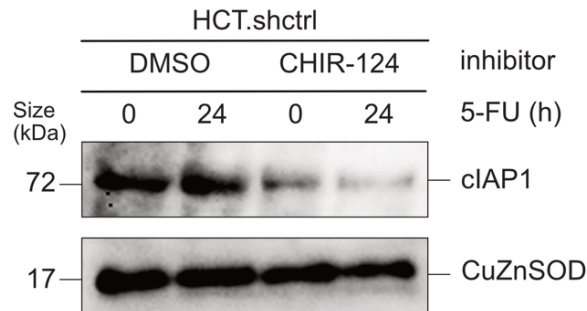
Figure 65. Levels of cIAP1 in HCT.shctrl cells stimulated with 5-FU alone and CHIR-124 plus 5-FU.
In the untreated and 5-FU-treated control (HCT.shctrl plus DMSO) cells, the levels of cIAP1 were considerably increased. The levels of cIAP1 were slightly decreased in response to CHIR-124 alone and almost completely lost in the cells treated with CHiR-124 plus 5-FU. HCT.shctrl cells were stimulated with the combination of Chk1/Chk2 inhibitor CHIR-124 (250 nM) plus 5-FU. The HCT.shctrl cells exposed to DMSO only or DMSO plus 5-FU were used as a control. The cells were incubated for 24 h and assessed for cIAP1 levels by using Western blot. CuZnSOD was utilised as a loading control.

CHAPTER 5

DISCUSSION

5.1 Discussion

Application of 5-FU in anti-tumour therapies can improve the survival of patients with colorectal cancer. Nevertheless, acquisition of 5-FU-resiststance is still a common issue and a major cause of the limited clinical use of this chemotherapeutic agent (Longley et al., 2003). Moreover, our knowledge of the molecular mechanisms responsible for development of such resistance is still poor. Therefore, it is crucial to examine the factors and pathways involved in 5-FU-induced apoptosis in order to increase its therapeutic potential.

Chemotherapeutic drugs exert their anti-tumour effect by induction of apoptosis, including initiation of the intrinsic and extrinsic cell death networks (Petak and Houghton, 2001). A few novel apoptotic pathways and cell death-inducing protein complexes have been identified recently, which like the conventional intrinsic and extrinsic networks, have been reported to initiate apoptosis in cancer cells treated with chemotherapeutic drugs. It was described by Feokistova et al. (2011) and Tenev et al. (2011) that cell death can be triggered by the protein complex named RIPoptosome, which consists of caspase-8, FADD and RIP1. The authors reported that formation of this protein platform occurs in response to the treatment with IAP inhibitor alone or in combination with anti-tumour agents.

Recently, our group has shown that apoptosis can be induced by caspase-8, but not caspase-9 upon stimulation with 5-FU, irinotecan or raltitrexed (Mohr et al., 2018). Moreover, we have demonstrated that caspase-8 activation does not require involvement of the death receptors, including TRAIL-R1/2, CD95 and TNF-R1, but is mediated by the novel, apoptosis-inducing signalling platform we termed FADDosome, which consists of caspase-10, caspase-8, FADD, cFLIP-L, RIP1 and TRAF2. The complex formation is driven by caspase-10, which is upregulated in a p53-independent

manner upon treatment with anti-tumour agents. Loss of ATR, caspase-10, RIP1 or TRAF2 contribute to the switch to an alternative cell death mechanism in cancer cells, which requires assembly of another, novel apoptosis-inducing protein complex, we termed FLIPosome, consisting of caspase-8 and cFLIP-L (Mohr et al., 2018).

Thus, in this study it was asked, what is the biological importance and the exact roles of the main FADDosome constituents in terms of the complex formation and caspase-8 activation. Moreover, it was asked, how the signal from the 5-FU-induced DNA-damage site is translated into cell death signals in cancer cells and what molecular factors are involved in this process. Therefore, it was set out to elucidate and better understand the functions of the main FADDosome components as well as to investigate the molecular details of the 5-FU-induced signalling pathway transducing signals from the DNA damage site towards the FADDosome.

Part I of this study was focused on investigation of the functional relationships and interactions between its main FADDosome components, encompassing caspase-10, caspase-8, FADD and cFLIP-L, in the context of the complex formation and caspase-8 activation. Firstly, the aim of the present research was to establish the expression constructs for human recombinant proteins of these factors, namely ΔDEDs caspase-10, ΔDEDs caspase-8, FADD-FL and ΔDEDs cFLIP-L, followed by establishment of the optimal expression and purification protocols for the respective proteins. The next aim was to express and purify the proteins of interest, followed by the analysis of their functional relationships and interactions in the context of the FADDosome.

Part II of this study focused on examination of the molecular pathways responsible for transduction of the signal from 5-FU-induced DNA damage sites towards the apoptosis-inducing protein complex, the FADDosome. It has been described that induction of genotoxic stress can activate the ATR/Chk1- and ATM/Chk2-mediated DNA damage

responses, including initiation of DNA repair and cell survival or apoptosis (Woods and Turchi, 2013; Weber and Ryan, 2015). In this context, ATR, ATM, Chk1 and Chk2 seemed to be the most promising candidates, which we hypothesised could be involved in the 5-FU-induced DNA damage signalling as well as contribute to FADDosome formation followed by initiation of apoptosis in cancer cells. Thus, the aim of the present research was to examine the functions of the ATR/Chk1- and ATM/Chk2-signalling axes in terms of the anti-tumour drug-induced FADDosome assembly and apoptosis regulation in 5-FU-treated tumour cells.

In summary, a better understanding of the roles of the main FADDosome constituents in the context of the complex formation and caspase-8 activation as well as of the molecular events of the DNA damage signalling towards the FADDosome, induced by chemotherapeutic agents, is a critical step towards designing new and more effective anti-tumour strategies, which can help bypass the drug resistance and defeat cancer.

5.2 Expression of Human Recombinant Proteins by Using the pET-28a System and Their Purification

In order to reconstitute the FADDosome complex as well as to investigate the functional relationships and interactions between the main complex components *in vitro*, it was necessary to express these components, namely caspase-10, caspase-8, FADD and cFLIP-L, as recombinant proteins by using *E. coli* and to purify them by column chromatography.

Firstly, it was focused on the cloning strategy and establishment of the protein expression constructs for human recombinant ΔDEDs caspase-10, ΔDEDs caspase-8, ΔDEDs cFLIP-L and FADD-FL, including the wild-type and mutated variants of the selected

proteins. The next step was to establish the most optimal protein expression and purification protocols for the respective proteins.

By using the pET-28a system, the following expression constructs were successfully generated: ΔDEDs caspase-10 (wild-type, C401A active site and D415A linker mutants), ΔDEDs caspase-8 (wild type, C360A active site and D374A/D384A linker mutants), ΔDEDs cFLIP-L (wild-type) and FADD-FL (wild type, full-length). The DEDs of caspase-10, caspase-8 and cFLIP-L were excluded in the DNA expression constructs as proposed by Denault and Salvesen (2002).

Firstly, the expression levels of the wild type variants of the recombinant protein constructs were tested. The recombinant production was induced by using 0.1 mM (final concentration) IPTG and was carried out at 18°C overnight. We observed that N-(His)$_6$ ΔDEDs caspase-10 (wild-type), N-(His)$_6$ ΔDEDs caspase-8 (wild-type), N-(His)$_6$ ΔDEDs cFLIP-L (wild-type) and C-(His)$_6$ FADD-FL were successfully expressed in the host BL21(DE3) cells. The analysis of the bacterial whole cell extracts revealed that the levels of expressed proteins of interest were decent and satisfactory, indicating that the chosen expression system and conditions for the recombinant production were good.

Nevertheless, after the IMAC purification of N-(His)$_6$ ΔDEDs caspase-10 (wild-type) and N-(His)$_6$ ΔDEDs caspase-8 (wild-type) we found that the proteins were processed into smaller fragments. Since we were interested in purification of the desired proteins in their uncleaved forms, the cleaved N-(His)$_6$ caspase-10 (wild-type) and N-(His)$_6$ ΔDEDs caspase-8 (wild-type) could not be used for the purpose of this study. As expected, C-(His)$_6$ FADD-FL was purified in its full-length form, thus further processing and purification of this protein was performed. This resulted in obtaining a very good level of a highly pure C-(His)$_6$ FADD-FL protein, satisfactory enough for experimental purposes.

Due to some unknown limitation(s), we were unable to purify N-(His)$_6$ ΔDEDs cFLIP-L (wild-type) by using IMAC chromatography. The protein was not detectable in the elution fractions collected at the major elution peak at 280 nm. Undoubtedly, a self-processing of cFLIP-L was excluded, as this protein is not capable to proteolytically process itself like caspases. This is due to the fact that the cysteine residue, which is crucial for the enzymatic activity of caspases, is not present in the cFLIP-L structure. Shorter variants of cFLIP-L, such as cFLIP-S or cFLIP-R, are generated via alternative mRNA splicing, resulting in the smaller or lacking caspase-like domain, whereas the DEDs remain intact (Golks et al., 2005; Riley et al., 2015). Other variants of cFLIP, such as cFLIP-p43 and cFLIP-p22, are generated by the caspase-8-mediated cleavage (Tsuchiya et al., 2015). Thus, it was assumed that N-(His)$_6$ ΔDEDs cFLIP-L (wild-type) could not be purified due to a few possible scenarios: (I) protein expression levels, which initially were satisfactory, were still too low to produce a good amount of the protein and/or (II) only a small part of the protein of interest was solubilised and isolated from inclusion bodies. Expanding the scale of the recombinant protein production and optimisation of solubilisation under denaturing conditions did not improve nor increase the yield after purification of N-(His)$_6$ ΔDEDs cFLIP-L (wild-type). Thus, a different protein expression system was considered.

Next, the expression levels of ΔDEDs caspase-10 (C401A), ΔDEDs caspase-10 (D415A), ΔDEDs caspase-8 (C360A) and ΔDEDs caspase-8 (D374A/D384A) constructs was examined. The recombinant production was induced by using 0.1 mM (final concentration) IPTG and incubated at 18°C overnight. Surprisingly, the levels of N-(His)$_6$ ΔDEDs caspase-10 (C401A) and N-(His)$_6$ ΔDEDs caspase-10 (D415A) were very low, when expressed in the host BL21(DE3) cells. Further optimisation of the recombinant production conditions, such as an increased final concentration of IPTG (0.5 and 1 mM), did not improve the yield of the proteins of interest. After considering that these protein variants could be too toxic, when expressed in *E. coli*, we added glucose to a final

concentration of 1% to the bacteria medium. The role of glucose is to enable a more tight and controlled expression of the genes, when using the pET-28a system (or other pET vectors), which prevents the "leaky" expression of the inserted genes in their uninduced state and as a result, reduces the toxic effect on the host cells. As suggested by Denault and Salvesen (2002), a lower 0.02 mM (final concentration) of IPTG was used. These adjustments resulted in an increased expression levels of N-(His)$_6$ ΔDEDs caspase-10 (C401A) and N-(His)$_6$ ΔDEDs caspase-10 (D415A), when compared with the previous method, which were satisfactory enough to process with purification steps. These results indicate, that addition of glucose and lowering of the IPTG concentration provided a more controlled, yet less stringent recombinant production conditions, which seemed to be preferable for N-(His)$_6$ ΔDEDs caspase-10 (C401A) and N-(His)$_6$ ΔDEDs caspase-10 (D415A).

Furthermore, similar to the N-(His)$_6$ ΔDEDs caspase-8 (wild-type), N-(His)$_6$ ΔDEDs caspase-8 (C360A) and N-(His)$_6$ ΔDEDs caspase-8 (D374A/D384A) were successfully expressed in the host BL21(DE3) cells. The assessment of the bacterial whole cell extracts showed that the levels of the produced proteins were very high, when compared with the expression of the wild-type construct. This indicates that the chosen expression system and conditions for the recombinant production was optimal and that the expression of mutated variants was more efficient than the wild-type one.

The selected N-(His)$_6$ ΔDEDs caspase-10 (D415A) and N-(His)$_6$ ΔDEDs caspase-8 (C360A) were purified as full-length proteins, thus they were subjected to further processing (N-terminal (His)$_6$ tag removal) and purification on SEC. Similar to C-(His)$_6$ FADD-FL, this resulted in obtaining a decent level of a highly pure ΔDEDs caspase-8 (C360A), which could be used for experimental purposes. Purification of ΔDEDs caspase-10 (D415A) was also successful, however it resulted in a much lower yield,

which was only enough for selected experiments. Similar to N-(His)$_6$ ΔDEDs cFLIP-L (wild-type), upscaling the recombinant protein expression and optimisation of solubilisation under denaturing conditions did not lead to obtaining higher yields after purification of ΔDEDs caspase-10 (D415A). Therefore, it was necessary to utilise a different system for protein production.

In the case of all expressed constructs, the assessment of the protein solubility revealed that the proteins of interest were aggregated in inclusion bodies formed by the bacteria, which happens very commonly during expression of eukaryotic proteins in bacterial systems. Our observation was in contrast to some reports, which showed that caspases, including caspase-8 and -10, could be expressed as soluble proteins in *E. coli* (Blanchard et al., 1999; Denault and Salvesen, 2002; Yu et al., 2008). Moreover, Denault and Salvesen (2002) proposed a basic protocol and described a procedure for recombinant production and purification of caspases by using the IPTG-inducible pET expression system and BL21(DE3) cells. Even though in the present study we tested the same expression system as proposed by Denault and Salvesen (2002), the recombinant production of N-(His)$_6$ ΔDEDs caspase-10 (wild type), N-(His)$_6$ ΔDEDs caspase-10 (D415A), N-(His)$_6$ ΔDEDs caspase-8 (wild-type) and N-(His)$_6$ ΔDEDs caspase-8 (C360A) resulted in formation of inclusion bodies. The same phenomenon was observed for N-(His)$_6$ ΔDEDs cFLIP-L (wild-type) and C-(His)$_6$ FADD-FL. The temperature used for the protein expression was lower than suggested by Denault and Salvesen (2002), however it still did not prevent aggregation of the proteins in inclusion bodies.

Some studies reported that expression of caspases, including caspase-8, resulted in a production of insoluble proteins (Garcia-Calvo et al., 1999; Watt et al., 1999; Keller et al., 2009), which is consistent with our results. Similar to Garcia-Calvo et al. (1999), Watt et al. (1999) and Keller et al. (2009) we performed the solubilisation of inclusion bodies

under denaturing conditions by using a buffer containing 6M GuHCl (or 8M urea), which currently is the most commonly used technique for the protein isolation from inclusion bodies. It was described that alternatively, buffers containing detergents (such as Triton X-100 or sarkosyl) can be used to solubilise proteins form inclusion bodies or other fusion tags can be utilised to enhance the protein solubility after expression (such as the well-known MBP (Maltose-binding protein), TrxA (thioredoxin), SUMO (Small ubiquitin modified) or NusA (N-utilization substance) (Costa et al., 2014).

In the current study, using a buffer containing 6M GuHCl (or 8M urea) enabled the solubilisation of N-(His)$_6$ ΔDEDs caspase-8 (wild-type), N-(His)$_6$ ΔDEDs caspase-8 (C360A), N-(His)$_6$ ΔDEDs caspase-10 (wild-type), N-(His)$_6$ ΔDEDs caspase-10 (D415A) and C-(His)$_6$ FADD-FL with different effects and efficiency, but overall resulted in obtaining supernatants containing soluble proteins. Moreover, the circular dichroism analysis revealed that C-(His)$_6$ FADD-FL, ΔDEDs caspase-8 (C360A) and ΔDEDs caspase-10 (D415A) were folded after purification, indicating a successful refolding of the proteins, which is critical to restore their functionality and/or activity.

5.3 Expression of Human Recombinant Proteins by Using the pGEX-4T-3 System and Their Purification

In the present study, several proteins, including C-(His)$_6$ FADD-FL, untagged ΔDEDs caspase-8 (C360A) and untagged ΔDEDs caspase-10 (D415A) were successfully expressed by using the pET-28a system and purified. Purification of the first two proteins led to obtaining a good and satisfactory yield, whereas the yield of the third protein was low and only enough for selected experiments. When using the pET-28a system, purification N-(His)$_6$ ΔDEDs cFLIP-L (wild type) was unsuccessful. It was assumed that this could be caused by too low protein expression levels and/or not efficient

solubilisation and isolation of the desired proteins from inclusion bodies. Moreover, a higher scale for the recombinant protein production and optimisation of solubilisation under denaturing conditions did not improve nor increase the yield of the proteins of interest after purification.

In response to these findings, using a different protein expression system was considered, namely pGEX-4-T3 vector. Using this system could enable more efficient recombinant production and it allows expression of the proteins fused to the GST tag, which can act as the solubility enhancer (Costa et al., 2014). For this, an empty pGEX-4T-3 vector was modified by inserting of DNA fragments containing C-terminal $(His)_6$ tag with thrombin or TEV cleavage site. The $(His)_6$ tag was added to facilitate purification on the Ni-NTA column and to utilise an already established protocol for the pET-28a system as a starting point. Therefore, only minor adjustments to the protein expression conditions would be required, when testing the pGEX-4-T3 system.

By using the pGEX-4-T3 system, the expression vectors containing the same DNA constructs as designed for the pET-28a system were established. Additionally, the cleavage mutant of cFLIP-L (D376A) was generated. This resulted in a successful establishment of the following vectors: ΔDEDs caspase-10 (C401A), ΔDEDs caspase-10 (D415A), ΔDEDs cFLIP-L (wild type) and ΔDEDs cFLIP-L (D376A) with both thrombin-$(His)_6$ and TEV-$(His)_6$ tags. Empty pGEX-4-T3/thrombin-$(His)_6$ and ΔDEDs caspase-8 (C360A)/thrombin-$(His)_6$ were generated to serve as controls.

All established protein constructs were tested for the expression levels. The recombinant production was induced by using 0.1 mM (final concentration) IPTG and was carried out at 30°C for 3 h and 15 h (overnight). We observed that N-GST ΔDEDs caspase-10 (C401A), N-GST ΔDEDs caspase-10 (D415A), N-GST ΔDEDs cFLIP-L (wild type) and

N-GST ΔDEDs cFLIP-L (D376A) with both thrombin-(His)$_6$ and TEV-(His)$_6$ tags as well as the control GST/thrombin-C-(His)$_6$ and N-GST ΔDEDs caspase-8 (C360A)/thrombin-C-(His)$_6$ were successfully expressed in the host BL21-RIL cells. The examination of bacterial whole cell extracts unveiled that the levels of expressed proteins of interest were high and satisfactory, which indicated that the pGEX-4-T3 expression system and the chosen conditions for the recombinant production were optimal.

Unexpectedly, the expression of the recombinant proteins fused with the GST tag did not result in their increased solubility. The only exception was the control GST/thrombin-C-(His)$_6$, which as expected was found in the supernatant. Considering that the conditions with a low stringency were chosen for the protein expression and despite that it still did not prevent the formation of inclusion bodies, it was assumed that there might be other parameters that need optimisation in order to facilitate the production of soluble proteins. Nevertheless, in the present study, solubilisation under denaturing conditions to isolate and purify the proteins of interest from the inclusion bodies was performed, as it allowed to utilise the already established protocol for the pET-28a system.

As expected, purification of GST/thrombin-C-(His)$_6$ was successful and led to obtaining of an exceptionally high yield of a pure protein, which could be used as a control in experimental assays. The first step of purification of N-GST ΔDEDs caspase-10 (D415A)/thrombin-(His)$_6$ by using IMAC was also successful and the levels of purified proteins were good and satisfactory to further process and purify the protein of interest. Surprisingly, after the GST and (His)$_6$ tag removal followed by the second IMAC purification, we found that the levels of untagged ΔDEDs caspase-10 (D415A) were considerably reduced, when compared with the fraction obtained and concentrated after the first purification step. Purification on the SEC column revealed that the untagged ΔDEDs caspase-10 (D415A) eluted at the end of the purification process, as opposed to

the expected elution at 45 ml. Thus, it was concluded that the protein of interest was not stable/underwent degradation after the tags removal and/or purification. However, the exact mechanism responsible for such instability and/or degradation still remains enigmatic. Purification of N-GST ΔDEDs caspase-10 (D415A)/thrombin-(His)$_6$ was attempted several times and detailed analyses were performed after each purification step in order to address this issue, nevertheless the possible point leading to the protein instability is yet to be identified.

Due to the yet unknown limitation(s) of the purification of the proteins expressed by using the pGEX-4-T3 system, the purification of the remaining proteins of interest, including N-GST ΔDEDs caspase-10 (C401A), N-GST ΔDEDs cFLIP-L (wild type) and N-GST ΔDEDs cFLIP-L (D376A) with both thrombin-(His)$_6$ and TEV-(His)$_6$ tags, remains unravelled. Therefore, it was assumed that optimisation of the parameters for the fusion tag removal and/or the following purification process could possibly address this issue. Additionally, possibly a new method and further research are needed to identify the differences or issues related to the fusion tag removal and unsuccessful purification of the proteins expressed by using the pGEX-4-T3 system. Alternatively, a new system for the protein expression and purification could be tested.

5.4   Caspase-10 Cleaves Caspase-8 *In Vitro*

The present study was focused examination of the functions and interactions between the main FADDosome components, namely caspase10, caspase-8, FADD and cFLIP-L. In particular, it was asked, whether caspase-10, which acts as the core driver of the FADDosome formation in 5-FU-induced apoptosis (Mohr et al., 2018), could function as a potential caspase-8 activator. In order to elucidate that, an activity assay *in vitro* was performed. For this, purified untagged ΔDEDs caspase-10 (D415A) and untagged

ΔDEDs caspase-8 (C360A), which played the role of potential enzyme and substrate, respectively, were used.

Initially, the activity assay by using physiological conditions was performed. It was observed that the levels of single-chained ΔDEDs caspase-8 (C360A) were considerably decreased, proportionally to the time of incubation. However, the same event was observed for the control. Thus, it was assumed, that the observed reduction of the control ΔDEDs caspase-8 (C360A) was caused by one of the following possible scenarios: (I) instability or (II) self-processing of the protein, which increased proportionally to the time of incubation. In order to address these issues, ΔDEDs caspase-8 (C360A) alone was tested by using different conditions, such as a stabilisation buffer, which has been described as the optimal reaction buffer for the caspases (Garcia-Calvo et al., 1999), and kosmotropic salts buffer, which promotes dimerization and subsequently, proteolysis and activation of proteins (Boatright et al., 2004). It was found that ΔDEDs caspase-8 (C360A) was unable to cleave itself in stabilising conditions and after addition of the kosmotropic salts, as no decrease of the protein, proportional to the time of incubation, was observed. Thus, these results suggested that the levels of single-chained ΔDEDs caspase-8 (C360A) were decreased previously due to its instability rather than the self-cleavage.

With respect to that, the activity assay by using stabilising conditions was performed. The obtained results revealed that ΔDEDs caspase-10 (D415A) was capable of cleaving ΔDEDs caspase-8 (C360A) *in vitro*. Thus, it was concluded that processing and activation of caspase-8 could be mediated by caspase-10 *in vitro*. Nevertheless, at this stage it was not possible to assess, whether such event could be affected, either positively or negatively, by FADD and/or cFLIP-L in terms of reconstitution of the

FADDosome complex. Moreover, the stoichiometry of the FADDosome constituents remains unclear and is yet to be resolved.

Moreover, it is noteworthy that another reason for the considerable decrease of the single-chained ΔDEDs caspase-8 (C360A) levels in the control assay could be a possibility of contamination with other proteinases, which was not tested in this study. Thus, in the next stages of this research, it would be beneficial to perform a screening for and detection of potential contaminating proteases, which could be present in the purified protein samples. Such experiments can be performed using commercially available kits that are able to detect primary or trace protease activity using fluorometric or colorimetric assays and contain all necessary controls, standards and buffers to perform these assays. The range of proteases, that can be detected using the commercial kits include serine, aspartic, cysteine and metalloproteases (Mohan et al., 2018). Based on the class of identified protease(s), appropriate inhibitors can be added to protect the purified proteins from proteinase degradation.

Moreover, in the next stages of this study, it would be necessary to test the functionality of ΔDEDs caspase-10 (D415A) using activity assays, as described by Watchmann et al. (2010). In order to perform the activity assays, the authors used the following caspase-10 substrates: Ac-DEVD-AFC, Ac-LEHD-AFC and Ac-IETD-AFC, which were mixed with various variants of purified human recombinant caspase-10, including ΔDEDs caspase-10 (wild type) and ΔDEDs caspase-10 (D415A). The activity of the desired proteins was then measured by monitoring the levels of hydrolysis of these substrates (Wachmann et al., 2010). Therefore, testing the activity of purified ΔDEDs caspase-10 (D415A) used in this study would provide a positive control for the ΔDEDs caspase-10 (D415A) / ΔDEDs caspase-8 (C360A) activity assay and serve as a confirmation for the functionality of ΔDEDs caspase-10 (D415A).

Caspases belong to the family of conserved cysteine proteases, which preferably cleave other caspases or substrates after an aspartate residue. Caspase-10 and -8 are known as initiator caspases, which conventionally are involved in the DISC formation and initiation of the extrinsic apoptotic pathways. Nevertheless, the most recent findings have demonstrated that, upon cytotoxic stress induced by anti-tumour drugs, caspase-8 is able to form intracellular complexes, such as FADDosome (Mohr et al., 2018) or RIPoptosome (Feoktistova et al., 2011; Tenev et al., 2011) and act as an initiator of the intrinsic apoptotic network. We have found that, at the FADDosome, caspase-8 undergoes activation which in turn leads to triggering of apoptosis in response to 5-FU. However, the exact mechanism of the caspase-8 activation at the complex remains unknown. For activation of the initiator caspase two model have been proposed, including the induced proximity model (Salvesen and Dixit, 1999) and proximity-induced dimerization model (Boatright and Salvesen, 2003, Wachmann et al., 2010). The first model suggests that bringing initiator caspases into close proximity drives the proteolytic processing of the molecules. The second model proposes that the force driving the cleavage of the initiator caspases requires dimerization of the molecules and this happens as a result of bringing caspases into close proximity (Boatright and Salvesen, 2003; Wachmann et al., 2010). The models and molecular mechanisms responsible for caspases activation was investigated and clarified a few years later by Keller et al., (2009). The authors demonstrated that the proximity-induced dimerization model was responsible for promoting the dimerization of caspase-8, which was found to be necessary for subsequent cleavage of the protein. This indicated that caspase-8 can only be processed after successful dimerization.

Conventionally, initiator caspases are believed to activate themselves via auto-cleavage. They can also proteolytically process the effector (executioner) caspases and other substrates. To date, it has not been reported that one initiator caspase could cleave and activate another initiator caspase. Moreover, it still remains controversial whether

caspase-10 can functionally substitute caspase-8 in death receptor-induced signalling pathways (Kischkell et al., 2001; Sprick et al., 2002). However, it has been described that caspase-8 and -10 share substrate specificity and therefore, their functions may partially overlap (Parrish et al., 2013; Riley et al., 2015).

Interestingly, in contrast to the findings presented in this research, the most recent study by Horn et al., (2017) has demonstrated that caspase-10 negatively regulates activation of caspase-8 in HeLa cells. In particular, the authors have shown that caspase-10 abolishes the caspase-8 activation at the CD95-DISC, which in turn leads to inhibition of apoptosis. Instead, the NF-kB pathway is activated, which as a result, contributes to cell survival. Nevertheless, it is noteworthy that our group has investigated the role of caspase-10 in caspase-8 activation in terms of the FADDosome complex, without involvement of the death receptors. Whereas Horn et al., (2017) studied the effect of caspase-10 functions on caspase-8 activity in terms of the CD95-DISC assembly. Thus, this indicates that caspase-10 can perform different functions and affect the caspase-8 activity depending on the context (death receptor independent FADDosome vs. CD95-DISC). Therefore, further studies are necessary to investigate and clarify in more detail the exact roles of caspase-10 in caspase-8 activation with respect to both the intrinsic and extrinsic apoptotic pathways.

5.5 Caspase-8 and FADD Possibly Interact via a Novel DED-Independent Mechanism

FADD is an adaptor molecule, which was identified and first characterised by Chinnaiyan et al. (1995). This protein is known to play a role in the DISC assembly, which is involved in initiation of the extrinsic apoptotic network. Following binding to a death receptor, FADD associates with caspase-8, which in turn undergoes cleavage and activation at

the DISC. Subsequently, these events lead to the initiation of the cell death (Grunert et al., 2012). It is believed that FADD and caspase-8 can associate through a homotypic interaction between their DEDs (Riley et al., 2015). To date, there has only been one study, which described the underlying mechanism of such interaction. Carrington et al. (2006) proposed a model for the FADD/caspase-8 interaction, based on studying different FADD mutants and their binding abilities to pro-caspase-8 in the context of the CD95-DISC assembly. The authors performed a CD95 co-immunoprecipitation, which allowed to identify the FADD binding surface for pro-caspase-8 within the FADD DED. These results were supported by examination of the crystal structure of MC159 protein, also known as vFLIP, which contains DEDs, structurally resembling the DEDs of FADD and zymogen caspase-8 (Carrington et al., 2006). However, to date, it has not been demonstrated, how FADD and caspase-8 interact in the context of the apoptosis-inducing protein complexes assembly, such as FADDosome, which are formed without engagement of the death receptors.

Thus, in order to examine the interaction between FADD and caspase-8 in the context of the FADDosome formation, a pull-down assay was performed. In this experiment, purified C-(His)$_6$-tagged FADD-FL (bait protein) and untagged ΔDEDs caspase-8 (C360A) (prey protein) were used. Additionally, a control assay by using purified GST/thrombin-C-(His)$_6$ and untagged ΔDEDs caspase-8 (C360A) was performed. The obtained results revealed that both C-(His)$_6$ FADD-FL and untagged ΔDEDs caspase-8 (C360A) eluted in the same fraction and their levels were comparable. Additionally, iy was observed that C-(His)$_6$ FADD-FL eluted in the next fraction, whereas ΔDEDs caspase-8 (C360A) was not detectable in this fraction.

Interestingly, the control assay has revealed that both C-(His)$_6$ GST and ΔDEDs caspase-8 (C360A) eluted in the same fraction, however the levels of ΔDEDs caspase-

8 (C360A) were lower, when compared with the C-(His)$_6$ FADD-FL / untagged ΔDEDs caspase-8 (C360A) results. In order to assess and compare the levels of eluted ΔDEDs caspase-8 (C360A) in both experiments, the elution fractions from the C-(His)$_6$ FADD-FL / untagged ΔDEDs caspase-8 (C360A) and the control C-(His)$_6$ GST and ΔDEDs caspase-8 (C360A) assays were examined. The fractions were run together on one SDS-PAGE and analysed by Western blot. Such analysis was necessary to provide a better view at the levels of eluted ΔDEDs caspase-8 (C360A) in both assays and to confirm the reliability of the C-(His)$_6$ FADD-FL / untagged ΔDEDs caspase-8 (C360A) experiment.

The results showed that the levels of eluted ΔDEDs caspase-8 (C360A) during the control C-(His)$_6$ GST and ΔDEDs caspase-8 (C360A) assay was considerably decreased, when compared with the protein levels eluted during the C-(His)$_6$ FADD-FL / untagged ΔDEDs caspase-8 (C360A) assay. Thus, these data indicated that C-(His)$_6$ FADD-FL and ΔDEDs caspase-8 (C360A) were capable to associate, however the exact mechanism responsible for such interaction and the stoichiometry of bound C-(His)$_6$ FADD-FL and ΔDEDs caspase-8 (C360A) remain unravelled and require further investigation.

Thus, it was concluded that FADD and caspase-8 can possibly interact via a novel, DED-independent mechanism *in vitro*. Nevertheless, at this stage it still remains unclear, whether the presence of caspase-10 and/or cFLIP-L could affect, either positively or negatively, the FADD/caspase-8 binding in the context of the FADDosome reconstitution. Moreover, the possible preferences and/or competition for binding between the FADDosome components in the context of the complex formation as well as their role in the switch between the FADDosome and FLIPosome, still remain unravelled.

Importantly, considering that ΔDEDs caspase-8 (C360A) did not contain its pro-domains, the question arises, what force and/or molecular mechanisms could possibly drive such interaction. Moreover, considering that the findings presented in this study are not in line with other reports, which describe that DEDs are believed to be necessary to associate with FADD (Carrington et al., 2006; Riley et al., 2015) and therefore, refute the classical model of the FADD/caspase-8 interaction, it is crucial to investigate the possible DED-independent interaction of FADD/caspase-8 in more detail and to find, which residues might be responsible for such interaction. Therefore, using a different experimental method and further research are required to address this matter.

5.6 ATR, Chk1 and Chk2 Regulate the 5-FU-Induced Apoptosis

Another aim of this study was to investigate the pathways and factors involved in the DNA damage signal transduction towards the 5-FU-induced caspase-10 upregulation and subsequent FADDosome formation. It was hypothesised that the ATR and/or ATM kinases could act as the 5-FU-induced DNA damage sensors and, together with Chk1 and/or Chk2, can translate the sensed lesion into the apoptotic signals in HCT116 cells (HCT.shctrl cells were used in this study, as they provided control cells for other HCT116 knockdown clones. HCT.shctrl and HCT116 cells respond in the same way to 5-FU).

First of all, it was focused on examination of the ATR and ATM phosphorylation status in HCT.shctrl cells after the treatment with 5-FU. The cells were examined for ATR and ATM activation by using antibodies against the Thr1989 and Ser1981 phosphorylation sites, respectively. We found that only ATR was phosphorylated in HCT.shctrl cells in response to 5-FU. Importantly, we observed that ATR was phosphorylated at Thr1989 after exposure to the anti-tumour drug. Other studies have also reported that ATR

undergoes phosphorylation at Thr1989 in cancer cells subjected to various treatments. Nam et al. (2011) demonstrated that upon treatment with hydroxyurea, ATR could be phosphorylated at Ser428 and Thr1989 in HeLa cells. Similar results were described in the study by Liu et al. (2011), which showed that ATR underwent phosphorylation at Thr1989 in 293T cells treated with hydroxyurea. Glanzer et al. (2014) also reported the same phosphorylation event in UMSCC30 cells subjected to treatment with etoposide. Interestingly, these reports emphasised the fact that the Thr1989 site is believed to function as a hallmark of an active state of ATR (Liu et al., 2011; Nam et al., 2011; Glanzer et al., 2014). Thus, the results obtained in the present research indicate that ATR, but not ATM, is activated in response to 5-FU and suggest that this kinase acts as the key sensor of the anti-tumour drug-induced DNA damage in HCT.shctrl cells (Figure 66).
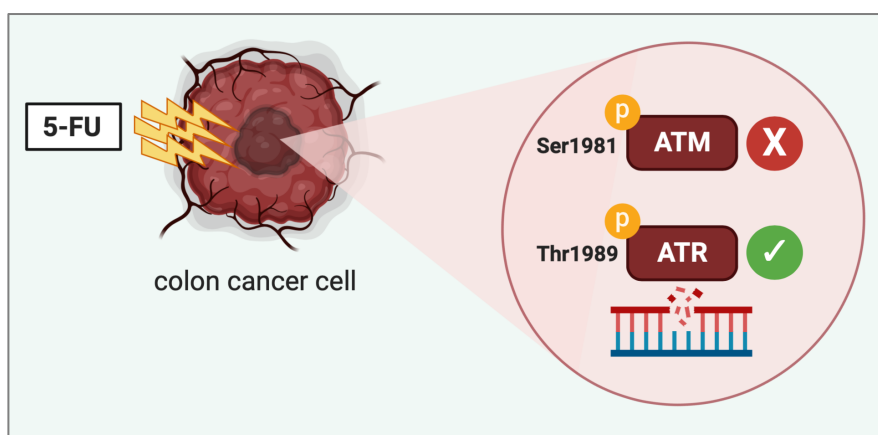
Figure 66. ATR is the key sensor of the 5-FU-induced DNA damage in cancer cells.
Treatment with 5-FU leads to DNA damage in colon cancer cells, which in turn contributes to the recruitment of ATR, but not ATM, to the damage site. As a result, ATR undergoes phosphorylation at Thr1981 and subsequent activation. Therefore, this indicates that ATR acts as the critical sensor of the 5-FU-induced DNA damage in colon cancer cells.[16]

In the present study, it was found that both Chk1 and Chk2 were phosphorylated in HCT.shctrl cells in response to 5-FU. We have demonstrated that Chk1 underwent

---

[16] Image created with BioRender.com

phosphorylation at Ser317 site, which is believed to be the critical site for activation of this kinase (Smith et al., 2010; Zhang and Hunter, 2013). Such observation was consistent with the results described in other studies, which reported that Chk1 was phosphorylated in response to 5-FU in HCT116 and SW480 cells (Martino-Echarri et al., 2014). Additionally, the Western blot results revealed that in HCT.shctrl cells exposed to 5-FU, Chk2 was phosphorylated at the Thr68 site, which is considered as crucial for its full activation (Smith et al., 2010). Such observation was similar to the results reported by Huelsenbeck et al. (2012), which described that Chk2 underwent phosphorylation in response to anti-tumour agents, such as doxorubicin and etoposide. These findings indicate that, similar to ATR, Chk1 and Chk2 kinases are activated in response to 5-FU and are involved in DNA damage signalling in 5-FU-induced apoptosis in HCT.shctrl cells.

Moreover, a very recent study by Jaarsveld et al. (2019) also reported an elevation of the Chk1 and Chk2 activation in response to chemotherapeutic drugs, such as cisplatin or doxorubicin. Interestingly, the authors suggested that the activation of these kinases contributes to resistance development in tumour cells rather than apoptosis induction (Jaarsveld et al., 2019). Thus, taken these and our findings together, it is noteworthy, that the roles of activated Chk1 and Chk2 in determining of the cell fate (survival vs. apoptosis) are very likely to be cell type- and/or stimulus-specific.

5.7 ATR Mediates Chk1 Activation and p53 Induction, Whereas Both ATR and ATM Regulate Chk2 Activation

As described in the classical DNA damage response model, ATR and ATM are involved in phosphorylation and activation of Chk1 and Chk2, respectively (Zinkel et al., 2005;

Matsuoka et al., 2007; Shiloh and Ziv, 2013; Zhang and Hunter, 2013). Thus, it was asked, whether the same molecular events were triggered in response to 5-FU in cancer cells. The Western blot analysis revealed that application of 5-FU in combination with ATR inhibitor AZD6738 led to a complete block of Chk1 phosphorylation at Ser317 in HCT.shctrl cells. In contrast, in the presence of ATM inhibitor KU55933, chemotherapeutic agent treated HCT.shctrl cells were able to phosphorylate Chk1 to the same degree as the control cell line, suggesting that ATR, but not ATM, was involved in the anti-tumour drug induced Chk1 activation (Figure 67).

Interestingly, treatment with 5-FU plus ATR or ATM inhibitor led to a strong reduction of the Chk2 phosphorylation at Thr68, when compared with the control cell line. These results suggest that both ATR and ATM were required for the Chk2 activation in HCT.shctrl cells treated with 5-FU. Initially, our findings ruled out the involvement of ATM in 5-FU-induced DNA damage signalling and apoptosis, as this kinase was not found to be phosphorylated in response to 5-FU. Nevertheless, finding out that ATM was involved in the Chk2 phosphorylation upon the 5-FU treatment, led to a conundrum, that requires further experiments with respect to the role of ATM in 5FU-treated HCT.shctrl cells.

In order to further investigate the role of ATR in phosphorylation and regulation of its substrates in 5-FU-induced apoptosis, a stable ATR knockdown clone of HCT116 cells, namely HCT.shATR, was generated. This cell line was checked for Chk1 and Chk2 activation by analysis of their phosphorylation status in response to 5-FU. In contrast to HCT.shctrl cells, we found that treatment of HCT.shATR with 5-FU led to an almost complete attenuation of Chk1 and Chk2 phosphorylation. Thus, these data further confirmed the requirement of ATR for 5-FU-induced Chk1 and Chk2 activation in cancer cells (Figure 67).

Induction of genotoxic stress typically contributes to accumulation of the tumour suppressor p53, which plays a crucial role in prevention of cancer development and regulation of numerous processes, including cell cycle, cellular responses to DNA damage and induction of apoptosis (Russo et al., 2005; Ju et al., 2007; Collavin et al., 2010; Li et al., 2015). Many studies reported that upon the genotoxic stress, p53 is activated and acts as transcriptional activator and can regulate a wide range of substrates, that are also involved in the above processes (Heeren et al., 2004; Balmer et al., 2014).

Thus, as expected, it was observed that the levels of p53 were strongly increased in HCT.shctrl cells in response to 5-FU. Moreover, we found that application of the ATR inhibitor blocked the 5-FU-induced elevation in p53. In contrast, the attenuation of the 5-FU-induced increase in p53 was not observed in response to 5-FU combined with ATM inhibitor alone or with both ATR and ATM inhibitors. Furthermore, our results showed that the levels of p53 were markedly reduced in 5-FU-treated HCT.shATR cells, when compared with the control HCT.shctrl cells subjected to the same treatment. Thus, we concluded that ATR functions as a key regulator of the Chk1 and Chk2 activation as well as p53 induction in 5-FU-initiated apoptosis in cancer cells (Figure 67).
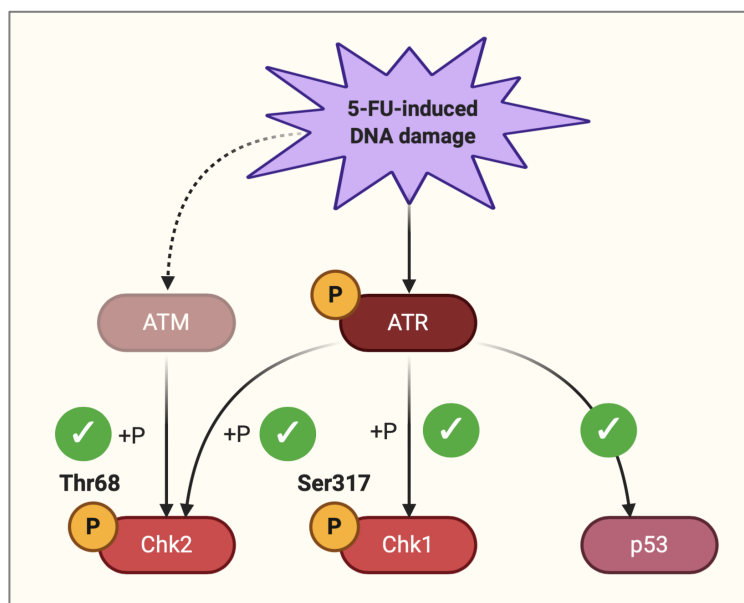
Figure 67*. Regulation of Chk1 and Chk2 phosphorylation and p53 induction in cancer cells treated with 5-FU.*
Upon 5-FU-induced DNA damage, activated ATR mediates phosphorylation of Chk1 at Ser317 and accumulation of p53. Moreover, Chk2 undergoes phosphorylation at Thr68 and therefore, also undergoes activation in response to 5-FU. However, this process is positively regulated by both ATR and ATM. [17]

Moreover, many studies have correlated the p53 status with therapy responses (Longley et al., 2003; Boyer et al., 2004; Sui et al., 2014). As mentioned above, we observed that blocking and knocking-down of ATR led to a strong reduction of p53 levels in the cells treated with 5-FU. In our previous report we described that HCT.p53-/- cells were protected from 5-FU-induced apoptosis (Mohr et al., 2018). Such observation was in line with the results obtained by others, which demonstrated that the absence of p53 strongly decreases the sensitivity of HCT.p53-/- cells to 5-FU (Longley et al., 2003; Boyer et al., 2004; Sui et al., 2014). Additionally, we found that caspase-9 was not required for 5-FU-induced apoptosis (Mohr et al., 2018). Therefore, considering that the resistance of HCT.p53-/- cells to 5-FU was not associated with inhibition of the conventional apoptotic pathway, we proposed a model of 5-FU-induced apoptosis and the alternative functions of p53 therein.

---

[17] Image created with BioRender.com

With respect to that, it was shown by our group that 5-FU-induced apoptosis was modulated by the p53-driven TRAIL-R2/JNK axis, which we assumed would signal to mitochondria (Mehrabadi, 2018). It was demonstrated that p53 was responsible for the transcriptional regulation of TRAIL-R2 (DR5) in 5-FU-treated HCT116 cells. Moreover, our group discovered, that in 5-FU-induced apoptosis, DR5 was not involved in caspase-8 activation, as described in the classical model of apoptosis, but in activation of JNK (Mehrabadi, 2018). Moreover, other molecular factors, which were associated with DR5 and responsible for the 5-FU-induced JNK activation, namely, caspase-8 and FADD, were also identified (Mehrabadi, 2018). The obtained data indicated that upon treatment with 5-FU, DR5 can form a complex with caspase-8 and FADD, without caspase-8 activation function, that mediates activation of JNK. This complex was termed JIST (JNK-inducing signal transduction complex). Thus, it was concluded that DR5 functions as the molecular platform for JNK activation in cancer cells treated with 5-FU (Mehrabadi, 2018). Since it was assumed that the p53-driven TRAIL-R2/JNK axis most likely signals to mitochondria, the initial apoptosis signal emitted by activated caspase-8 at the FADDosome would be amplified via the mitochondria leading to the release of pro-apoptotic factors, such as Smac/DIABLO (Mehrabadi, 2018). In the light of these findings, the question arises, whether ATR could regulate the TRAIL-R2/JNK pathway via p53 in response to 5-FU. Nevertheless, this remains to be resolved.

5.8 ATR is Required for Caspase-10 Upregulation and FADDosome Formation

Next, it was asked, whether the ATR- and ATM-mediated signalling pathways were involved in 5-FU-induced upregulation of caspase-10, which we showed to act as the core molecular driver of the FADDosome complex formation (Mohr et al. 2018). The results obtained by Western blot showed that in the presence of ATR inhibitor AZD6738,

upregulation of caspase-10 was strongly attenuated in HCT.shctrl cells treated with 5-FU. On the contrary, blocking of ATM with KU55933 had no effect on caspase-10 upregulation in the 5-FU treated cells, ruling out the role of ATM in controlling the anti-cancer drug-induced caspase-10 upregulation.

In order to further investigate the involvement of ATR in regulation of caspase-10 levels in response to 5-FU, it was tested the HCT.shATR cells, which were analysed for caspase-10 upregulation by using Western blot and compared them with the results obtained for HCT.shctrl cells. Similar to the findings observed for HCT.shctrl cells treated with 5-FU plus ATR inhibitor, caspase-10 was not detectable in HCT.shATR cells after exposure to 5-FU. Thus, it was concluded that, upon treatment with 5-FU, caspase-10 is upregulated in ATR-dependent manner, whereas ATM is dispensable for this process (Figure 68).

5.9 Activated Chk1 and Chk2 Act Independently of p53 and Are Required for Caspase-10 Upregulation and FADDosome Formation

in this study, it was demonstrated that blocking and knocking-down of ATR contributed to a strong decrease of the Chk1 and Chk2 phosphorylation, p53 induction and caspase-10 upregulation after treatment with 5-FU. Next, we investigated the order of molecular events downstream of ATR in more detail by using HCT.p53-/- and HCT.shC10 cells, which were examined for Chk1 and Chk2 phosphorylation levels after exposure to the chemotherapeutic drug.

It was observed that phosphorylation of Chk1 and Chk2 was markedly elevated in both HCT.p53-/- and HCT.shC10 cells stimulated with 5-FU, which was comparable with the

results obtained for the control HCT.shctrl cells subjected to the same treatment. Thus, it was concluded, that activation of Chk1 and Chk2 in 5-FU-induced apoptosis is p53-independent and occurs upstream of caspase-10. Additionally, the results obtained by Western blot revealed that the loss of caspase-10 did not affect the levels of p53 and p21 in response to 5-FU. It was observed that these proteins were induced in HCT.shC10 cells to the same degree as in HCT.shctrl cells treated with the anti-tumour drug. These results indicated that the cells lacking caspase-10 showed the same molecular response to the chemotherapeutic as HCT.shctrl cells as far as p53 and p21 activation was concerned. Thus, both cell types were principally able to respond to cytotoxic drug-inflicted stress and damage.

Next, it was asked, whether activated Chk1 and Chk2 were involved in the signal transduction towards the 5-FU-induced caspase-10 upregulation and FADDosome formation. Prior to the analysis, we examined the action of a potent and selective inhibitor CHIR-124, which primarily attenuates the activity of Chk1, however it can also block activation of Chk2 (Tse et al., 2007). The Western blot analysis revealed that after application of CHIR-124, the Chk1 and Chk2 phosphorylation was considerably reduced in HCT.shctrl cells treated with 5-FU or etoposide. Moreover, it was found that the HCT.shctrl cells exposed to CHIR-124 plus 5-FU or etoposide combination mounted the same molecular response to the treatment as HCT.shctrl cells stimulated with 5-FU or etoposide alone, as we observed that the levels of p53 and p21 were increased to the same degree in the control and treated cells.

Next, HCT.shctrl cells treated with CHIR-124 plus 5-FU or etoposide were checked for the levels of caspase-10. The results obtained by Western blot unveiled that application of the inhibitor led to a strong decrease of caspase-10 in response to 5-FU. Additionally, it was observed that upon treatment with etoposide, caspase-10 upregulation was not increased. Subsequently, stimulation with CHIR-124 plus etoposide did not influence the

caspase-10 upregulation levels. Our results indicated that upregulation of caspase-10 was Chk1/Chk2-dependent and that this molecular event is important for the cell death triggered by 5-FU, but not etoposide. Thus, other molecular factors, namely Chk1/Ch2, which like ATR, which are involved in signalling from the DNA damage site towards the 5-FU-induced caspase-10 upregulation, were identified (Figure 68).
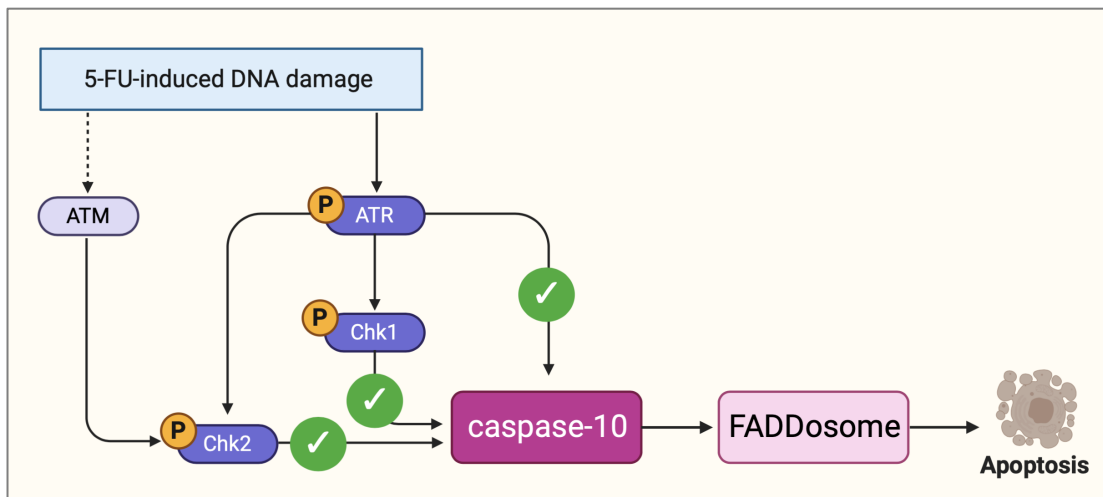
Figure 68. ATR, Chk1 and Chk2 are involved in signalling from the DNA damage site towards the 5-FU-induced caspase-10 upregulation and FADDosome formation.
Following treatment with 5-FU leading to the DNA damage, caspase-10 undergoes upregulation, which is mediated either directly by activated ATR or indirectly by ATR-regulated downstream Chk1 and Chk2. Activation of the latter is also positively regulated by ATM, nevertheless ATM was found dispensable for 5-FU-induced caspase-10 upregulation. Increased caspase-10 levels lead to formation of the FADDosome complex, which in turn initiates apoptosis.[18]

Additionally, it was observed that in HCT.shctrl cells exposed to the CHIR-124 plus 5-FU or etoposide, the p53 and p21 levels were strongly increased, which was comparable with the results obtained for the HCT.shctrl cells stimulated with 5-FU or etoposide alone. Thus, in contrast to the ATR findings, blocking of Chk1 and Chk2 did not lead to the decrease of p53 in response to 5-FU. This indicated that induction of p53 does not require the involvement of activated Chk1 and Chk2 in 5-FU-induced apoptosis.

---

[18] Image created with BioRender.com

To date, the role of caspase-10 and its activity in the initiation of the programmed cell death in response to anti-tumour treatments has been examined and reported only by a few studies *in vitro*. It was demonstrated, that application of adriamycin and etoposide could promote transcription of the Casp10 gene through activation of p53, leading to the increase of the caspase-10 amount at the mRNA and protein levels in tumour cells (Rikhof et al., 2003). Such results were in contrast to the observations present in this study, as it was found that etoposide did not contribute to the elevation of caspase-10 levels in HCT.shctrl cells. Moreover, contrary to Rikhof et al. (2003), it was demonstrated, that upregulation of caspase-10 was p53-independent in cancer cells exposed to chemotherapeutic drugs, such as 5-FU. However, it is noteworthy, that Rikhof et al. (2003) examined the types of cells, that were different from HCT.shctrl cells, namely H460 (lung cancer), PA-1 (ovarian cancer) and U2OS (osteosarcoma). Taken together, the results suggest that the increase of the caspase-10 levels and its regulation mechanisms is very like to be treatment type- and/or cell-type specific.

Interestingly, it was suggested by some studies that caspase-10 can trigger apoptosis in a FADD-dependent manner, without involvement of the death receptor pathways after exposure to cytotoxic chemotherapeutic drugs (Park et al., 2004; Filomenko et al., 2006; Lee et al., 2007), which is in line with our findings (Mohr et al., 2018). Such cell death-inducing mechanisms were found in human U937, 293T and HeLa cell lines stimulated with etoposide (Filomenko et al., 2006) and in human lymphoblastic leukaemia cells exposed to paclitaxel (taxol) (Park et al., 2004). Taken together, it is becoming more evident that apoptosis induction, which requires involvement of caspase-10 (and caspase-8) can occur without engagement of the death receptors and that this process is not limited to HCT116 cells and 5-FU treatment only.

5.10 Inhibition of Chk1/Chk2 Activation Leads to a Switch to the FLIPosome Mode of Apoptosis

Next, it was asked, whether Chk1 and Chk2 were involved in regulation of the 5-FU-induced apoptosis and whether they could be responsible for determining the mode of cell death (FADDosome vs. FLIPosome) in cancer cells treated with the anti-tumour drug. In this context, it was hypothesised that blocking of Chk1/Chk2 could lead to the significant elevation of the cell death levels in response to 5-FU.

When the levels of apoptosis in HCT.shctrl cells, which were treated with a CHIR-124/5-FU combination, were examined, it was observed that blocking of Chk1 and Chk2 significantly increased the cell death triggered by 5-FU after 24 h. Following the 48 h stimulation with CHIR-124 plus 5-FU, the levels of apoptosis in HCT.shctrl cells were also strongly elevated and slightly higher, when compared with the result obtained for HCT.shctrl cells treated with 5-FU alone. Similar results were obtained for HCT116 cells, which were lacking ATR, caspase-10, RIP1 or TRAF2, as we observed that these cells could still undergo apoptosis in response to 5-FU. Thus, similar to the findings reported by our group previously (Mohr et al., 2018), the data obtained in this study for HCT.shctrl cells stimulated with CHIR-124 plus 5-FU suggest, that the cells might be able to switch to an alternative mode of apoptosis.

Furthermore, our group showed that in the absence of ATR, caspase-10, RIP1 or TRAF2, cIAP1 was degraded in response to 5-FU, which is one of the main characteristics of the FLIPosome-mediated apoptosis. (Mohr et al., 2018). Having found that HCT.shctrl cells with blocked Chk1/Chk2 could still undergo apoptosis in response to 5-FU, it was asked, whether inhibition of these kinases could lead to the switch to the FLIPosome mode of apoptosis in cancer cells. Therefore, it was assumed, that in

HCT.shctrl cells treated with CHIR-124 plus 5-FU, cIAP1 could also undergo proteolytic degradation after the treatment. As expected, application of the CHIR-124/5-FU combination led to cIAP1 degradation. Thus, similar to the results obtained for the caspase-10-, ATR-, RIP1- and TRAF2-deficient cells (Mohr et al., 2018), when Chk1 and Chk2 are not present, it appears that HCT.shctrl cells can switch to the alternative mechanism of the FLIPosome.

The findings presented in this study indicate that application of Chk1/Chk2 inhibitor sensitises cancer cells to treatment with anti-tumour drugs, leading to induction of more effective apoptotic response, which is in line with the observations described by others (Tse et al., 2007; Akasaka et al., 2014; Qiu et al., 2018). Similar to the results obtained in the present research, Akasaka et al. (2014) found that the synergistic effect of the Chk1 inhibitor and 5-FU enhances apoptosis in the treatment of colorectal cancer. The authors also demonstrated that blocking Chk1 can increase cell death in the treatment of gastric tumours in response to 5-FU (Akasaka et al., 2014). Moreover, Tse et al. (2007) and Qiu et al. (2018) reported that application of the Chk1/Chk2 inhibitor, CHIR-124, combined with topoisomerase poisons promotes apoptosis in breast cancer and p53-mutated solid tumour cell lines. Thus, taken these and our findings together, application of Chk1/Chk2 inhibitors combined with anti-tumour drugs holds a significant promise and might provide therapeutic advantages in the treatment of various cancers, including p53-null or p53-mutated tumours.

5.11 Conclusions

In the present study, it was observed that ΔDEDs caspase-10 (wild-type), ΔDEDs caspase-8 (wild type), ΔDEDs cFLIP-L (wild-type) and FADD-FL were successfully expressed using induction with 0.1 mM (final concentration) IPTG and incubation at 18°C overnight, leading to production of good levels of proteins. The same expression conditions were optimal for production of ΔDEDs caspase-8 (C360A and D374A/D384A mutants), whereas expression of ΔDEDs caspase-10 (C410A and D415A mutants) required supplementation of the bacterial medium with 1% (final concentration) glucose and induction with 0.02 mM (IPTG) followed by incubation at 18°C overnight.

Moreover, the results showed that the control ΔDEDs caspase-8 (C360A) and C-(His)$_6$ GST (a product of an empty modified pGEX-4-T3 vector) were successfully expressed after induction with 0.1 mM (final concentration) IPTG followed by incubation at 30°C for 3 h. This led to production of very high levels of proteins. For expression of ΔDEDs caspase-10 (C401A and D415A mutants) and ΔDEDs cFLIP-L (wild type and D376A linker mutant), same expression conditions were found optimal.

It was found that ΔDEDs caspase-8 (C360A) and C-(His)$_6$ FADD-FL were successfully purified using column chromatography, leading to obtaining very good and satisfactory yields of highly pure proteins, which can be used in small-scale experiments, such as activity or pull-down assays, co-immunoprecipitation or ELISA.

Furthermore, the novel function of the core driver of the FADDosome formation, caspase-10 as a potential caspase-8 activator was studied. It was discovered that caspase-10 is able to process caspase-8 *in vitro*. Moreover, the interaction between other key FADDosome components, namely FADD and caspase-8 was also

investigated. It was found that FADD and caspase-8 possibly interact via a novel mechanism *in vitro* that is independent of DED.

In summary, the work presented in this study provides methods for protein expression and purification, which can be utilised in the next stages of this research as well as serve as a starting point in these studies, which aim to express and purify proteins for crystallography and protein structure studies. Moreover, the activity and pull-down assays results provide a better understanding of the functional relationships and interactions between the FADDosome components and serve as a foundation for further work to be carried out in the context of the complex reconstitution and switch to the FLIPosome.

In this study, it was discovered that ATR, Chk1 and Chk2 kinases, which are conventionally involved in the regulation of the DNA damage response and the DNA repair, were phosphorylated after stimulation with 5-FU and required for the caspase-10 upregulation followed by FADDosome formation. Moreover, it was discovered that Chk1 and Chk2 kinases were activated in an ATR-dependent manner in response to 5-FU. (Figure 69). Thus, it was concluded that ATR acts as the key sensor of the 5-FU-induced DNA damage in colorectal cancer cells. Moreover, it was concluded that in the further signalling pathway downstream of ATR, Chk1 and Chk2 function as the DNA damage signal transducers towards caspase-10 and the FADDosome (Figure 69).

Additionally, it was found that activated ATR plays a role in regulation of p53 accumulation in response to 5-FU, suggesting that ATR is not only involved in the DNA damage response signalling towards the FADDosome, but also very likely regulates other 5-FU induced pathways, which depend on p53 (Figure 69). Thus, it was concluded that like Chk1 and Chk2, p53 acts as a DNA damage signal transducer downstream of ATR, however it regulates an apoptotic pathway that is distinct from the caspase-10-

driven FADDosome (Figure 69).

Moreover, it was discovered that, similar to inhibition of ATR, blocking of Chk1 and Chk2 in 5-FU-treated HCT.shctrl cells appeared to promote a switch to an alternative cell death mechanism, which requires assembly of the FLIPosome platform (Figure 69).

In summary, in the present study, ATR, Chk1 and Chk2 were identified as the novel factors involved in 5-FU-induced DNA damage signalling, caspase-10 upregulation and FADDosome formation in response to 5-FU. This led to discovery of the novel ATR/Chk1/Chk2/caspase-10 apoptotic network triggered in colorectal cancer cells exposed to 5-FU (Figure 69). Moreover, p53 was also identified as the molecular factor, which acts downstream of ATR and plays a role in the DNA damage signalling in 5-FU-induced apoptosis, suggesting an involvement of another novel ATR/p53 cell death pathway in colorectal cancer cells (Figure 69).

Moreover, the findings presented in this research indicate a novel mode of action of the ATR inhibitor AZD6738 and the Chk1/Chk2 inhibitor CHIR-124, when combined with other anti-tumour drugs, such as 5-FU, in the treatment of colorectal cancer. Since our group demonstrated previously that the FLIPosome executes apoptosis more effectively than the FADDosome and it does not require involvement of p53, promoting a switch to the FLIPosome mode of apoptosis holds a significant promise and provides therapeutic advantages in the treatment of p53-null or p53-mutated tumours.
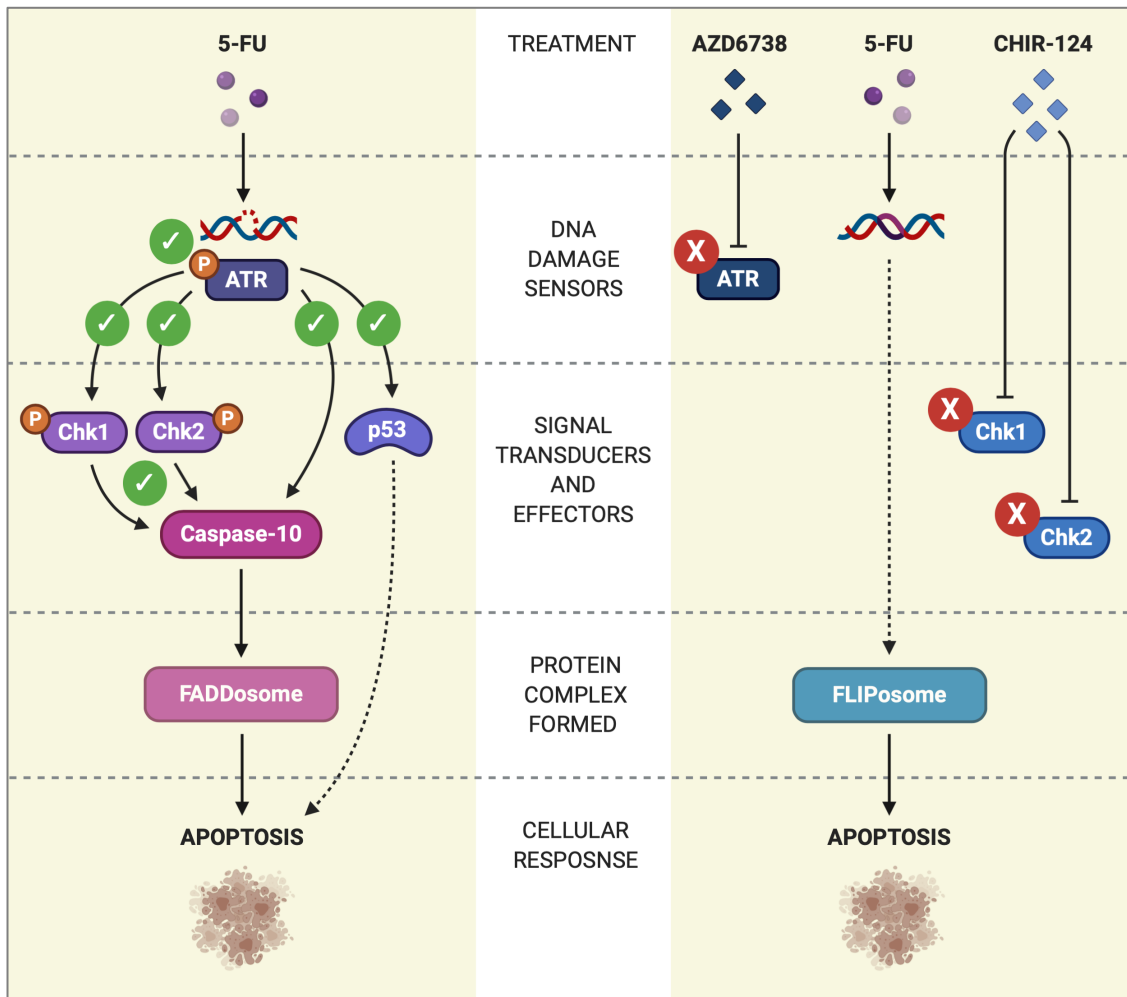
Figure 69. Novel signalling pathways and the mechanisms of the FADDosome and FLIPosome formation in HCT.shctrl cells treated with 5-FU.

The 5-FU-induced DNA damage is sensed by ATR and the signals from the DNA lesion site are transduced in the ATR-dependent manner towards the caspase-10 upregulation followed by FADDosome formation and subsequent apoptosis (left panel). In this signalling pathway, ATR also mediates phosphorylation of Chk1 and Chk2, which like ATR, are required for the 5-FU-stimulated caspase-10 upregulation. Moreover, ATR also plays a role in induction of p53 in response to 5-FU. Therefore, we assume that ATR very likely mediates another, p53-regulated pathway and the molecular factors involved in this pathway need to be identified. Furthermore, similar to the loss of caspase-10, RIP1 and TRAF2, inhibition of ATR with AZD6738 (ATR inhibitor) as well as blocking of Chk1 and Chk2 with CHIR-124 (Chk1/Chk2 inhibitor) causes a shift to the FLIPosome mode of apoptosis in HCT.shctrl cells treated with 5-FU (right panel). However, the molecular factors involved in the DNA damage sensing and signal transduction toward the FLIPosome in response to 5-FU are yet to be identified.[19]

---

[19] Image created with BioRender.com

5.12 Future Work

In the present study, it was discovered that caspase-10 has the ability to cleave caspase-8 *in vitro*. However, the question arises, whether caspase-10-mediated activation of caspase-8 could be possibly affected, either positively or negatively, after addition of FADD and/or cFLIP-L to the setting. This could provide more insights into the roles of FADD and cFLIP-L in terms of the FADDosome formation as well as into the mechanisms responsible for activation of caspase-8 at the complex.

The mechanism of caspase-10-mediated caspase-8 activation in the presence of FADD and/or cFLIP-L could be tested by performing the activity assay. In one setting, caspase-10, caspase-8 and FADD would be mixed and the cleavage of caspase-8 would be analysed after indicated timepoints, as described in this study. In another setting, caspase-10, caspase-8 and cFLIP-L would be mixed and the processing of caspase-8 would be examined in the same manner. The cleavage efficiency could be then compared between all settings at selected timepoints, to detect any possible delays or acceleration of the caspase-8 activation.

Moreover, it was found that FADD and caspase-8 can possibly interact via a novel DED-independent mechanism. However, the exact details regarding the mechanism responsible for this interaction as well as the stoichiometry of the bound FADD and caspase-8 remain unknown. Thus, further research and application of different techniques are required in order to confirm this interaction and resolve the stoichiometry of the bound FADD and caspase-8 molecules. The binding between the proteins can be confirmed by performing immunoprecipitation, whereas the stoichiometry of associated FADD and caspase-8 can be assessed by using gel filtration chromatography analysis. Moreover, the structure modelling of the protein-protein interaction between FADD and

caspase-8 could provide more insights into what residues are responsible for the potential DED-independent binding between these proteins.

Furthermore, it is hypothesised that upon 5-FU treatment, upregulated capsase-10 can outcompete cFLIP-L for binding to caspase-8, which results in formation of the FADDosome. Thus, it was asked, what are the actual binding preferences between caspase-10 and caspase-8/cFLIP-L. Investigation of this matter could provide more details regarding the potential switch mechanism from the FADDosome to the FLIPosome complex and *vice versa*. Also, it was asked, what effect would different/increasing concentrations of caspase-10 have on its binding preference and whether an increased concentration of caspase-10 would indeed outcompete cFLIP-L for binding to caspase-8, as hypothesised.

The binding preferences between caspase-10 and caspase-8/cFLIP-L can be tested by mixing caspase-10 at different/increasing concentrations and caspase-8/cFLIP-L at constant concentrations. The effect of the increased amount of caspase-10 could be assessed by performing the binding assay and analysis of elution fractions for the presence of the proteins of interest, as described in this study. Alternatively, the binding preference of caspase-10 could also be tested by carrying out the activity assay and examination of the caspase-10-mediated cleavage of caspase-8 and cFLIP-L after selected timepoints.

In the present study, it was shown that 5-FU-induced DNA damage signalling is mediated by ATR, Chk1 and Chk2 and that these kinases are involved in positive regulation of caspase-10 upregulation in response to the anti-tumour drug, leading to the formation of the FADDosome and apoptosis. Initially, the role of ATM in this process was ruled out, however further experiments revealed, that the activity of Chk2 was dependent on ATM,

leading to a conundrum that requires more detailed investigation and answers with respect to ATM phosphorylation status in 5-FU-treated cells.

In the present study, an antibody that detects the Ser1981 phosphorylation site in ATM was used. It has been described that, upon occurrence of the DNA damage, ATM undergoes autophosphorylation at Ser1981, which is considered a hallmark of its activation and stabilisation (So et al., 2009). However, some studies reported that this kinase requires phosphorylation at Ser367, Ser1893, and Ser1981, in order to reach its full activity potential (Kozlov et al., 2011). Thus, examination of the ATM phosphorylation at Ser367 and Ser1893 is necessary to further assess the activity status and the role of this kinase in the DNA damage-induced signal transduction and apoptosis in response to 5-FU.

In the light of the results obtained so far, the detailed information on how ATR, Chk1 and Chk2 mediate the 5-FU-induced caspase-10 upregulation remains unclear and requires further investigation. In this context, it is essential to identify the molecular factors that might be involved in regulation of caspase-10 expression. The Chk1 and Chk2 kinases phosphorylate and control a wide range of substrates, of which many play an important role in the DNA damage-induced gene transcription and apoptosis (Bartek and Lukas, 2003; Christmann and Kaina, 2013). The most common substrates are the transcription factors BRCA1 and BRCA2, which normally are phosphorylated in the Chk2- and Chk1-dependent manner, respectively. Moreover, it was reported that BRCA1 and BRCA2 can be also activated by ATR and ATM. Additionally, BRCA1 is known to interact with p53 and transcriptionally regulate the activation of some genes involved in the DNA repair and apoptosis (Christmann and Kaina, 2013). Thus, examination of BRCA1 and BRCA2 as potential members of the ATR/Chk1/Chk2 signalling pathway could provide more insights into the regulation of the 5-FU-induced caspase-10 expression in cancer cells.

In the present study, it was discovered that the loss of ATR led to a considerable decrease of p53 levels in the cells exposed to 5-FU. Moreover, in our previous report we found that HCT.p53-/- cells were protected from 5-FU-induced apoptosis and that caspase-9 was dispensable for this process (Mohr et al., 2018). Moreover, it was discovered by our group that 5-FU-induced apoptosis was regulated by the p53-meduated TRAIL-R2/JNK network (Mehrabadi, 2018). Thus, a question arised, whether ATR could regulate the TRAIL-R2/JNK pathway through p53 after stimulation with 5-FU. Moreover, it was reported that BRCA1 transcriptionally activates GADD45a, which is believed to mediate the DNA repair process and activation of MEKK4. Once activated, this kinase regulates MKK4 and MKK7, which are responsible for regulation of the cytotoxic stress-induced activation of JNK (c-Jun-N-terminal kinase) (Takekawa et al., 1998; Mita et al., 2002; Christmann and Kaina, 2013). Therefore, investigation of the roles of ATR in the regulation of p53-driven TRAIL-R2/JNK axis and BRCA1 in JNK activation would provide more insights into the mechanisms involved in the novel signalling pathways of the 5-FU-induced apoptosis.

Moreover, it is hypothesised that the p53-regulated TRAIL-R2/JNK signalling pathway might be involved in the 5-FU-induced phosphorylation of Bid, as it was previously shown that JNK can activate and regulate Bid (Dhanasekaran and Reddy, 2008). Thus, we believe that phosphorylated Bid might potentially function as the meeting point of the FADDosome complex and the p53-driven TRAIL-R2/JNK signalling axis. It has been reported that ATR and ATM are involved in phosphorylation of Bid at Ser61 and Ser78 (Kamer et al., 2005; Zinkel et al., 2006; Liu et al., 2011; Wang et al., 2014). Moreover, Liu et al. (2011) described that Bid plays an important role in the DNA damage response by interacting with ATR and ATRIP (ATR-interacting protein), which in turn leads to formation of a complex that is involved in initiation of ssDNA repair. The authors also reported that Bid can interact with RPA (replication protein A), which is involved in recognition and coating ssDNA. Upon the Bid-mediated ssDNA coating with RPA, the

Bid-regulated ATR-ATRIP complex is recruited to the point of DNA damage and thereby, initiates its repair. Most importantly, Liu et al. (2011) emphasises the fact that the functions of ATR in the replicative stress response are highly dependent on Bid activity and its interaction with RPA. Such observations suggest that Bid can be involved in a wide range of processes associated with the DNA damage response, including both pro-apoptotic and pro-survival events, as well as it can interact with numerous proteins. Thus, the question arises, whether Bid could perform similar functions in the 5-FU-induced apoptosis in cancer cells. Therefore, more detailed investigation of different Bid functions and its interactions with other proteins can contribute to better understanding of the roles of Bid in the DNA damage response and novel 5-FU-induced pathways of apoptosis in cancer cells.

The work presented in this study provided answers for the factors and pathways involved in regulation of the caspase-10 upregulation and the FADDosome in 5-FU-induced apoptosis. However, it still leaves the question, what molecular factors are responsible for the DNA damage signal transduction towards the FLIPosome-mediated apoptosis in response to 5-FU. Having found that ATR acts as the key regulator of the DNA damage-induced signalling towards the caspase-10-dependent FADDosome formation, it was asked, whether ATM could be phosphorylated and signal towards the caspase-10-independent FLIPosome in response to 5-FU. Furthermore, it was asked, whether, as shown for the FADDosome, Chk1 and Chk2 could also play a role in FLIPosome-dependent apoptosis signalling and the complex formation. Thus, more detailed examination is needed in order to assess the importance of ATM and Chk1/Chk2 and their activation in signalling towards the 5-FU-induced FLIPosome formation. This hypothesis can be tested by using HCT.shC10 and HCT.shATR knockdown cells treated with 5-FU plus ATM inhibitor, which could be analysed for apoptosis levels by flow cytometry as well as cIAP1 levels by Western blot and TNF-α production by ELISA.

REFERENCE LIST

Abraham, R.T. (1998). Mammalian target of rapamycin: immunosuppressive drugs uncover a novel pathway of cytokine receptor signaling. *Current Opinion in Immunology*, 10, 330–336.

Akasaka, T., Tsujii, M., Kondo, J., Hayashi, Y., Ying, J. and Lu, Y. et al. (2014). 5-FU resistance abrogates the amplified cytotoxic effects induced by inhibiting checkpoint kinase 1 in p53-mutated colon cancer cells. *International Journal of Oncology*, 46, 63-70.

Amaral, J.D., Xavier, J.M., Steer, C.J. and Rodrigues, C.M. (2010). The role of p53 in apoptosis. *Discovery Medicine*, 9, 145–152.

Ando, K., Kernan, J.L., Liu, P.H., Sanda, T., Logette, E., Tschopp, J., Look, A.T., Wang, J., Bouchier-Hayes, L. and Sidi, S. (2012). PIDD Death-Domain Phosphorylation by ATM Controls Prodeath versus Prosurvival PIDDosome Signaling. *Molecular Cell*, 47, 681–693.

Ariumi, Y., Turelli, P., Masutani, M., and Trono, D. (2005). DNA Damage Sensors ATM, ATR, DNA-PKcs, and PARP-1 Are Dispensable for Human Immunodeficiency Virus Type 1 Integration. *Journal of Virolo*gy, 79, 2973-2978.

Ashkenazi, A. and Dixit, V.M. (1998). Death Receptors: Signaling and Modulation. *Science*, 281, 1305–1308.

Awasthi, P., Foiani, M. and Kumar, A. (2016). ATM and ATR signaling at a glance. *Journal of Cell Science*, 129, 1285–1285.

Bai, L. and Wang, S. (2014). Targeting Apoptosis Pathways for New Cancer Therapeutics. *Annual Review of Medicine*, 65, 139–155.

Bakkenist, C.J. and Kastan, M.B. (2003). DNA damage activates ATM through intermolecular autophosphorylation and dimer dissociation. *Nature*, 421, 499–506.

Balmer, M.T., Katz, R.D., Liao, S., Goodwine, J.S. and Gal, S. (2014). Doxorubicin and 5-fluorouracil induced accumulation and transcriptional activity of p53 are independent of the phosphorylation at serine 15 in MCF-7 breast cancer cells. *Cancer Biology & Therapy*, 15, 1000–1012.

Baptiste-Okoh, N., Barsotti, A.M. and Prives, C. (2008). A role for caspase 2 and PIDD in the process of p53-mediated apoptosis. *Proceedings of the National Academy of Sciences*, 105, 1937–1942.

Bartek, J. and Lukas, J. (2003). Chk1 and Chk2 kinases in checkpoint control and cancer. *Cancer Cell*, 3, 421–429.

Bauer, J.H. and Helfand, S.L. (2006). New tricks of an old molecule: lifespan regulation by p53. *Aging Cell*, 5, 437–440.

Belz, K., Schoeneberger, H., Wehner, S., Weigert, A., Bonig, H., Klingebiel, T., Fichtner, I. and Fulda, S. (2014). Smac mimetic and glucocorticoids synergize to induce apoptosis in childhood ALL by promoting ripoptosome assembly. *Blood*, 124, 240–250.

Bentley, N.J., Holtzman, D.A., Flaggs, G., Keegan, K.S., DeMaggio, A., Ford, J.C., Hoekstra, M. and Carr, A.M. (1996). The Schizosaccharomyces pombe rad3 checkpoint gene. *The EMBO Journal*, 15, 6641–6651.

Berglund, H., Olerenshaw, D., Sankar, A., Federwisch, M., McDonald, N.Q. and Driscoll, P.C. (2000). The three-dimensional solution structure and dynamic properties of the human FADD death domain 1 1Edited by A. Fersht. *Journal of Molecular Biology*, 302, 171–188.

Bertsch, U., Röder, C., Kalthoff, H. and Trauzold, A. (2014). Compartmentalization of TNF-related apoptosis-inducing ligand (TRAIL) death receptor functions: emerging role of nuclear TRAIL-R2. *Cell Death & Disease*, 5, 1–10.

Berube, C., Boucher, L.-M., Ma, W., Wakeham, A., Salmena, L., Hakem, R., Yeh, W.-C., Mak, T.W. and Benchimol, S. (2005). Apoptosis caused by p53-induced protein with death domain (PIDD) depends on the death adapter protein RAIDD. *Proceedings of the National Academy of Sciences*, 102, 14314–14320.

Biton, S. and Ashkenazi, A. (2011). NEMO and RIP1 Control Cell Fate in Response to Extensive DNA Damage via TNF-α Feedforward Signaling. *Cell*, 145, 92–103.

Blackford, A.N. and Jackson, S.P. (2017). ATM, ATR, and DNA-PK: The Trinity at the Heart of the DNA Damage Response. *Molecular Cell*, 66, 801–817.

Blanchard, H., Kodandapani, L., Mittl, P.R., Marco, S.D., Krebs, J.F., Wu, J.C., Tomaselli, K.J. and Grütter, M.G. (1999). The three-dimensional structure of caspase-8: an initiator enzyme in apoptosis. *Structure*, 7, 1125–33.

Boatright, K., Deis, C., Denault, J., Sutherlin, D. and Salvesen, G. (2004). Activation of caspases-8 and -10 by FLIPL. *Biochemical Journal*, 382, 651-657.

Boatright, K.M. and Salvesen, G.S. (2003). Mechanisms of caspase activation. *Current Opinion in Cell Biology*, 15, 725–31.

Bock, F.J., Krumschnabel, G., Manzl, C., Peintner, L., Tanzer, M.C., Hermann-Kleiter, N., Baier, G., Llacuna, L., Yelamos, J. and Villunger, A. (2012a). Loss of PIDD limits NF-κB activation and cytokine production but not cell survival or transformation after DNA damage. *Cell Death & Differentiation*, 20, 546–557.

Bock, F.J., Peintner, L., Tanzer, M., Manzl, C. and Villunger, A. (2012b). P53-induced protein with a death domain (PIDD): master of puppets? *Oncogene*, 31, 4733–4739.

Boyer, J., McLean, E.G., Aroori, S., Wilson, P., McCulla, A., Carey, P.D., Longley, D.B. and Johnston, P.G. (2004). Characterization of p53 Wild-Type and Null Isogenic Colorectal Cancer Cell Lines Resistant to 5-Fluorouracil, Oxaliplatin, and Irinotecan. *Clinical Cancer Research*, 10, 2158–2167.

Brenner, D., Blaser, H. and Mak, T.W. (2015). Regulation of tumour necrosis factor signalling: live or let die. *Nature Reviews Immunology*, 15, 362–374.

Brody, H. (2015). Colorectal cancer. *Nature*, 521, S1–S1.

Brosh, R. and Rotter, V. (2009). When mutants gain new powers: news from the mutant p53 field. *Nature Reviews Cancer*, 9, 701–713.

Carrington, P.E., Sandu, C., Wei, Y., Hill, J.M., Morisawa, G., Huang, T., Gavathiotis, E., Wei, Y. and Werner, M.H. (2006). The Structure of FADD and Its Mode of Interaction with Procaspase-8. *Molecular Cell*, 22, 599–610.

Chinnaiyan, A., O'Rourke, K., Tewari, M. and Dixit, V. (1995). FADD, a novel death domain-containing protein, interacts with the death domain of Fas and initiates apoptosis. *Cell*, 81, 505-512.

Christmann, M. and Kaina, B. (2013). Transcriptional regulation of human DNA repair genes following genotoxic stress: trigger mechanisms, inducible responses and genotoxic adaptation. *Nucleic Acids Research*, 41, 8403–8420.

Ciccia, A., and Elledge, S. (2010). The DNA Damage Response: Making It Safe to Play with Knives. *Molecular Cell*, 40, 179-204.

Cimprich, K.A., Shin, T.B., Keith, C.T. and Schreiber, S.L. (1996). cDNA cloning and gene mapping of a candidate human cell cycle checkpoint protein. *Proceedings of the National Academy of Sciences*, 93, 2850–2855.

Collavin, L., Lunardi, A. and Del Sal, G. (2010). p53-family proteins and their regulators: hubs and spokes in tumor suppression. *Cell Death & Differentiation*, 17, 901–911.

Costa, S., Almeida, A., Castro, A. and Domingues, L. (2014). Fusion tags for protein solubility, purification and immunogenicity in Escherichia coli: the novel Fh8 system. *Frontiers in Microbiology*, 5.

Cuenin, S., Tinel, A., Janssens, S. and Tschopp, J. (2007). p53-induced protein with a death domain (PIDD) isoforms differentially activate nuclear factor-kappaB and caspase-2 in response to genotoxic stress. *Oncogene*, 27, 387–396.

Cullen, S.P. and Martin, S.J. (2009). Caspase activation pathways: some recent progress. *Cell Death & Differentiation*, 16, 935–938.

Daniel, J.A., Pellegrini, M., Lee, J.-H., Paull, T.T., Feigenbaum, L. and Nussenzweig, A. (2008). Multiple autophosphorylation sites are dispensable for murine ATM activation in vivo. *The Journal of Cell Biology*, 183, 777–783.

Daub, H., Olsen, J.V., Bairlein, M., Gnad, F., Oppermann, F.S., Körner, R., Greff, Z., Kéri, G., Stemmann, O. and Mann, M. (2008). Kinase-selective enrichment enables quantitative phosphoproteomics of the kinome across the cell cycle. *Molecular Cell*, 31, 438–448.

David, R. (2012). Apoptosis: A lipid trigger of MOMP. *Nature Reviews Molecular Cell Biology*, 13, 208–209.

De Angelis, P.M., Svendsrud, D.H., Kravik, K.L. and Stokke, T. (2006). Cellular response to 5-fluorouracil (5-FU) in 5-FU-resistant colon cancer cell lines during treatment and recovery. *Molecular Cancer*, 5, 20.

van Delft, M.F., Smith, D.P., Lahoud, M.H., Huang, D.C.S. and Adams, J.M. (2009). Apoptosis and non-inflammatory phagocytosis can be induced by mitochondrial damage without caspases. *Cell Death & Differentiation*, 17, 821–832.

Denault, J.-B. and Salvesen, G.S. (2003). Expression, purification, and characterization of caspases. *Current Protocols in Protein Science*, Chapter 21, Unit 21.13.

Dephoure, N., Zhou, C., Villen, J., Beausoleil, S.A., Bakalarski, C.E., Elledge, S.J. and Gygi, S.P. (2008). A quantitative atlas of mitotic phosphorylation. *Proceedings of the National Academy of Sciences*, 105, 10762–10767.

Dhanasekaran, D.N. and Reddy, E.P. (2008). JNK signaling in apoptosis. *Oncogene*, 27, 6245–6251.

Dickens, L.S., Boyd, R.S., Jukes-Jones, R., Hughes, M.A., Robinson, G.L., Fairall, L., Schwabe, J.W.R., Cain, K. and MacFarlane, M. (2012). A Death Effector Domain Chain DISC Model Reveals a Crucial Role for Caspase-8 Chain Assembly in Mediating Apoptotic Cell Death. *Molecular Cell*, 47, 291–305.

Eberstadt, M., Huang, B., Chen, Z., Meadows, R.P., Ng, S.-C., Zheng, L., Lenardo, M.J. and Fesik, S.W. (1998). NMR structure and mutagenesis of the FADD (Mort1) death-effector domain. *Nature*, 392, 941–945.

Ehrenschwender, M., Bittner, S., Seibold, K. and Wajant, H. (2014). XIAP-targeting drugs re-sensitize PIK3CA-mutated colorectal cancer cells for death receptor-induced apoptosis. *Cell Death & Disease*, 5, 1–12.

Elmore, S. (2007). Apoptosis: A Review of Programmed Cell Death. *Toxicologic Pathology*, 35, 495–516.

Falck, J., Lukas, C., Protopopova, M., Lukas, J., Selivanova, G. and Bartek, J. (2001). Functional impact of concomitant versus alternative defects in the Chk2-p53 tumour suppressor pathway. *Oncogene*, 20, 5503–10.

Fava, L.L., Schuler, F., Sladky, V., Haschka, M.D., Soratroi, C., Eiterer, L., Demetz, E., Weiss, G., Geley, S., Nigg, E.A. and Villunger, A. (2017). The PIDDosome activates p53 in response to supernumerary centrosomes. *Genes & Development*, 31, 34–45.

Feoktistova, M., Geserick, P., Kellert, B., Dimitrova, D.P., Langlais, C., Hupe, M., Cain, K., MacFarlane, M., Häcker, G. and Leverkus, M. (2011). cIAPs Block Ripoptosome Formation, a RIP1/Caspase-8 Containing Intracellular Cell Death Complex Differentially Regulated by cFLIP Isoforms. *Molecular Cell*, 43, 449–463.

Feoktistova, M., Geserick, P., Panayotova-Dimitrova, D. and Leverkus, M. (2012). Pick your poison: The Ripoptosome, a cell death platform regulating apoptosis and necroptosis. *Cell Cycle*, 11, 460–467.

Filomenko, R., Prévotat, L., Rébé, C., Cortier, M., Jeannin, J.-F., Solary, E. and Bettaieb, A. (2006). Caspase-10 involvement in cytotoxic drug-induced apoptosis of tumor cells. *Oncogene*, 25, 7635–7645.

Fu, J., Jin, Y. and Arend, L.J. (2003). Smac3, a novel Smac/DIABLO splicing variant, attenuates the stability and apoptosis-inhibiting activity of X-linked inhibitor of apoptosis protein. *The Journal of Biological Chemistry*, 278, 52660–52672.

Fuchs, Y. and Steller, H. (2011). Programmed Cell Death in Animal Development and Disease. *Cell*, 147, 742–758.

Fuchs, Y. and Steller, H. (2015). Live to die another way: modes of programmed cell death and the signals emanating from dying cells. *Nature Reviews Molecular Cell Biology*, 16, 329–344.

Fulda, S. and Vucic, D. (2012). Targeting IAP proteins for therapeutic intervention in cancer. *Nature Reviews Drug Discovery*, 11, 109–124.

Galluzzi, L., Vitale, I., Aaronson, S.A., Abrams, J.M., Adam, D., Agostinis, P., Alnemri, E.S., Altucci, L., Amelio, I. and Andrews, D.W. (2018). Molecular mechanisms of cell death: recommendations of the Nomenclature Committee on Cell Death 2018. *Cell Death & Differentiation*, 25, 486–541.

Gandhi, L., Camidge, D.R., Ribeiro de Oliveira, M., Bonomi, P., Gandara, D., Khaira, D., Hann, C.L., McKeegan, E.M., Litvinovich, E. and Hemken, P.M. (2011). Phase I Study of Navitoclax (ABT-263), a Novel Bcl-2 Family Inhibitor, in Patients With Small-Cell Lung Cancer and Other Solid Tumors. *Journal of Clinical Oncology*, 29, 909–916.

García, V., Lara-Chica, M., Cantarero, I., Sterner, O., Calzado, M., and Muñoz, E. (2015). Galiellalactone induces cell cycle arrest and apoptosis through the ATM/ATR pathway in prostate cancer cells. *Oncotarget*, 7, 4490-4506.

Garcia-Calvo, M., Peterson, E.P., Rasper, D.M., Vaillancourt, J.P., Zamboni, R., Nicholson, D.W. and Thornberry, N.A. (1999). Purification and catalytic properties of human caspase family members. *Cell Death & Differentiation*, 6, 362–369.

Garrido, C., Galluzzi, L., Brunet, M., Puig, P.E., Didelot, C. and Kroemer, G. (2006). Mechanisms of cytochrome c release from mitochondria. *Cell Death & Differentiation*, 13, 1423–1433.

Geserick, P., Hupe, M., Moulin, M., Wong, W.W.-L., Feoktistova, M., Kellert, B., Gollnick, H., Silke, J. and Leverkus, M. (2009). Cellular IAPs inhibit a cryptic CD95-induced cell death by limiting RIP1 kinase recruitment. *The Journal of Cell Biology*, 187, 1037–1054.

Glanzer, J.G., Liu, S., Wang, L., Mosel, A., Peng, A. and Oakley, G.G. (2014). RPA Inhibition Increases Replication Stress and Suppresses Tumor Growth. *Cancer Research*, 74, 5165–5172.

Golks, A., Brenner, D., Fritsch, C., Krammer, P.H. and Lavrik, I.N. (2005). c-FLIPR, a New Regulator of Death Receptor-induced Apoptosis. *Journal of Biological Chemistry*, 280, 14507–14513.

Gonzalez, S., Prives, C. and Cordon-Cardo, C. (2003). p73alpha regulation by Chk1 in response to DNA damage. *Molecular and Cellular Biology*, 23, 8161–8171.

Gonzalvez, F. and Ashkenazi, A. (2010). New insights into apoptosis signaling by Apo2L/TRAIL. *Oncogene*, 29, 4752–4765.

Gotoff, S.P., Amirmokri, E. and Liebner, E.J. (1967). Ataxia Telangiectasia. *American Journal of Diseases of Children*, 114, 617.

Grossman, T.H., Kawasaki, E.S., Punreddy, S.R. and Osburne, M.S. (1998). Spontaneous cAMP-dependent derepression of gene expression in stationary phase plays a role in recombinant expression instability. *Gene*, 209, 95–103.

Grunert, M., Gottschalk, K., Kapahnke, J., Gündisch, S., Kieser, A. and Jeremias, I. (2012). The adaptor protein FADD and the initiator caspase-8 mediate activation of NF-κB by TRAIL. *Cell Death & Disease*, 3, 1-13.

Guo, Y., Srinivasula, S.M., Druilhe, A., Fernandes-Alnemri, T. and Alnemri, E.S. (2002). Caspase-2 Induces Apoptosis by Releasing Proapoptotic Proteins from Mitochondria. *Journal of Biological Chemistry*, 277, 13430–13437.

Hakem, R., Hakem, A., Duncan, G.S., Henderson, J.T., Woo, M., Soengas, M.S., Elia, A., de la Pompa, J.L., Kagi, D., Khoo, W., Potter, J., Yoshida, R., Kaufman, S.A., Lowe,

S.W., Penninger, J.M. and Mak, T.W. (1998). Differential Requirement for Caspase 9 in Apoptotic Pathways In Vivo. *Cell*, 94, 339–352.

Hao, Z., Duncan, G.S., Chang, C.-C., Elia, A., Fang, M., Wakeham, A., Okada, H., Calzascia, T., Jang, Y., You-Ten, A., Yeh, W.-C., Ohashi, P., Wang, X. and Mak, T.W. (2005). Specific Ablation of the Apoptotic Functions of Cytochrome c Reveals a Differential Requirement for Cytochrome c and Apaf-1 in Apoptosis. *Cell*, 121, 579–591.

Hartlerode, A.J., Morgan, M.J., Wu, Y., Buis, J. and Ferguson, D.O. (2015). Recruitment and activation of the ATM kinase in the absence of DNA-damage sensors. *Nature Structural & Molecular Biology*, 22, 736–743.

He, K., Zheng, X., Li, M., Zhang, L. and Yu, J. (2015). mTOR inhibitors induce apoptosis in colon cancer cells via CHOP-dependent DR5 induction on 4E-BP1 dephosphorylation. *Oncogene*, 35, 148–157.

Heeren, P.A.M., Kloppenberg, F.W.H., Hollema, H., Mulder, N.H., Nap, R.E. and Plukker, J.T.M. (2004). Predictive effect of p53 and p21 alteration on chemotherapy response and survival in locally advanced adenocarcinoma of the esophagus. *Anticancer Research*, 24, 2579–83.

Henry, C.M. and Martin, S.J. (2017). Caspase-8 Acts in a Non-enzymatic Role as a Scaffold for Assembly of a Pro-inflammatory "FADDosome" Complex upon TRAIL Stimulation. *Molecular Cell*, 65, 715–729.

Hirao, A., Cheung, A., Duncan, G., Girard, P.-M., Elia, A.J., Wakeham, A., Okada, H., Sarkissian, T., Wong, J.A. and Sakai, T. (2002). Chk2 Is a Tumor Suppressor That Regulates Apoptosis in both an Ataxia Telangiectasia Mutated (ATM)-Dependent and an ATM-Independent Manner. *Molecular and Cellular Biology*, 22, 6521–6532.

Ho, L., Taylor, R., Dorstyn, L., Cakouros, D., Bouillet, P., and Kumar, S. (2009). A tumor suppressor function for caspase-2. *Proceedings Of The National Academy Of Sciences*, 106(1), 5336-5341.

Holzinger, A., Phillips, K. and Weaver, T. (1996). Single-Step Purification/Solubilization of Recombinant Proteins: Application to Surfactant Protein B. *Biotechniques*, 20, 804-808.

Hong, S.-J., Wu, W.-C., Lai, Y.-H. and Wu, K.-Y. (2014). Mechanism of 5-Fluorouracil-Induced Apoptosis on Cultured Corneal Endothelial Cells. *Open Journal of Apoptosis*, 3, 5–15.

Horn, S., Hughes, M.A., Schilling, R., Sticht, C., Tenev, T., Ploesser, M., Meier, P., Sprick, M.R., MacFarlane, M. and Leverkus, M. (2017). Caspase-10 Negatively Regulates Caspase-8-Mediated Cell Death, Switching the Response to CD95L in Favor of NF-κB Activation and Cell Survival. *Cell Reports*, 19, 785–797.

Houldsworth, J. and Lavin, M.F. (1980). Effect of ionizing radiation on DNA synthesis in ataxia telangiectasia cells. *Nucleic Acids Research*, 8, 3709–3720.

Huelsenbeck, S.C., Schorr, A., Roos, W.P., Huelsenbeck, J., Henninger, C., Kaina, B. and Fritz, G. (2012). Rac1 Protein Signaling Is Required for DNA Damage Response Stimulated by Topoisomerase II Poisons. *Journal of Biological Chemistry*, 287, 38590–38599.

Hwang, E., Jeong, M., Park, S. and Jang, S. (2014). Evidence of complex formation between FADD and c-FLIP death effector domains for the death inducing signaling complex. *BMB Reports*, 47, 488-493.

Imre, G., Larisch, S. and Rajalingam, K. (2011). Ripoptosome: a novel IAP-regulated cell death-signalling platform. *Journal of Molecular Cell Biology*, 3, 324–326.

van Jaarsveld, M.T.M., Deng, D., Wiemer, E.A.C. and Zi, Z. (2019). Tissue-Specific Chk1 Activation Determines Apoptosis by Regulating the Balance of p53 and p21. *iScience*, 12, 27–40.

Jack, M.T., Woo, R.A., Hirao, A., Cheung, A., Mak, T.W. and Lee, P.W.K. (2002). Chk2 is dispensable for p53-mediated G1 arrest but is required for a latent p53-mediated apoptotic response. *Proceedings of the National Academy of Sciences*, 99, 9825–9829.

Jang, T., Zheng, C., Li, J., Richards, C., Hsiao, Y.-S., Walz, T., Wu, H. and Park, H.H. (2014). Structural Study of the RIPoptosome Core Reveals a Helical Assembly for Kinase Recruitment. *Biochemistry*, 53, 5424–5431.

Janssens, S. and Tinel, A. (2011). The PIDDosome, DNA-damage-induced apoptosis and beyond. *Cell Death & Differentiation*, 19, 13–20.

Ju, J., Schmitz, J.C., Song, B., Kudo, K. and Chu, E. (2007). Regulation of p53 Expression in Response to 5-Fluorouracil in Human Cancer RKO Cells. *Clinical Cancer Research*, 13, 4245–4251.

Kamer, I., Sarig, R., Zaltsman, Y., Niv, H., Oberkovitz, G., Regev, L., Haimovich, G., Lerenthal, Y., Marcellus, R.C. and Gross, A. (2005). Proapoptotic BID Is an ATM Effector in the DNA-Damage Response. *Cell*, 122, 593–603.

Kandoth, C., McLellan, M.D., Vandin, F., Ye, K., Niu, B., Lu, C., Xie, M., Zhang, Q., McMichael, J.F. and Wyczalkowski, M.A. (2013). Mutational landscape and significance across 12 major cancer types. *Nature*, 502, 333–339.

Keller, N., Mareš, J., Zerbe, O. and Grütter, M.G. (2009). Structural and Biochemical Studies on Procaspase-8: New Insights on Initiator Caspase Activation. *Structure*, 17, 438–448.

Kemp, M., and Sancar, A. (2016). ATR Kinase Inhibition Protects Non-cycling Cells from the Lethal Effects of DNA Damage and Transcription Stress. *Journal of Biological Chemistry*, 291, 9330-9342.

Kerr, J.F.R., Wyllie, A.H. and Currie, A.R. (1972). Apoptosis: A Basic Biological Phenomenon with Wideranging Implications in Tissue Kinetics. *British Journal of Cancer*, 26, 239–257.

Kim, I.R., Murakami, K., Chen, N.-J., Saibil, S.D., Matysiak-Zablocki, E., Elford, A.R., Bonnard, M., Benchimol, S., Jurisicova, A., Yeh, W.-C. and Ohashi, P.S. (2009). DNA damage- and stress-induced apoptosis occurs independently of PIDD. *Apoptosis*, 14, 1039–1049.

Kischkel, F.C., Lawrence, D.A., Tinel, A., LeBlanc, H., Virmani, A., Schow, P., Gazdar, A., Blenis, J., Arnott, D. and Ashkenazi, A. (2001). Death receptor recruitment of endogenous caspase-10 and apoptosis initiation in the absence of caspase-8. *The Journal of Biological Chemistry*, 276, 46639–46646.

Kitagawa, R. and Kastan, M.B. (2005). The ATM-dependent DNA damage signaling pathway. *Cold Spring Harbor Symposia on Quantitative Biology*, 70, 99–109.

Kleiblova, P., Shaltiel, I.A., Benada, J., Ševčík, J., Pecháčková, S., Pohlreich, P., Voest, E.E., Dundr, P., Bartek, J., Kleibl, Z., Medema, R.H. and Macurek, L. (2013). Gain-of-function mutations of PPM1D/Wip1 impair the p53-dependent G1 checkpoint. *The Journal of Cell Biology*, 201, 511–521.

Koff, J., Ramachandiran, S. and Bernal-Mizrachi, L. (2015). A Time to Kill: Targeting Apoptosis in Cancer. *International Journal of Molecular Sciences*, 16, 2942–2955.

Kohli, M., Yu, J., Seaman, C., Bardelli, A., Kinzler, K.W., Vogelstein, B., Lengauer, C. and Zhang, L. (2004). SMAC/Diablo-dependent apoptosis induced by nonsteroidal

antiinflammatory drugs (NSAIDs) in colon cancer cells. *Proceedings of the National Academy of Sciences*, 101, 16897–16902.

Konopleva, M., Contractor, R., Tsao, T., Samudio, I., Ruvolo, P., Kitada, S. et al. (2006). Mechanisms of apoptosis sensitivity and resistance to the BH3 mimetic ABT-737 in acute myeloid leukemia. *Cancer Cell*, 10, 375-388.

Kozlov, S.V., Graham, M.E., Jakob, B., Tobias, F., Kijas, A.W., Tanuji, M., Chen, P., Robinson, P.J., Taucher-Scholz, G., Suzuki, K., So, S., Chen, D. and Lavin, M.F. (2011). Autophosphorylation and ATM activation: additional sites add to the complexity. *The Journal of Biological Chemistry*, 286, 9107–9119.

Kozlov, S.V., Graham, M.E., Peng, C., Chen, P., Robinson, P.J. and Lavin, M.F. (2006). Involvement of novel autophosphorylation sites in ATM activation. *The EMBO Journal*, 25, 3504–3514.

Kuida, K., Haydar, T.F., Kuan, C.-Y., Gu, Y., Taya, C., Karasuyama, H., Su, M.S.-S., Rakic, P. and Flavell, R.A. (1998). Reduced Apoptosis and Cytochrome c–Mediated Caspase Activation in Mice Lacking Caspase 9. *Cell*, 94, 325–337.

Kurz, E.U. and Lees-Miller, S.P. (2004). DNA damage-induced activation of ATM and ATM-dependent signaling pathways. *DNA Repair*, 3, 889–900.

LaCasse, E.C., Mahoney, D.J., Cheung, H.H., Plenchette, S., Baird, S. and Korneluk, R.G. (2008). IAP-targeted therapies for cancer. *Oncogene*, 27, 6252–6275.

Lavrik, I. (2005). Death receptor signaling. *Journal of Cell Science*, 118, 265–267.

Leber, B., Lin, J. and Andrews, D.W. (2007). Embedded together: The life and death consequences of interaction of the Bcl-2 family with membranes. *Apoptosis*, 12, 897–911.

Lee, H.-J., Pyo, J.-O., Oh, Y., Kim, H.-J., Hong, S., Jeon, Y.-J., Kim, H., Cho, D.-H., Woo, H.-N., Song, S., Nam, J.-H., Kim, H.J., Kim, K.-S. and Jung, Y.-K. (2007). AK2 activates a novel apoptotic pathway through formation of a complex with FADD and caspase-10. *Nature Cell Biology*, 9, 1303–1310.

Lee, J.-H. and Paull, T.T. (2005). ATM Activation by DNA Double-Strand Breaks Through the Mre11-Rad50-Nbs1 Complex. *Science*, 308, 551–554.

Li, H., Zhu, H., Xu, C.J. and Yuan, J. (1998). Cleavage of BID by caspase 8 mediates the mitochondrial damage in the Fas pathway of apoptosis. *Cell*, 94, 491–501.

Li, S., Zhang, L., Yao, Q., Li, L., Dong, N., Rong, J., Gao, W., Ding, X., Sun, L., Chen, X., Chen, S. and Shao, F. (2013). Pathogen blocks host death receptor signalling by arginine GlcNAcylation of death domains. *Nature*, 501, 242–246.

Li, X.-L., Zhou, J., Chen, Z.-R. and Chng, W.-J. (2015). p53mutations in colorectal cancer- molecular pathogenesis and pharmacological reactivation. *World Journal of Gastroenterology*, 21, 84.

Lin, Y., Ma, W. and Benchimol, S. (2000). Pidd, a new death-domain–containing protein, is induced by p53 and promotes apoptosis. *Nature Genetics*, 26, 122–127.

Liu, F.-T., Newland, A.C. and Jia, L. (2003). Bax conformational change is a crucial step for PUMA-mediated apoptosis in human leukemia. *Biochemical and Biophysical Research Communications*, 310, 956–962.

Liu, Q., Guntuku, S., Cui, X.S., Matsuoka, S., Cortez, D., Tamai, K., Luo, G., Carattini-Rivera, S., DeMayo, F., Bradley, A., Donehower, L.A. and Elledge, S.J. (2000). Chk1 is an essential kinase that is regulated by Atr and required for the G(2)/M DNA damage checkpoint. *Genes & Development*, 14, 1448–59.

Liu, X., Kim, C.N., Yang, J., Jemmerson, R. and Wang, X. (1996). Induction of Apoptotic Program in Cell-Free Extracts: Requirement for dATP and Cytochrome c. *Cell*, 86, 147–157.

Liu, Y., Bertram, C.C., Shi, Q. and Zinkel, S.S. (2010). Proapoptotic Bid mediates the Atr-directed DNA damage response to replicative stress. *Cell Death & Differentiation*, 18, 841–852.

Liu, Y., Vaithiyalingam, S., Shi, Q., Chazin, W.J. and Zinkel, S.S. (2011). BID Binds to Replication Protein A and Stimulates ATR Function following Replicative Stress. *Molecular and Cellular Biology*, 31, 4298–4309.

Logette, E., Schuepbach-Mallepell, S., Eckert, M.J., Leo, X.H., Jaccard, B., Manzl, C., Tardivel, A., Villunger, A., Quadroni, M., Gaide, O. and Tschopp, J. (2011). PIDD orchestrates translesion DNA synthesis in response to UV irradiation. *Cell Death & Differentiation*, 18, 1036–1045.

Longley, D.B., Harkin, D.P. and Johnston, P.G. (2003). 5-fluorouracil: mechanisms of action and clinical strategies. *Nature Reviews Cancer*, 3, 330–338.

van Loo, G., van Gurp, M., Depuydt, B., Srinivasula, S.M., Rodriguez, I., Alnemri, E.S., Gevaert, K., Vandekerckhove, J., Declercq, W. and Vandenabeele, P. (2002). The serine protease Omi/HtrA2 is released from mitochondria during apoptosis. Omi interacts with caspase-inhibitor XIAP and induces enhanced caspase activity. *Cell Death & Differentiation*, 9, 20–26.

Lopez, J. and Tait, S.W.G. (2015). Mitochondrial apoptosis: killing cancer using the enemy within. *British Journal of Cancer*, 112, 957–962.

Lowe, J., Cha, H., Lee, M.-O., Mazur, S.J., Appella, E. and Fornace, A.J. (2012). Regulation of the Wip1 phosphatase and its effects on the stress response. *Frontiers in Bioscience,* 17, 1480–1498.

Lu, X., Nguyen, T.-A., Moon, S.-H., Darlington, Y., Sommer, M. and Donehower, L.A. (2008). The type 2C phosphatase Wip1: An oncogenic regulator of tumor suppressor and DNA damage response pathways. *Cancer and Metastasis Reviews*, 27, 123–135.

Luo, X., Budihardjo, I., Zou, H., Slaughter, C. and Wang, X. (1998). Bid, a Bcl2 Interacting Protein, Mediates Cytochrome c Release from Mitochondria in Response to Activation of Cell Surface Death Receptors. *Cell*, 94, 481–490.

Manzl, C., Fava, L.L., Krumschnabel, G., Peintner, L., Tanzer, M.C., Soratroi, C., Bock, F.J., Schuler, F., Luef, B., Geley, S. and Villunger, A. (2013). Death of p53-defective cells triggered by forced mitotic entry in the presence of DNA damage is not uniquely dependent on Caspase-2 or the PIDDosome. *Cell Death & Disease*, 4, 1–9.

Manzl, C., Krumschnabel, G., Bock, F., Sohm, B., Labi, V., Baumgartner, F., Logette, E., Tschopp, J. and Villunger, A. (2009). Caspase-2 activation in the absence of PIDDosome formation. *The Journal of Cell Biology*, 185, 291–303.

Márquez-Jurado, S., Díaz-Colunga, J., das Neves, R.P., Martinez-Lorente, A., Almazán, F., Guantes, R. and Iborra, F.J. (2018). Mitochondrial levels determine variability in cell death by modulating apoptotic gene expression. *Nature Communications*, 9.

Marsden, V.S., Ekert, P.G., Van Delft, M., Vaux, D.L., Adams, J.M. and Strasser, A. (2004). Bcl-2–regulated apoptosis and cytochromecrelease can occur independently of both caspase-2 and caspase-9. *The Journal of Cell Biology*, 165, 775–780.

Marsden, V.S., O'Connor, L., O'Reilly, L.A., Silke, J., Metcalf, D., Ekert, P.G., Huang, D.C.S., Cecconi, F., Kuida, K., Tomaselli, K.J., Roy, S., Nicholson, D.W., Vaux, D.L.,

Bouillet, P., Adams, J.M. and Strasser, A. (2002). Apoptosis initiated by Bcl-2-regulated caspase activation independently of the cytochrome c/Apaf-1/caspase-9 apoptosome. *Nature*, 419, 634–637.

Martino-Echarri, E., Henderson, B.R. and Brocardo, M.G. (2014). Targeting the DNA replication checkpoint by pharmacologic inhibition of Chk1 kinase: a strategy to sensitize APC mutant colon cancer cells to 5-fluorouracil chemotherapy. *Oncotarget*, 5.

Matsuoka, S., Ballif, B.A., Smogorzewska, A., McDonald, E.R., Hurov, K.E., Luo, J., Bakalarski, C.E., Zhao, Z., Solimini, N., Lerenthal, Y., Shiloh, Y., Gygi, S.P. and Elledge, S.J. (2007). ATM and ATR Substrate Analysis Reveals Extensive Protein Networks Responsive to DNA Damage. *Science*, 316, 1160–1166.

Matthews, T.P., Jones, A.M. and Collins, I. (2013). Structure-based design, discovery and development of checkpoint kinase inhibitors as potential anticancer therapies. *Expert Opinion on Drug Discovery*, 8, 621–640.

Mavridis, L. and Janes, R. (2016). PDB2CD: a web-based application for the generation of circular dichroism spectra from protein atomic coordinates. *Bioinformatics*, 33, 56-63.

McIlwain, D.R., Berger, T. and Mak, T.W. (2013). Caspase functions in cell death and disease. *Cold Spring Harbor Perspectives in Biology*, 5, 1–28.

Mehrabadi, Y. (2018). Regulation of cytotoxic drug-induced apoptosis by death receptor 5 in human colon cancer cells [Doctoral dissertation, University of Essex]. Albert Sloman Library.

Micheau, O. and Tschopp, J. (2003). Induction of TNF receptor I-mediated apoptosis via two sequential signaling complexes. *Cell*, 114, 181–90.

Mita, H., Tsutsui, J., Takekawa, M., Witten, E.A. and Saito, H. (2002). Regulation of MTK1/MEKK4 Kinase Activity by Its N-Terminal Autoinhibitory Domain and GADD45 Binding. *Molecular and Cellular Biology*, 22, 4544–4555.

Mohan, M., Kozhithodi, S., Nayarisseri, A. and Elyas, K. (2018). Screening, Purification and Characterization of Protease Inhibitor from Capsicum frutescens. *Bioinformation*, 14, 285-293.

Mohr, A., Deedigan, L., Jencz, S., Mehrabadi, Y., Houlden, L., Albarenque, S.-M. and Zwacka, R.M. (2018). Caspase-10: a molecular switch from cell-autonomous apoptosis to communal cell death in response to chemotherapeutic drug treatment. *Cell Death & Differentiation*, 25, 340–352.

Mohr, A., Yu, R. and Zwacka, R.M. (2015). TRAIL-receptor preferences in pancreatic cancer cells revisited: Both TRAIL-R1 and TRAIL-R2 have a licence to kill. *BMC Cancer*, 15, 1–11.

Muller, P.A.J. and Vousden, K.H. (2013). p53 mutations in cancer. *Nature Cell Biology*, 15, 2–8.

Nam, E.A., Zhao, R., Glick, G.G., Bansbach, C.E., Friedman, D.B. and Cortez, D. (2011). Thr-1989 Phosphorylation Is a Marker of Active Ataxia Telangiectasia-mutated and Rad3-related (ATR) Kinase. *Journal of Biological Chemistry*, 286, 28707–28714.

Nicoletti, I., Migliorati, G., Pagliacci, M., Grignani, F. and Riccardi, C. (1991). A rapid and simple method for measuring thymocyte apoptosis by propidium iodide staining and flow cytometry. *Journal of Immunological Methods*, 139, 271-279.

Oda, E., Ohki, R., Murasawa, H., Nemoto, J., Shibue, T., Yamashita, T., Tokino, T., Taniguchi, T. and Tanaka, N. (2000). Noxa, a BH3-Only Member of the Bcl-2 Family and Candidate Mediator of p53-Induced Apoptosis. *Science*, 288, 1053–1058.

Ohtsuka, T., Buchsbaum, D., Oliver, P., Makhija, S., Kimberly, R. and Zhou, T. (2003). Synergistic induction of tumor cell apoptosis by death receptor antibody and chemotherapy agent through JNK/p38 and mitochondrial death pathway. *Oncogene*, 22, 2034–2044.

Painter, R.B. and Young, B.R. (1980). Radiosensitivity in ataxia-telangiectasia: a new explanation. *Proceedings of the National Academy of Sciences*, 77, 7315–7317.

Pan, Y., Ren, K., He, H., and Shao, R. (2009). Knockdown of Chk1 sensitizes human colon carcinoma HCT116 cells in a p53-dependent manner to lidamycin through abrogation of a G2/M checkpoint and induction of apoptosis. *Cancer Biology & Therapy*, 8, 1559-1566.

Park, S.-J., Wu, C.-H., Gordon, J.D., Zhong, X., Emami, A. and Safa, A.R. (2004). Taxol Induces Caspase-10-dependent Apoptosis. *Journal of Biological Chemistry*, 279, 51057–51067.

Parrish, A.B., Freel, C.D. and Kornbluth, S. (2013). Cellular Mechanisms Controlling Caspase Activation and Function. *Cold Spring Harbor Perspectives in Biology*, 5, 1–24.

Patil, M., Pabla, N. and Dong, Z. (2013). Checkpoint kinase 1 in DNA damage response and cell cycle regulation. *Cellular and Molecular Life Sciences*, 70, 4009–4021.

Peták, I. and Houghton, J.A. (2001). Shared pathways: death receptors and cytotoxic drugs in cancer therapy. *Pathology Oncology Research*, 7, 95–106.

Peter, M.E., Hadji, A., Murmann, A.E., Brockway, S., Putzbach, W., Pattanayak, A. and Ceppi, P. (2015). Erratum: The role of CD95 and CD95 ligand in cancer. *Cell Death & Differentiation*, 22, 885–886.

Qiu, Z., Oleinick, N. and Zhang, J. (2018). ATR/CHK1 inhibitors and cancer therapy. *Radiotherapy and Oncology*, 126, 450-464.

Ribe, E.M., Jean, Y.Y., Goldstein, R.L., Manzl, C., Stefanis, L., Villunger, A. and Troy, C.M. (2012). Neuronal caspase 2 activity and function requires RAIDD, but not PIDD. *Biochemical Journal*, 444, 591–599.

Rikhof, B., Corn, P.G. and El-Deiry, W.S. (2003). Caspase 10 Levels are Increased Following DNA Damage in a p53-Dependent Manner. *Cancer Biology & Therapy*, 2, 705–710.

Riley, J.S., Malik, A., Holohan, C. and Longley, D.B. (2015). DED or alive: assembly and regulation of the death effector domain complexes. *Cell Death & Disease*, 6, 1–16.

Roberts, A.W., Seymour, J.F., Brown, J.R., Wierda, W.G., Kipps, T.J., Khaw, S.L., Carney, D.A., He, S.Z., Huang, D.C.S. and Xiong, H. (2012). Substantial Susceptibility of Chronic Lymphocytic Leukemia to BCL2 Inhibition: Results of a Phase I Study of Navitoclax in Patients With Relapsed or Refractory Disease. *Journal of Clinical Oncology*, 30, 488–496.

Roberts, D.L., Merrison, W., MacFarlane, M. and Cohen, G.M. (2001). The inhibitor of apoptosis protein-binding domain of Smac is not essential for its proapoptotic activity. *The Journal of Cell Biology*, 153, 221–228.

Robertson, J.D., Enoksson, M., Suomela, M., Zhivotovsky, B. and Orrenius, S. (2002). Caspase-2 Acts Upstream of Mitochondria to Promote Cytochromec Release during Etoposide-induced Apoptosis. *Journal of Biological Chemistry*, 277, 29803–29809.

Robertson, J.D., Gogvadze, V., Kropotov, A., Vakifahmetoglu, H., Zhivotovsky, B. and Orrenius, S. (2004). Processed caspase-2 can induce mitochondria-mediated apoptosis independently of its enzymatic activity. *EMBO Reports*, 5, 643–648.

Russo, A., Bazan, V., Iacopetta, B., Kerr, D., Soussi, T. and Gebbia, N. (2005). The TP53 Colorectal Cancer International Collaborative Study on the Prognostic and Predictive

Significance ofp53Mutation: Influence of Tumor Site, Type of Mutation, and Adjuvant Treatment. *Journal of Clinical Oncology*, 23, 7518–7528.

Ryan, E., Hollingworth, R., and Grand, R. (2016). Activation of the DNA Damage Response by RNA Viruses. *Biomolecules*, 6, 1-24.

Ryan, K.M., Phillips, A.C. and Vousden, K.H. (2001). Regulation and function of the p53 tumor suppressor protein. *Current Opinion in Cell Biology*, 13, 332–337.

Salvesen, G.S. and Dixit, V.M. (1999). Caspase activation: The induced-proximity model. *Proceedings of the National Academy of Sciences*, 96, 10964–10967.

Savitsky, K., Bar-Shira, A., Gilad, S., Rotman, G., Ziv, Y., Vanagaite, L., Tagle, D., Smith, S., Uziel, T. and Sfez, S. (1995). A single ataxia telangiectasia gene with a product similar to PI-3 kinase. *Science*, 268, 1749–1753.

Sax, J.K., Fei, P., Murphy, M.E., Bernhard, E., Korsmeyer, S.J. and El-Deiry, W.S. (2002). BID regulation by p53 contributes to chemosensitivity. *Nature Cell Biology*, 4, 842–849.

Schilling, R., Geserick, P. and Leverkus, M. (2014). Characterization of the Ripoptosome and Its Components. *Methods in Enzymology*, 545, 83–102.

Schleich, K., Warnken, U., Fricker, N., Öztürk, S., Richter, P., Kammerer, K., Schnölzer, M., Krammer, P.H. and Lavrik, I.N. (2012). Stoichiometry of the CD95 Death-Inducing Signaling Complex: Experimental and Modeling Evidence for a Death Effector Domain Chain Model. *Molecular Cell*, 47, 306–319.

Schroeder, A., Warnken, U., Röth, D., Klika, K.D., Vobis, D., Barnert, A., Bujupi, F., Oberacker, T., Schnölzer, M., Nicolay, J.P., Krammer, P.H. and Gülow, K. (2017). Targeting Thioredoxin-1 by dimethyl fumarate induces ripoptosome-mediated cell death. *Scientific Reports*, 7.

Scott, F.L., Stec, B., Pop, C., Dobaczewska, M.K., Lee, J.J., Monosov, E., Robinson, H., Salvesen, G.S., Schwarzenbacher, R. and Riedl, S.J. (2008). The Fas–FADD death domain complex structure unravels signalling by receptor clustering. *Nature*, 457, 1019–1022.

Seaton, B.L., Yucel, J., Sunnerhagen, P. and Subramani, S. (1992). Isolation and characterization of the Schizosaccharomyces pombe rad3 gene, involved in the DNA damage and DNA synthesis checkpoints. *Gene*, 119, 83–89.

Selmi, T., Alecci, C., dell' Aquila, M., Montorsi, L., Martello, A., Guizzetti, F., Volpi, N., Parenti, S., Ferrari, S., Salomoni, P., Grande, A. and Zanocco-Marani, T. (2015). ZFP36 stabilizes RIP1 via degradation of XIAP and cIAP2 thereby promoting ripoptosome assembly. *BMC Cancer*, 15.

Sheikh, M.S., Burns, T.F., Huang, Y., Wu, G.S., Amundson, S., Brooks, K.S., Fornace, A.J. and el-Deiry, W.S. (1998). p53-dependent and -independent regulation of the death receptor KILLER/DR5 gene expression in response to genotoxic stress and tumor necrosis factor alpha. *Cancer Research*, 58, 1593–1598.

Shen, C., Pei, J., Guo, X., Zhou, L., Li, Q. and Quan, J. (2018). Structural basis for dimerization of the death effector domain of the F122A mutant of Caspase-8. *Scientific Reports*, 8.

Shen, J., Vakifahmetoglu, H., Stridh, H., Zhivotovsky, B. and Wiman, K.G. (2008). PRIMA-1MET induces mitochondrial apoptosis through activation of caspase-2. *Oncogene*, 27, 6571–6580.

Shiloh, Y. and Ziv, Y. (2013). The ATM protein kinase: regulating the cellular response to genotoxic stress, and more. *Nature reviews. Molecular cell biology*, 14, 197–210.

Sidi, S. and Bouchier-Hayes, L. (2017). Direct pro-apoptotic role for NPM1 as a regulator of PIDDosome formation. *Molecular & Cellular Oncology*, 4, 1–3.

Sidi, S., Sanda, T., Kennedy, R.D., Hagen, A.T., Jette, C.A., Hoffmans, R., Pascual, J., Imamura, S., Kishi, S. and Amatruda, J.F. (2008). Chk1 Suppresses a Caspase-2 Apoptotic Response to DNA Damage that Bypasses p53, Bcl-2, and Caspase-3. *Cell*, 133, 864–877.

Sladky, V., Schuler, F., Fava, L.L. and Villunger, A. (2017). The resurrection of the PIDDosome – emerging roles in the DNA-damage response and centrosome surveillance. *Journal of Cell Science*, 130, 3779–3787.

Smith, J., Tho, L.M., Xu, N. and Gillespie, D.A. (2010). The ATM-Chk2 and ATR-Chk1 pathways in DNA damage signaling and cancer. *Advances in Cancer Research*, 108, 73–112.

Song, J., Han, H.-S., Sabapathy, K., Lee, B.-M., Yu, E. and Choi, J. (2010). Expression of a Homeostatic Regulator, Wip1 (Wild-type p53-induced Phosphatase), Is Temporally Induced by c-Jun and p53 in Response to UV Irradiation. *Journal of Biological Chemistry*, 285, 9067–9076.

Song, J.-Y., Ryu, S.-H., Cho, Y.M., Kim, Y.S., Lee, B.-M., Lee, S.-W. and Choi, J. (2013). Wip1 suppresses apoptotic cell death through direct dephosphorylation of BAX in response to γ-radiation. *Cell Death & Disease*, 4, 1–8.

Sørensen, C.S., Syljuåsen, R.G., Falck, J., Schroeder, T., Rönnstrand, L., Khanna, K.K., Zhou, B.-B., Bartek, J. and Lukas, J. (2003). Chk1 regulates the S phase checkpoint by coupling the physiological turnover and ionizing radiation-induced accelerated proteolysis of Cdc25A. *Cancer Cell*, 3, 247–258.

Sprick, M.R., Rieser, E., Stahl, H., Grosse-Wilde, E., Weigand, M.A. and Walczak, H. (2002). Caspase-10 is recruited to and activated at the native TRAIL and CD95 death-inducing signalling complexes in a FADD-dependent manner but cannot functionally substitute caspase-8. *The EMBO Journal*, 21, 4520–4530.

Srinivasula, S.M., Datta, P., Fan, X.-J., Fernandes-Alnemri, T., Huang, Z. and Alnemri, E.S. (2000). Molecular Determinants of the Caspase-promoting Activity of Smac/DIABLO and Its Role in the Death Receptor Pathway. *Journal of Biological Chemistry*, 275, 36152–36157.

Stavridi, E. S., Huyen, Y., Sheston, E. A. and Halazonetis, T. D. (2005). 'The three-dimensional structure of p53', in Zambetti, G. (ed.) *The p53 tumor suppressor pathway and cancer. Springer*, 25-40.

Sui, X., Kong, N., Wang, X., Fang, Y., Hu, X., Xu, Y., Chen, W., Wang, K., Li, D. and Jin, W. (2014). JNK confers 5-fluorouracil resistance in p53-deficient and mutant p53-expressing colon cancer cells by inducing survival autophagy. *Scientific Reports*, 4.

Tait, S.W.G. and Green, D.R. (2010). Mitochondria and cell death: outer membrane permeabilization and beyond. *Nature Reviews Molecular Cell Biology*, 11, 621–632.

Takai, H., Naka, K., Okada, Y., Watanabe, M., Harada, N., Saito, S., Anderson, C.W., Appella, E., Nakanishi, M., Suzuki, H., Nagashima, K., Sawa, H., Ikeda, K. and Motoyama, N. (2002). Chk2-deficient mice exhibit radioresistance and defective p53-mediated transcription. *The EMBO Journal*, 21, 5195–5205.

Takai, H., Tominaga, K., Motoyama, N., Minamishima, Y.A., Nagahama, H., Tsukiyama, T., Ikeda, K., Nakayama, K., Nakanishi, M. and Nakayama, K. (2000). Aberrant cell cycle checkpoint function and early embryonic death in Chk1(-/-) mice. *Genes & Development*, 14, 1439–47.

Takekawa, M. and Saito, H. (1998). A Family of Stress-Inducible GADD45-like Proteins Mediate Activation of the Stress-Responsive MTK1/MEKK4 MAPKKK. *Cell*, 95, 521–530.

Taylor, A.M.R., Harnden, D.G., Arlett, C.F., Harcourt, S.A., Lehmann, A.R., Stevens, S. and Bridges, B.A. (1975). Ataxia telangiectasia: a human mutation with abnormal radiation sensitivity. *Nature*, 258, 427–429.

Taylor, A.M.R., Lam, Z., Last, J.I. and Byrd, P.J. (2015). Ataxia telangiectasia: more variation at clinical and cellular levels. *Clinical Genetics*, 87, 199–208.

Tenev, T., Bianchi, K., Darding, M., Broemer, M., Langlais, C., Wallberg, F., Zachariou, A., Lopez, J., MacFarlane, M., Cain, K. and Meier, P. (2011). The Ripoptosome, a Signaling Platform that Assembles in Response to Genotoxic Stress and Loss of IAPs. *Molecular Cell*, 43, 432–448.

Thant, A.A., Wu, Y., Lee, J., Mishra, D.K., Garcia, H., Koeffler, H.P. and Vadgama, J.V. (2008). Role of caspases in 5-FU and selenium-induced growth inhibition of colorectal cancer cells. *Anticancer Research*, 28, 3579–3592.

Tinel, A., Janssens, S., Lippens, S., Cuenin, S., Logette, E., Jaccard, B., Quadroni, M. and Tschopp, J. (2006). Autoproteolysis of PIDD marks the bifurcation between pro-death caspase-2 and pro-survival NF-κB pathway. *The EMBO Journal*, 26, 197–208.

Tinel, A. and Tschopp, J. (2004). The PIDDosome, a Protein Complex Implicated in Activation of Caspase-2 in Response to Genotoxic Stress. *Science*, 304, 843–846.

Tovar, C., Rosinski, J., Filipovic, Z., Higgins, B., Kolinsky, K., and Hilton, H. et al. (2006). Small-molecule MDM2 antagonists reveal aberrant p53 signaling in cancer: Implications for therapy. *Proceedings of The National Academy Of Sciences*, 103, 1888-1893.

Tse, A.N., Rendahl, K.G., Sheikh, T., Cheema, H., Aardalen, K., Embry, M., Ma, S., Moler, E.J., Ni, Z.J., Lopes de Menezes, D.E., Hibner, B., Gesner, T.G. and Schwartz, G.K. (2007). CHIR-124, a Novel Potent Inhibitor of Chk1, Potentiates the Cytotoxicity of Topoisomerase I PoisonsIn vitroandIn vivo. *Clinical Cancer Research*, 13, 591–602.

Tsuchiya, Y., Nakabayashi, O. and Nakano, H. (2015). FLIP the Switch: Regulation of Apoptosis and Necroptosis by cFLIP. *International Journal of Molecular Sciences*, 16, 30321–30341.

Uren, R.T., Iyer, S. and Kluck, R.M. (2017). Pore formation by dimeric Bak and Bax: an unusual pore? *Philosophical Transactions of the Royal Society of London. Series B, Biological Sciences*, 372, 20160218.

Urist, M., Tanaka, T., Poyurovsky, M.V. and Prives, C. (2004). p73 induction after DNA damage is regulated by checkpoint kinases Chk1 and Chk2. *Genes & Development*, 18, 3041–3054.

Vakifahmetoglu, H., Olsson, M., Orrenius, S. and Zhivotovsky, B. (2006). Functional connection between p53 and caspase-2 is essential for apoptosis induced by DNA damage. *Oncogene*, 25, 5683–5692.

Varfolomeev, E., Blankenship, J.W., Wayson, S.M., Fedorova, A.V., Kayagaki, N., Garg, P., Zobel, K., Dynek, J.N., Elliott, L.O. and Wallweber, H.J.A. (2007). IAP antagonists induce autoubiquitination of c-IAPs, NF-kappaB activation, and TNFalpha-dependent apoptosis. *Cell*, 131, 669–681.

Vercammen, E., Staal, J. and Beyaert, R. (2008). Sensing of Viral Infection and Activation of Innate Immunity by Toll-Like Receptor 3. *Clinical Microbiology Reviews*, 21, 13–25.

Verhagen, A.M., Ekert, P.G., Pakusch, M., Silke, J., Connolly, L.M., Reid, G.E., Moritz, R.L., Simpson, R.J. and Vaux, D.L. (2000). Identification of DIABLO, a Mammalian Protein that Promotes Apoptosis by Binding to and Antagonizing IAP Proteins. *Cell*, 102, 43–53.

Villunger, A., Michalak, E.M., Coultas, L., Mullauer, F., Bock, G., Ausserlechner, M., Adams, J. and Strasser, A. (2003). p53- and Drug-Induced Apoptotic Responses Mediated by BH3-Only Proteins Puma and Noxa. *Science*, 302, 1036–1038.

Violette, S., Poulain, L., Dussaulx, E., Pepin, D., Faussat, A.-M., Chambaz, J., Lacorte, J.-M., Staedel, C. and Lesuffleur, T. (2002a). Resistance of colon cancer cells to long-term 5-fluorouracil exposure is correlated to the relative level of Bcl-2 and Bcl-XL in addition toBax andp53 status. *International Journal of Cancer*, 98, 498–504.

Violette, S., Poulain, L., Dussaulx, E., Pepin, D., Faussat, A.-M., Chambaz, J., Lacorte, J.-M., Staedel, C. and Lesuffleur, T. (2002b). Resistance of colon cancer cells to long-term 5-fluorouracil exposure is correlated to the relative level of Bcl-2 and Bcl-XL in addition toBax andp53 status. *International Journal of Cancer*, 98, 498–504.

W Owens, T., Gilmore, A.P., Streuli, C.H. and Foster, F.M. (2013). Inhibitor of Apoptosis Proteins: Promising Targets for Cancer Therapy. *Journal of Carcinogenesis & Mutagenesis*, S14, 1–9.

Wachmann, K., Pop, C., van Raam, B.J., Drag, M., Mace, P.D., Snipas, S.J., Zmasek, C., Schwarzenbacher, R., Salvesen, G.S. and Riedl, S.J. (2010). Activation and Specificity of Human Caspase-10. *Biochemistry*, 49, 8307–8315.

Wajant, H. (2002). The Fas Signaling Pathway: More Than a Paradigm. *Science*, 296, 1635–1636.

Wang, C. and Youle, R.J. (2009). The Role of Mitochondria in Apoptosis. *Annual Review of Genetics*, 43, 95–118.

Wang, L., Yang, J.K., Kabaleeswaran, V., Rice, A.J., Cruz, A.C., Park, A.Y., Yin, Q., Damko, E., Jang, S.B., Raunser, S., Robinson, C.V., Siegel, R.M., Walz, T. and Wu, H. (2010). The Fas–FADD death domain complex structure reveals the basis of DISC assembly and disease mutations. *Nature Structural & Molecular Biology*, 17, 1324–1329.

Wang, P., Lindsay, J., Owens, T.W., Mularczyk, E.J., Warwood, S., Foster, F., Streuli, C.H., Brennan, K. and Gilmore, A.P. (2014). Phosphorylation of the Proapoptotic BH3-Only Protein Bid Primes Mitochondria for Apoptosis during Mitotic Arrest. *Cell Reports*, 7, 661–671.

Watt, W., Koeplinger, K.A., Mildner, A.M., Heinrikson, R.L., Tomasselli, A.G. and Watenpaugh, K.D. (1999). The atomic-resolution structure of human caspase-8, a key activator of apoptosis. *Structure*, 7, 1135–1143.

Weber, A.M. and Ryan, A.J. (2015). ATM and ATR as therapeutic targets in cancer. *Pharmacology & Therapeutics*, 149, 124–138.

Wilson, W.H., O'Connor, O.A., Czuczman, M.S., LaCasce, A.S., Gerecitano, J.F., Leonard, J.P., Tulpule, A., Dunleavy, K., Xiong, H. and Chiu, Y.-L. (2010). Navitoclax, a targeted high-affinity inhibitor of BCL-2, in lymphoid malignancies: a phase 1 dose-escalation study of safety, pharmacokinetics, pharmacodynamics, and antitumour activity. *The Lancet Oncology*, 11, 1149–1159.

Woods, D. and Turchi, J.J. (2013). Chemotherapy induced DNA damage response. *Cancer Biology & Therapy*, 14, 379–389.

Wu, G.S., Burns, T.F., McDonald, E.R., Jiang, W., Meng, R., Krantz, I.D., Kao, G., Gan, D.D., Zhou, J.Y. and Muschel, R. (1997). KILLER/DR5 is a DNA damage-inducible p53-regulated death receptor gene. *Nature Genetics*, 17, 141–3.

Xiao, Z., Chen, Z., Gunasekera, A.H., Sowin, T.J., Rosenberg, S.H., Fesik, S. and Zhang, H. (2003). Chk1 Mediates S and G2Arrests through Cdc25A Degradation in Response to DNA-damaging Agents. *Journal of Biological Chemistry*, 278, 21767–21773.

Xiaodong Wang (2001). The expanding role of mitochondria in apoptosis. *Genes & Development*, 15, 2922–2933.

Yamaguchi, H., Durell, S.R., Chatterjee, D.K., Anderson, C.W. and Appella, E. (2007). The Wip1 Phosphatase PPM1D Dephosphorylates SQ/TQ Motifs in Checkpoint Substrates Phosphorylated by PI3K-like Kinases†. *Biochemistry*, 46, 12594–12603.

Yu, J.W., Jeffrey, P.D. and Shi, Y. (2009). Mechanism of procaspase-8 activation by c-FLIPL. *Proceedings of the National Academy of Sciences of the United States of America*, 106, 8169–8174.

Zabludoff, S.D., Deng, C., Grondine, M.R., Sheehy, A.M., Ashwell, S., Caleb, B.L., Green, S., Haye, H.R., Horn, C.L. and Janetka, J.W. (2008). AZD7762, a novel checkpoint kinase inhibitor, drives checkpoint abrogation and potentiates DNA-targeted therapies. *Molecular Cancer Therapeutics*, 7, 2955–66.

Zhang, L. and Yu, J. (2013). Role of apoptosis in colon cancer biology, therapy, and prevention. *Current Colorectal Cancer Reports*, 9, 331–340.

Zhang, N., Yin, Y., Xu, S.-J. and Chen, W.-S. (2008). 5-Fluorouracil: Mechanisms of Resistance and Reversal Strategies. *Molecules*, 13, 1551–1569.

Zhang, Y. and Hunter, T. (2013). Roles of Chk1 in cell biology and cancer therapy. *International Journal of Cancer*, 134, 1013–1023.

Zhao, H., Watkins, J.L. and Piwnica-Worms, H. (2002). Disruption of the checkpoint kinase 1/cell division cycle 25A pathway abrogates ionizing radiation-induced S and G2 checkpoints. *Proceedings of the National Academy of Sciences*, 99, 14795–14800.

Zinkel, S., Gross, A. and Yang, E. (2006). BCL2 family in DNA damage and cell cycle control. *Cell Death & Differentiation*, 13, 1351–9.

Zinkel, S.S., Hurov, K.E., Ong, C., Abtahi, F.M., Gross, A. and Korsmeyer, S.J. (2005). A Role for Proapoptotic BID in the DNA-Damage Response. *Cell*, 122, 579–591.

Zong, W.-X., Lindsten, T., Ross, A.J., MacGregor, G.R. and Thompson, C.B. (2001). BH3-only proteins that bind pro-survival Bcl-2 family members fail to induce apoptosis in the absence of Bax and Bak. *Genes & Development*, 15, 1481–1486.